The momentum spectrum and charge ratio of cosmic ray muons in the vertical direction between 200 and 5000 GeV/c

R. Thornley

THE MOMENTUM SPECTRUM AND CHARGE RATIO OF COSMIC RAY MUONS IN THE VERTICAL DIRECTION BETWEEN 200 AND 5000 GeV/c

by

R. THORNLEY B.Sc.

A Thesis submitted to
the University of Durham
for the Degree of Doctor of Philosophy

October, 1979

ABSTRACT

The sea-level vertical muon momentum spectrum and charge ratio have been measured in the momentum range 200 GeV/c to 3000 GeV/c using the MARS spectrograph at Durham.

The analysis of approximatley 80,000 muons is described, and the various instrumental effects which affect the shape or absolute intensity of the spectrum are discussed in detail. Muons accompanied and unaccompanied by extensive air showers are included in the measurement of the muon spectrum.

A simple muon production and propogation model has been used to predict the pion and kaon production spectra from the present measurement of the muon spectrum. It has not been possible to predict the proportion of kaons and pions produced in primary cosmic ray interactions in the atmosphere.

The present measurement of the muon spectrum is in good agreement with the shape and absolute intensity of the previous measurement of the muon spectrum using the MARS spectrograph (Ayre et al, 1975). The prediction by Whalley (1974) of a flatter pion and kaon spectrum above 100 GeV/c is substantiated.

The shape of the present measurement of the muon spectrum is in agreement, within the limits of statistical accuracy, with the results from other spectrographs, but there are differences in absolute intensity. Comparisons with indirect measurements of the muon spectrum show that the present spectrum is flatter and higher in intensity above 1 TeV/c.

The overall value of the charge ratio of muons between 100 GeV/c and 3000 GeV/c is 1.305 ±0.015. There is an indication of a slight rise of the charge ratio with momentum. This result is consistant with the previous measurement of the charge ratio between 20 and 500 GeV/c using

using the MARS spectrograph (Baxendale et al, 1975) and with the results of Ashley et al (1975) above 1 TeV/c.

PREFACE

The results presented in this thesis represent the research carried out by the author in the period 1974 - 1977 while he was a research student under the supervision of Dr. M. G. Thompson in the Cosmic Ray Group of the Physics Department of the University of Durham.

When the author joined the group the construction of the blue side of the spectrograph was complete and the collection of the data presented here had already begun. The author took over responsibility for running the spectrograph early in 1975. The author was also responsible for the analysis of the collected data using the MARS2 analysis program previously developed by members of the Cosmic Ray Group. The interpretation of the results of the computer analysis has been the sole responsibility of the author. The results presented here represent the final measurements of the muon momentum spectrum and charge ratio using the MARS spectrograph at Durham.

ACKNOWLEDGEMENTS

I would like to express my sincere thanks to the following people:

Professor A.W. Wolfendale, F.R.S., for the provision of the facilities for this work and for his many encouraging and stimulating discussions.

The Science Research Council for the provision of a Research Studentship and for funding this experiment.

Dr. M.G. Thompson, my supervisor and leader of the MARS Cosmic Ray Group, for his advice and guidance throughout this work.

To all past members of the MARS Cosmic Ray Group for without their help in the design, construction, understanding and running of the spectrograph, this work would not have been possible.

Dr. M.R. Whalley for his help in the interpretation of the data.

Mr. J.M. Baxendale for repairing the momentum selector a countless number of times, for his expert adjustment of the high voltage spark-gaps and for his help in running the spectrograph.

Mr. K. Tindale for his daily checking of the spectrograph instrumentation.

Dr. B.J. Daniels and Mrs. S.E. Davidson for their extremely well managed handling of the muon data and for their advice on computer programming matters.

Mrs. A. Gregory, Mrs. P.A. Russell for their expert drawing of some of the diagrams.

Mrs. G. Snawdon for her transformation of this thesis through her speedy and precise typing.

My wife for her patience during the writing of this thesis and for her help in drawing some of the diagrams and in reading through the manuscript.

CONTENTS

CHAPTER 1

INTRODUCTION

1.1 THE DISCOVERY OF COSMIC RAYS

The effect of cosmic rays on physical apparatus had been noticed as long ago as the end of the eighteenth century. Coulomb observed that a charged sphere hung by a long silk thread gradually lost its charge, and he suspected that the charge had leaked away along the thread rather than through the air. Later, it was noticed that a gold leaf electroscope, far removed from any known source of radiation, would gradually lose its charge.

At first it was thought that this was caused by natural radioactivity from the matter around the electroscope, but when Hess (1911, 1912) flew an ionisation counter in a balloon up to a height of 5 km and noted that after an initial slight decrease, the ionisation gradually increased with height, it was realised that the radiation emanated from above.

It was natural for physicists at that time to assume that this radiation was gamma radiation, as this was the most penetrating form of radiation then known. However, with the advent of coincidence counter telescopes (Bothe and Kolhorster 1928, 1929) it soon became clear that cosmic rays consisted of charged particles. Further, by introducing a 4.1 cm slab of gold between the Geiger-Müller tubes of the telescope. Bothe and Kolhorster were able to show that the cosmic radiation had a soft and a hard component, the hard component being able to penetrate the gold slab.

More evidence that the cosmic radiation consisted of charged particles came from the work of Clay (1927) who made several voyages from Amsterdam to Java carrying ionisation chambers. He found that the

cosmic ray intensity decreased at the equator, where the horizontal component of the magnetic field is at its strongest. If the cosmic radiation was entirely neutral this effect would not have been observed.

The identification of the two components of the cosmic radiation was achieved after the development of the counter-controlled cloud chamber (Blackett and Occhialini, 1933), in which the tracks of charged particles could be observed in a magnetic field. The soft component was seen to consist of equal numbers of negatively and positively charged particles which sometimes appeared in groups or showers. The former particles were soon identified as being electrons, and it was Anderson (1932) who correctly identified the positively charged particles as the anti-particle of the electron, or the positron, which was predicted in Dirac's theory. This discovery was a major achievement of cosmic ray physics.

The mass of the particles constituting the penetrating component was first measured by Street and Stevenson (1937). They were found to be $\sim$200 times heavier than the mass of the electron and were first thought to be the particles responsible for carrying the strong nuclear force, postulated by Yukawa (1935). They were therefore called μ-mesons. There was some doubt about this interpretation, however, when they did not interact with nuclei as strongly as expected. This problem was overcome when Lattes et al (1949) observed, in nuclear emulsions, the decay of a particle into the μ-meson. This particle, with a mass of $\sim$273 electron masses, was correctly interpreted as the Yukawa particle and was called the π-meson, or pion for short. The μ-meson, later found not to be a meson, is now known as the muon.

The study of the nature of cosmic rays resulted in the discovery of many new particles. Some of these, such as the positron, muon and

pion, have already been mentioned, others include the Λ and Σ^+ (Rochester and Butler, 1947) and the K^+ (Brown et al 1949).

With the development of the theories of bremsstrahlung and pair production came a realisation that the particles observed at sea level are the interaction and decay products of extra-terrestrial particles as they descend through the atmosphere. The study of cosmic rays therefore splits naturally into the study of the primary radiation at the top of the atmosphere and its secondary products at mountain attitudes and ground level. Each of these components will be considered in turn.

1.2 THE PRIMARY COSMIC RADIATION AND ITS ORIGIN

The fact that the primary radiation consists mainly of positively charged particles has been known for some time from observations of the East-West effect (Johnson and Street, 1933). However, it has not been until recently, with the advent of balloons and satellites which are able to carry particle detectors high into the atmosphere, that the composition and energy spectrum of the primary cosmic radiation have been measured in detail.

Wolfendale (1973) has summarised the measurements of the primary spectrum and this is shown in figure 1.1. Protons are the most abundant particle, and α-particles are the next most abundant having an intensity of a factor of $\sim$8 lower. Nuclei of $Z>2$ are also present, but in much smaller quantities and nuclei with Z as high as $\sim$96 have been detected in the primary radiation by means of nuclear emulsions (Fowler et al 1967, 1970). A comparison of cosmic ray abundances with universal abundances shows an excess of light nuclei (Li, Be and B) in the cosmic ray beam. It is generally agreed that these excess light nuclei are spallation products caused by collisions of heavier nuclei during their

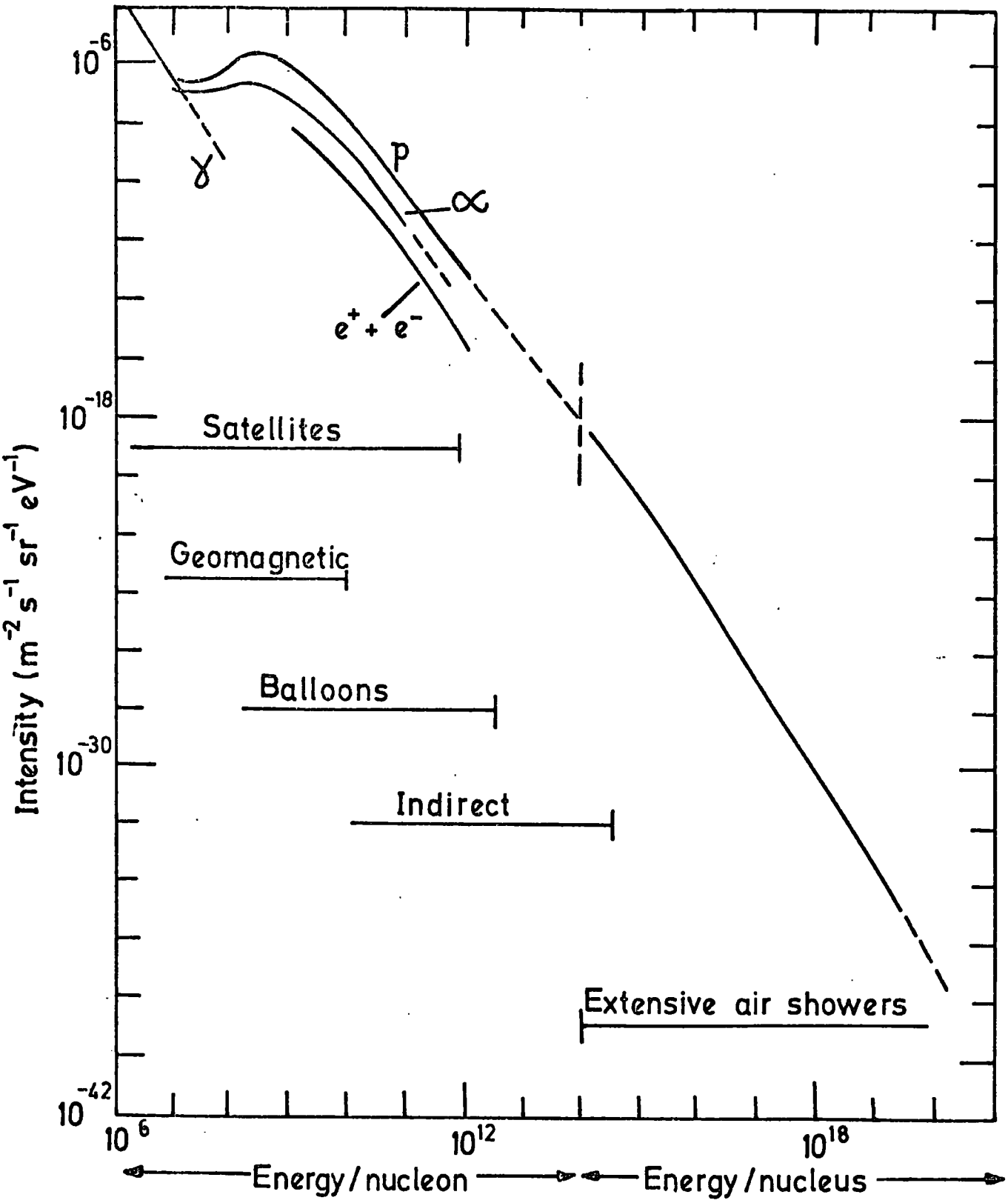

Figure 1.1 The primary energy spectrum of cosmic ray particles. (after Wolfendale 1973)

propogation from their source to earth..

The information about individual nuclei stops at about 5 $\times 10^{11}$ eV/nucleon and above this energy only the flux of protons can be measured. Grigorov (1971) has measured the proton spectrum up to $\sim 10^{15}$ eV/nucleon and his measurements show a falling off of the proton spectrum above $\sim 10^{12}$ eV. This is at variance with indirect measurements in this region and this is why the proton intensity is shown as being uncertain in the range 10^{12} - 10^{14} eV (Wolfendale, 1973).

Above 10^{16} eV/nucleon, direct measurements are impracticable because of the extremely low flux of particles (about 1 m^{-2} sr^{-1} $year^{-1}$). However, primary particles of energy $\geq 10^{13}$ eV induce showers of particles (mainly electrons and positrons) in the atmosphere which have enough energy to reach ground level. These are called extensive air showers (or EAS for short) and by measuring their size spectrum, the primary energy spectrum up to $\sim 10^{20}$ eV/nucleus may be determined. However, it is difficult to determine the nature of the primary particle from EAS measurements, and the energy spectrum in this region must be expressed in units of energy/nucleus.

The primary spectrum falls exponentially with energy. Above 10^{10} eV/nucleon, where the effect of the interplanetary magnetic field is insignificant, to about 3 $\times 10^{15}$ eV/nucleon, the exponent is ~ 2.6. Above 3 $\times 10^{15}$ eV/nucleon, the exponent increases sharply to ~ 3.2 and continues with this value until $\sim 10^{18}$ eV where the spectrum appears to flatten once again (Cunningham et al, 1977).

The origin of the cosmic radiation, and hence the interpretation of the shape and the composition of the primary spectrum, is still open to much conjecture. Ginzburg (1975) favours, on energetic grounds, a galactic origin for the majority of cosmic rays. Possible galactic

sources having sufficient energy are supernova (Colgate, 1966) and pulsars. The latter source has been proposed to explain the 'kink' in the spectrum at $\sim 10^{15}$ eV (Karakula et al, 1974). Another explanation for the change in slope of the primary spectrum is that above $\sim 10^{15}$ eV cosmic rays have sufficient energy to escape from the galactic magnetic field.

Burbidge (1975) argues in favour of an extra-galactic contribution to the flux of protons between 10^{16} and 10^{19} eV. The extra-galactic cosmic rays fill up clusters and super-clusters of galaxies which occupy $\sim 1\%$ of the universe. This circumvents the problem, on energetic grounds, of cosmic rays pervading the whole universe. Possible extra-galactic sources are active galaxies in the Virgo cluster, Centauris A or M82.

The existence of the ultra-high energy cosmic rays of energy $\sim 10^{20}$ eV is one of the biggest problems confronting astrophysicists (see Stocker, 1978). Greisen (1966) and Zatsepin and Kuzmin (1966) point out that cosmic rays of this energy should not be observed because of electron pair production, photodisintegration and photopion production interactions of the cosmic rays with the 3°K background radiation. Thus, the primary spectrum should cut-off at about $10^{18} - 5 \times 10^{19}$ eV (Stecker, 1978).

The absence of a cut-off may be because the ultra-high energy cosmic rays are of local origin produced in the galaxy or supercluster of galaxies so that they have not lived long enough for their energies to be attenuated.

The primary cosmic radiation also contains electrons (and positrons) and γ rays. The intensity of the electron component is $\sim 1/100$th of the proton-nuclei conponent. Electrons, positrons and γ's are all produced as a result of interactions between primary cosmic rays

and interstellar matter. The γ's come from the decay of neutral pions and the electrons and positrons from the decay of charged pions. However, above 10^9 eV, the positron/electron ratio is only ∿5%, so there must be sources of elecrons within the galaxy. Extra-galactic sources of electrons are ruled out because of Compton interactions with the 3°K background radiation.

The importance of γ-ray studies lies in the fact that γ-rays are not deflected in the galactic magnetic field and their arrival direction can indicate the region of their production. The γ-ray intensity is highest in the centre of the galaxy, therefore indicating a high density of cosmic rays there.

The diffuse background of γ-rays is thought to be of extra-galactic origin.

1.3 COSMIC RAYS AT GROUND LEVEL

On entering the atmosphere, primary cosmic ray protons travel ∿80 gm cm^{-2} before interacting with the nucleus of an air molecule. α-particles travel ∿45 gm cm^{-2} and heavier nuclei somewhat less. As a result of this interaction, three cascades develop coincidentally within the atmosphere. They are the nucleon, the electromagnetic and the muon cascade.

A nucleon cascade develops because a number of secondary protons and neutrons are produced in the proton-air nucleus interaction for the expense of only about a half of the proton's energy. The proton can therefore make, on average, a further 11 interactions before reaching ground level.

Also produced in these interactions are pions and a small proportion (10 - 15%) of kaons. Other particles such as hyperons are produced, but these are of lesser importance for the production of secondary particles.

Uncharged pions decay in about 10^{-15} s into two γ-rays. Each γ-ray then produces an electron-positron pair by the process of pair production, and these electrons and positrons produce further γ's by the process of bremsstrahlung. Thus, an electromagnetic cascade builds up in the atmosphere and the number of electrons, positrons and photons increases until the mean energy of the electrons and positrons reaches the critical energy for air (84 MeV). When this happens, absorption of the electrons by the air tends to dominate and the shower size decreases. If the primary energy is $\gtrsim 10^{13}$ eV, the shower can reach ground level.

The muon cascade arises from the decay of charged pions and kaons.

$$\pi^{\pm} \rightarrow \mu^{\pm} + \nu_{\mu} \ (\bar{\nu}_{\mu}) \qquad \text{(branching ratio 100\%)}$$

$$K^{\pm}_{\mu 2} \rightarrow \mu^{\pm} + \nu_{\mu} \ (\bar{\nu}_{\mu}) \qquad \text{(branching ratio 64.5\%)}$$

The mean lifetime of pions and kaons at rest are 2.6×10^{-8}s and 1.2×10^{-8}s respectively, but because of relativistic time dilation the mean lifetimes are considerably extended. This results in an increasing chance of interaction with an air nucleus as energy increases. However, because the mass of the kaon is about 4 times greater than the mass of the pion, time dilation will have a smaller effect on kaons. This results in an increasing contribution to the muon flux from kaons as energy increases. For example, at 10 GeV, kaons supply ∿5% of the muons at ground level, whereas above 10^4 GeV, this increases to ∿25%.

The competition between interaction and decay of pions and kaons results in the 'sec θ' enhancement of the muon intensity. As the zenith angle, θ, increases, pions and kaons travel for longer periods in the less dense upper atmosphere. The probability of interaction is therefore smaller and more pions and kaons decay. This is not observed at low

energies because the resulting muons have less chance of reaching ground level before they decay!

Muons decay into and electron and two neutrinos with a mean lifetime of 2.2×10^{-6} s.

$$\mu^{\pm} \rightarrow e^{\pm} + \nu_e \ (\bar{\nu}_e) + \bar{\nu}_\mu \ (\nu_\mu)$$

Although muons are produced at an average atmospheric depth of only 100 gm cm^{-2}, because of time dilation nearly all muons with an energy above 100 GeV are able to reach ground level. At lower energies, the effects of energy loss and decay reduce the number of muons reaching ground level.

1.4 MUON STUDIES AND THEIR SIGNIFICANCE

The quantities usually measured in relation to the muon component are its momentum spectrum and positive to negative charge ratio.

Figure 1.2 shows some of the most recent direct measurements of the muon momentum spectrum above 1 GeV/c. It can be seen that there are differences in absolute intensity and systematic differences between the measurements at all but the lowest momenta. Also, above 500 GeV/c there are large errors on the measurements.

The present measurement extends from ∿200 GeV/c and significantly improves the precision of the muon spectrum up to ∿3000 GeV/c. Further, the measurement is absolute, therefore it is free of the problems associated with normalisation procedures.

Recent measurements of the charge ratio (Allkofer et al, 1971(a), Nandi & Sinha, 1972(a) and Baxendale et al, 1975) indicate that it is fairly constant between 10 GeV/c and 100 GeV/c with a value of ∿1.29. However, the results of Ashley et al (1975) above 1 TeV indicate a significant rise in the charge ratio to ∿1.38. The present results extend from 100 GeV/c and tend to confirm the observed rise in the charge ratio.

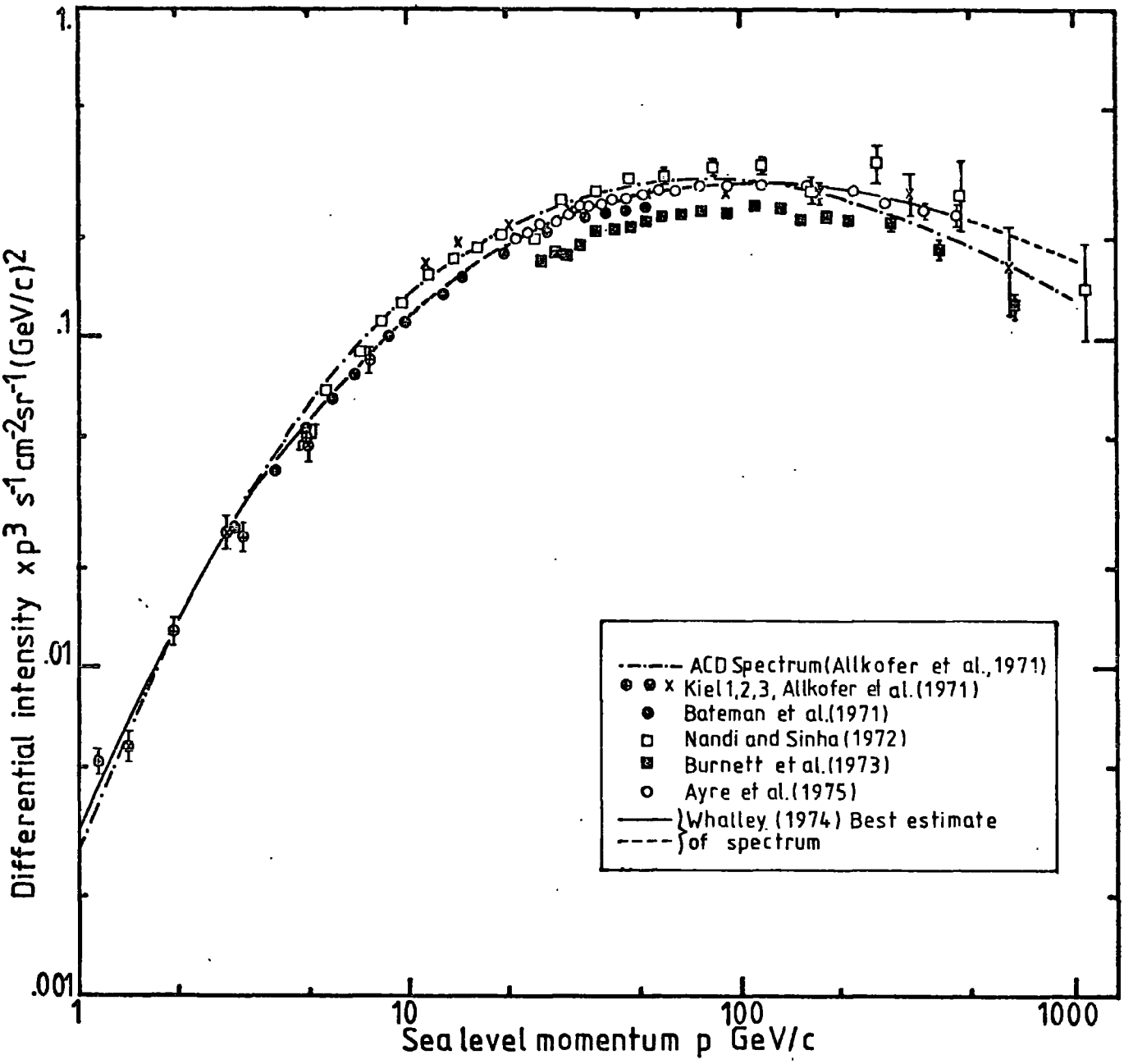

Figure 1.2 Recent measurements of the muon spectrum (After Whalley, 1974)

Recently, many authors (for example, Hume et al, 1973, Erlykin et al, 1974, Hoffman, 1975 and Thompson and Whalley, 1977) have used measurements of the muon momentum spectrum and, more particularly, of the muon charge ratio, to make predictions about the nuclear physics of interactions of primary cosmic rays in the atmosphere and about the shape and composition of the primary cosmic ray nucleon spectrum.

The interest in these calculations has been aroused mainly by the availability of data on proton-proton interactions at very high energies from the Intersecting Storage Ring (ISR) facility at CERN. Data from other high energy accelerators such as the NAL accelerator in the USA have also been used.

These data provide information on the inclusive production of nucleons, pions and kaons in proton-proton interactions up to equivalent laboratory energies of 1.5×10^3 GeV. Inclusive interactions are those in which only one (or two) of the interaction products are observed. Although proton-proton interactions are complex, the scaling hypothesis of Feynman (1969) and the hypothesis of limiting fragmentation of Benecke et al (1969) suggest that theoretically, these interactions should have a simple scaling property. That is, as the energy increases, the cross-sections for inclusive reactions should become energy independent and reach limiting values.

Experiments performed using the ISR facility have shown that, with a few exceptions, particle distributions scale over the ISR energy range up to 1.5×10^3 GeV and confirm the hypothesis of limiting fragmentation and the scaling hypothesis. Therefore the use of such data to calculate the production spectra of pions and kaons in the atmosphere, and hence the muon momentum spectrum and charge ratio, implicitly assumes that scaling holds up to cosmic ray energies. The

comparison between observed and predicted values can therefore be used as a test of scaling.

The situation is not as clear cut as this, however, because the primary composition has not been measured beyond 100 GeV/nucleon. Therefore, any predictions about nuclear interactions above 100 GeV/nucleon rely on assumptions about the primary cosmic ray composition. Similarly any predictions about the primary composition assume that scaling holds up to cosmic ray energies

The muon charge ratio is particularly sensitive to the ratio of protons to neutrons in the primary cosmic radiation and to the charge ratio of pions and kaons produced in primary cosmic ray interactions in the atmosphere. Therefore, much of the recent work has been concerned with predicting the charge ratio, which is known to $\sim$1% at momenta <100 GeV/c.

The results of these calculations have not been very consistant, however, and the predicted charge ratio has been found to be higher than the measured value in many cases. Possible explanations for this discepancy are that the hypothesis of limiting fragmentation breaks down at high energy (Hume et al, 1973, Erlykin et al, 1974), there is an increase in the relative number of nuclei in the primary radiation (Erlykin et al, 1974) or that the charge ratio of pions and kaons produced in proton-air nucleus interactions is smaller than in proton-proton interactions (Thompson and Whalley, 1977). Support for this latter suggestion comes from recent calculations by Badhwar et al (1977), Liland (1979) and Minorikawa and Saito (1977) who all allow for the nuclear effects and obtain good agreement with the measured charge ratio.

However, there are still difficulties in predicting the observed

increase in the charge ratio between 100 GeV/c and 1000 GeV/c. This increase is primarily caused by the increasing production of muons from kaons at high energy, but it is also influenced by the ratio of protons to neutrons in the primary radiation. Also, there is uncertainty about the production of kaons from neutrons (Thompson and Whalley, 1977, and Thompson et al, 1978).

Predictions based upon the muon momentum spectrum are also contradictory. Erlykin et al (1974) conclude that in order to obtain agreement between the primary spectrum predicted from direct and indirect measurements of the muon spectrum, and the primary spectrum predicted from EAS data, there must either be a breakdown in scaling above 10^3 GeV/nucleon with no change in primary composition, or an increase in the fraction of heavy nuclei in the primary radiation. Thompson and Whalley (1977) came to substantially the same conclusion. However, Badhwar et al (1977) obtain good agreement with direct measurements of the muon spectrum using a primary spectrum of constant composition without invoking a breakdown in scaling.

It is believed that this and further measurements of the muon momentum spectrum and charged ratio should enable more precise predictions to be made concerning the nature of nuclear interactions at cosmic ray energies and the composition of the primary spectrum above 100 GeV/nucleon.

1.5 THE MUON AND ELEMENTARY PARTICLES

Since the discovery ofthe muon in the cosmic radiation over 40 years ago, the reason for its existence remains unsolved. The muon has the same weak and electromagnetic interactions as the electron, but it is simply 207 times as heavy. The muon and the electron each have associated with them a neutral particle, called a neutrino, which

allows them to conserve their lepton number in decays and interactions.

However, some light has recently been thrown on this problem by the discovery of a fifth lepton in electron-positron annihilation (see Perl, 1978 for a review of this discovery). This lepton, called the τ, has a mass of $\sim$1782 MeV/c^2 and there is good evidence to suggest that it has an associated neutrino. This discovery opens up the possibility that a whole spectrum of leptons exist.

In parallel with discovery of a fifth lepton are the discoveries of two massive vector mesons, the J/Ψ (mass 3095 MeV/c^2) (Augustin et al, 1974 and Aubert et al, 1974) and the Υ (mass 9.46 GeV/c^2) (see Miller, 1978) in electron-positron annihilation and in high energy proton-nucleus interactions, which require two new quarks, the c and b quarks, to explain their existence.

The significance of this is that the leptons are similar to quarks in that they appear to have no internal structure and there appears to be a symmetry between quarks and leptons which might point towards a unification of the weak and electromagnetic forces (Close, 1979). This symmetry is shown below:

$$\begin{pmatrix} u \\ d \end{pmatrix} \quad \begin{pmatrix} c \\ s \end{pmatrix} \quad \begin{pmatrix} t? \\ b \end{pmatrix} \qquad \text{quarks}$$

$$\begin{pmatrix} e \\ \nu_e \end{pmatrix} \quad \begin{pmatrix} \mu \\ \nu_\mu \end{pmatrix} \quad \begin{pmatrix} \tau \\ \nu_\tau \end{pmatrix} \qquad \text{leptons}$$

where u, d and s quarks were postulated by Gell-Mann (1964) and Zweig (1964, 1965) to explain the observed multiplet structure of the baryons and the mesons which were then known. Evidence for the existence of a sixth quark, t, has not been found, but it is strongly believed to exist (Close, 1979).

The mystery surrounding the muon now seems to be lessening and

future high energy experiments may uncover a new field of quark-lepton spectroscopy. However, the investigation of massive leptons and mesons requires particle beams of very high energy. Koshiba (1977) has suggested that a large (10 m^3) spectrograph, of high resolving power, could be used to investigate the $\mu^-\mu^+$ decays of massive vector mesons and charmed meson and lepton pairs produced in cosmic ray nuclear interactions. Also, if the yield of such particles is high enough, then a flattening of the muon spectrum should be observed at energies above 10 TeV. Cosmic rays may once again, as they were in the 1930's and 1940's, be used as a means of examining the nature and properties of the elementary particles.

CHAPTER 2

A DESCRIPTION OF THE SPECTROGRAPH

2.1 INTRODUCTION

The Muon Automated Research Spectrograph, or MARS for short, is a multilayer, solid iron magnet spectrograph, using scintillation counters for muon detection and trays of flash-tubes for trajectory location, which was designed to measure the momentum spectrum and charge ratio of muons arriving in the vertical direction up to a momentum of about 5000 GeV/c.

The spectrograph is situated at an altitude of 200 ft above mean sea level and the geographical co-ordinates are latitude 54.5°N and longitude 1.3°W. The spectrograph is aligned such that the front of the spectrograph faces North.

Since its construction, which commenced in 1968, several experiments have been performed. Notable among them are precise measurements of the muon spectrum and charge ratio from 20 to 500 GeV/c (Ayre et al 1975 and Baxendale et al 1975), measurements of electromagnetic interactions of muons in iron (Hansen 1975, 1975(a) and 1976) and measurements of muons in extensive air showers and the rate of multiple muons (Rada 1977 and Hawkes 1977). The present work is a measurement of the muon spectrum and charge ratio from 200 to 3000 GeV/c, thus extending the previous measurement of Ayre et al to higher momenta. This is the final piece of major work to be carried out on MARS, the spectrograph having been dismantled in early 1978.

A schematic diagram of MARS drawn in perspective is shown in figure 2.1. It can be seen that it consists of four solid iron

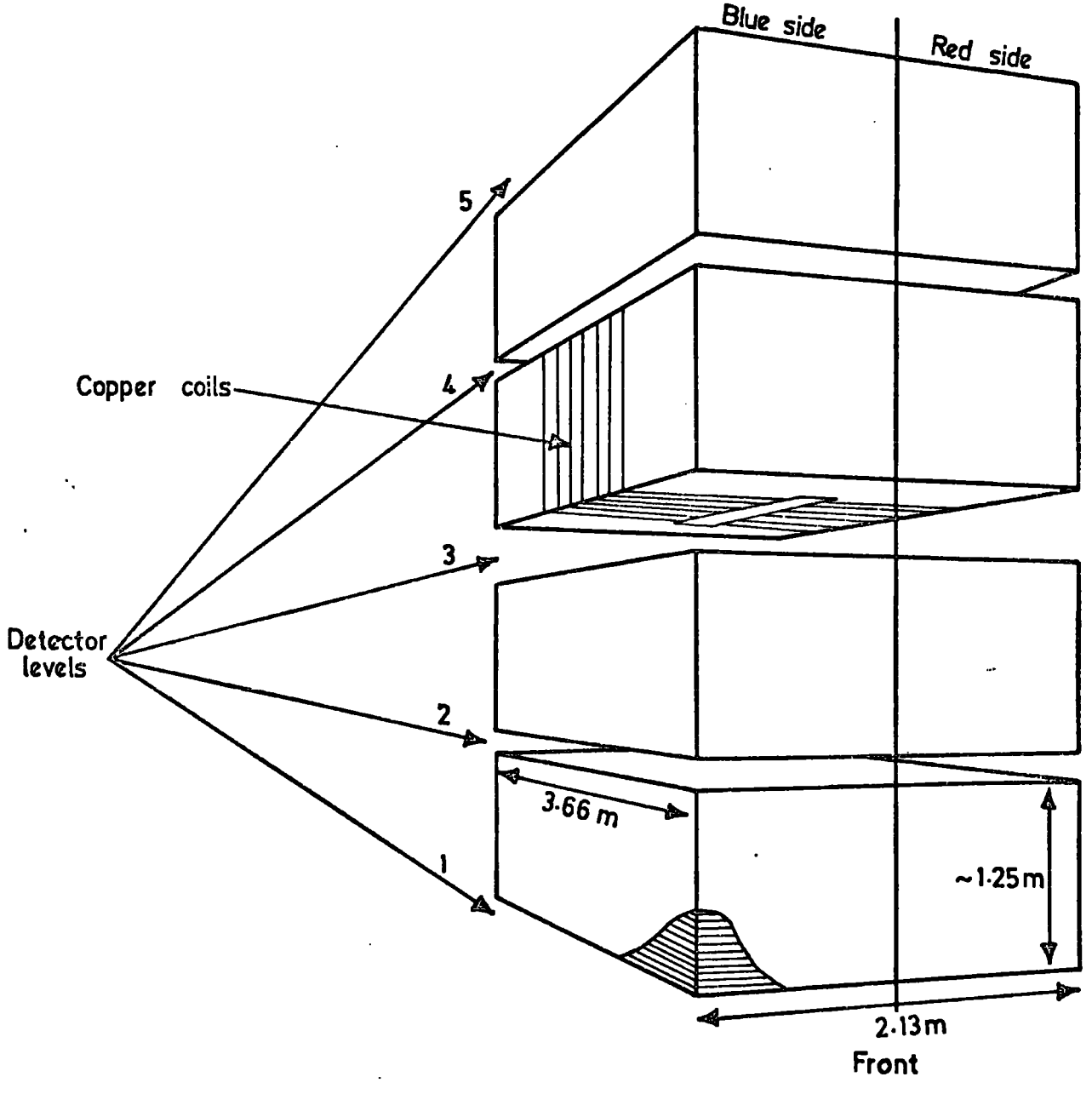

Figure 2.1 Schematic diagram of spectrograph drawn in perspective

toroidal magnets placed one above the other with gaps between them for the particle detectors. Each magnet weighs about 71 tons, thus making the total weight of the magnets equal to 284 tons. Four different particle detectors were used on the spectrograph and their arrangement is shown in figure 2.2. Scintillation counters at levels 1, 3 and 5 were used for muon detection, trays of large diameter (1.5 cm) flash-tubes were used at levels 1, 3 and 5 for momentum selection, trays of small diameter (0.5 cm) were used at levels 1,2,3,4 and 5 for trajectory location and finally, trays of Geiger counters were used at levels 1 and 5 to determine whether the muon passed through the front or the back of the spectrograph at those levels.

A multilayer arrangement was chosen to minimise the problems associated with burst production in the magnet blocks which is a particular problem in solid iron spectrographs. On its passage through an iron block a muon may initiate an electromagnetic cascade through the process of bremsstrahlung and direct pair production, and if this accompanies the muon from the magnet, it may mask the trajectory of the muon in the flash-tube tray. The probability that one or more particles accompany a muon from a magnet block has been calculated by Said (1966) and Hansen (1975), and their results are shown in figure 2.3. The burst probability is seen to rise sharply with momentum. By having flash-tube trays at five levels, there is then a good chance (99.6% at 100 GeV/c, 97.3% at 1000 GeV/c and 85.4% at 5000 GeV/c) that at least three of them will contain unambiguous tracks so that the trajectory of the muon can be reconstructed and the muon momentum determined.

The spectrograph splits naturally into two halves, corresponding to the two long sides of the toroidal magnets, and they are known as the blue side and the red side. Each half has its own detectors

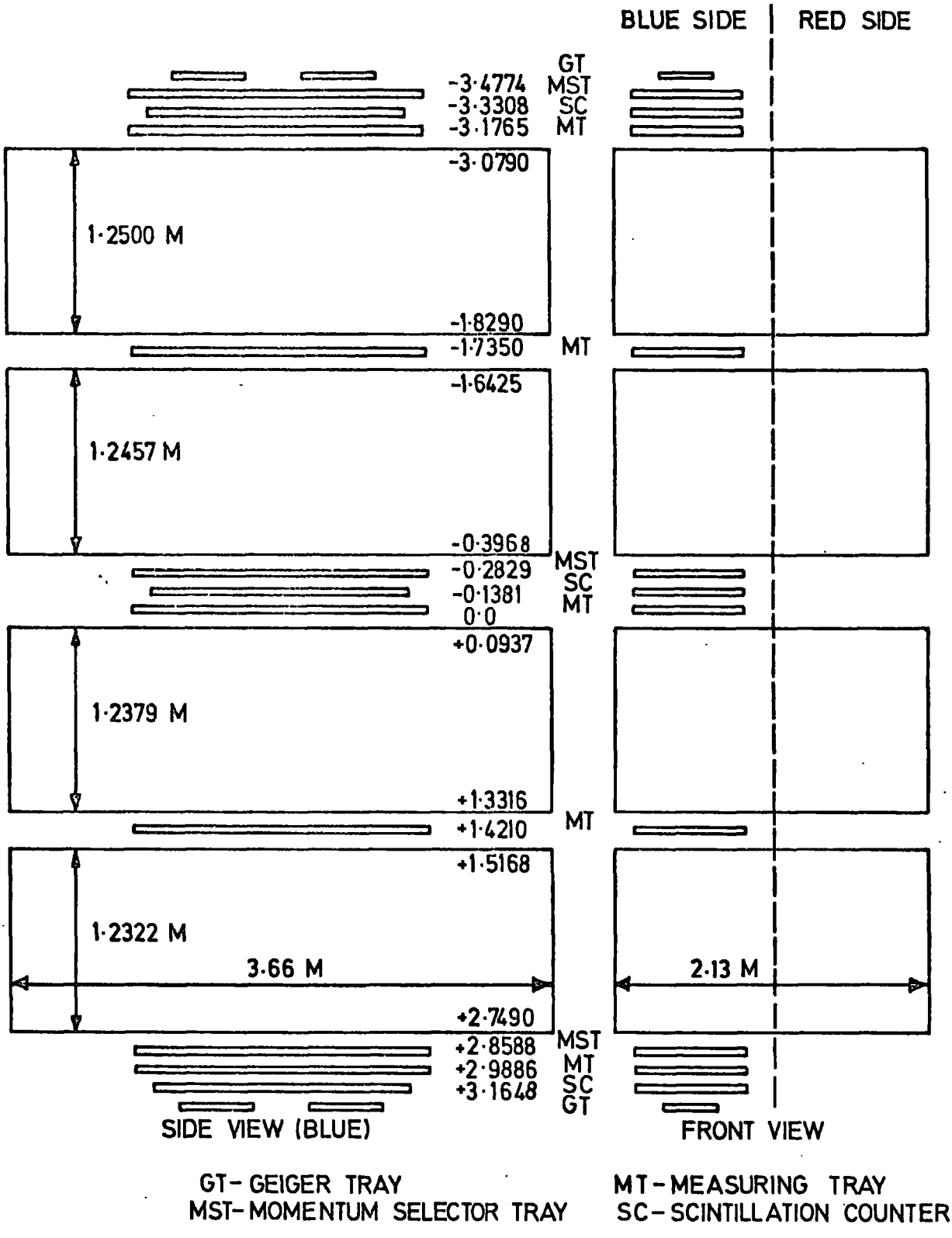

Figure 2.2 A side view and front view of the spectrograph showing its dimensions

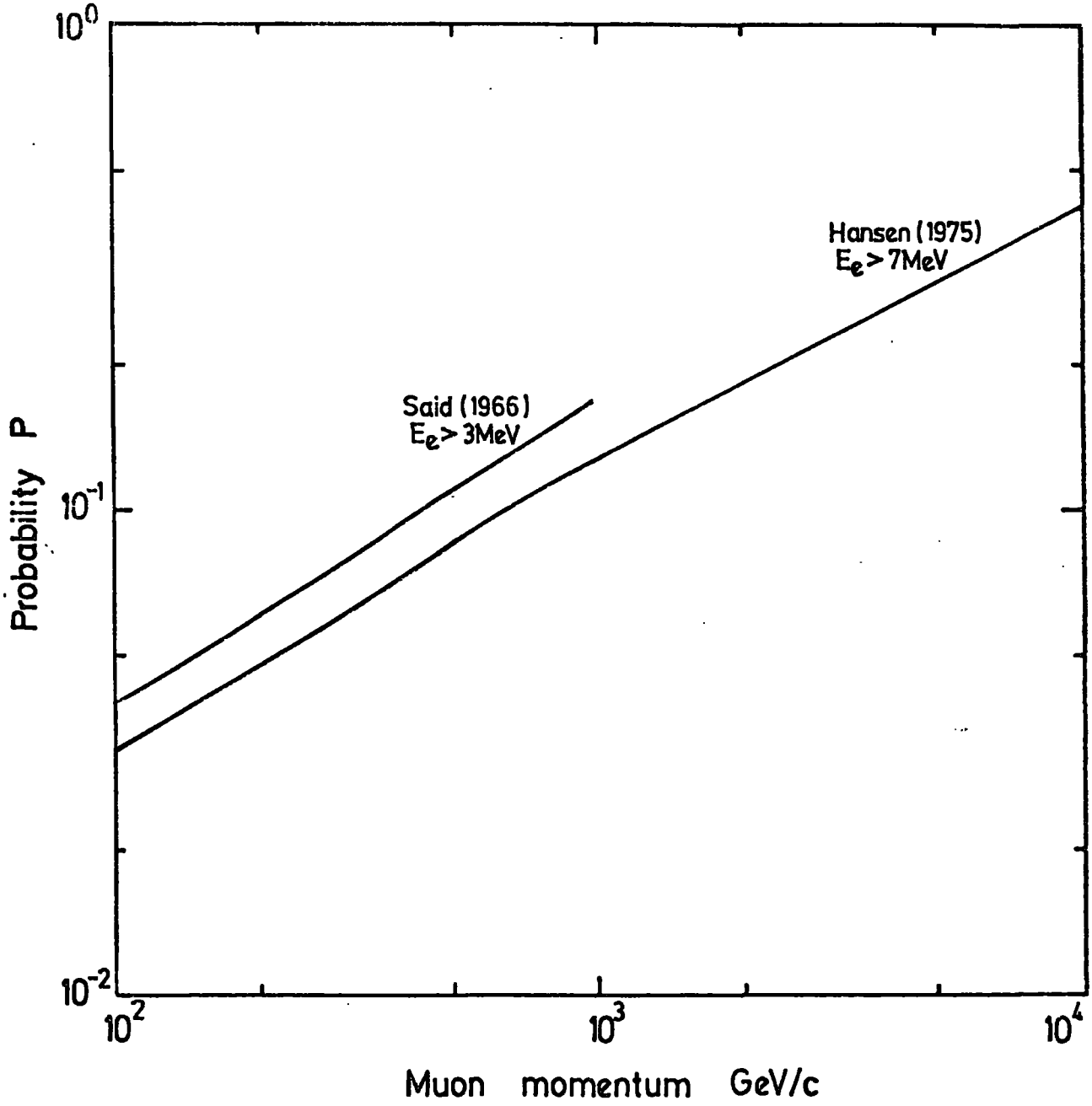

Figure 2.3 The probability P that one or more particles of energy greater than E_e accompany a muon from a magnet block

associated with it and it can be operated independently of the other side. The results presented here were measured on the blue side of MARS, the red side being used by Hawkes (1977) for the measurement of muons in extensive air showers (the air showers being detected by the Durham Extensive Air Shower Automated Research Array) and for the measurement of the rate of multiple muons. All references to the spectograph from now onwards will refer implicitly to the blue side unless otherwise stated.

As mentioned earlier, the MARS spectrograph has already been the subject of several major experiments and full descriptions of the spectrograph will be found in publications by Ayre (1971) and Ayre et al 1972 (a) and (b). Therefore only a brief description of the spectrograph will be given here. This will start by considering the design of the magnets, then there will be a description of the particle detectors and finally the controlling electronics and the method of data collection will be discussed.

2.2 THE MAGNETS

The arrangement of the magnets can be seen in figure 2.1. They are constructed from seventy-eight $\frac{5}{8}$ inch iron plates with rectangular slots cut in their centres for the copper energising coils. An unstabilised power supply capable of delivering 100 Amps at 100 Volts is used to power the magnets.

It is clear from the coil windings that the magnetic field will be from the back to the front of the spectrograph or vice versa depending upon the current direction. Muons pass downwards through the spectrograph and their trajectories are located in the front plane of the spectrograph by means of the trays of flash-tubes at all five levels. Therefore, from simple theory governing the motion of charged particles in a magnetic field and assuming a continuous magnetic

field through the spectrograph and energy loss to be negligable, the trajectory of the muon in the front plane will follow the path of a circle. By measuring the radius of curvature of the circle, the momentum of the muon can be determined from equation 2.1, where p is the momentum in eV, B is the magnetic field strength in kGauss and r is the radius

$$p = 300 \times B \times r \qquad (2.1)$$

of curvature in cm. In fact the magnetic field is not continuous, because of the gaps between the magnets, and the energy loss is not negligible. However, Wells (1972) showed that all that was needed to correct the calculated momentum for these effects is to add to it a constant. (See section 4.6). This basically is the technique used to measure the momentum of muons passing through the spectrograph. The charge of muons can be determined from the direction in which the trajectories bend in a particular magnetic field, hence the charge ratio of muons can be measured.

The strength of the magnetic field is related to the maximum muon momentum which the spectrograph can reliably measure. Following the method of Allkofer (1971(b)), Wells (1972) showed that the Maximum Detectable Momentum, or MDM for short, is related to the magnetic field strength B, and the error in track location at the measuring levels σ, in the following way:

$$MDM \doteq \frac{K \times B}{\sigma}$$

K is a constant which is dependent upon physical constants and upon the geometry of the spectrograph (for a definition and full discussion of the MDM, see section 5.4). Therefore to achieve the highest MDM, the magnetic field strength must be as large as practically possible. When MARS was designed, it was required to have an MDM of about 5000 GeV/c. Therefore with a trajectory location error estimated

to be about 0.3 mm a magnetic field strength of 16 kGauss was sufficient. However, it has since been found that the trajectory location error was underestimated and is in fact about 0.6 mm, thus giving an MDM of about 2500 GeV/c.

The measured momentum is directly proportional to the magnetic field strength as shown in equation 2.1. Therefore it is important to know accurately the magnetic field strength and how uniform it is in the region through which the muons pass. The magnetic field was measured by means of search coils inserted in the magnet blocks during their construction (Ayre,1971). The induced voltage in the search coils was measured as the energising current was reversed. Taking into account the errors of measurement and possible variations in the mains voltage, the magnitude of the magnetic field is estimated to be 16.3(±1%) kGauss with a non-uniformity of ±4% over the region through which the muons pass.

2.3 THE SCINTILLATION COUNTERS

Three scintillation counters at levels 1, 3 and 5 define the acceptance of the spectrograph and serve to trigger the momentum selector electronics if a three fold coincidence of pulses is detected on the passage of a muon through the spectrograph. The construction of a scintillation counter with its associated electronics is shown in figure 2.4. The plastic scintillator and photomultiplier tubes are enclosed in a light-tight aluminium box. The efficiency of the scintillation counter system will be discussed in section 4.5.

2.4 THE MOMENTUM SELECTOR TRAYS AND THE MOMENTUM SELECTOR

In this experiment, because only muons of momentum greater than 100 GeV/c are of interest, MARS is equipped with a momentum selector system to filter out as many of the unwanted muons as possible.

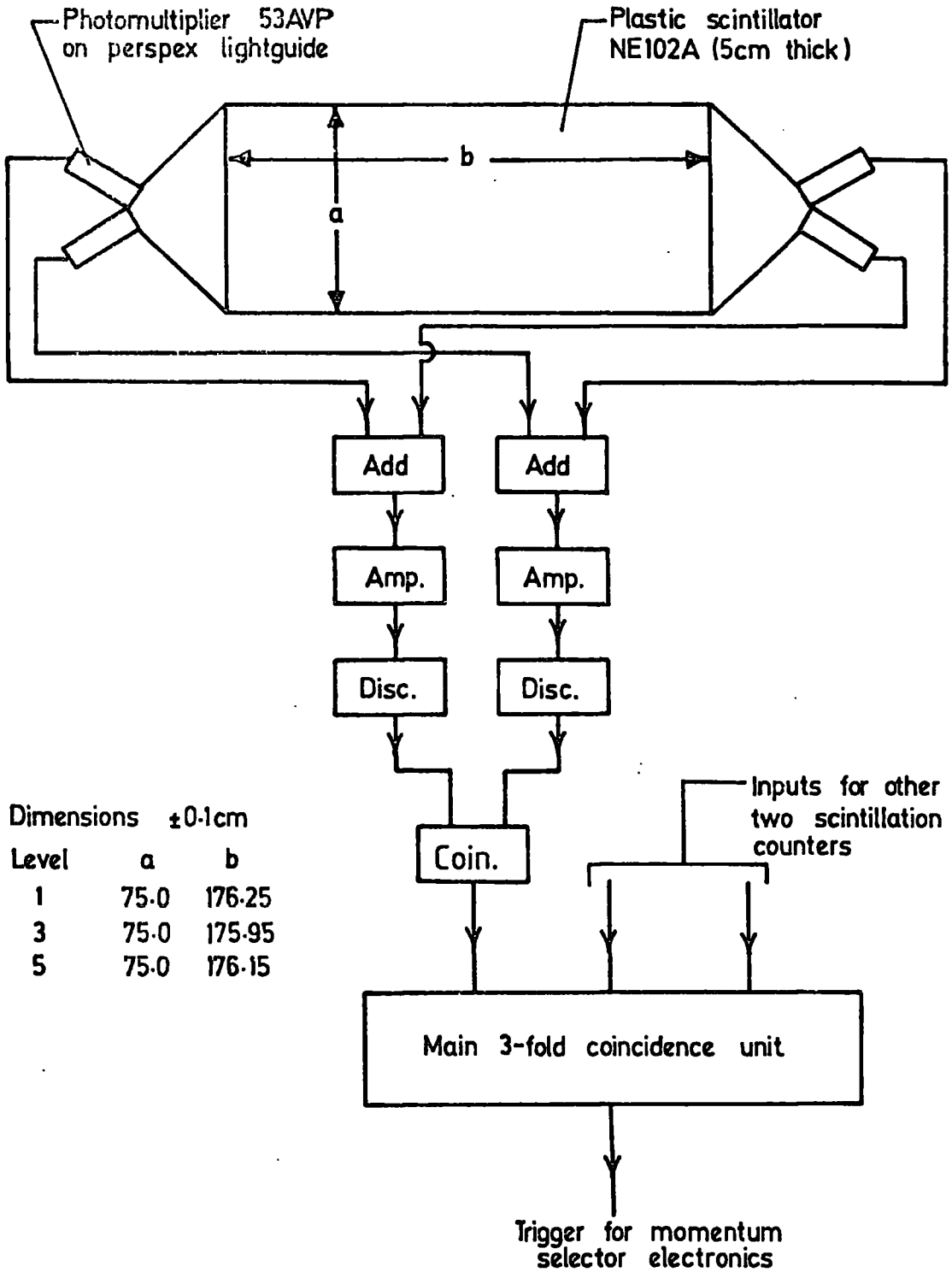

Dimensions ±0·1cm

Level	a	b
1	75·0	176·25
3	75·0	175·95
5	75·0	176·15

Figure 2.4 Schematic diagram showing the construction of a scintillation counter with its associated electronics

An idea of the number of unwanted muons can be obtained from the integral intensities of muons at 7.0 GeV/c (this is approximately the low momentum cut-off of MARS) and 100 GeV/c which are $1.52\ 10^{-3}\ cm^{-2}\ s^{-1}\ sr^{-1}$ and $1.38\ 10^{-5}\ cm^{-2}\ s^{-1}\ sr^{-1}$ respectively (Allkofer 1971). There are therefore about 110 times more muons with a momentum greater than 7 GeV/c than there are with a momentum greater than 100 GeV/c. The small acceptance of the spectrograph to the low energy muons will reduce this excess, but the need for a momentum selector is quite obvious if a large amount of unwanted data is not to be collected.

The momentum selector system consists of three trays, called Momentum Selector Trays or MST for short, of large diameter flash-tubes (1.5 cm internal diameter) at levels 1, 3 and 5, which define the muon trajectory, and an electronic momentum selector unit, which serves to trigger the main data collection system if the muon satisfies a certain deflection criterion. The momentum selector trays will first be described.

The arrangement of flash-tubes in a momentum selector tray is shown in figure 2.5. The flash-tubes are 2 metres long and contain neon (2% helium) at a pressure of 0.8 Atmospheres. On the passage of a muon through a flash-tube, ionisation is caused around the path of the muon and on the application of a high voltage pulse across the flash-tube by means of the aluminium electrodes, the gas breaks down due to secondary ionisation and the flash-tube discharges. The rows of flash-tubes are staggered as shown in figure 2.5 so that there is no clear path for muons incident in the angular range $\pm 7°$ about the vertical. In this way the position of the muon in the MST can be determined. The way in which the discharged flash-tubes are detected

and how this information is used will now be described.

The flash-tubes are digitised by the method of Ayre and Thompson (1969). Each flash-tube has a brass probe positioned close to its face so that when a flash-tube discharges, a voltage pulse is electrostatically induced into the probe and is used to 'set' an electronic memory. Thus it is possible to assess automatically which flash-tubes have discharged in each momentum selector tray.

Each MST is divided into one hundred and fifty one $\frac{1}{2}$ cm cells defined as the position at which the trajectory of the muon crosses the middle of layer 3, see figure 2.5. Electronic cell allocation logic on the front of the trays , which receive information from the electronic memories attached to the brass probes, automatically determine, from the pattern of discharged flash-tubes, which cell the muon most likely crossed. The cell allocation logic, which is shown in table 2.1, was designed to be as accurate as possible over the angular range of $\pm 7^{\circ}$. Where either of two cells could be set by a given flash-tube configuration, the most probable cell is allocated. Each cell is connected directly to the electronic momentum selector unit where they are combined together in overlapping groups of 4 at levels 3 and 5 and in overlapping groups of 6 at level 1. Table 2.2 shows the original tray front cell numbers and the group numbers in the momentum selector unit.

Consider figure 2.7, which represents the path of a muon through the spectrograph. The momentum selector levels are indicated and it is assumed that they are equally spaced. If a, b and c ($1 \leqslant a,b,c, \leqslant 51$) are the group numbers allocated in the momentum selector unit at levels 1, 3 and 5, then the deflection of the trajectory, defined in figure 2.7, is given by $\Delta = 2b-a-c$. A high momentum event is then signified

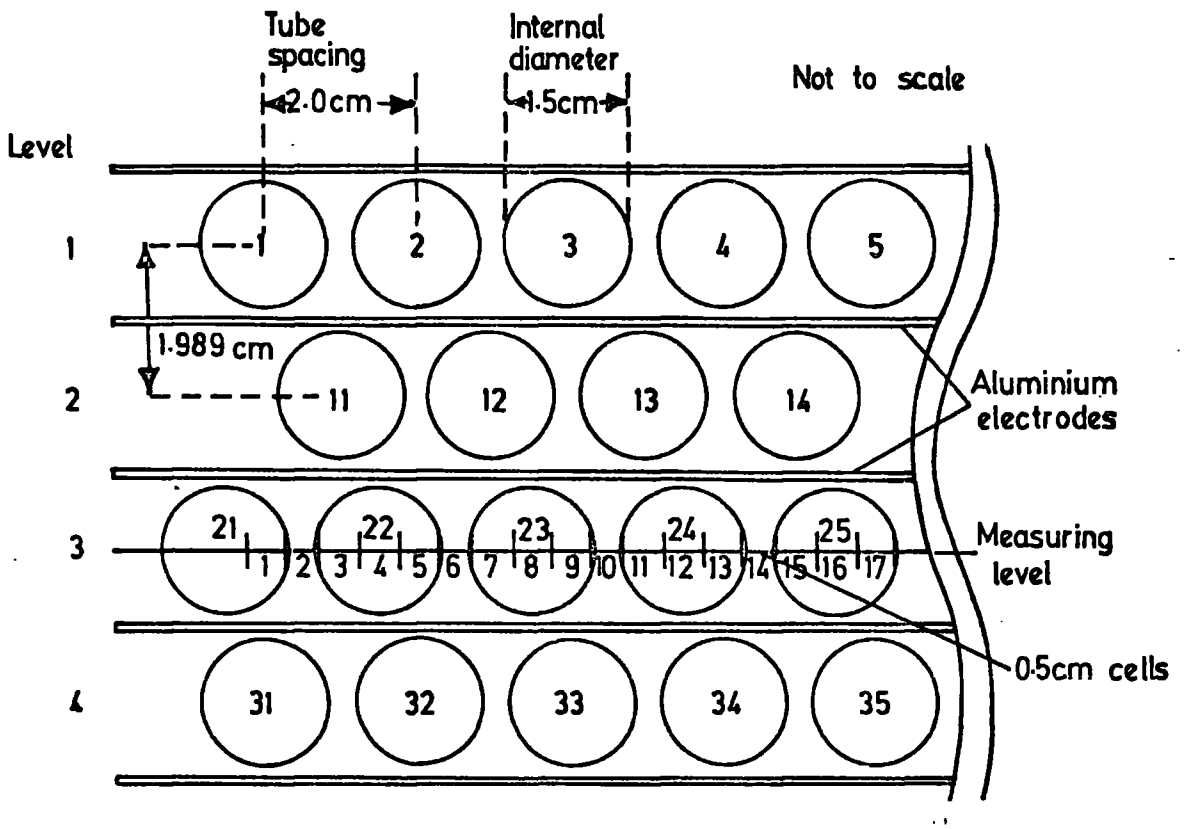

Figure 2.5 The arrangement of flash-tubes in a momentum selector tray

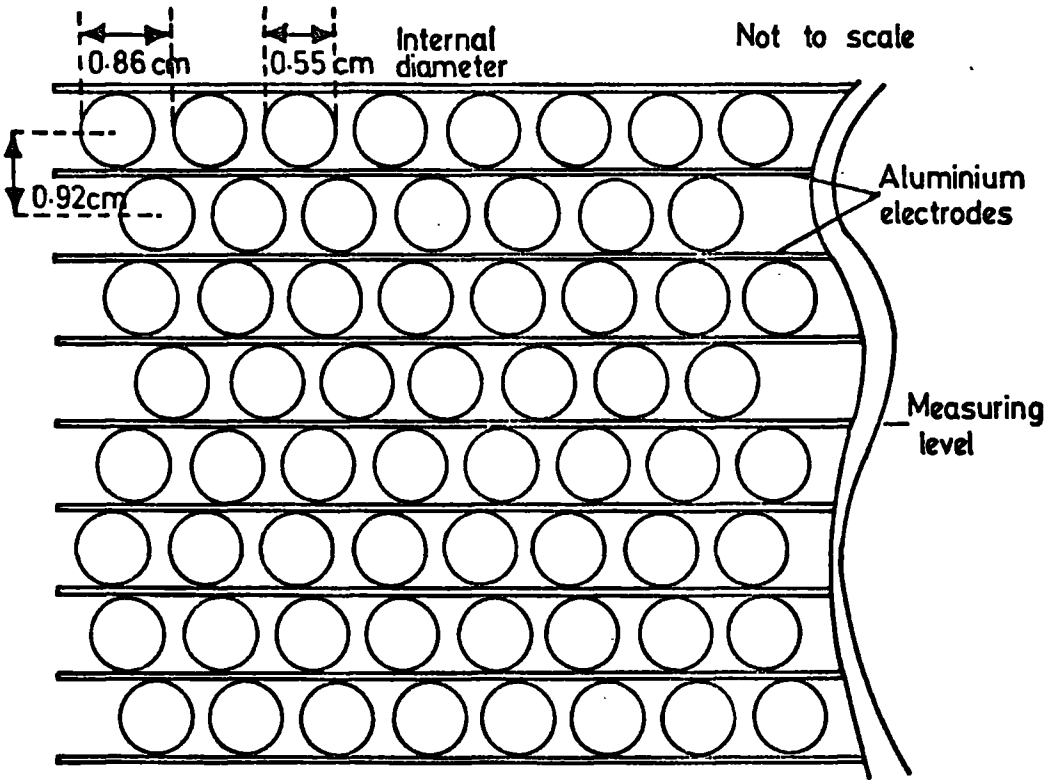

Figure 2.6 The arrangement of flash-tubes in a measuring tray

	LAYER			
	1	2	3	4
CELL NUMBER	TUBES DISCHARGED			
1	1		21	31
1	1	11	21	31
1	1		21	
2	1	11		31
2		11		31
2	1			31
3	1	11	22	31
3		11	22	31
3	2	11	22	31
4	2	11	22	
4		11	22	
4		11	22	32
4	2	11	22	32

TABLE 2.1 THE RELATION BETWEEN THE PREDETERMINED FLASH-TUBE CONFIGURATION AND THE ALLOCATED CELLS

TRAY FRONT CELL NUMBERS	GROUP NUMBERS AT LEVEL 1	GROUP NUMBERS AT LEVELS 3 AND 5
1	1	1
2	1	1
3	1 and 2	1
4	1 and 2	1 and 2
5	1 and 2	2
6	2 and 3	2
7	2 and 3	2 and 3
8	2 and 3	3
9	3 and 4	3
10	3 and 4	3 and 4

TABLE 2.2 THE RELATIONSHIP BETWEEN THE TRAY FRONT CELL NUMBERS AND THE MOMENTUM SELECTOR UNIT GROUP NUMBERS

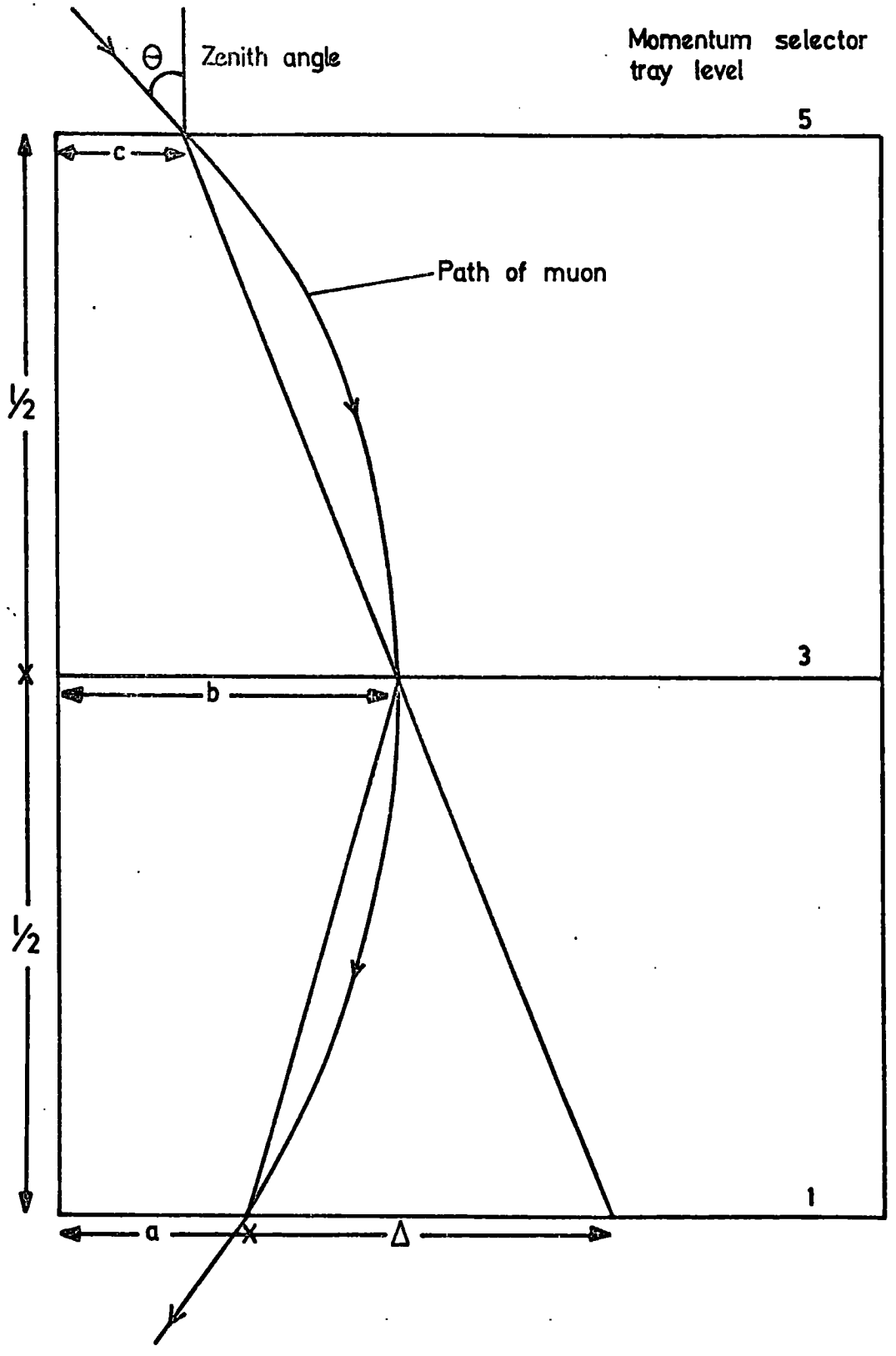

Figure 2.7 Schematic diagram of the spectrograph showing the definition of deflection Δ

if the deflection Δ is zero. This condition is indicated by triple input nand gates in the momentum selector unit, which are connected to all possible zero deflection combinations. When a high momentum event is indicated, a pulse is sent to trigger the high resolution measuring trays and the data collection electronics is activated.

The efficiency of the momentum selector in detecting high momentum events will be considered in detail in section 4.4.

2.5 THE MEASURING TRAYS

Trays of small diameter flash-tubes known as the measuring trays are situated at all five levels of the spectrograph. These form the main detecting elements of the spectrograph and are used to determine the trajectory of the muon in the front plane. Figure 2.6 shows the arrangement of flash-tubes in a measuring tray. There are 89 flash-tubes in each row, the flash-tubes having an internal diameter of 0.55 cm and a length of 2 metres and being filled with neon (2% helium) to a pressure of 2.4 Atmospheres. The flash-tube pattern was designed to have an even response for muons in the zenith angular range of ±7°. The resolution of individual flash-tubes is poor, but arranged in this way, the track of a muon on the measuring tray can be located to within about 0.6 mm.

When a high momentum event is signified by the momentum selector, a high voltage pulse is applied to the electrodes on the measuring trays and the flash-tubes along the muon trajectory discharge. The flash-tubes are digitised in the same way as on the momentum selector trays, so that electronic memories are 'set' corresponding to the discharged flash-tubes. The way in which this 'information' is collected and stored will be discussed in section 2.7, but first, the Geiger counter trays will be described.

2.6 THE GEIGER COUNTER TRAYS

Four trays containing 23 Geiger Muller tubes each are positioned with two of the trays being above and two below the spectrograph as shown in figure 2.2. Each tray covers approximately 2/9 of the area of a scintillation counter. Their purpose is to determine which part of the spectrograph the muon passed through (i.e. from front-to-front, from back-to-back, from front-to-back or from back-to-front). This information is needed to calculate the relative positions and skewness of the measuring trays. This will be covered in more detail in section 4.3.

Each tray is assigned one bit of a four bit word in the event header stored with each event and it is set equal to 1 if a Geiger counter in that tray is triggered. The Geiger counter tray information is collected and stored with the measuring tray information.

2.7 THE METHOD OF DATA COLLECTION AND STORAGE

After the passage of a high momentum muon through the spectrograph, the data for that event is stored temporarily on a small ferrite core store of capacity 1024 8-bit words or bytes. The header information for the event is first read into the core store. The header information consists of the event number, the time, the date, the current in the magnet windings, the magnetic field direction, the trigger mode of the spectrograph, the Geiger counter data and the atmospheric pressure. Each tray is then scanned in turn and if a column is found which contains at least one 'set' memory (i.e. discharged flash-tube) the column number and the flash-tube pattern are read into the core store. When all the measuring trays have been scanned, an IBM 1130 computer is interrupted and the data are off loaded onto a magnetic disk on the computer. The reason for this procedure

is that the IBM 1130 is normally servicing another experiment, and all the data must be ready in the core store as soon as the IBM 1130 is interrupted from its normal tasks.

The IBM 1130 does not have a large enough memory and it is not fast enough to analyse the data, therefore when a magnetic disk becomes full, with approximately 3600 events, the data are transfered to the Northern Universities Multiple Access Computer (an IBM 370) for analysis. The data analysis program will be discussed in the next chapter.

A summary of the operation of the spectrograph is shown in figure 2.8.

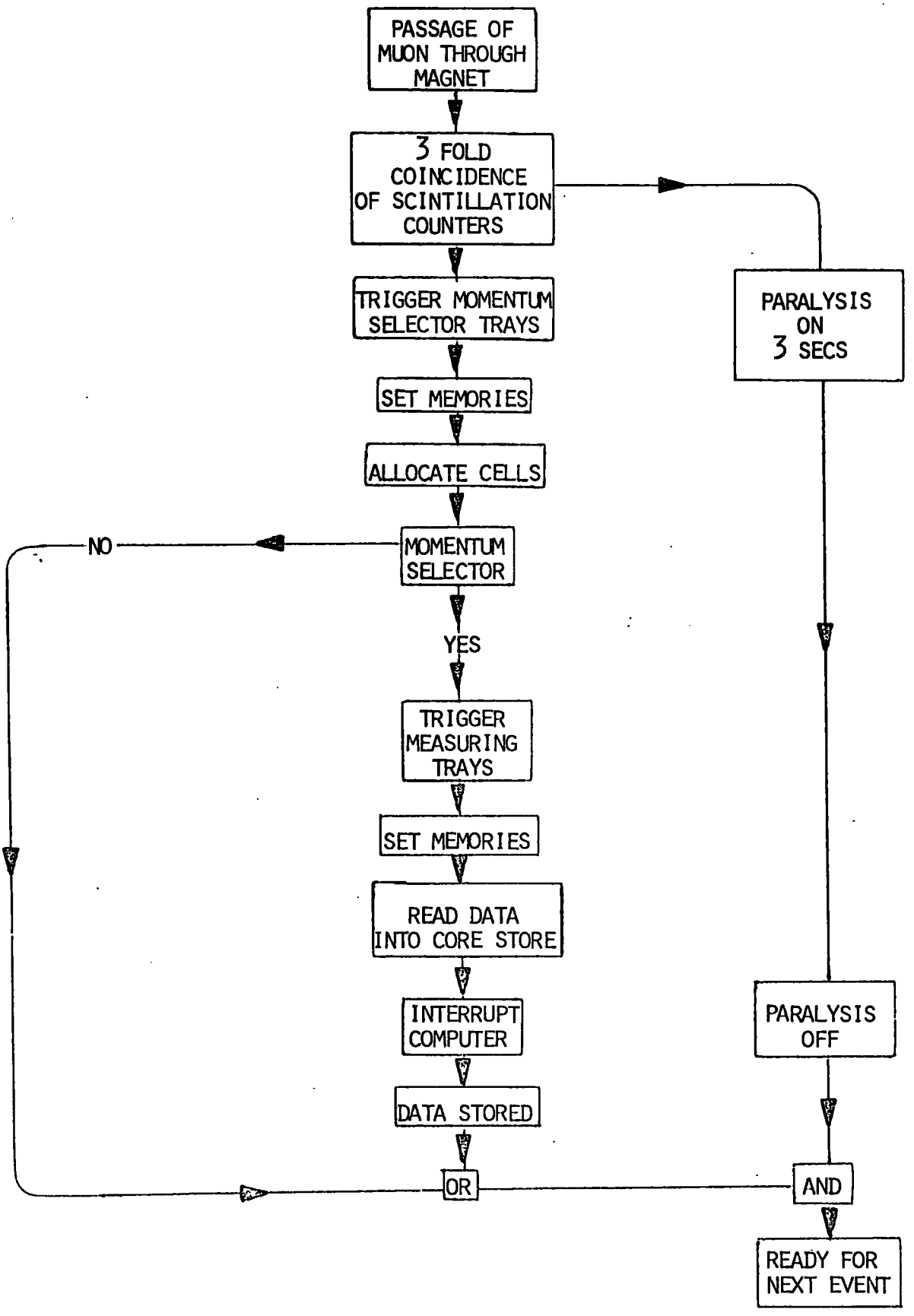

FIGURE 2.8 THE OPERATION OF THE SPECTROGRAPH

CHAPTER 3

THE COLLECTION AND ANALYSIS OF THE DATA

3.1 THE COLLECTION OF THE DATA

The data to be presented in this thesis were collected over a period of two years from mid-1974 to mid-1976, the author being responsible for the collection of the latter 75% of the data.

The data were collected in a series of runs, each run lasting approximately 24 hours or 72 hours if it was at the weekend. At the end of each run, the efficiency and the count rates of the various detectors on MARS were checked to ensure the spectrograph was operating correctly. The magnetic field direction was reversed and the momentum selector unit was tested by a purpose-built electronic tester to check the correct operation of the logic circuits. This testing procedure was found necessary because faults often developed in the triple input nand gates in the momentum selector. (See section 2.4 for a description of the momentum selector). Either an input on a particular gate became open circuit which had the effect of making that gate inoperative and hence slightly reducing the 'high momentum' muon rate, or an input would remain permanently high, so that if a low momentum muon passed through the cells which set the other two inputs high, the output would fall, indicating a 'high momentum' muon event. This latter fault was most troublesome and, because of the steeply falling spectum, it had the effect of substantially increasing the 'high momentum' muon rate. If a fault was detected at the end of a run, the offending nand gate was found and replaced, and if the rate of high momentum events was substantially higher than the normal rate the data were placed in the class II category. If there was no fault in the momentum selector

or if there was a fault but the rate of high momentum events was not significantly different from normal (it was assumed the fault developed near the end of the run) the data for that run were accepted and placed in the class I category. Only class I data have been considered in this work.

A total of 79,729 class I events were collected in a total live time of 5118 hr 24 min and 31 seconds. The ratio of positive field live time to negative field live time being 0.9947%.

3.2 INTRODUCTION TO THE DATA ANALYSIS TECHNIQUE

The purpose of any analysis technique is to identify events in which the muon trajectory lies within the acceptance of the spectrograph and from the flash-tube data, determine the momentum and the charge of the muon. The analysis technique must have the following important characteristics:

a) Speed - there are 79,729 events to analyse.

b) Accuracy - the information in the flash-tubes must be used as accurately and as fully as possible to determine the co-ordinates of the muon tracks in the measuring trays.

c) Objectivity - the results should not depend upon the analyst.

To these ends a computer analysis technique was developed by Wells (1972) and was further developed by Piggott (1975) and Daniels (1975), which is fast, objective and has greater accuracy than previous manual analysis techniques. The resulting analysis program, called MARS2, has been used to analyse the present data and it will be briefly described in this chapter.

3.3 THE METHOD OF DETERMINING THE MUON MOMENTUM

Having identified an event which is within the acceptance of the spectrograph, the analysis program locates the co-ordinates of the muon's trajectory in each of the measuring trays and fits a parabola to these co-ordinates by the method of least squares. The momentum and charge of the muon are then determined from one of the coefficients of the fitted parabola.

Assuming that the spectrograph has one continuous magnet and that the energy loss of the muon is negligible, then the trajectory of the muon, as seen in the front plane of the spectrograph, will follow the arc of a circle as shown in figure 3.1. If (x,y) are the co-ordinates of the muon in the front plane, (x_c,y_c) are the co-ordinates of the centre of the circle and r is the radius of the circle, then

$$(y - y_c)^2 + (x - x_c)^2 = r^2$$

If this equation is re-arranged and expanded binomially, neglecting terms higher than x^2, then

$$y = \frac{x^2}{2r} - \frac{x_c x}{r} + \left[y_c + \frac{x^2}{2r} - r \right]$$

Therefore if a parabola of the form

$$y = ax^2 + bx + c$$

is fitted to the co-ordinates of the muon in the measuring trays then the radius of curvature of the trajectory is given by

$$r = 1/2a$$

and given that $p = 300\ B\ r$ (equation 2.1) the momentum is given by:

$$p = \frac{300\ B}{2a}$$

For B = 16.3 kGauss, and correcting for the magnet gaps for muons with vertical trajectories, this expression becomes $p = \frac{0.2445}{a}$ GeV/c when a is measured in metres. This is the formula used in the analysis program

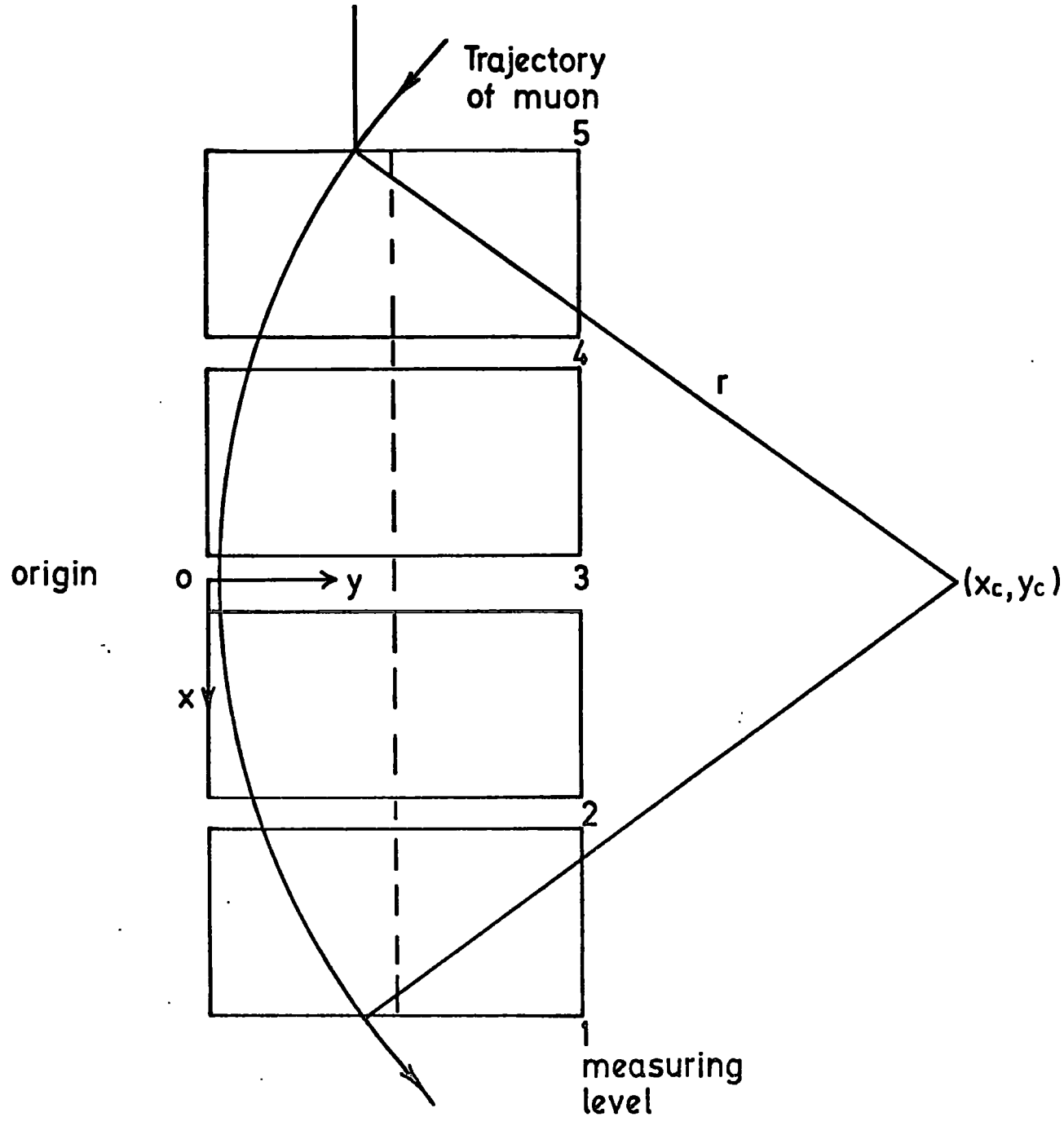

Figure 3.1 Coordinate system of the spectrograph.

to calculate the momentum of muons. The charge of the muon is determined from the sign of a and the direction of the magnetic field.

To correct the momentum for the effect of the gaps between the magnet blocks and for energy loss, Wells (1972) gives tables of the corrections to be added to the computed momenta. For details of these corrections see section 4.7.

3.4 THE INTERPRETATION OF THE FLASH-TUBE DATA

Typical events which the analysis program must be able to interpret are shown in figures 3.2 and 3.3. The events are shown plotted on a diagram of the measuring tray fronts. These diagrams are drawn with the trays in their correct relative vertical and lateral positions. However, the measuring tray depth, which is in reality about 10 cm, is not in proportion to the separation of the trays, which is about 150 cm. The event shown in figure 3.2 has a momentum of 633 GeV/c. It has four clear tracks in the upper four trays and a group of tracks in the lower tray which is called a burst. The burst is caused by the muon initiating an electromagnetic cascade within the magnet which accompanies the muon into the measuring tray.

The event shown in figure 3.3 has a momentum of 209 GeV/c. Two clear tracks are seen in trays 4 and 5, there is an inefficient track in tray 3, the track in tray 2 contains a knock-on electron and there is again a group of particles in tray 1. In this case, the density of the particles is not large and the analysis program must have some means of selecting the correct track.

To enable the computer program to interpret these flash-tube patterns, they are arranged in groups, where a group is defined as follows:

A group is defined as two or more discharged flash-tubes

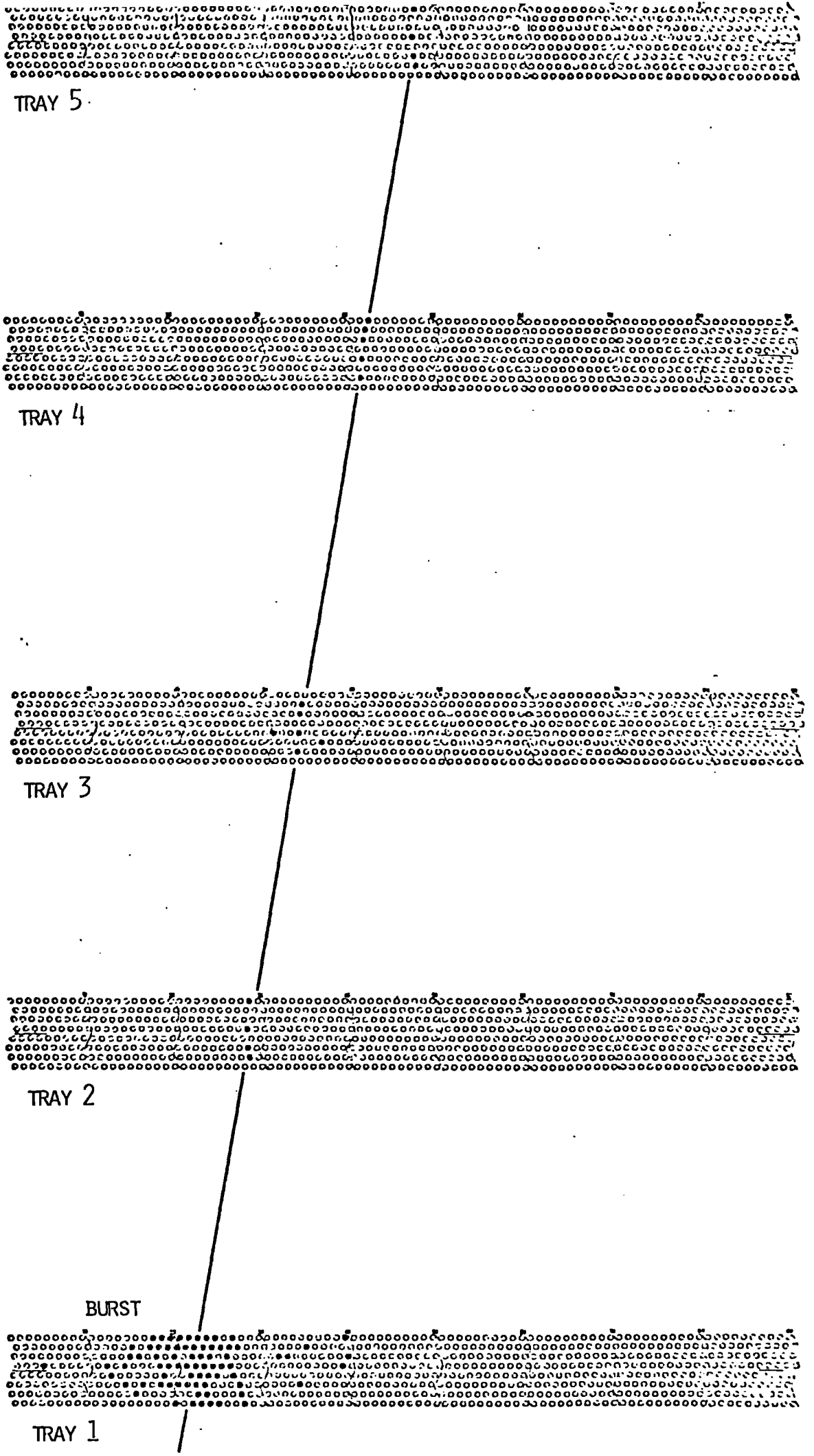

FIGURE 3.2 A TYPICAL MARS EVENT

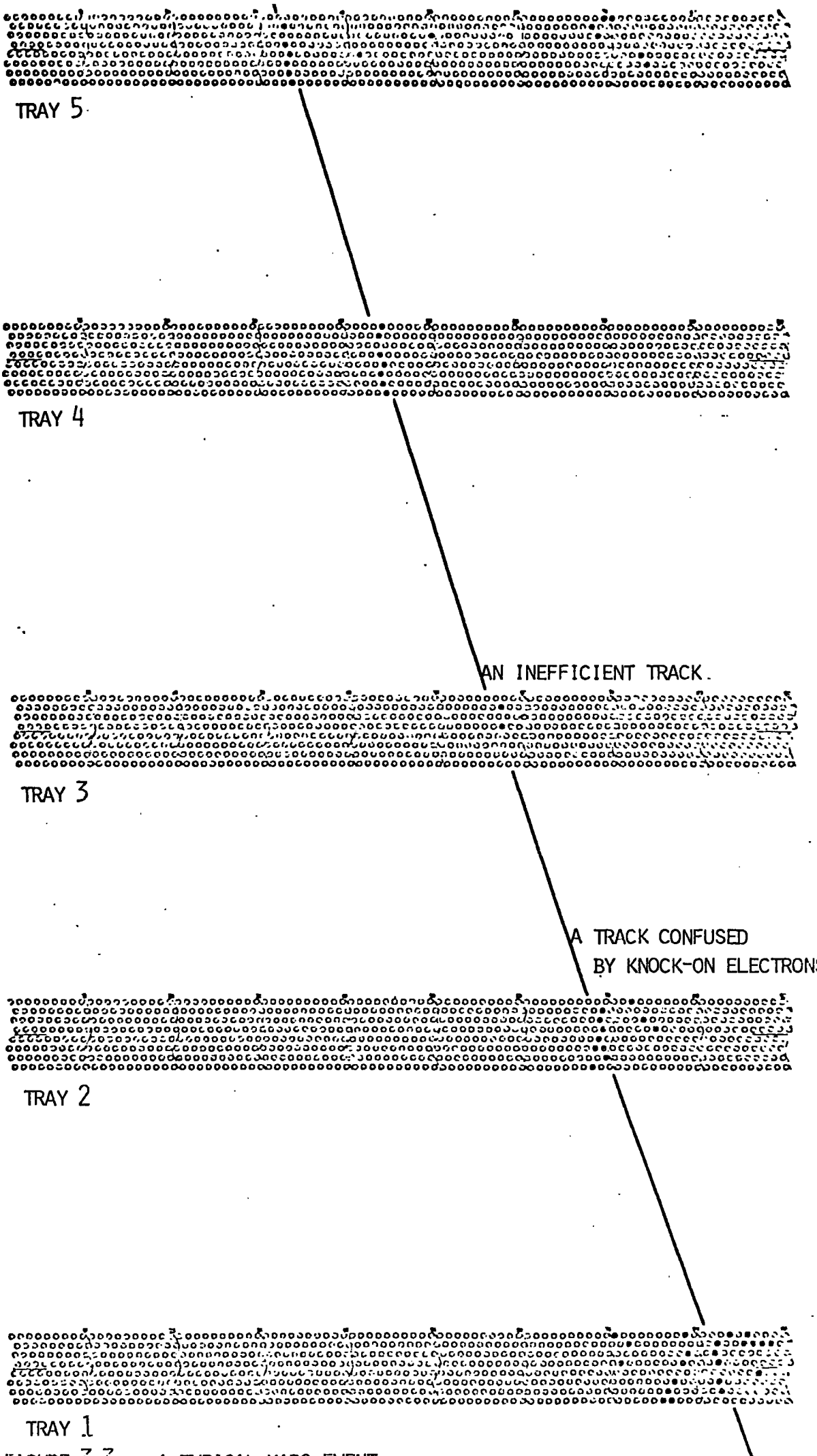

FIGURE 3.3 A TYPICAL MARS EVENT

separated from any other group by at least one column of un-discharged flash-tubes or by two columns with only one discharged flash-tube in each.

Thus, in figure 3.3, there are four groups in the measuring tray at level 1.

In some cases, a group, as defined above contains too many flash-tubes to reliably fix the position of the muon, therefore the program is able to split a group into a number of sub-groups. The definition of a sub-group is as follows:

If a group is more than three columns wide, then it is split into sub-groups of three columns width.

Thus if a group spans five columns of flash-tubes, three sub-groups are defined corresponding to the first, middle and final three columns of the group.

If a group is too large for trajectory defining purposes, it is called a burst.

A burst is defined as a group which contains more than 10 discharged flash-tubes or which spans more than 5 columns.

An example of a burst is seen in figure 3.2.

There are two reasons for adopting this definition of a burst. The first is because when a muon passes through a measuring tray, the mean number of discharged flash-tubes is 4.57. Therefore if a group contains more than 10 discharged flash-tubes there are likely to be two or more particle tracks present. The second reason is that a single particle track traversing a measuring tray in the zenith angular range $\pm 7^{\circ}$ is unlikely to discharge flash-tubes in more than three columns. Therefore if a group spans more than five columns again it is likely that there are two or more particles present. If there are two

particle tracks close together, it is not considered possible to split them and the group is not used in the trajectory fitting procedure.

A group is also not used in the trajectory fitting procedure if it is too small.

An inefficient group is defined as a group which contains only two discharged flash-tubes.

An example of such a group is seen in figure 3.3.

When a group is not used in the trajectory fitting procedure because it is inefficient or because it is a burst, the fitted trajectory must pass the acceptance test. This means that the fitted trajectory must lie on or within one tube spacing of the rejected group.

With these definitions of a group, sub-group, burst and inefficient group, the program is able to interpret the flash-tube data in the measuring trays in an unambiguous way.

3.5 THE LOCATION OF THE TRAJECTORY CO-ORDINATES

After the groups and sub-groups in an event have been identified, all the possible combinations of groups are analysed in an attempt to fit a muon trajectory. Usually there is only one group per tray, but occasionally there are more. Only those group combinations which satisfy certain criteria are accepted as genuine trajectories.

The method of locating the co-ordinates of the muon in the measuring trays is a two stage process. The first stage consists of selecting a combination of groups and defining a narrow channel through each measuring tray. These channels are based upon the pattern of discharged flash-tubes and also on the gaps in layers containing no discharged flash-tubes. A parabola is then fitted by the method of least squares, to the co-ordinates of the centres of the channels. The second stage of the analysis consists of calculating, from the

the previously fitted parabola, the angle of the trajectory at each measuring level. Then, by using this extra information the channels are re-defined more precisely. A second parabola is then fitted to the centres of the new channels from which the momentum and the charge of the muon are determined.

3.6 THE TRACK FITTING OPTIONS

The analysis program is not always able to define a channel through a measuring tray without violating a part of the flash-tube data. There are two reasons why this is so.

The first is that a flash-tube does not always discharge when a muon passes through its sensitive volume. The mean flash-tube efficiency in MARS is 88.5%. The probability that a flash-tube will discharge is related to the distance of the trajectory from the centre of the tube. If the trajectory is near the wall of the flash-tube, the path length in the gas and the number of ion pairs produced by the muon are small. Therefore there is less chance that the flash-tube will discharge. When this happens, it is called a 'tube inefficiency' and some means is required within the program to locate and 'turn on' the inefficient tube.

The second reason why the program cannot always define a channel is because a knock-on electron is sometimes produced by the muon when it passes through an aluminium electrode or the glass wall of a flash-tube. If the electron has sufficient energy it may discharge a flash-tube and confuse the muon track. If the knock-on electron discharges a flash-tube in a layer in which there is already a discharged flash-tube, see figure 3.4b, the analysis program tries the group with each of the flash-tubes in turn. The group producing the 'best fit' is accepted. However, if the knock-on electron discharges a flash-tube

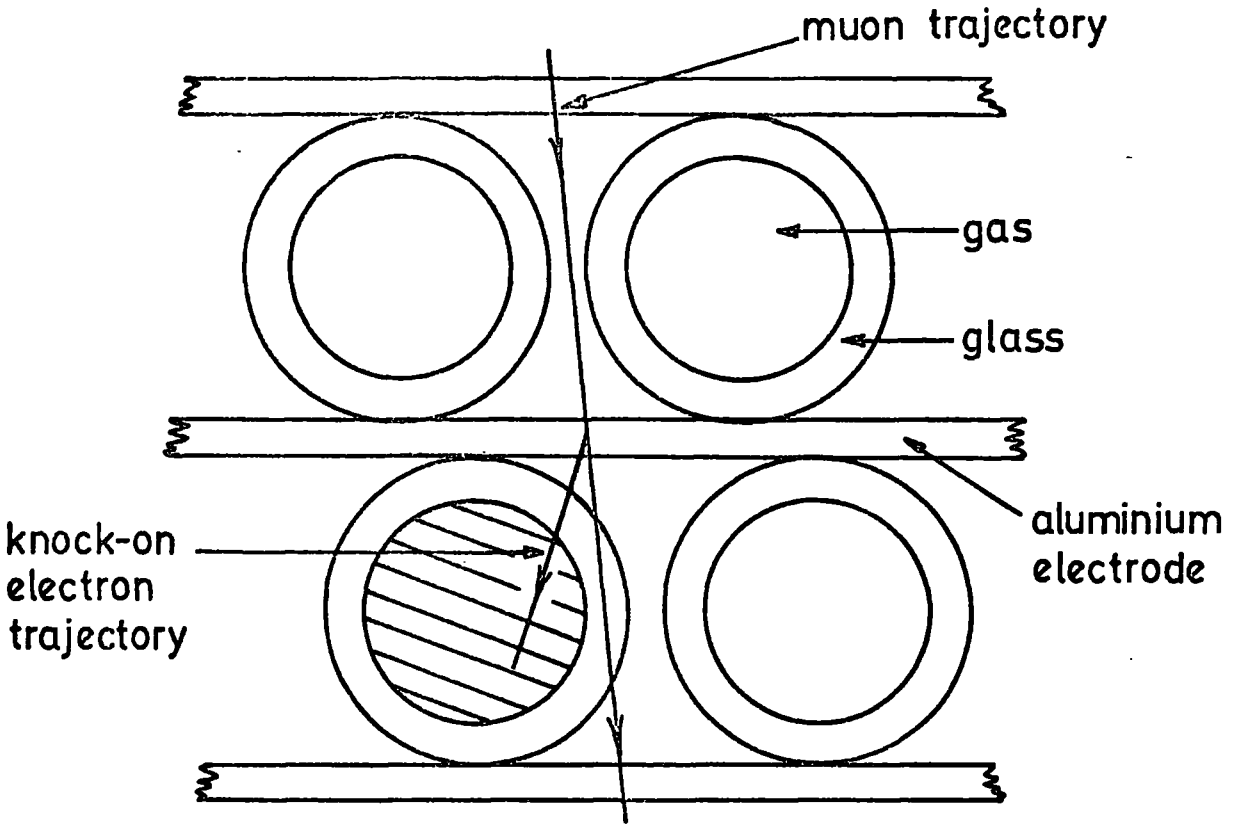

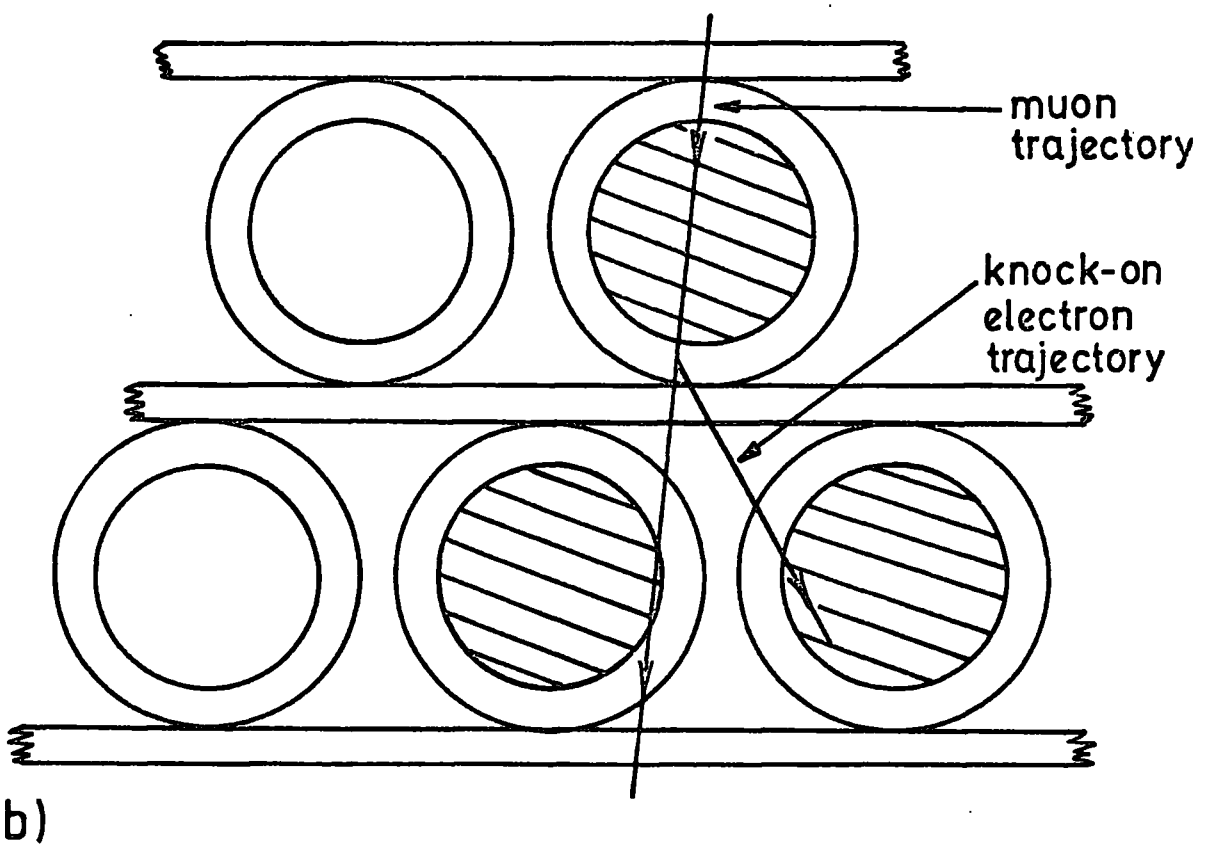

Figure 3.4 The consequences of knock-on production in the measuring trays.

in a layer in which the muon passed through a gap between the flash-tubes, see figure 3.4a, some means is needed of 'turning off' the offending tube so that the correct muon track is used in the analysis.

The method which has been adopted to overcome these problems is to give the program twelve track fitting options which are descibed in table 3.1 and shown in figure 3.5. The track fitting options allow the program to effectively turn flash-tubes on or off in a well defined way. The options most likely to be used have the low option numbers and are tried first. Therefore the most likely option is option zero, which represents a good fit. If the program is unable to define a channel through the group it assumes there is a knock-on electron (option 1) and neglects each discharged tube in turn until it can define a channel. If this is unsuccessful, a tube inefficiency (option 2) is assumed and undischarged tubes are systematically turned on. The program goes through the options until it can unambiguously define a channel. If this does not prove possible, then the group is rejected and not used further in the trajectory fitting procedure. However, the fitted trajectory must pass within one tube spacing of the rejected group and hence satisfy the acceptance test.

In any choice between groups or sub-groups in the same tray, the group with the lowest track fitting option is prefered.

This method of turning on or off flash-tubes has been checked extensively by Wells (1972) and is found to be satisfactory.

3.7 THE STANDARD DEVIATION OF THE FITTED PARABOLA

For events in which four or five trays are used in the analysis, a measure of the goodness of fit of the parabola is provided by its standard deviation s, which is given by

OPTION	DESCRIPTION
0	Good fit - no information has to be assumed
1	A knock-on electron is assumed (a discharged tube is neglected).
2	A tube inefficiency is assumed (an undischarged tube is assumed to have discharged).
3	A knock-on electron and a tube inefficiency in different layers are assumed.
4	Two knock-on electrons in different layers are assumed.
5	Two inefficiencies in different layers are assumed.
6	One single knock-on and one double knock-on are assumed in different layers.
7	A tube inefficiency and a knock-on in the same layer are assumed.
8	Two knock-ons in the same layer are assumed (muon passed between them).
9	Two knock-ons in the same layer are assumed (muon passed to one side of them).
10	An inefficiency and a double knock-on are assumed in the same layer.
11	Assumes an inefficient tube between two knock-ons.

TABLE 3.1 THE TRACK FITTING OPTIONS

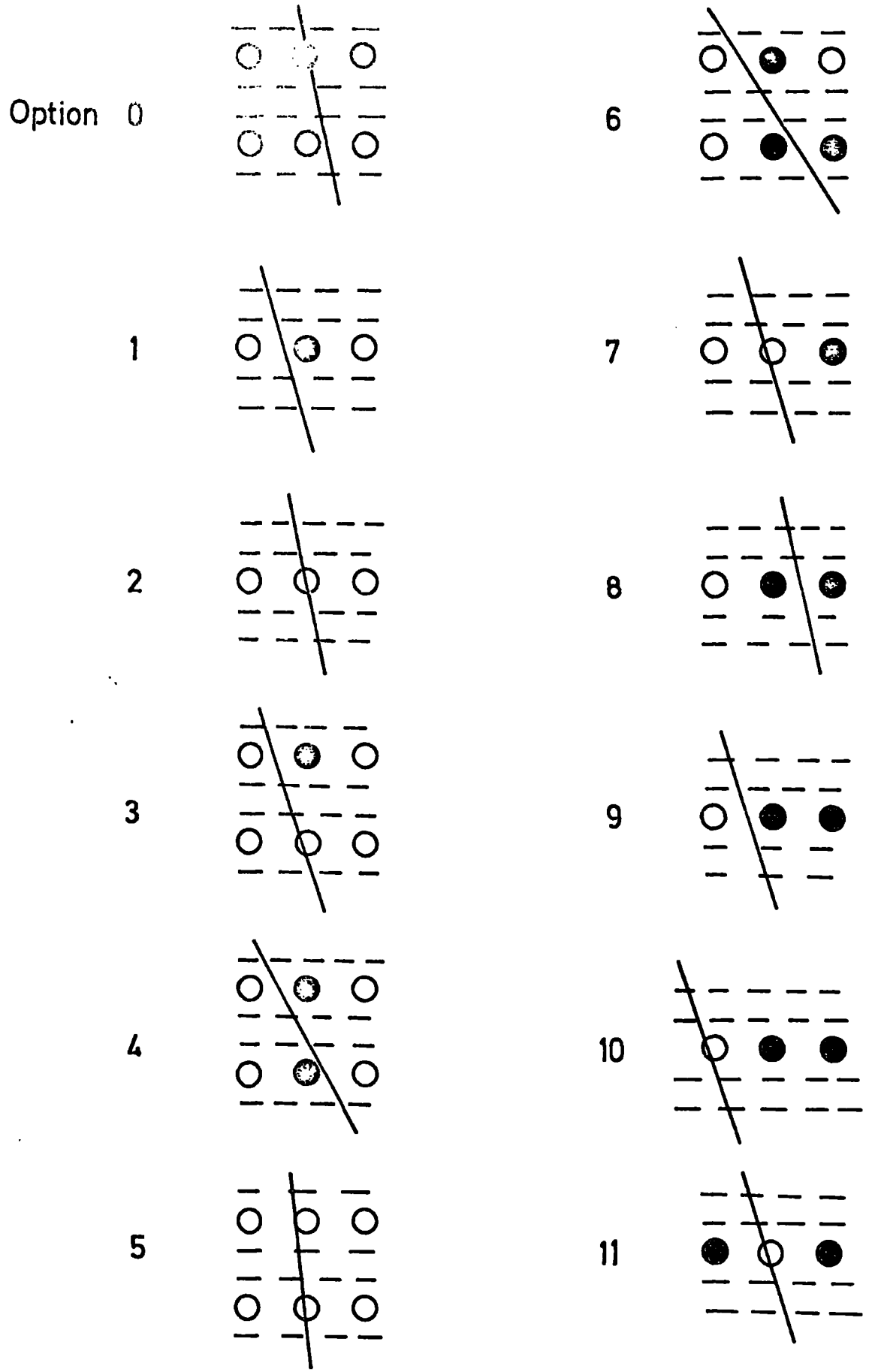

Figure 3.5 Illustration of track fitting options.

$$s = \sqrt{\sum_{i=1}^{n} \delta_i^2/n} \qquad n = 4 \text{ or } 5$$

where δ_i is the horizontal distance between the fitted parabola and the centre of the channel at level i and n is the number of trays used. Clearly this has no significance for three tray fit events for which a parabola can be fitted exactly.

The value of s depends upon the error in track location and on multiple Coulomb scattering in the magnet blocks, both of which are random in nature. Standard deviation distributions for the ranges 70 - 100 GeV/c, 100 -150 GeV/c and >150 GeV/c are shown in figure 3.6. It is found that events in the extreme tail of these distributions i.e. with large s, tend to be wrongly analysed. A cut is therefore introduced into these distributions at about three times the mean (this is approximately equivalent to a three standard deviation cut for a Gaussian distribution) and if an event has a standard deviation greater than this value it is rejected to be re-analysed at a later date.

3.8 TRAJECTORY SELECTION

If an event has more than one successful combination of groups, the trajectories are ordered according to the number of trays used and then to the standard deviation of the fitted parabola. The trajectory with the greatest number of trays and the smallest standard deviation is accepted as the best fit muon trajectory. The program then searches for a second muon by rejecting any group combination which uses a group in the best fit trajectory (unless this happens to a burst which can contain two muon tracks) and selecting the best fit of the remaining trajectories. If there are any group combinations left, a third independent muon is searched for and if it is found, the event is given an error code to signify a multiple muon event.

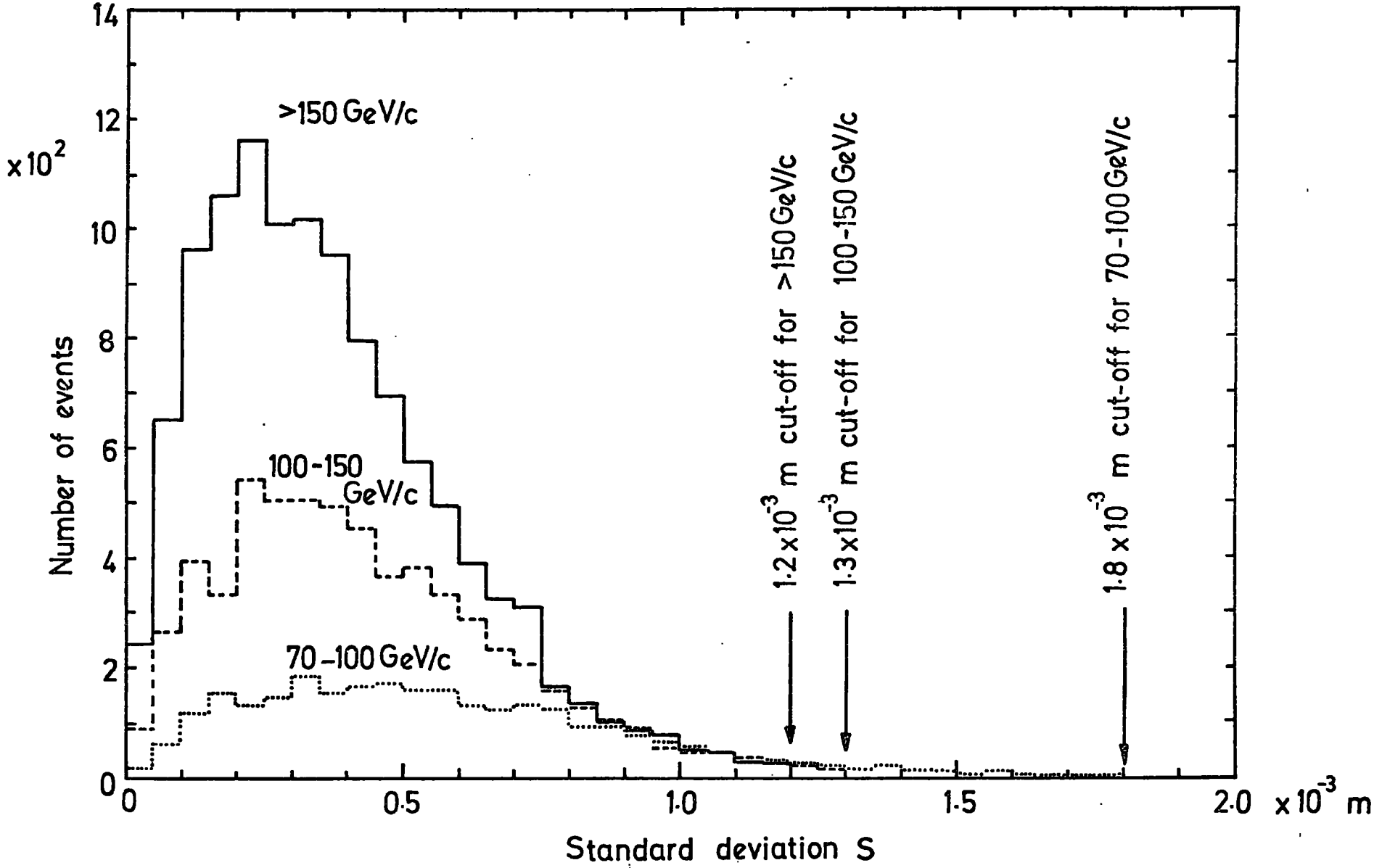

Figure 3.6 Frequency histograms of the standard deviation of the parabola.

3.9 THE REJECTION OF EVENTS

3.9.1 INTRODUCTION

The analysis of an event results in it being placed in either the 'pass' category, the 'shower' category or the 'fail' category. A shower event is defined as one in which tray 5 contains more than 30 columns of discharged flash-tubes. These events are more difficult to analyse than ordinary events because of the presence of air shower particles. Therefore, they are filtered out and analysed separately. A description of their analysis will be found in section 6.4. Events which fail the analysis are given an error code to indicate the reason for failure and they are either re-analysed or the spectrum is corrected for their loss. The treatment of the failed events will be considered in this section. Figure 3.7 is a flow chart showing the essential features of the analysis program and the order in which the error codes are assigned.

3.9.2 ERROR CODE SE1

An electronics fault has caused an error in the format of these events which makes them impossible to read by the analysis program. This fault is not momentum dependent and will only affect the absolute height of the momentum spectum.

Assuming that these events would have fallen into the pass, fail and shower categories in the same proportions as the rest of the data, and if N_T (= 79729) and N_{SE1} (= 1873) are the total number of events collected and the number of SE1 events respectively, then the upwards correction to be applied to the spectrum is given by

$$C_{SE1} = 1 + \frac{N_{SE1}}{N_T} = 1.023 \pm 0.001$$

3.9.3 ERROR CODES SE3 AND E91

The error codes SE3 and E91 are given to events if they have a

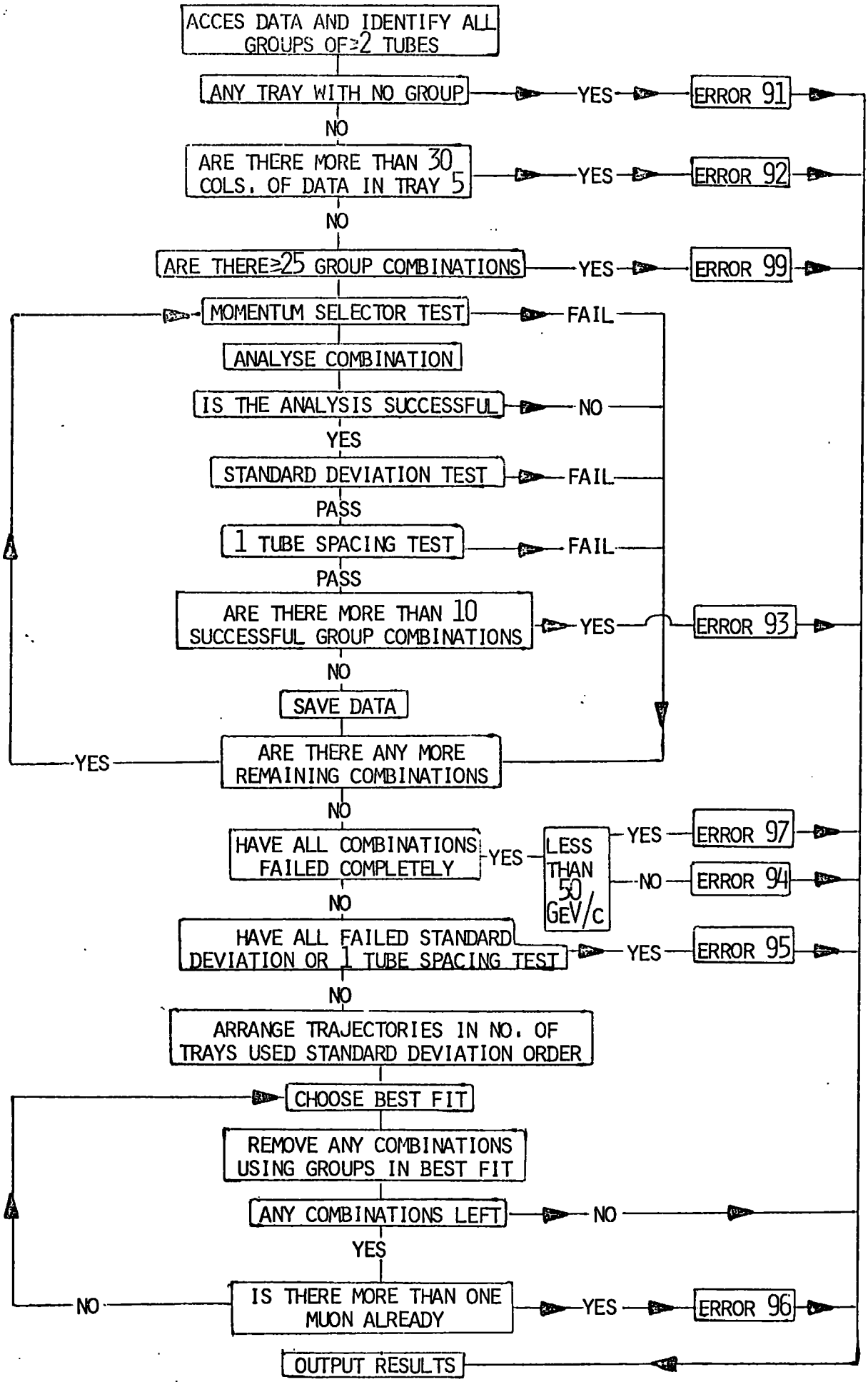

FIGURE 3.7 A FLOW CHART SHOWING THE ESSENTIAL FEATURES OF THE ANALYSIS PROGRAM

measuring tray containing no or only single discharged flash-tubes respectively. These error codes pick out events which have an inefficient flash-tube tray (for example see figure 3.8), events where the muon passes out of the acceptance of the spectrograph and is accompanied by other particles, (for example see figure 3.9), and events caused by extensive air shower particles triggering the spectrograph. However it is not always possible to determine whether an event has been rejected because a tray is inefficient or because the trajectory missed that tray (for example see figure 3.10). For this reason, the correction to the spectrum has been calculated theoretically. The correction is not momentum dependent because it only depends upon the flash-tube efficiency.

The correction was calculated by simulating the paths of muons through the spectrograph and generating a file containing the flash-tube information of the simulated events. This file was then analysed in the usual way and the proportion of SE3 and E91 events was calculated. All these events were within the acceptance of the spectrograph, therefore they were due only to flash-tube inefficiencies. The simulation program used the layer efficiencies of table 3.2 to determine the probability that a flash-tube would discharge. The efficiencies in table 3.2 were derived from the file of pass data by only considering tracks which fell on the muon trajectory. Only one tube per layer was allowed and bursts were excluded. Figure 3.11 shows a frequency histogram of the number of flash-tubes per group for the simulated data in comparison with the real data. The areas under the two histograms between 0 and 8 tubes per group have been equalised to facilitate comparison. The theoretical probability of an event being assigned an SE3 or E91 error code due to tube inefficiencies alone

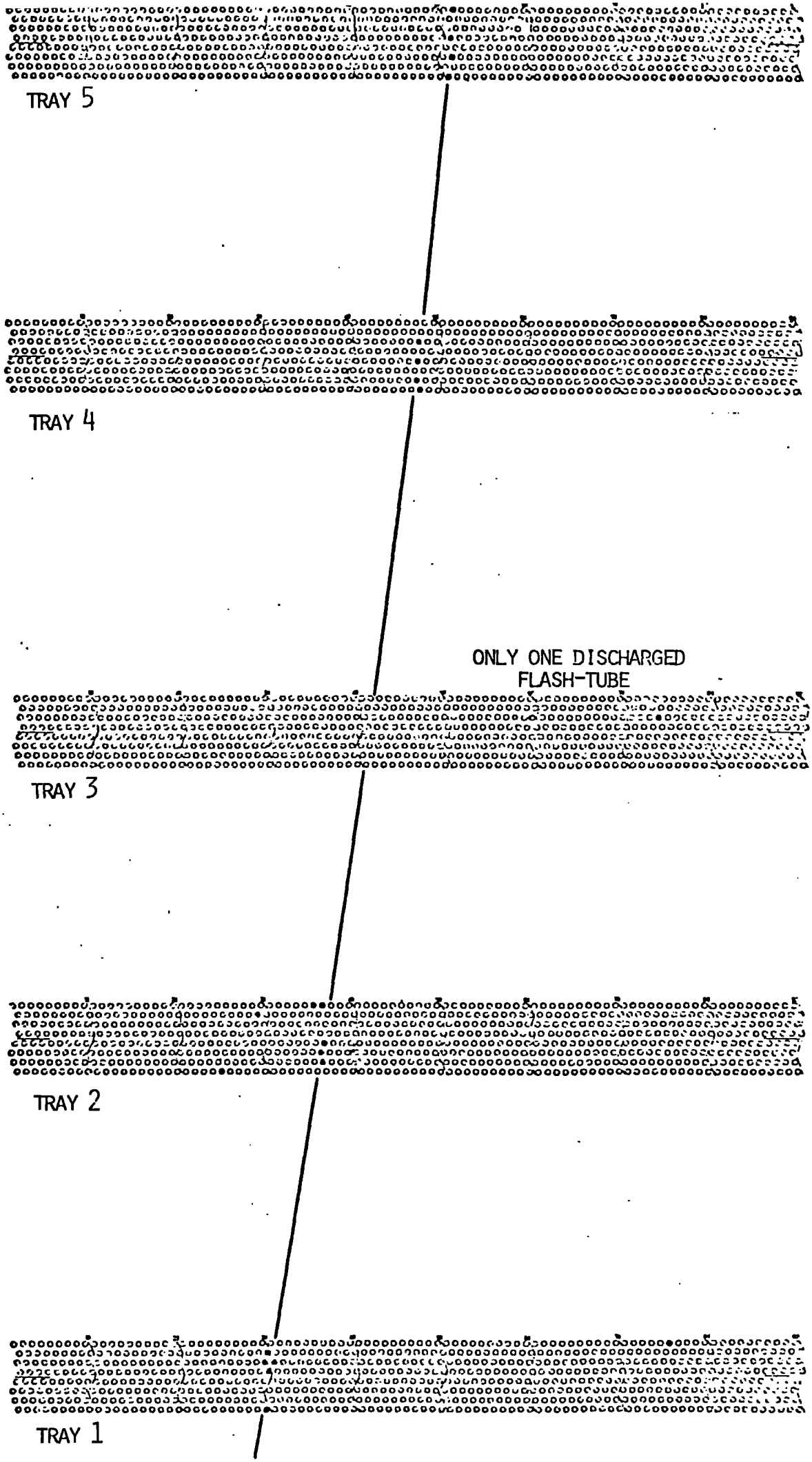

FIGURE 3.8 AN ERROR E91 EVENT

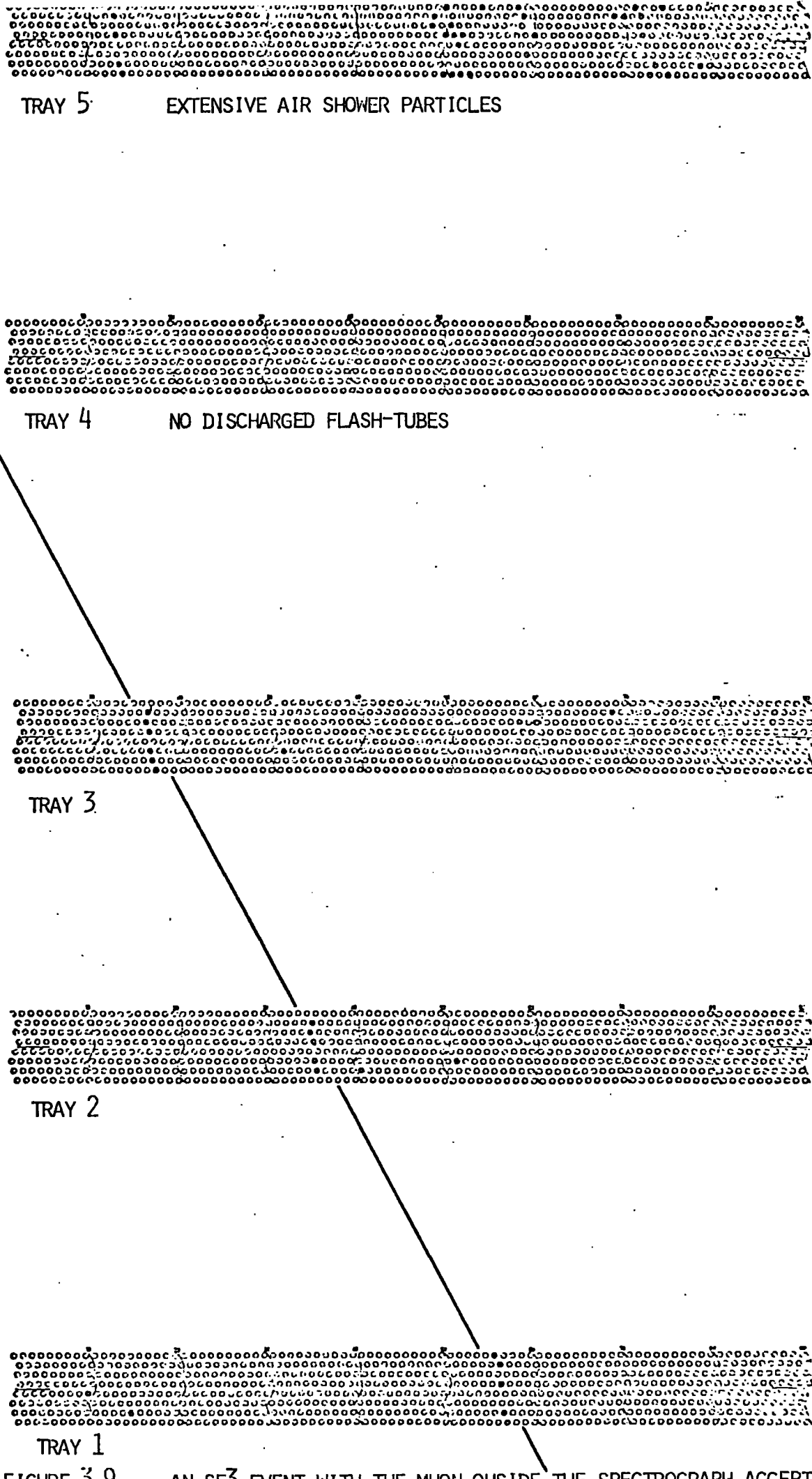

FIGURE 3.9 AN SE3 EVENT WITH THE MUON OUSIDE THE SPECTROGRAPH ACCEPTANCE

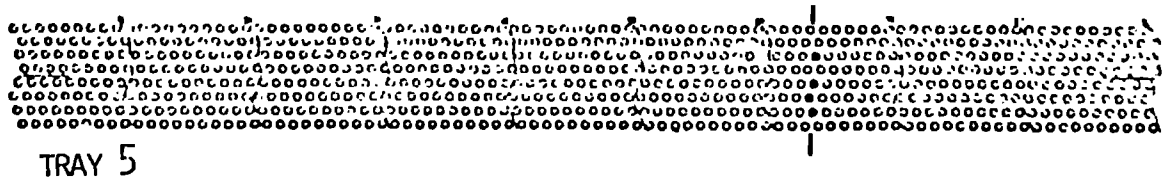

TRAY 5

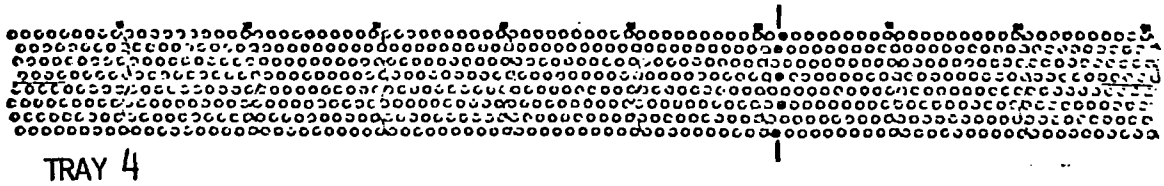

TRAY 4

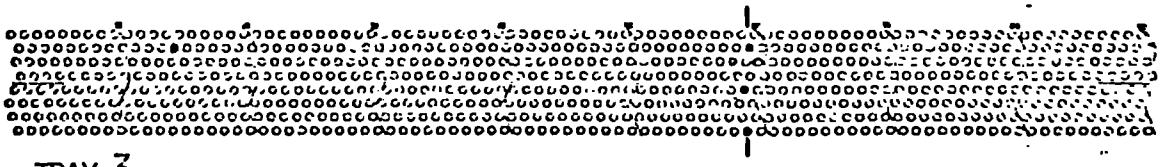

TRAY 3

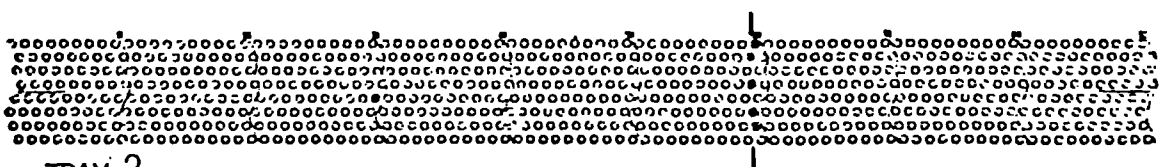

TRAY 2

IS TRAY 1 INEFFICIENT OR DID THE MUON

PASS OUT THE FRONT OR BACK PLANE OF THE SPECTROGRAPH?

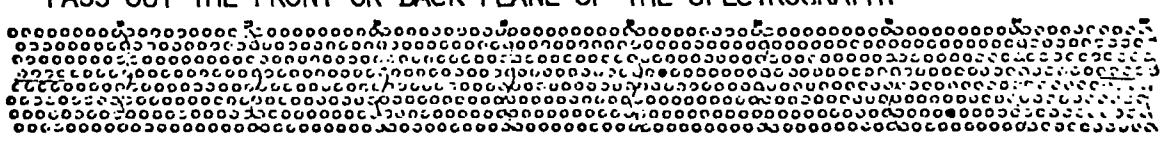

TRAY 1

FIGURE 3.10 AN E91 EVENT

LAYER	TRAY				
	1	2	3	4	5
1	58.8	53.7	60.5	59.1	55.6
2	60.3	59.1	60.2	59.5	56.8
3	58.0	49.5	33.0	59.0	55.4
4	60.0	58.7	59.7	59.0	57.1
5	59.5	59.9	42.9	59.3	44.6
6	60.4	60.4	55.6	58.3	57.9
7	58.7	62.2	60.8	59.3	56.7
8	60.3	61.2	58.1	59.7	56.7
MEAN TUBE DENSITY ±0.01	4.75	4.65	4.31	4.73	4.41

TABLE 3.2 THE LAYER EFFICIENCIES AND MEAN TUBE DENSITIES OF THE DATA WHICH PASSED THE ANALYSIS PROGRAM

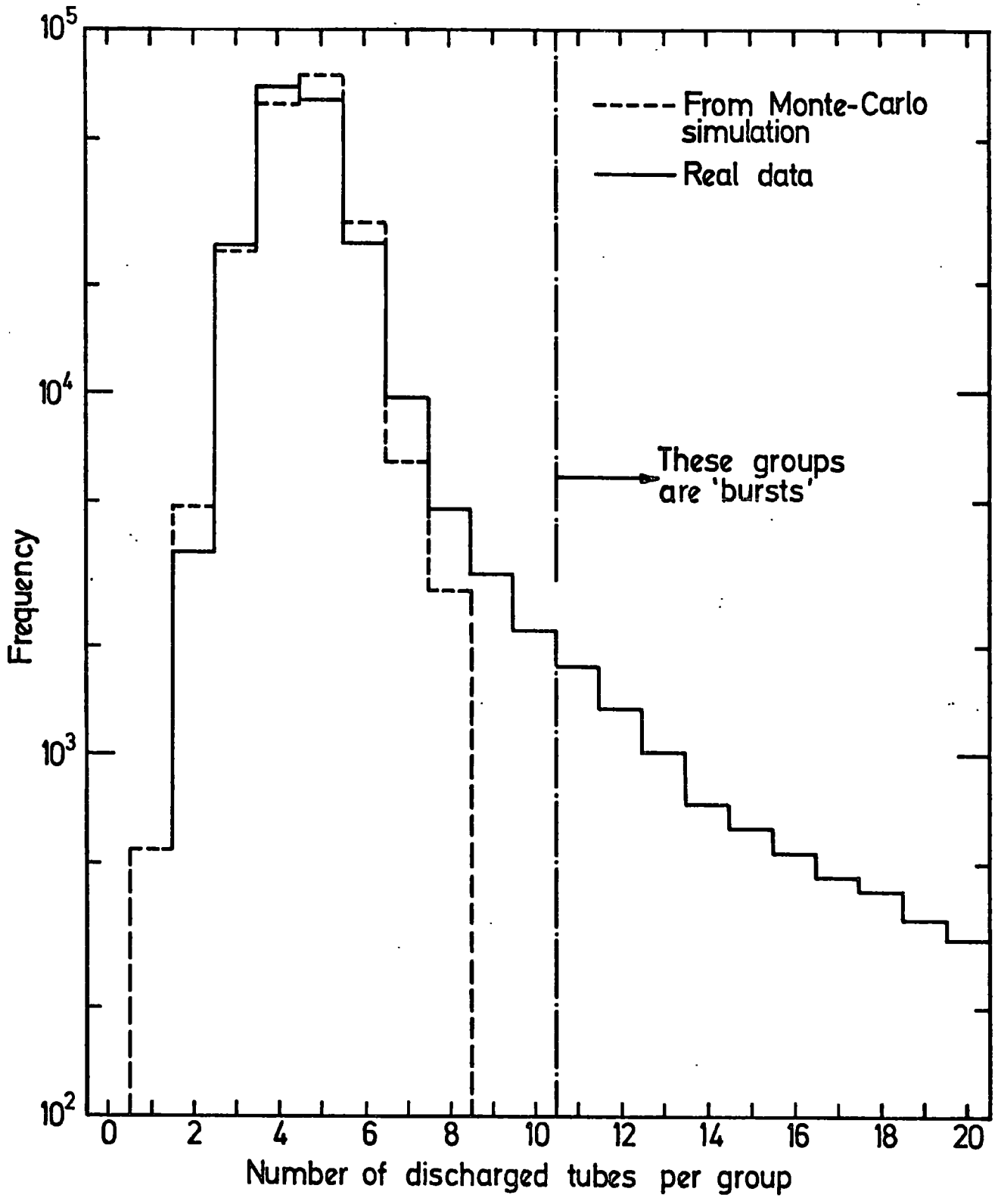

Figure 3.11 A frequency histogram of the number of discharged tubes per group.

is estimated to be 1.33 (±0.1)%.

To check this value, the file of E91 events was re-analysed using the analysis program modified so that it did not reject events with a tray containing only one discharged flash-tube. Shown in figure 3.12 is the ratio of the number of E91 events which passed the re-analysis to the number of events in the pass category plotted against momentum. Within the errors, the ratio is momentum independant and justifies the overall upwards correction for the loss of these events. From the number of events which passed re-analysis, the probability of an event being given an E91 error code is 1.22 (±0.1)%. This is less than the theoretical value because it does not include the SE3 events (which are difficult to re-analyse) and because bursts and knock-on electrons reduce in practice the number of groups which have only one tube. The number of genuine SE3 events in expected to be small, therefore it is considered that the theoretical value is correct and this has been used to calculate the upwards correction to the spectrum. The value of the correction is therefore $C_{3,91} = 1/(1 - 0.0133) = 1.013 \pm 0.001$.

3.9.4 ERROR CODE E94

These events fail because they have more than two rejected trays. They represent 0.4% of the collected data and no attempt has been made to re-analyse them. The spectrum has, however, been corrected for the loss of these events because although the correction is small ($\sim$ 0.4%) at 100 GeV/c, it amounts to $\sim$11% at 4000 GeV/c because of the increasing production of bursts with momentum. For details of these corrections see section 6.3.

3.9.5 ERROR CODE E97

In order to speed up the analysis of the data, a 'momentum selector' was built into the program to reject events of momentum

Figure 3.12 A comparison of the spectra of the reanalysed E91 events with events from the 'pass' category.

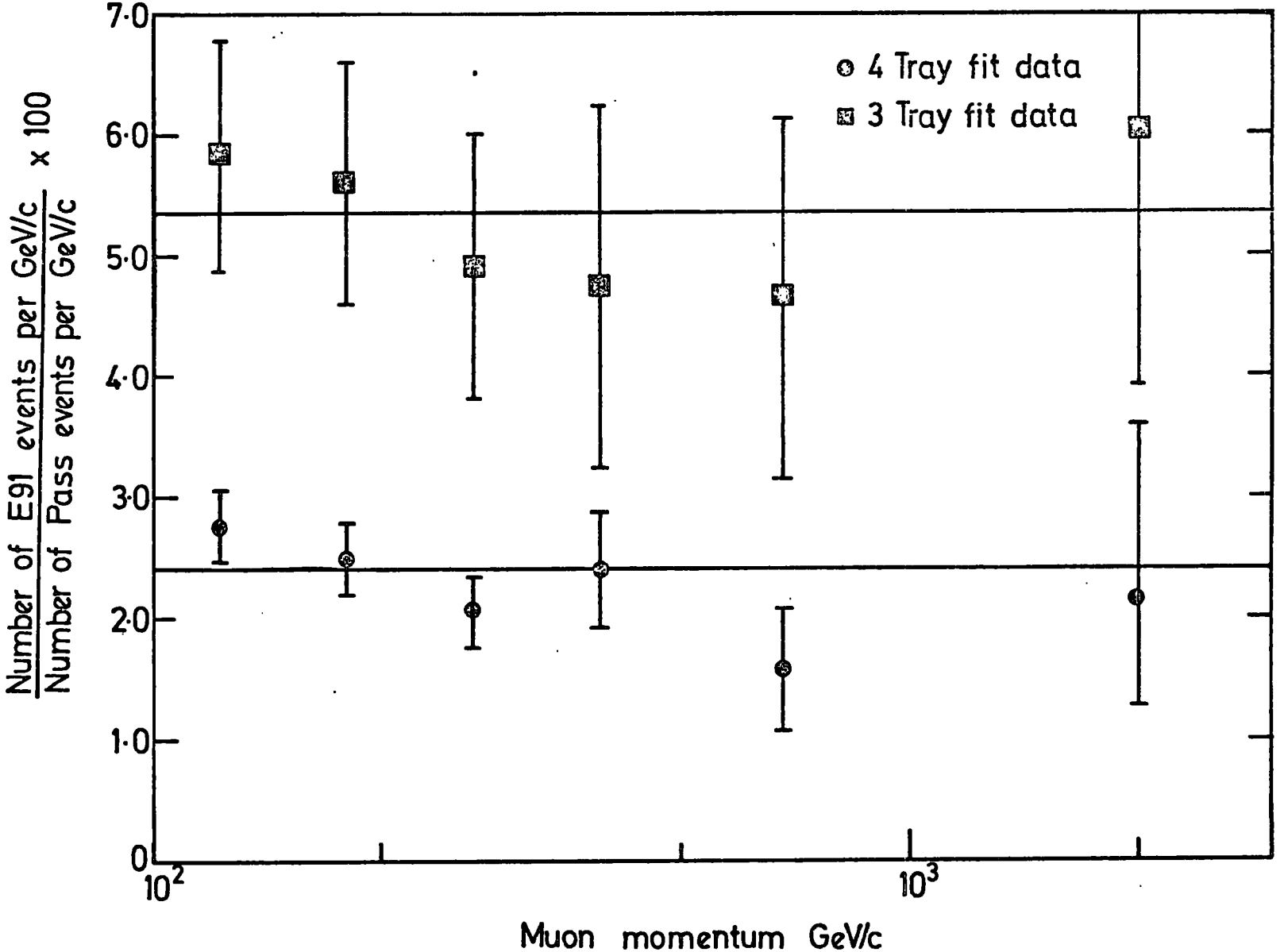

$\leq$ 50 GeV/c before their analysis.

This software momentum selector considers deflections between all combinations of columns containing one or more discharged flash-tubes. To check the efficiency of this momentum selector, a sample of 1319 E97 events were re-analysed with the error code suppressed. None of the analysed events had a momentum greater than 100 GeV/c. These events can therefore be rejected without further analysis.

3.9.6 ERROR CODES E19 AND E99

Events with more than 10 groups in any one tray are given an E19 error code, and events with more than 25 group combinations are given an E99 error code. These error codes were introduced to reduce the time taken for the initial analysis of the data and to filter out multiple muon events.

Many of the E19 and E99 events result from the spectrograph being triggered by extensive air showers. Typical E19 and E99 events are shown in figures 3.13 and 3.14.

The re-analysis of the data was carried out by simply removing the 25 group combination and 10 groups per tray limits from the analysis program. This ensures that as much of the data as possible are analysed in the same way, and avoids any systematic biases in the spectrum.

A sample of 50 E19 events and 192 E99 events were plotted out and checked to see if the program had analysed them correctly. The results proved satisfactory, therefore the 'pass' events from this analysis were added to the main file of 'pass' events. Also, any E95 events generated by this re-analysis were added to the main file of E95 events.

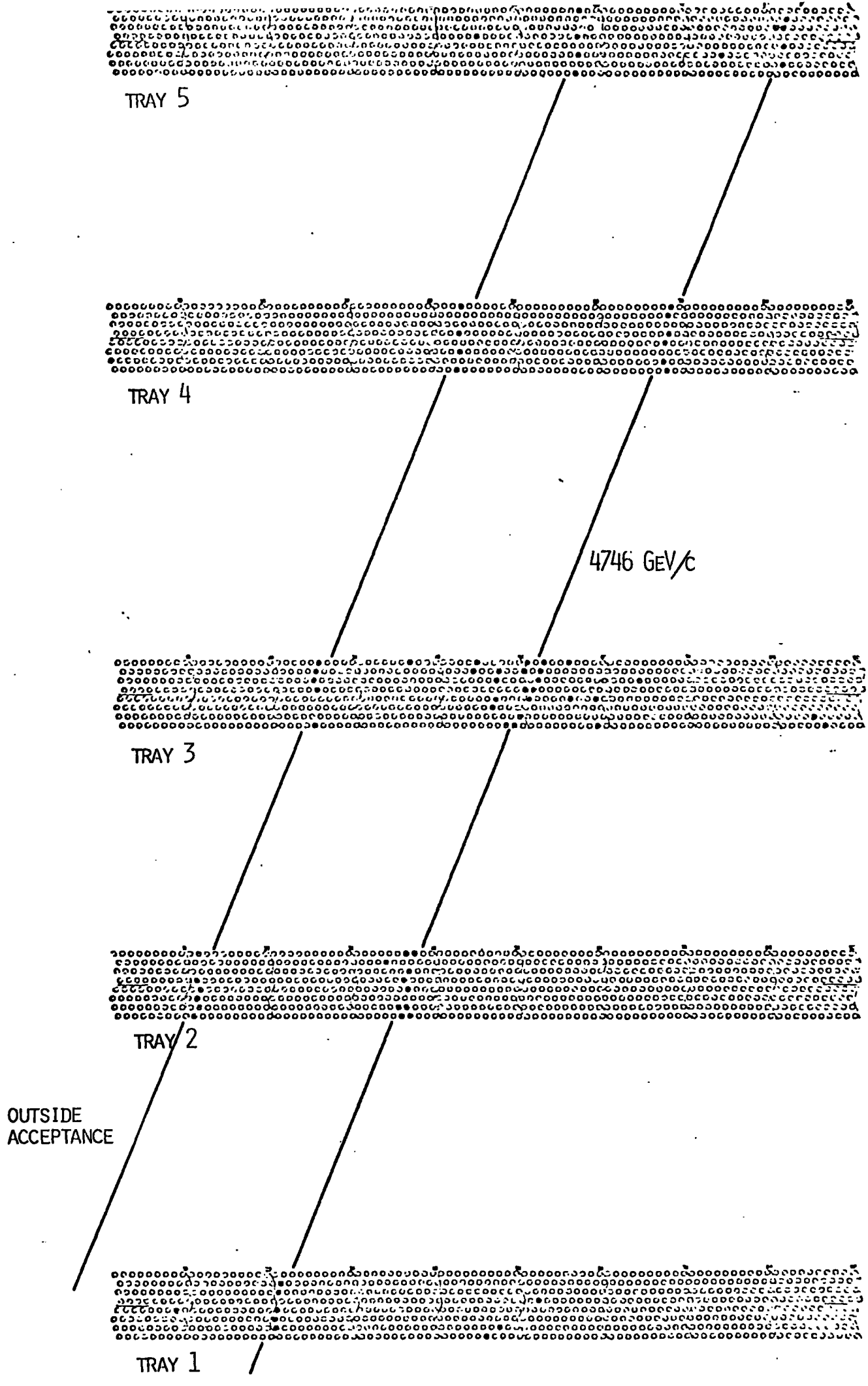

FIGURE 3.13 AN E99 EVENT

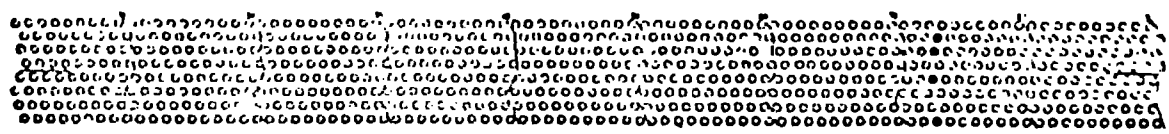

TRAY 5

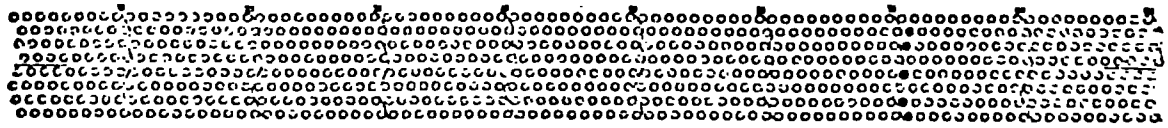

TRAY 4

FIVE TRAYS WERE USED ON RE-ANALYSIS

THE MOMENTUM WAS ESTIMATED TO BE 158 GeV/c

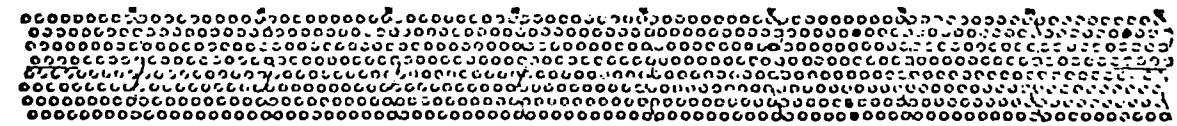

TRAY 3

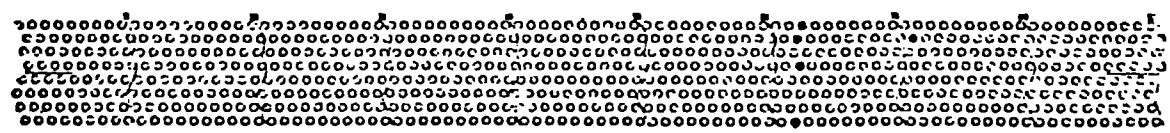

TRAY 2

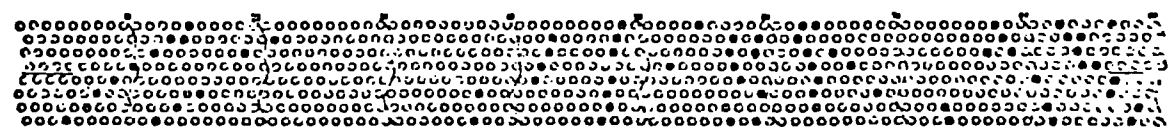

TRAY 1

FIGURE 3.14 AN E19 EVENT WITH A LARGE BURST IN TRAY 1

3.9.7. ERROR CODE E93

An event is given this error code if there are more than 10 successful group combinations. These events only arise on re-analysis of E99 events and they are very uncommon. When they arise, they are plotted out on tray front diagrams for visual inspection and then analysed by the program in the edit mode. In this mode, the data in a tray can be edited and individual tracks separated out for analysis. Individual groups are not split and only muons within the acceptance of the spectrograph are accepted.

3.9.8. ERROR CODE E96

These events contain more than two successful muon trajectories and must be analysed with the program in the edit mode. All muons within the acceptance of the spectrograph are accepted.

3.9.9 ERROR CODE E95

These events either fail the standard deviation test (i.e. the fitted trajectory has a large standard deviation) or they fail the acceptance test (i.e. the fitted trajectory lies ouside one tube spacing of a group in an unused tray). The events have either suffered severe multiple Coulomb scattering or they have been wrongly analysed because of confused tracks in a measuring tray. Both types of event should be included in the spectrum provided a reliable estimate of their momentum can be obtained and provided they are within the acceptance of the spectrograph.

The E95 events were re-analysed in two ways:

A) With the standard deviation test suppressed so that the best fit trajectory was not rejected even though it had a large standard deviation. However the one tube spacing acceptance test was still applied.

B) With a 4 cm acceptance test but with the usual standard deviation test.

Of 2324 events analysed, 728 events of momentum >100 GeV/c passed the analysis and are considered to be within the acceptance. They amount to, at most, 2.5% of the data in the 'pass' category.

Before the results of the re-analysis were checked, the spectra from the re-analysis of the E95 events were compared with the spectra of events in the 'pass' category. This comparison is shown in figure 3.15 where it can be seen that the spectra of E95 events are much flatter than the corresponding 'pass' event spectra. This suggests that many events are wrongly analysed because any error in the measurement of a steeply falling spectrum will tend to enhance the intensity at high energy.

Computer drawn diagrams of the measuring tray fronts, in which the flash-tube columns are straight, were generated for all E95 events. These diagrams were examined together with the results of the analysis above. Complex events were plotted out on the more accurate tray front diagrams for further consideration.

If an event passed analysis A or analysis B, see for example figures 3.16 and 3.17, then it was accepted provided that it had clear tracks in those trays used to determine the muon trajectory. These were considered highly scattered events.

If an event contained a muon track confused by knock-on electrons or shower electrons, see for example figure 3.18, the event was re-analysed without the data for that tray. This method was justified for five tray fit events because the resulting four tray fit trajectory usually had a standard deviation of about 1/10th of that of the five tray fit trajectory. The method was justified for four tray fit events

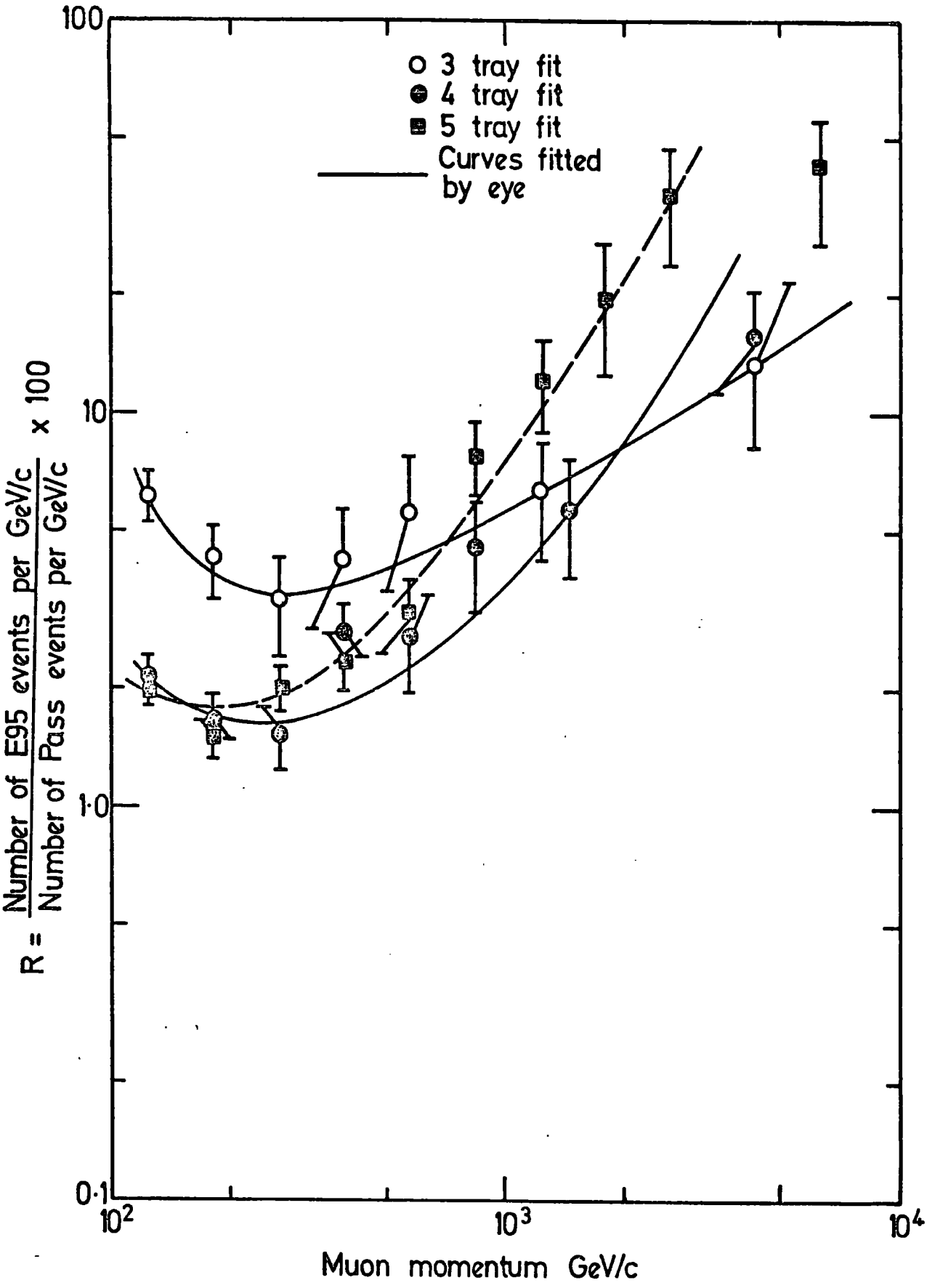

Figure 3.15 A comparison of the spectra of E95 events with events from the 'pass' category.

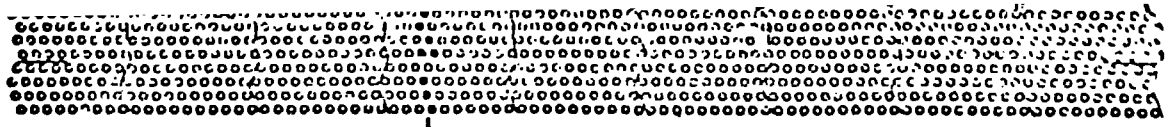

TRAY 5

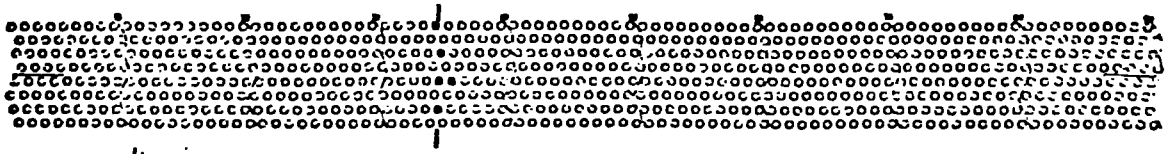

TRAY 4

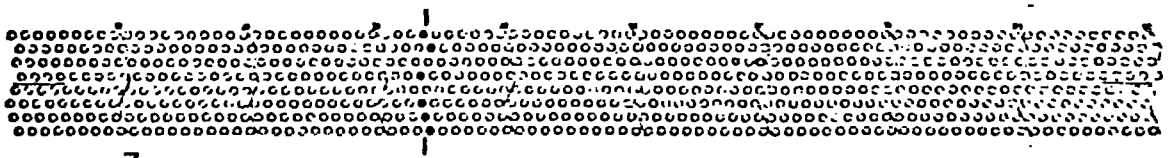

TRAY 3

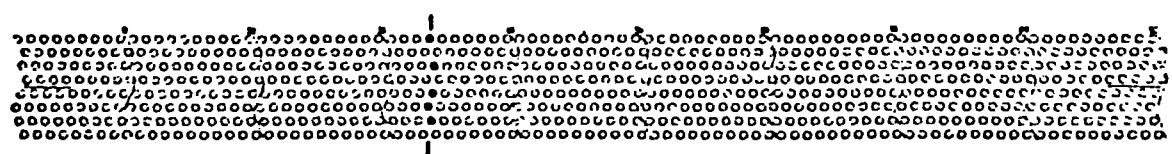

TRAY 2

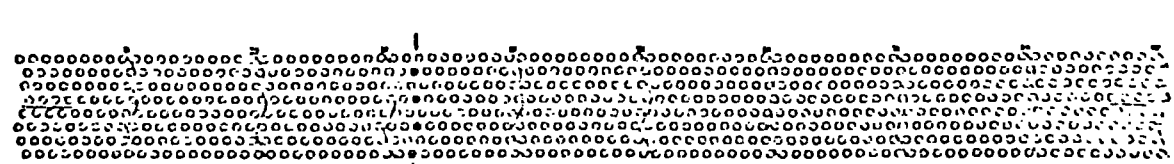

TRAY 1

FIGURE 3.16 AN E95 EVENT WHICH PASSED ANALYSIS A

TRAY 5

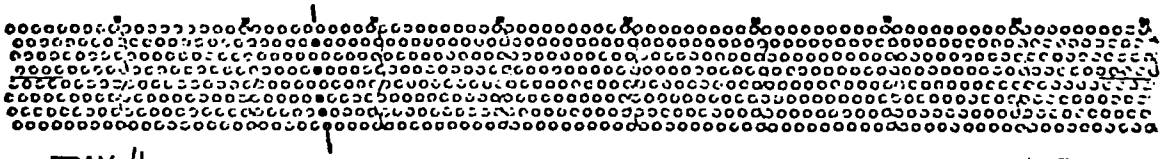

TRAY 4

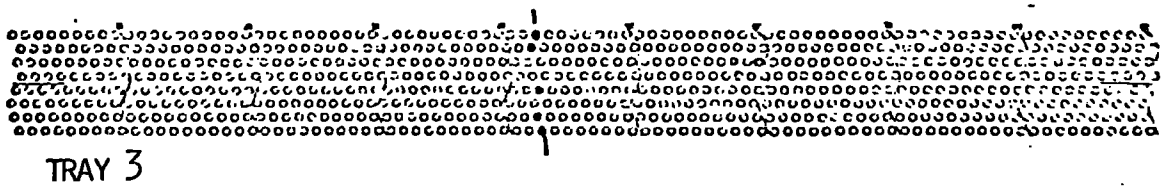

TRAY 3

THIS TRACK IS OUSIDE 1 TUBE SPACING BUT WITHIN 4CM OF THE FITTED TRAJECTORY

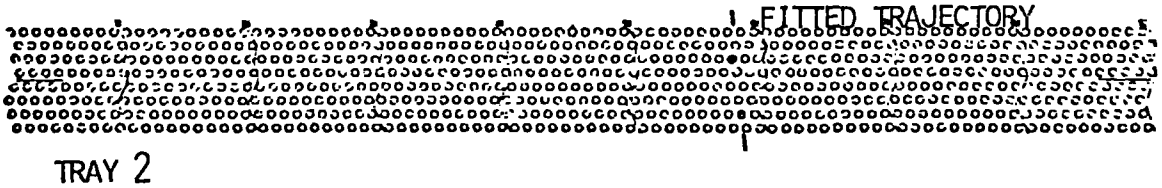

TRAY 2

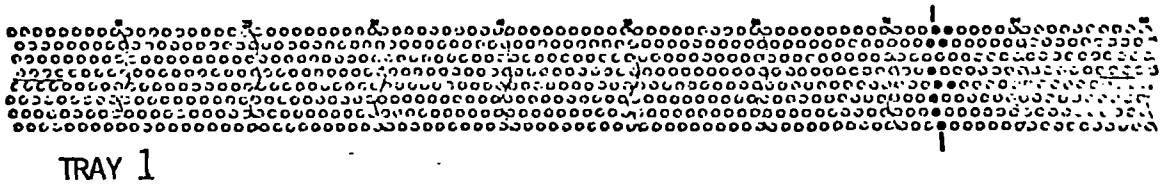

TRAY 1

FIGURE 3.17 AN E95 EVENT WHICH PASSED ANALYSIS B

TRAY 5

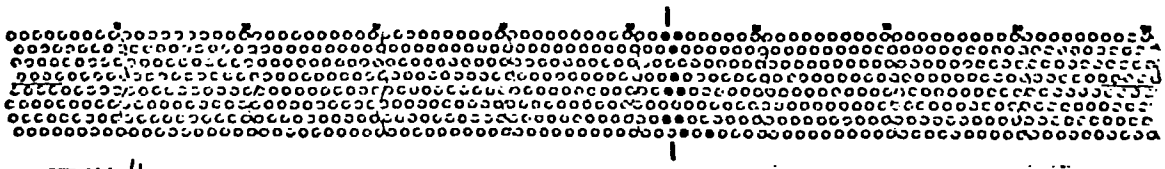

TRAY 4

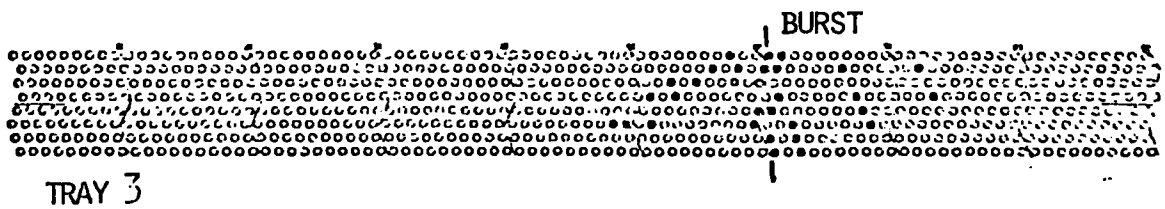

TRAY 3

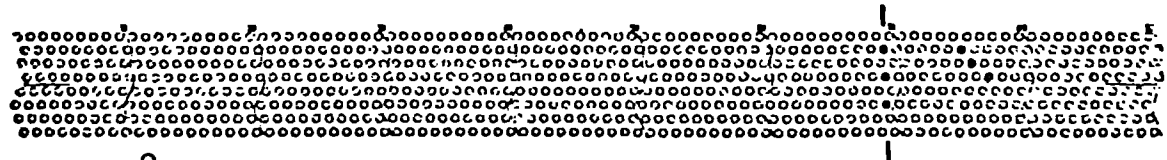

TRAY 2

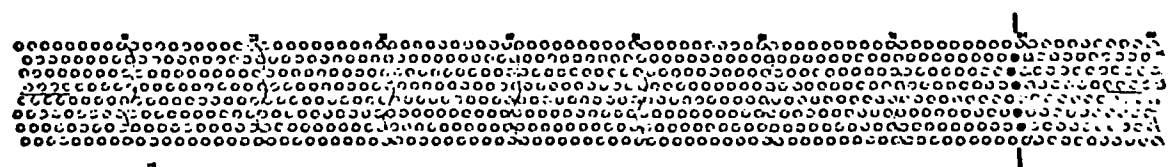

TRAY 1

FIGURE 3.18 AN E95 EVENT WITH CONFUSED MUON TRACKS IN TRAYS 3 AND 4

because the result of the three tray fit was often in agreement with the result of the four tray fit analysis when the confused muon track was edited to remove the offending electron track.

Events were rejected if they fell outside the acceptance of the spectrograph, see for example figure 3.19, or if they had an inefficient muon track next to an efficient electron track which had been erroneously used in the analysis, see for example figure 3.20. Events such as this were placed in the SE3 or E91 category.

To check that subjective bias had been kept to a minimum, a second person analysed a sample of 200 E95 events. Good agreement was seen between the results, therefore it was felt that subjective bias had been kept to a minimum. A further check on the analysis comes from looking at a comparison of the final E95 spectra with the spectra of the data in the 'pass' category. This is shown in figure 3.21, where it can be seen that the spectra are now in good agreement, showing that the error in the measurement of the E95 spectra has been substantially reduced.

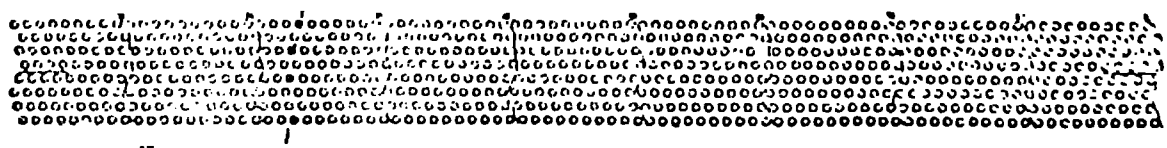

TRAY 5

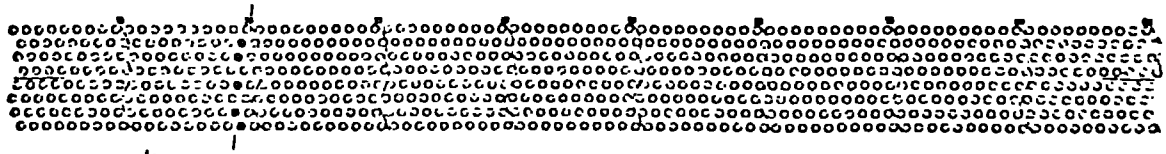

TRAY 4

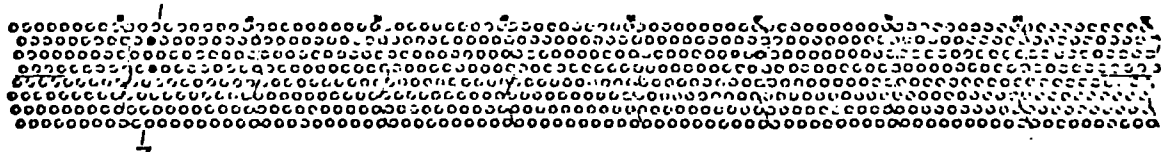

TRAY 3

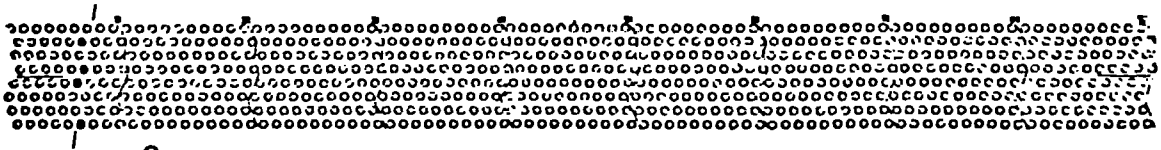

TRAY 2

ELECTRON BURST

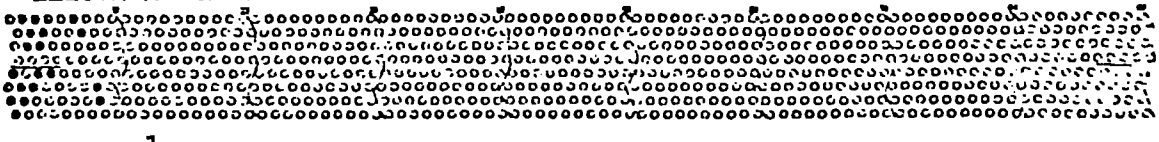

TRAY 1

FIGURE 3.19 AN E95 EVENT WHICH IS JUST OUSIDE THE SPECTROGRAPH ACCEPTANCE

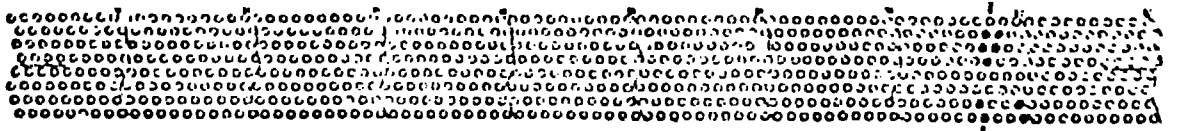

TRAY 5

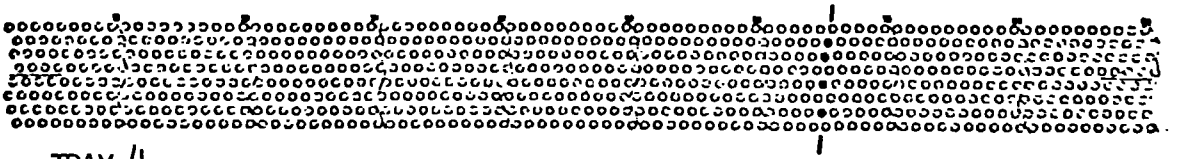

TRAY 4

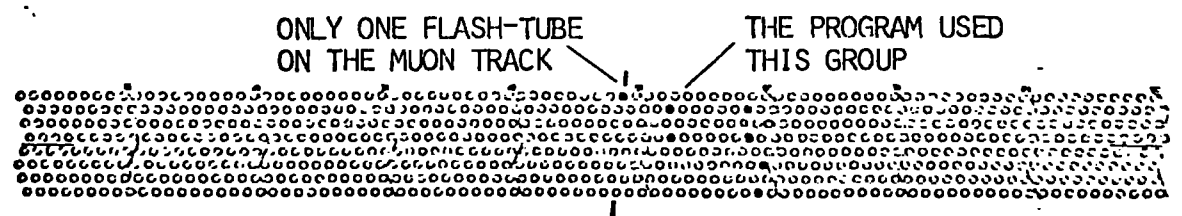

TRAY 3

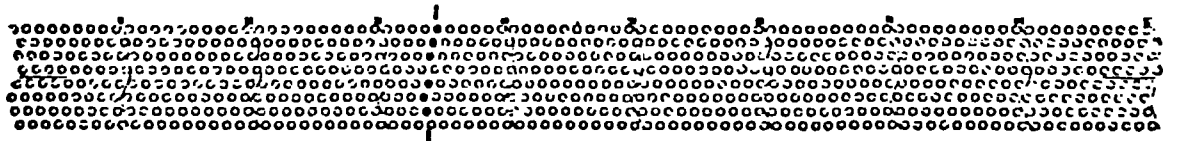

TRAY 2

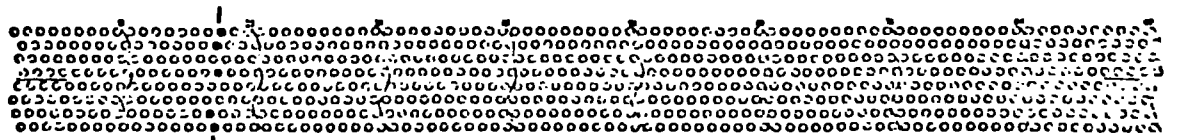

TRAY 1

FIGURE 3.20 AN E95 EVENT WHICH HAS BEEN PLACED IN THE E91 CATEGORY

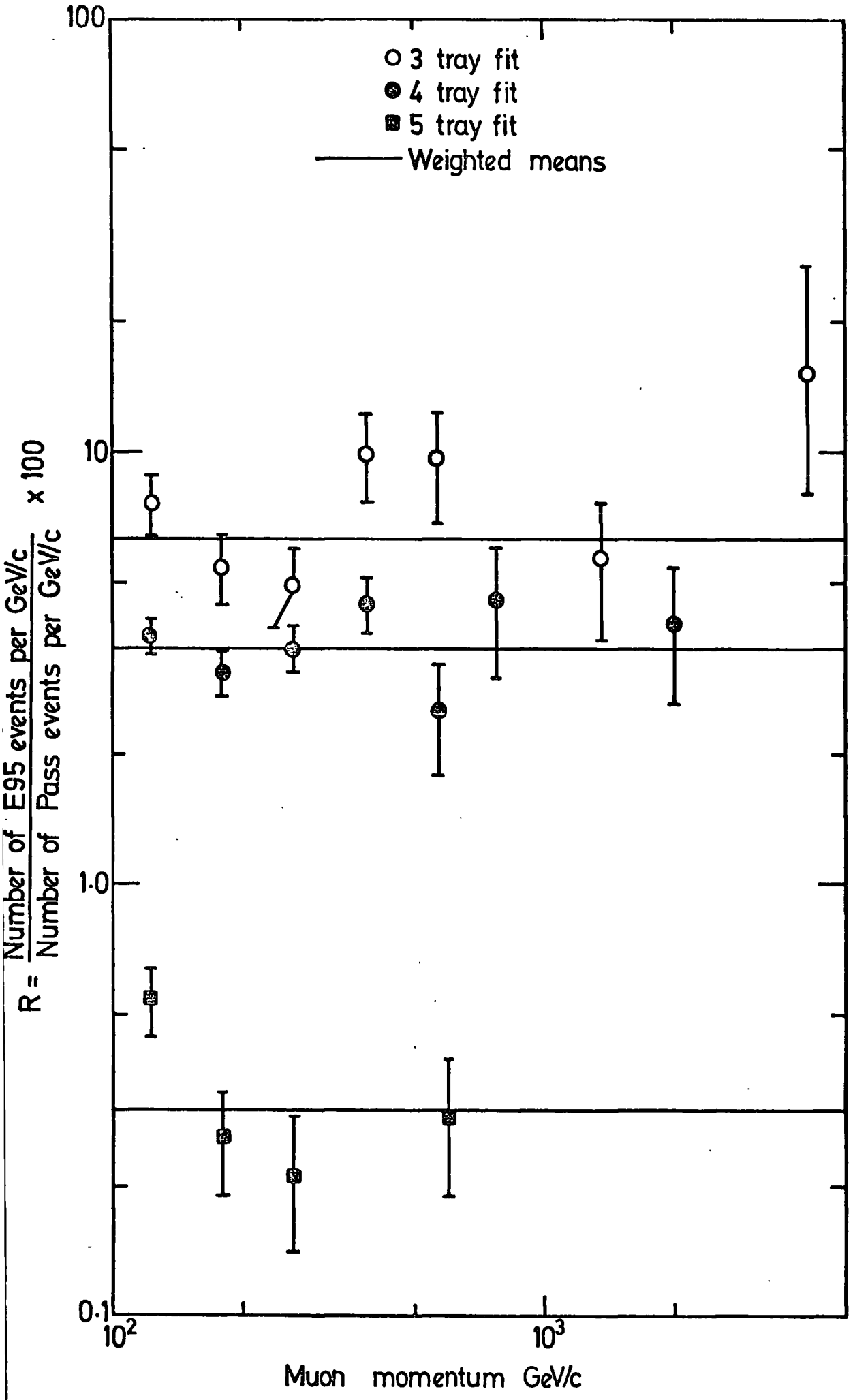

Figure 3.21 The spectra of E95 events after checking the results of the A and B analysis.

CHAPTER 4

THE ACCEPTANCE, ALIGNMENT AND EFFICIENCY OF THE SPECTROGRAPH

4.1 THE ACCEPTANCE OF THE SPECTROGRAPH

The acceptance of the spectrograph is that quantity which when multiplied by the flux of the cosmic ray muons at sea level (measured in units of m^{-2} s^{-1} sr^{-1} GeV/c^{-1}) gives the rate of muons through the spectrograph. Thus the acceptance has units on m^2 sr and is defined by the geometry of the spectrograph,

The acceptance is dependent upon the momentum of muons considered. Low energy muons which have large radii of curvature will have a small probability of staying within the sensitive volume of the spectrograph. The momentum dependence of the acceptance is shown in figure 4.1 which is taken from Whalley (1974).

For momenta of interest on this work ($\geq$200 GeV/c) the acceptance has reached its limiting value. This has been calculated by Whalley (1974) and Hawkes (1977) and has the value of 408±2 cm^2 sr. The errors are mainly caused by the difficulty in defining the plane of the scintillation counters because of their finite thickness.

4.2 THE ANGULAR ACCEPTANCE OF THE SPECTROGRAPH

It is shown in figure 4.1 that for muons of momenta >200 GeV/c the acceptance has reached its limiting value. This means that the trajectories of muons in this region can be considered to be along straight lines. Thus with x and l defined as in figure 4.2 the angular acceptance of the spectrograph is given by the ratio x/l, with $x = w\cos\theta - h\sin\theta$, and $l = w\cos\theta$.

A comparison of the measured and theoretical angular distributions of muons in the bending plane of the spectrograph is

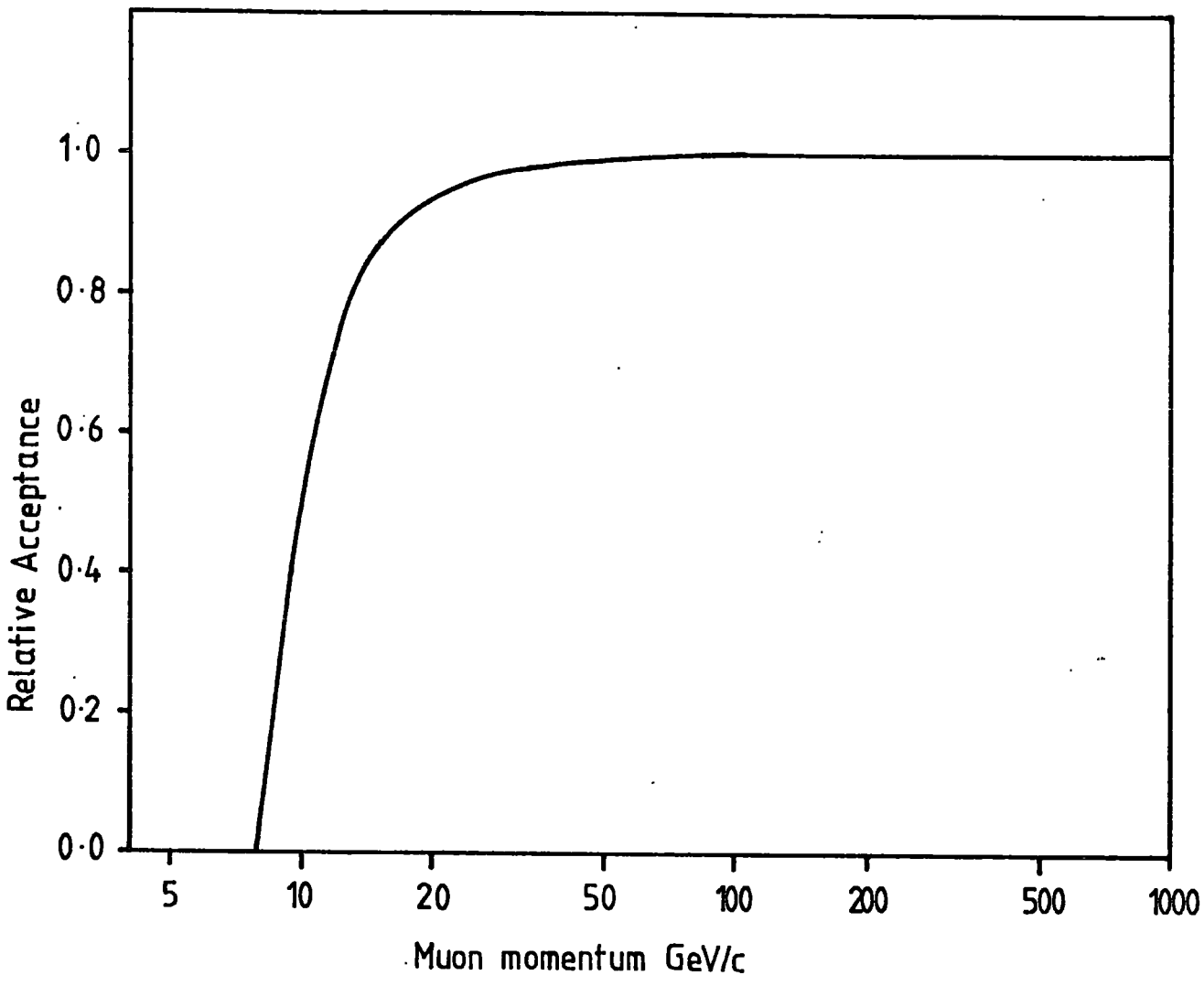

Figure 4.1 The relative acceptance of MARS

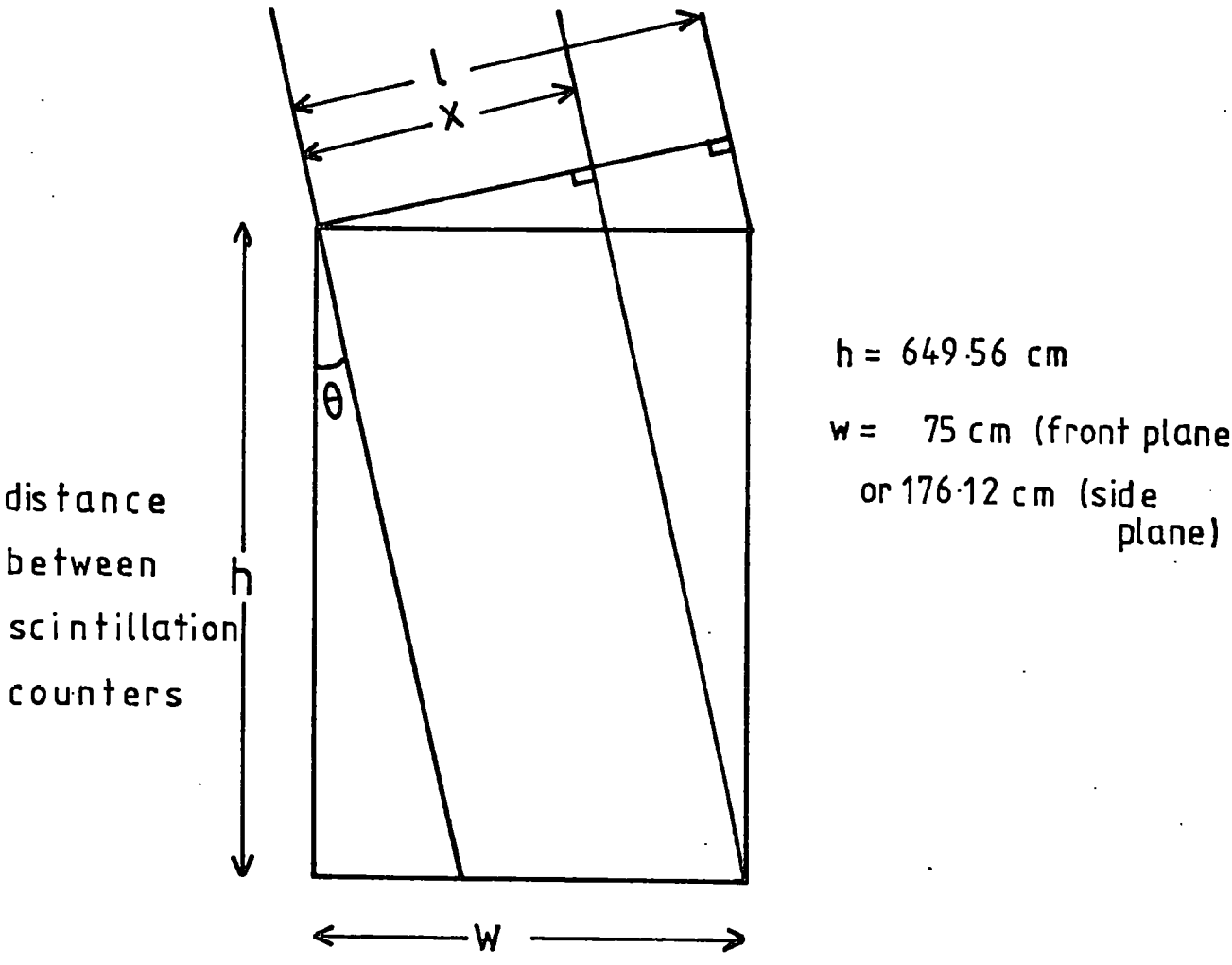

Figure 4.2 Schematic diagram of the spectrograph defining its angular acceptance : x/l

shown in figure 4.3a. Good agreement is seen between the two. For the side plane, the angular acceptance is shown in figure 4.3b.

The intensity of muons as a function of zenith angle is shown in figure 4.4 (Coates 1967). As can be seen, the variation over the angular range ±15 degrees is small. Thus it is considered that no correction is needed to the measured muon spectrum for the angular acceptance of the spectrograph.

4.3 THE ALIGNMENT OF THE MEASURING TRAYS

The maximum momentum, and hence the smallest deflection, which can be reliably measured by the spectrograph is partly dependant upon the accuracy with which the relative lateral positions and skewness of the measuring trays are known. These errors set a limit on the smallest deflection which can be measured but they can be neglected if they are significantly smaller than the errors of trajectory location.

The technique used to measure the relative lateral displacement of the measuring trays is to run the spectrograph with the magnetic field in the iron magnet blocks reduced to zero. Muons will then pass through the spectrograph along straight line paths with small random deviations caused by multiple scattering and measuring errors. The events are analysed by fitting a straight line rather than a parabola to the flash tube patterns, and the co-ordinates of the centres of the channels through the measuring trays are obtained in the usual way. The co-ordinates in trays one and five are then joined by a new straight line and the horizontal displacements of the co-ordinates in the trays 2, 3 and 4 from this straight line are calculated. These displacements, called z_2, z_3, and z_4 and which are shown in figure 4.5, are binned into three frequency histograms whose widths are dependent upon the scattering in the magnet blocks and trajectory location

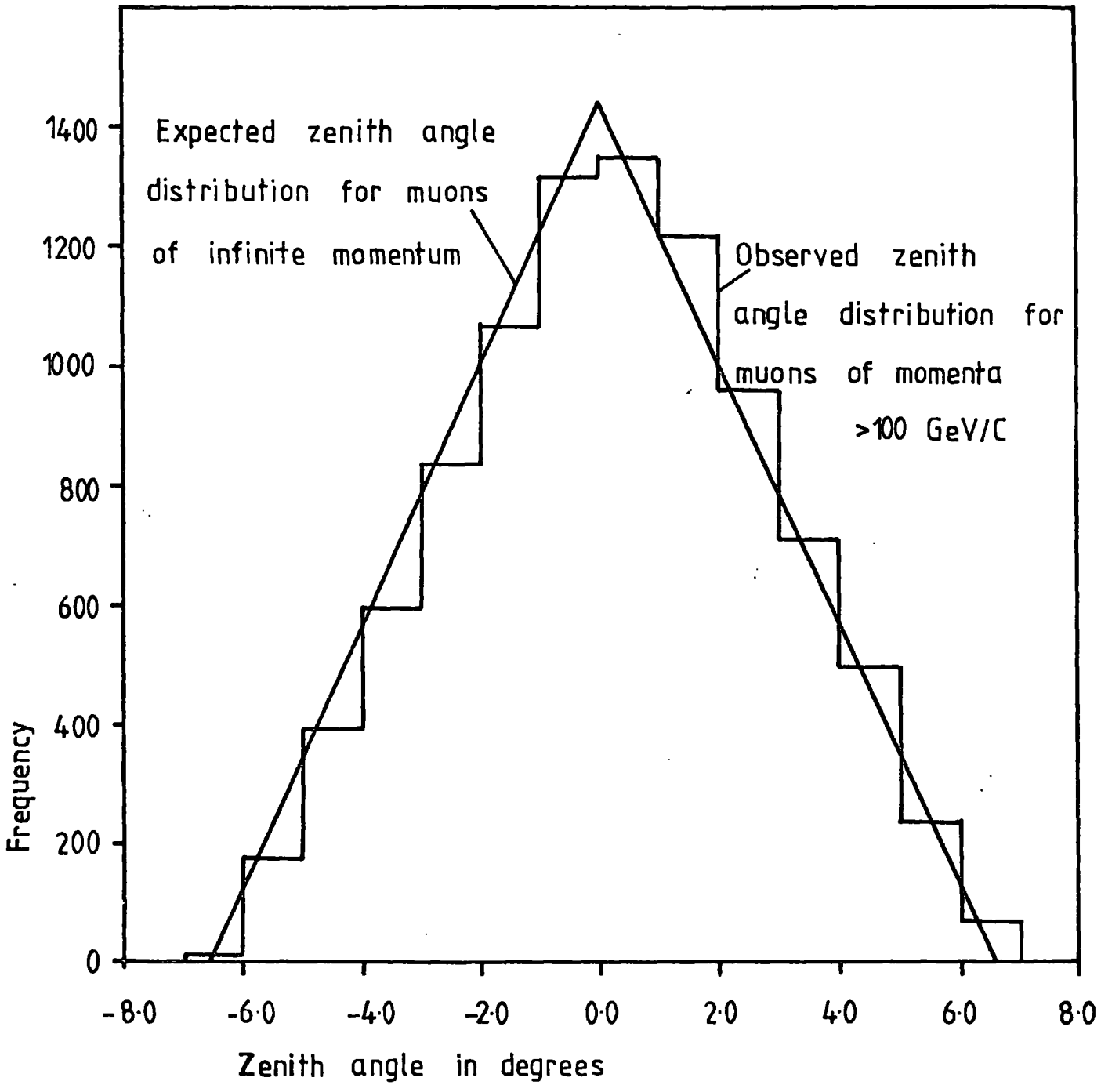

Figure 4.3a The zenith angle distribution in MARS

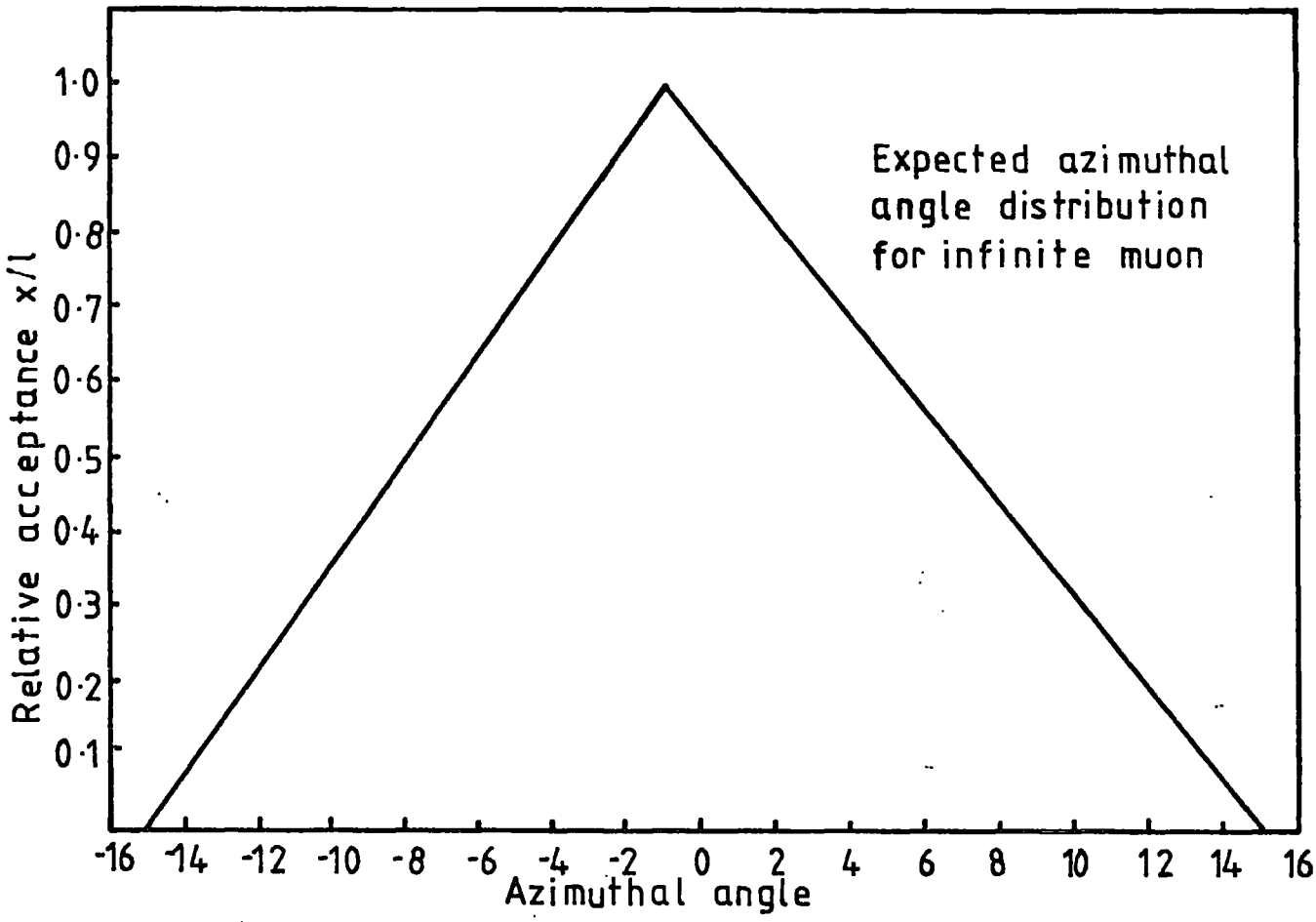

Figure 4.3b Azimuthal angle distribution

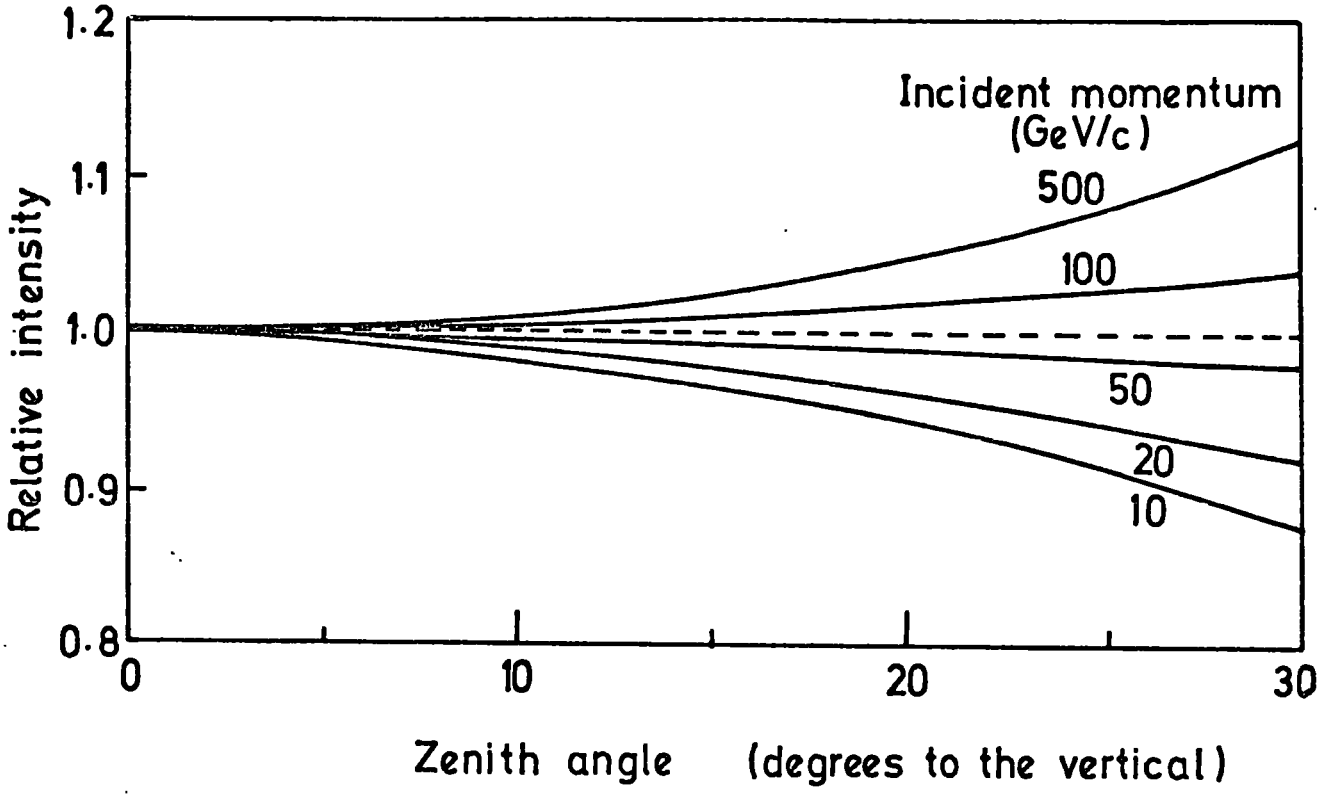

Figure 4.4 Variation of muon intensity with zenith angle. (after Whalley 1974)

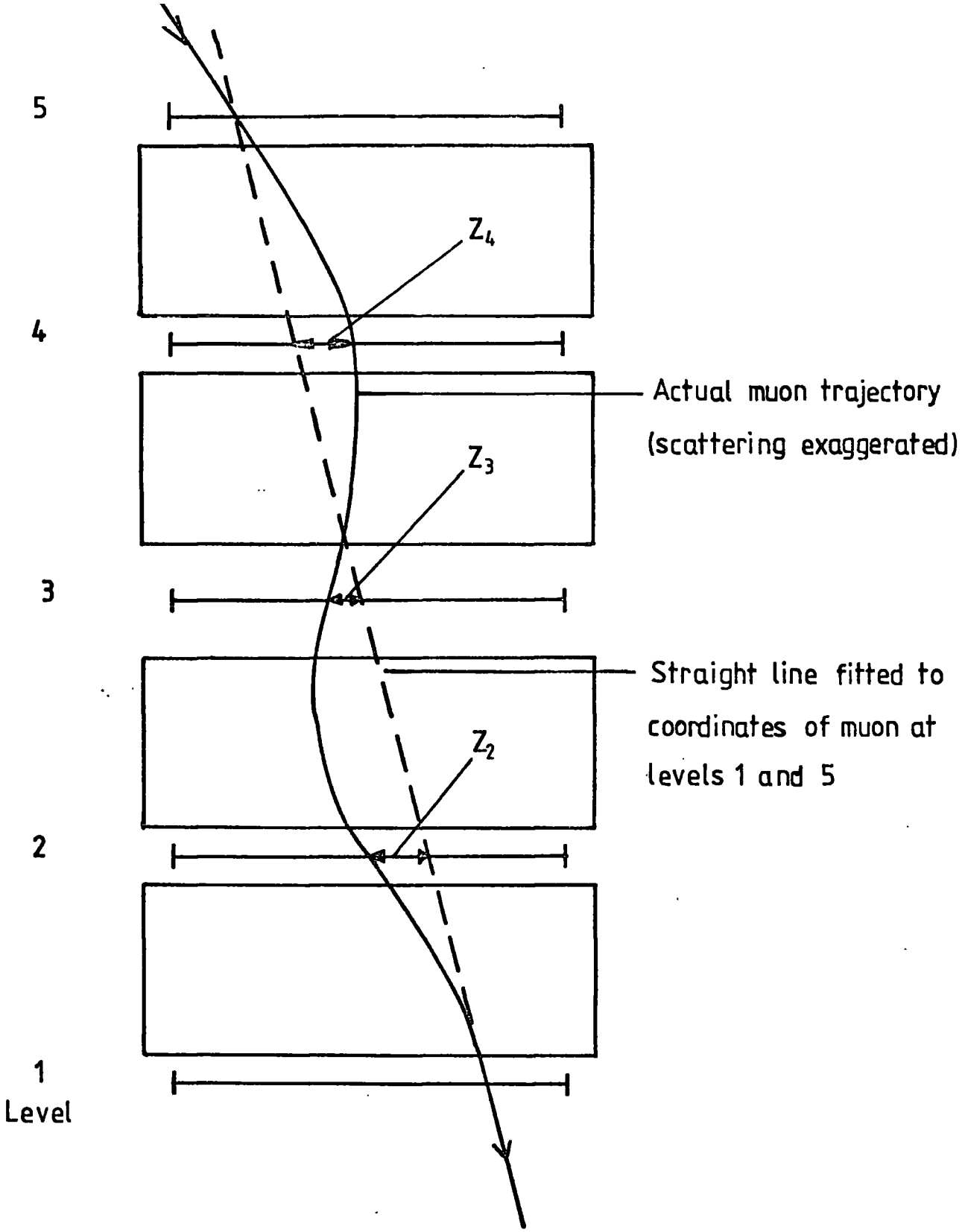

Figure 4.5 Diagram showing the path of a muon through the spectrograph with zero magnetic field

errors, and whose means or modes give the tray displacements at levels 2, 3 and 4 relative to the vertical line joining trays 1 and 5.

The relative skewness of the measuring trays has been estimated in a similar manner using the method of Ayre.(1975(a). The trays of Geiger Muller tubes located above and below the spectrograph are used to determine through which part of the spectrograph a proportion of the muon events pass. If FF, BB, BF, and FB represent muons passing down the front , down the back, from the back to the front, and from the front to the back of the spectrograph respectively, then for each of these four cases frequency histograms of z_2, z_3, and z_4 can be built up. If the trays are all parallel, the mean values of these histograms will be equal to those of the full histograms described above. Any skewness of the measuring trays will show up in the relative position of these mean values.

A zero field run was carried out before data collection began. The results of this run are shown in table 4.1 which is taken from Piggott (1975).

These displacements have been incorporated into the analysis program and used in the analysis of the data presented here. The skewness of the measuring trays was esimated to be <0.01 degrees.

At the end of data collection, the zero field run was repeated to check that the measuring trays had not moved during the course of the experiment. The magnetic field was reduced to zero by successively reducing and reversing the current in the energising coils around the iron blocks. A compass was used to check that the magnetic field reversed at each step, thus ensuring that no remnant magnetism was trapped in the blocks.

The data were collected with the momentum selector in operation

LEVEL	DISPLACEMENT mm
2	-1.37 ±0.2
3	2.19 ±0.2
4	-4.28 ±0.2

TABLE 4.1 THE HORIZONTAL TRAY DISPLACEMENTS TAKEN FROM PIGGOTT (1975)

to reject widely scattered events. A comparison between histograms with and without the momentum selector in operation is shown in figure 4.6. It is apparent that for an equal number of events, the histogram produced with the momentum selector will give the more accurate measurement.

The full displacement histograms for levels 2, 3 and 4 are shown in figure 4.7. If the tray displacements given in table 4.1 are correct, and the measuring trays have not moved during the course of the experiment, then the means and modes of the distributions in figure 4.7 should be centred on zero. However, since the distributions are slightly skew the mode will be a better estimate of tray position than the mean. (The skewness is thought to be caused by systematic effects in the momentum selector. However, distributions obtained by Piggott (1975) without the momentum selector still show some skewness).

The means and modes of the displacement histograms obtained from the zero field run after data collection are shown in table 4.2. It is concluded that the results are consistent with those obtained before data collection began, and that the measuring trays did not move significantly during the period of data collection.

The results of the analysis of the FF, BB, FB and BF distributions are shown in table 4.3. The errors on these measurements are large because of the low rate of events through the Geiger Muller tube trays. Therefore definite conclusions cannot easily be made on the skewness of the measuring trays. However it is concluded that the results are not inconsistent with the skewness being less than 0.01 degrees.

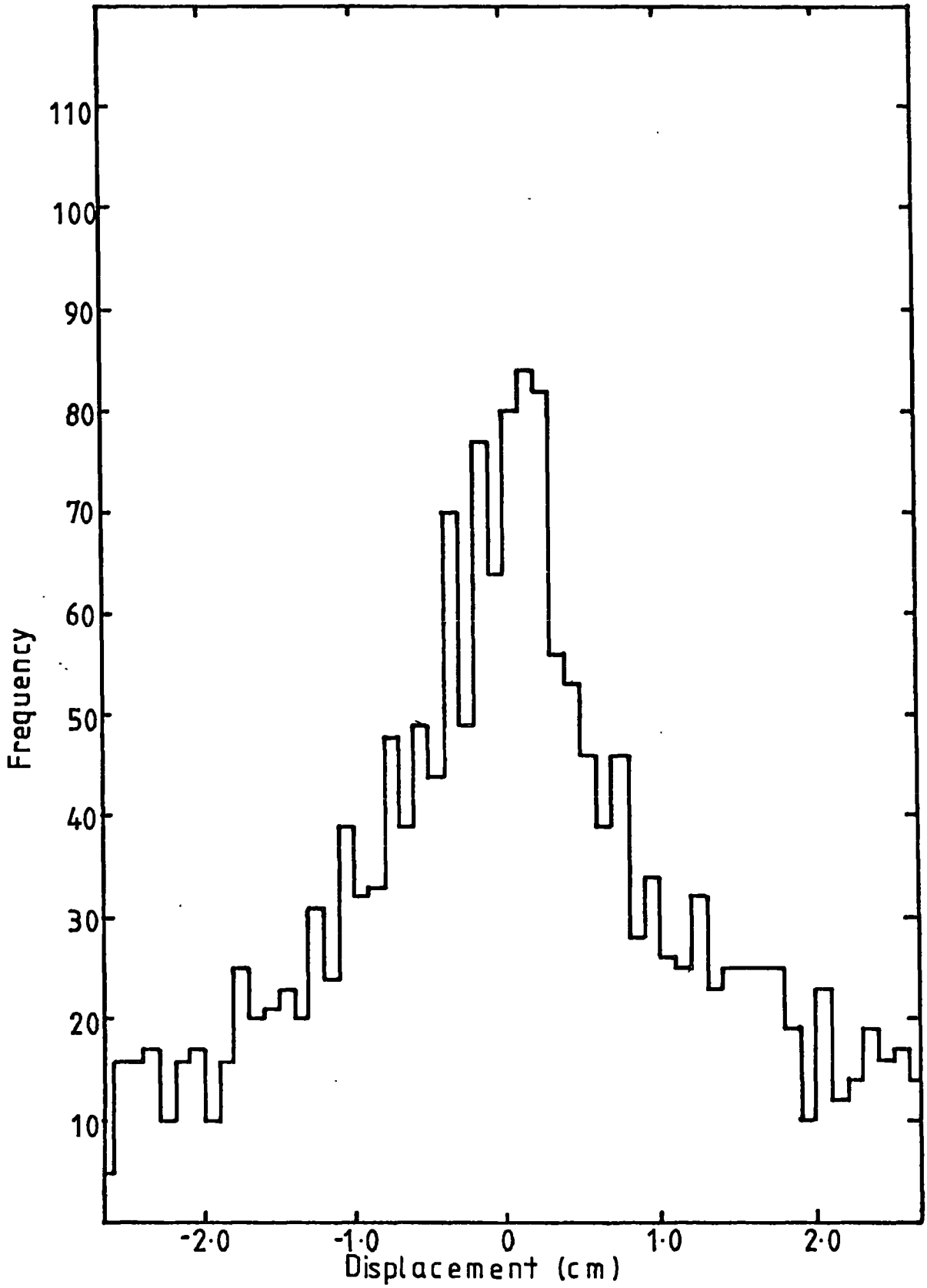

Figure 4.6a The displacement histogram for tray 3 for the data collected without the momentum selector (After Piggott 1975)

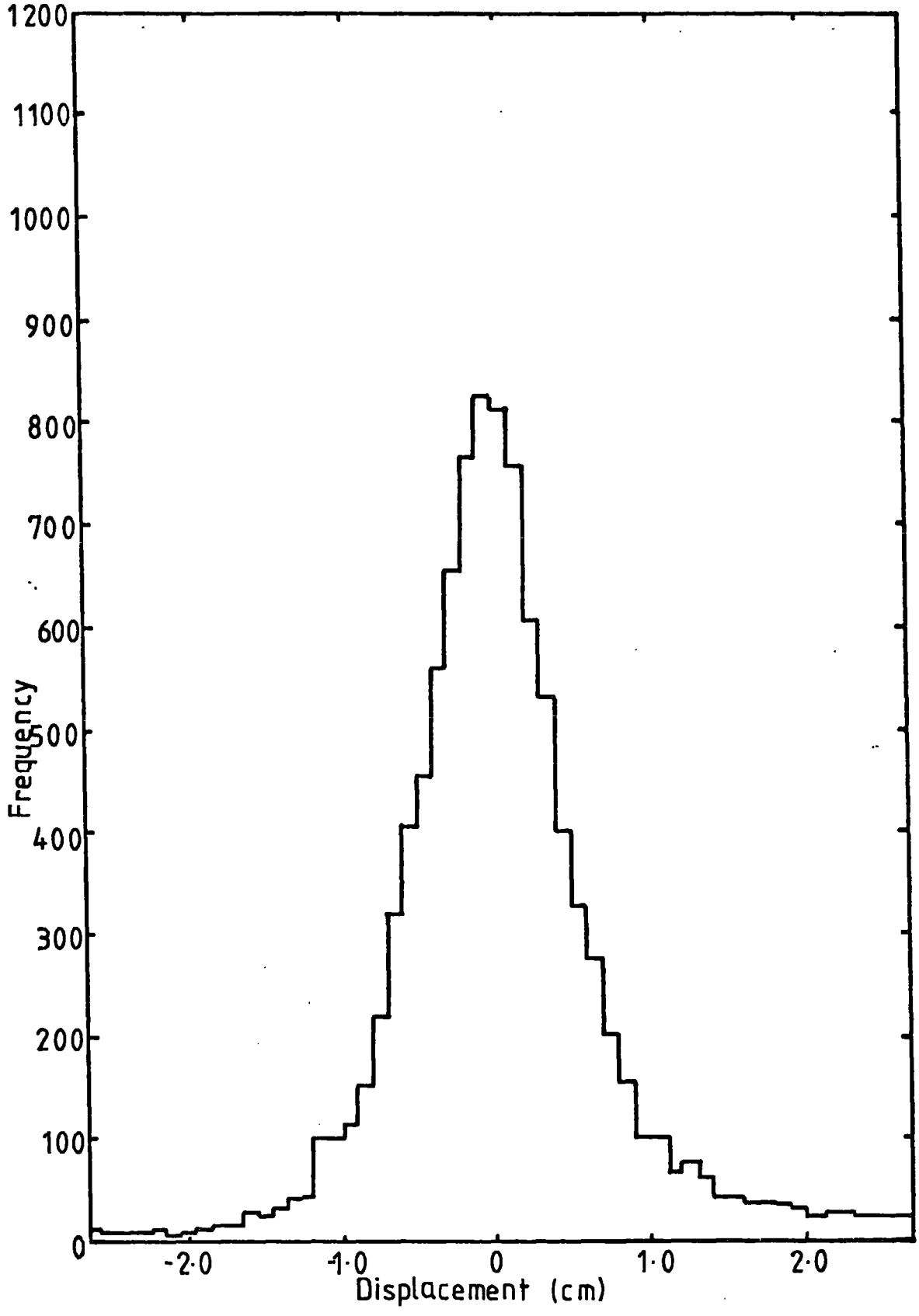

Figure 4.6b The displacement histogram for tray 3 for the data collected with the momentum selector (After Piggott, 1975)

Figure 4.7 The zero field displacement histograms

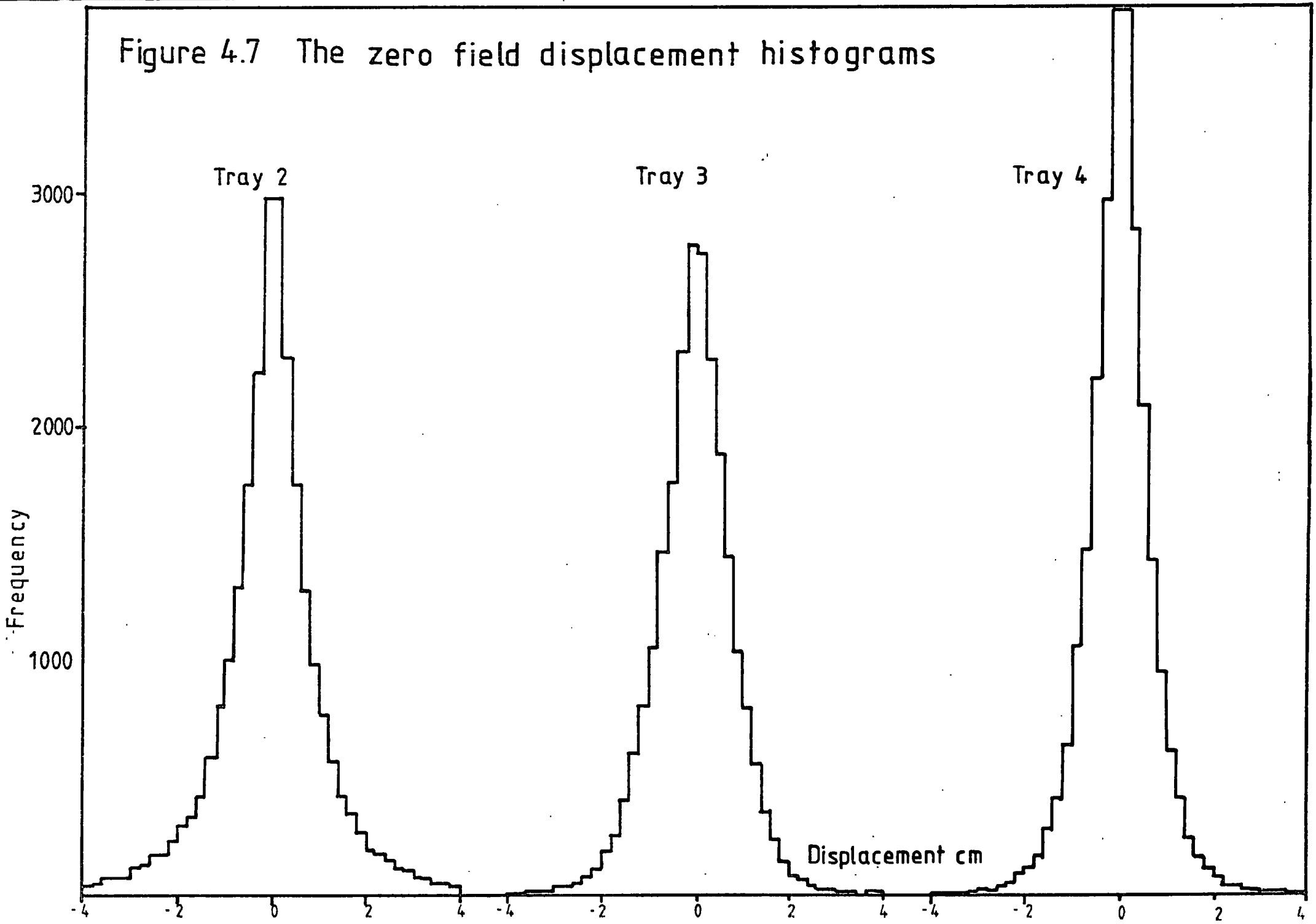

LEVEL	DISPLACEMENT mm	
	MEAN	MODE
2	-0.33 ±0.08	0.01 ±0.5
2 (3σ cut)	-0.11 ±0.06	
3	-0.20 ±0.06	0.99 ±0.5
3 (3σ cut)	-0.15 ±0.05	
4	-0.14 ±0.04	0.24 ±0.5
4 (3σ cut)	-0.13 ±0.04	

TABLE 4.2 THE MEANS AND MODES OF THE DISPLACEMENT HISTOGRAMS FOR THE ZERO FIELD RUN AFTER DATA COLLECTION

	DISPLACEMENT IN mm		
	LEVEL		
	2	3	4
MEAN	-0.57 ±0.5	-0.37 ±0.3	-0.52 ±0.3
FF MEAN (3σ cut)	-0.15 ±0.4	-0.28 ±0.3	-0.36 ±0.2
MODE	-0.70 ±3.0	-0.80 ±3.0	-0.50 ±3.0
MEAN	-0.19 ±0.5	-0.16 ±0.4	0.09 ±0.3
BB MEAN (3σ cut)	0.23 ±0.4	-0.03 ±0.3	-0.12 ±0.3
MODE	-1.10 ±3.0	0.20 ±3.0	0.50 ±3.0
MEAN	-0.24 ±0.5	-0.13 ±0.4	0.29 ±0.4
BF MEAN (3σ cut)	-0,20 ±0.4	-0.33 ±0.4	0.39 ±0.3
MODE	0.50 ±3.0	0.10 ±3.0	-1.20 ±3.0
MEAN	-0.60 ±0.5	0.17 ±0.4	0.19 ±0.3
FB MEAN (3σ cut)	-0.34 ±0.3	0.25 ±0.3	-0.05 ±0.2
MODE	0.10 ±3.0	2.00 ±3.0	0.80 ±3.0

TABLE 4.3 THE MEANS AND MODES OF THE DISPLACEMENT HISTOGRAMS FOR THE ZERO FIELD RUN AFTER DATA COLLECTION FOR FF, BB, FB AND BF EVENTS

4.4 MOMENTUM SELECTOR EFFICIENCY

4.4.1 INTRODUCTION

To obtain an estimate of the muon momentum spectrum, it is necessary to know the probability of a muon of given momentum triggering the momentum selector and hence being recorded by the spectrograph.

The efficiency of the momentum selector is mainly dependent on the momentum of the muon. Corrections have to made for wrong celling by the tray front electronics, the flash-tube inefficiency, the production of knock-on electrons in the measuring trays, the production of bursts in the magnets and multiple scattering of the muon. The production of bursts or knock-on electrons tends to set off more than one cell and therefore increases the apparent efficiency of the momentum selector. The other effects tend to set off a different cell from the one which the muon would have set off. This may increase or decrease the probability of triggering the momentum selector depending on the position of the muon within the momentum selector tray (MST).

A calculation of the momentum selector efficiency will first be made assuming that it is dependent only upon momentum. Then it will be recalculated by taking the above mentioned corrections into account.

4.42 THE MOMENTUM SELECTOR EFFICIENCY ASSUMING MOMENTUM DEPENDENCE ONLY

The efficiency of the momentum selector can be calculated in a simple way by assuming that it is only dependent upon muon momentum. This is done by finding, for a given muon momentum, all possible combinations of cells in the three momentum selector trays and calculating the fraction of these cell combinations which trigger the momentum selector. This fraction is then the momentum selector efficiency for that momentum.

All possible cell combinations for a given momentum can be calculated from the relationship between deflection Δ, and the cells a, b and c allocated at levels 1, 3 and 5 (see figure 2.7) which is:

$$\Delta = 2b - a - c$$

and the relationship given by Whalley (1974), between deflection Δ and momentum p for muons of momentum greater than 100 GeV/c which is:

$$p\Delta = 400 \text{ GeV/c. cm}$$

Figure 4.8 shows a schematic diagram of the momentum selector tray fronts with the ½ cm cells indicated and several trajectories of muons of momentum equal to 200 GeV/c incident at positive zenith angles through cell 4 at level 5.

The number of possible cell combinations can be reduced by making use of the cell groupings in the momentum selector. Thus cells 1, 4, 7, 11 .... etc in level 5 are equivalent to one another (neglecting the ends of the trays) and it is only necessary to consider three adjacent cells in tray 5 to find all the significant cell combinations. This has been done for a muon momentum of 200 GeV/c in table 4.4 using cells 4, 5 and 6 for positive zenith angles and cells 22, 21 and 20 for negative zenith angles. The cell group numbers in the momentum selector were used to find which cell combination would trigger the momentum selector and this is indicated in table 4.4 by a Y (yes) or a N (no). It can be seen that the proportion of the cell combinations which trigger the momentum selector is always a fraction of 6. It is therefore only necessary to consider the first 6 consecutive cell combinations in the columns of table 4.4 to give the momentum selector efficiency. In this case, 21 of the 36 combinations trigger the momentum selector, therefore its efficiency at

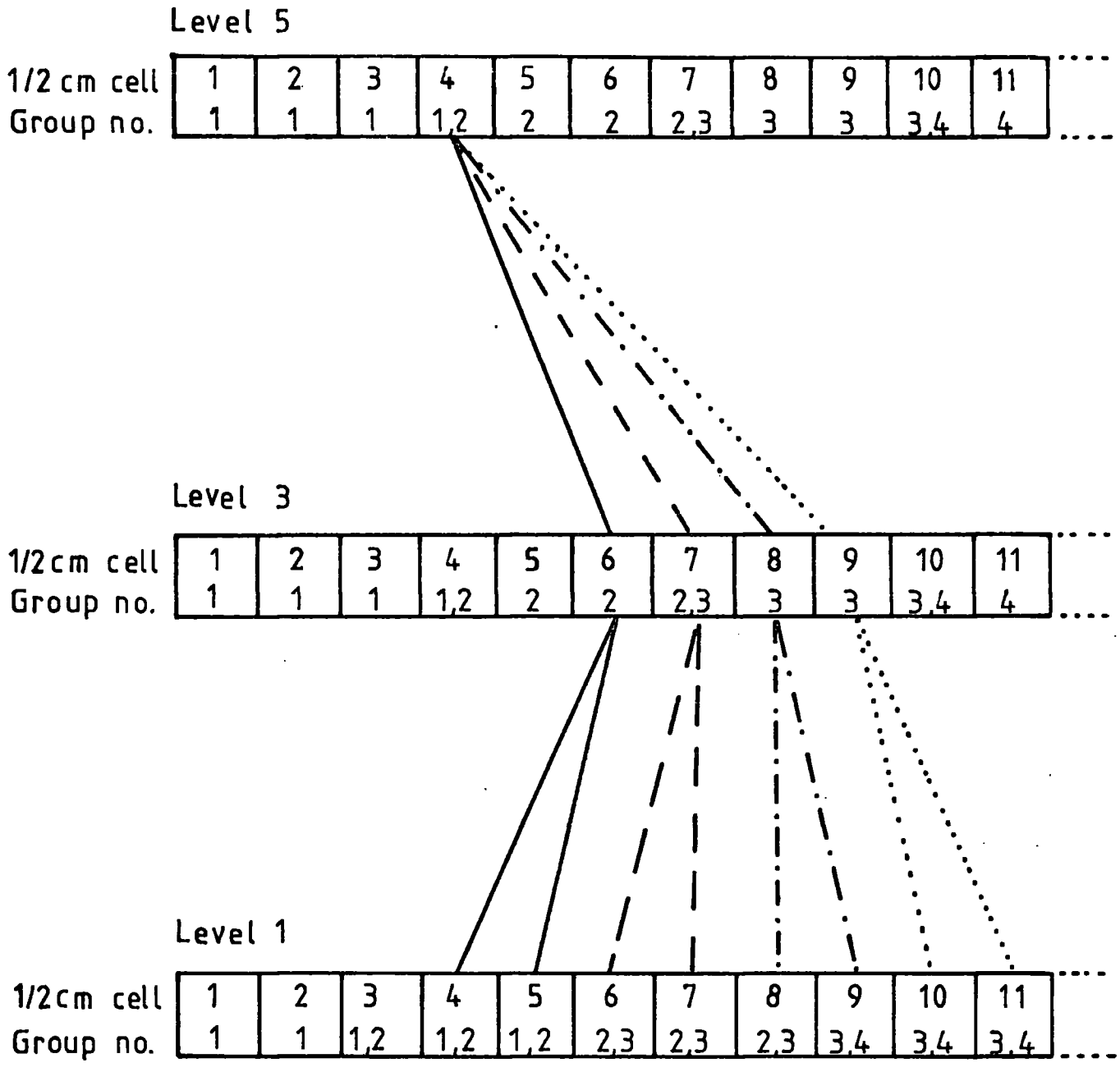

Figure 4.8 A schematic diagram of the momentum selector tray fronts showing the 1/2 cm cells and the group numbers in the momentum selector. Also shown are 8 possible trajectories of 200 GeV/c muons

ZENITH ANGLE	+ve				+ve				+ve				−ve				−ve				−ve			
LEVEL	5	3	1		5	3	1		5	3	1		5	3	1		5	3	1		5	3	1	
Only the first six cell combinations are required to calculate the momentum selector efficiency	4	6	4	Y	5	7	5	Y	6	8	6	N	22	20	22	Y	21	19	21	Y	20	18	20	N
	4	6	5	Y	5	7	6	Y	6	8	7	N	22	19	21	Y	21	18	20	N	20	17	19	N
	4	7	6	Y	5	8	7	N	6	9	8	N	22	19	20	Y	21	18	19	N	20	17	18	N
	4	7	7	Y	5	8	8	N	6	9	9	Y	22	18	19	N	21	17	18	N	20	16	17	Y
	4	8	8	N	5	9	9	Y	6	10	10	Y	22	18	18	N	21	17	17	Y	20	16	16	Y
	4	8	9	Y	5	9	10	Y	6	10	11	Y	22	17	17	Y	21	16	16	Y	20	15	15	N
	4	9	10	Y	5	10	11	N	6	11	12	N	22	17	16	Y	21	16	15	Y	20	15	14	N
	4	9	11	Y	5	10	12	N	6	11	13	N	22	16	15	Y	21	15	14	N	20	14	13	N
	4	10	12	Y	5	11	13	Y	6	12	14	N	22	16	14	Y	21	15	13	N	20	14	12	N
	4	10	13	Y	5	11	14	Y	6	12	15	Y	22	15	13	N	21	14	12	N	20	13	11	Y
	4	11	14	N	5	12	15	N	6	13	16	Y	22	15	12	N	21	14	11	Y	20	13	10	Y
	4	11	15	Y	5	12	16	N	6	13	17	Y	22	14	11	Y	21	13	10	Y	20	12	9	N
	4	12	16	Y	5	13	17	Y	6	14	18	N	22	14	10	Y	21	13	9	Y	20	12	8	N
	4	12	17	Y	5	13	18	Y	6	14	19	N	22	13	9	Y	21	12	8	N	20	11	7	N
	4	13	18	Y	5	14	19	N	6	15	20	N	22	13	8	Y	21	12	7	N	20	11	6	N
	4	13	19	Y	5	14	20	N	6	15	21	Y	22	12	7	N	21	11	6	N	20	10	5	Y
	4	14	20	N	5	15	21	Y	6	16	22	Y	22	12	6	N	21	11	5	Y	20	10	4	Y
	4	14	21	Y	5	15	22	Y	6	16	23	Y	22	11	5	Y	21	10	4	Y	20	9	3	N
	⋮	⋮	⋮	⋮	⋮	⋮	⋮	⋮	⋮	⋮	⋮	⋮	⋮	⋮	⋮	⋮	⋮	⋮	⋮	⋮	⋮	⋮	⋮	⋮
The proportion of combinations which trigger the momentum selector	5/6				4/6				3/6				4/6				3/6				2/6			

Hence Momentum Selector Efficiency = 21/36 = 0.583

Y If the combination triggers the momentum selector

N If the combination does not trigger the momentum selector

TABLE 4.4 THE CELL COMBINATIONS FOR A MUON MOMENTUM OF 200 GeV/c

200 GeV/c is 21/36 = 0.583. The efficiencies at other momenta are calculated in a similar way and are given in table 4.5.

4.4.3 THE MOMENTUM SELECTOR EFFICIENCY CORRECTED FOR WRONG CELLING, ENERGY LOSS, AND SCATTERING

In order to allow for the effects of wrong celling by the cell allocation logic and for multiple scattering and energy loss in the magnets, a computer program was used to simulate the paths of muons through the spectrograph. The program calculated the discharged flash-tube patterns in the momentum selector trays for each event. These patterns were then passed to a sub-program which simulated the cell allocation logic and gave the allocated cell for each pattern. These cells were then used to determine whether the event would have triggered the momentum selector. For each momentum, 10,000 trials were made and the results are shown in table 4.5. Good agreement is seen between the two methods of estimating the efficiency of the momentum selector. Wrong celling, multiple scattering and energy loss are seen to have very little effect on the result except at momenta close to the low energy cut-off.

4.4.4 THE MOMENTUM SELECTOR EFFICIENCY CORRECTED FOR THE EFFECT OF BURSTS

If a burst accompanies a muon from a magnet block in levels 3 or 1, extra cells may be allocated in the MST and the probability of the event triggering the momentum selector will be increased. This increase is not easily estimated as it not only depends upon the burst probability and distribution of burst size with momentum but it also depends upon the relative positions and angles of the trajectories of the burst electrons to that of the muon. Table 4.6 lists the thirty six significant cell combinations for muons of momentum 200 GeV/c.

DEFLECTION Δ CELLS	MOMENTUM p GeV/c	EFFICIENCY FROM CELL COMBINATIONS	EFFICIENCY FROM MONTE-CARLO PROGRAM
1	100	2.8 (1/36)	5.7
2	114	11.1 (4/36)	14.5
3	133	25.0 (9/36)	25.5
4	160	41.7 (15/36)	42.6
5	200	58.3 (21/36)	58.0
6	267	75.0 (27/36)	74.5
7	400	88.9 (32/36)	87.4
8	800	97.2 (35/36)	95.9

TABLE 4.5 THE EFFICIENCY OF THE MOMENTUM SELECTOR

LAYER	5	3	1	5	3	1	5	3	1
	4	6(0)	4(0)	5	7(0)	5(0)	6	8(1)	6(3)
	4	6(0)	5(0)	5	7(0)	6(0)	6	8(1)	7(2)
POSITIVE ZENITH ANGLES	4	7(0)	6(0)	5	8(1)	7(2)	6	9(2)	8(1)
ZENITH	4	7(0)	7(0)	5	8(1)	8(1)	6	9(0)	9(0)
ANGLES	4	8(1)	8(1)	5	9(0)	9(0)	6	10(0)	10(0)
	4	8(0)	9(0)	5	9(0)	10(0)	6	10(0)	11(0)
	22	20(0)	22(0)	21	19(0)	21(0)	20	18(1)	20(3)
	22	19(0)	21(0)	21	18(1)	20(3)	20	17(2)	19(2)
	22	19(0)	20(0)	21	18(1)	19(2)	20	17(2)	18(1)
	22	18(1)	19(2)	21	17(2)	18(1)	20	16(0)	17(0)
	22	18(1)	18(1)	21	17(0)	17(0)	20	16(0)	16(0)
	22	17(1)	17(0)	21	16(0)	16(0)	20	15(1)	15(4)

The figures in brackets refer to the distance of the nearest cell which must be selected for that combination to trigger the momentum selector.

The probabilities P_1^1, P_1^3,.....P_3^3 are deduced from this table as follows:

$P_1^1 = 6/15$ $P_2^1 = 5/15$ $P_3^1 = 3/15$ $P_4^1 = 1/15$

$P_1^3 = 11/15$ $P_2^3 = 4/15$ $P_3^3 = 0$ $P_4^3 = 0$

Where the number of combinations which do not trigger the momentum selector is 15

TABLE 4.6 THE 36 SIGNIFICANT CELL COMBINATIONS FOR A MUON OF 200 GeV/c AND THE CALCULATION OF THE PROBABILITIES P_1^1, P_1^3,.....P_3^3.

Also listed are the distances of the closest cells in levels 1 and 3 which need to be set for combinations to trigger the momentum selector. If these distances j and k, are both equal to zero then the combination will trigger the momentum selector. For example, for a momentum of 200 GeV/c and the cell combination c=6, b=9 and a=8 the momentum selector would only be triggered if cell b=7 or cell a=9 was allocated by a burst electron. Thus not only are adjacent cells important when considering burst electrons but sometimes a cell spaced 2 of 3 cells from the muon cell will cause the combination to trigger the momentum selector if it is set by a burst electron.

To estimate the effect of bursts, a method similar to that of Piggott (1975) has been used. A momentum selector tray front was superimposed on a measuring tray front. It was assumed that if more than half the area of a measuring tray flash-tube overlapped a momentum selector tray flash-tube then the latter flash-tube would have discharged assuming that the former had. Thus each measuring tray flash-tube had a particular momentum selector tray flash-tube assigned to it. A mask was then drawn on transparent film which could be placed over computer pictures of events, so that it was possible to determine which momentum selector tray flash-tubes would have discharged for a particular measuring tray flash-tube pattern. The mask was placed over all measuring tray 2 and tray 4 flash-tube patterns of a sample of 570 events. Trays 2 and 4 were selected because they are at the same relative position beneath the magnet blocks as are the momentum selector trays at levels 1 and 3. Thus bursts would have developed to the same extent. For each measuring tray, the number of cells allocated and their separation was determined. The probabilities that a cell is allocated at a separation of one cell-P_1 (adjacent), two cells-P_2 and

three cells-P_3 from the cell allocated by the muon were calculated to be 6.0 ±1.0%, 2.6 ±0.7% and 2.2 ±0.6% respectively.

If P_1^1, P_1^3, P_2^1, P_2^3, P_3^1, P_3^3 are the probabilities that an event of given momentum will pass the momentum selector if a cell is allocated at a separation of 1, 2 and 3 cells from the cell allocated by the muon at levels 1 and 3 respectively, (these probabilities are calculated from tables like 4.6) then the efficiency of the momentum selector, Effc, when corrected for bursts will be given approximately by equations 4.1 and 4.2. It is assumed that a burst will only occur

$$Effc = Eff + (1 - Eff) \times Pc \qquad (4.1)$$

$$Pc = P_1 \times (P_1^1 + P_1^3) + P_2 \times (P_2^1 + P_2^3) + P_3 \times (P_3^1 + P_3^3) \qquad (4.2)$$

in tray 1 or 3 separately and that only one extra cell is allocated in a tray at once. Also cells allocated at a separation of greater than three cells from that allocated by the muon have been neglected. The results of these calculations are shown in table 4.7. The quantity (1 - Eff) × Pc is plotted as a function of momentum in figure 4.9 and Effc is plotted as a function of momentum in figure 4.10.

4.5 THE EFFICIENCY OF THE MOMENTUM SELECTOR TRAYS

4.5.1 FACTORS AFFECTING THE MST EFFICIENCY

When a muon passes through a momentum selector tray, flash-tubes are discharged and depending on their pattern, a cell is usually allocated by the tray front electronics, (see chapter 3 for a more detailed description). As a cell is not always allocated after the passage of a muon through the tray, allowance has to be made for this in calculating the momentum selector efficiency. There are two reasons why a cell may not be allocated. The first one is the fact that the probability of a flash-tube discharging after the passage of a muon through its sensitive volume is less than unity. This means that

MOMENTUM GeV/c	MONTE CARLO Eff %	(1 - Eff) × Pc%	Effc
100	5.7	1.9	7.6
114	14.5	2.3	16.8
133	25.5	2.4	27.9
160	42.6	2.2	44.8
200	58.0	1.8	59.8
267	74.5	1.3	75.8
400	87.4	0.7	88.1
800	95.9	0.2	96.1

TABLE 4.7 THE MOMENTUM SELECTOR EFFICIENCY BURST CORRECTIONS

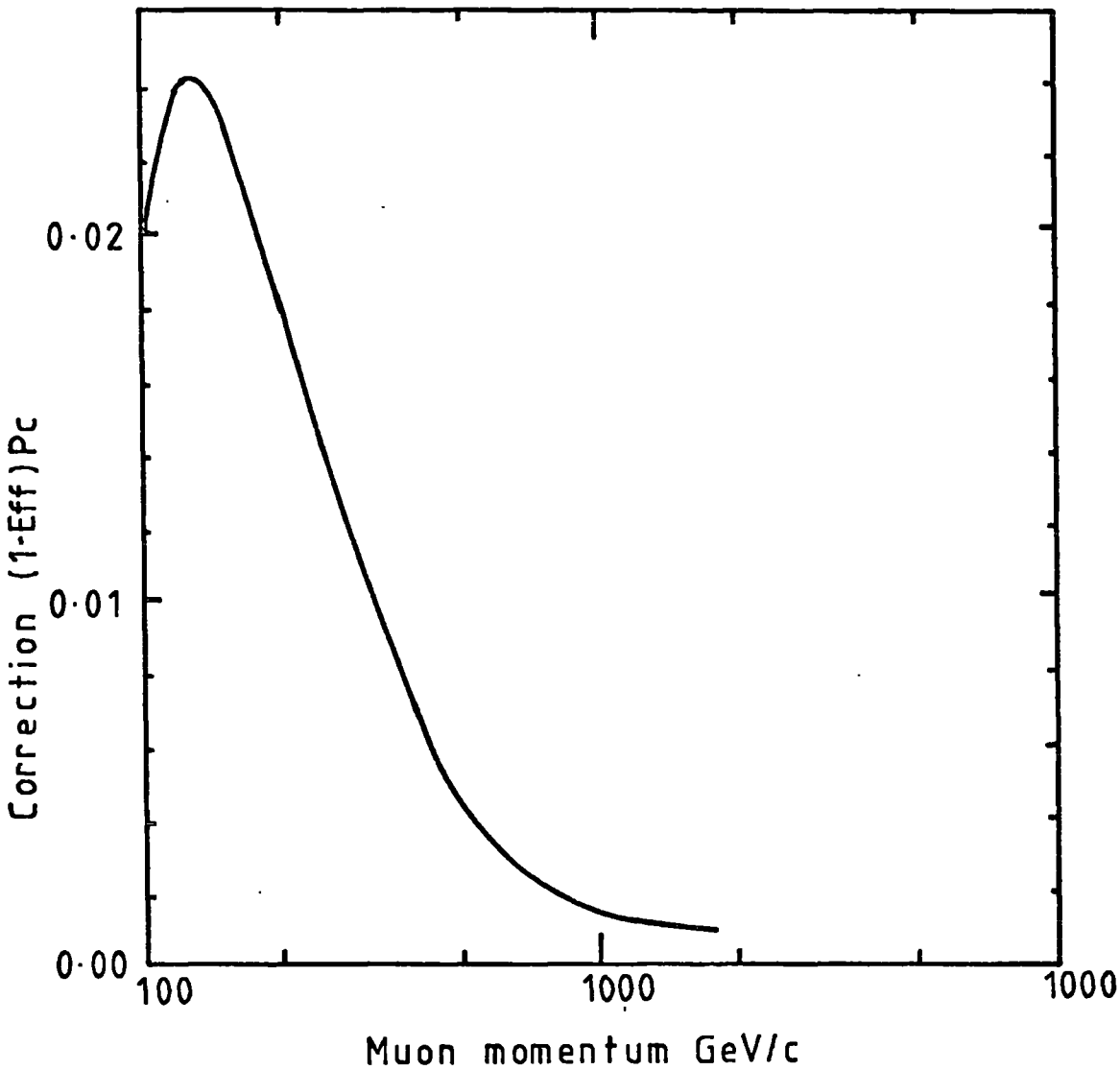

Figure 4.9 The correction to be added to the momentum selector efficiency as a result of bursts

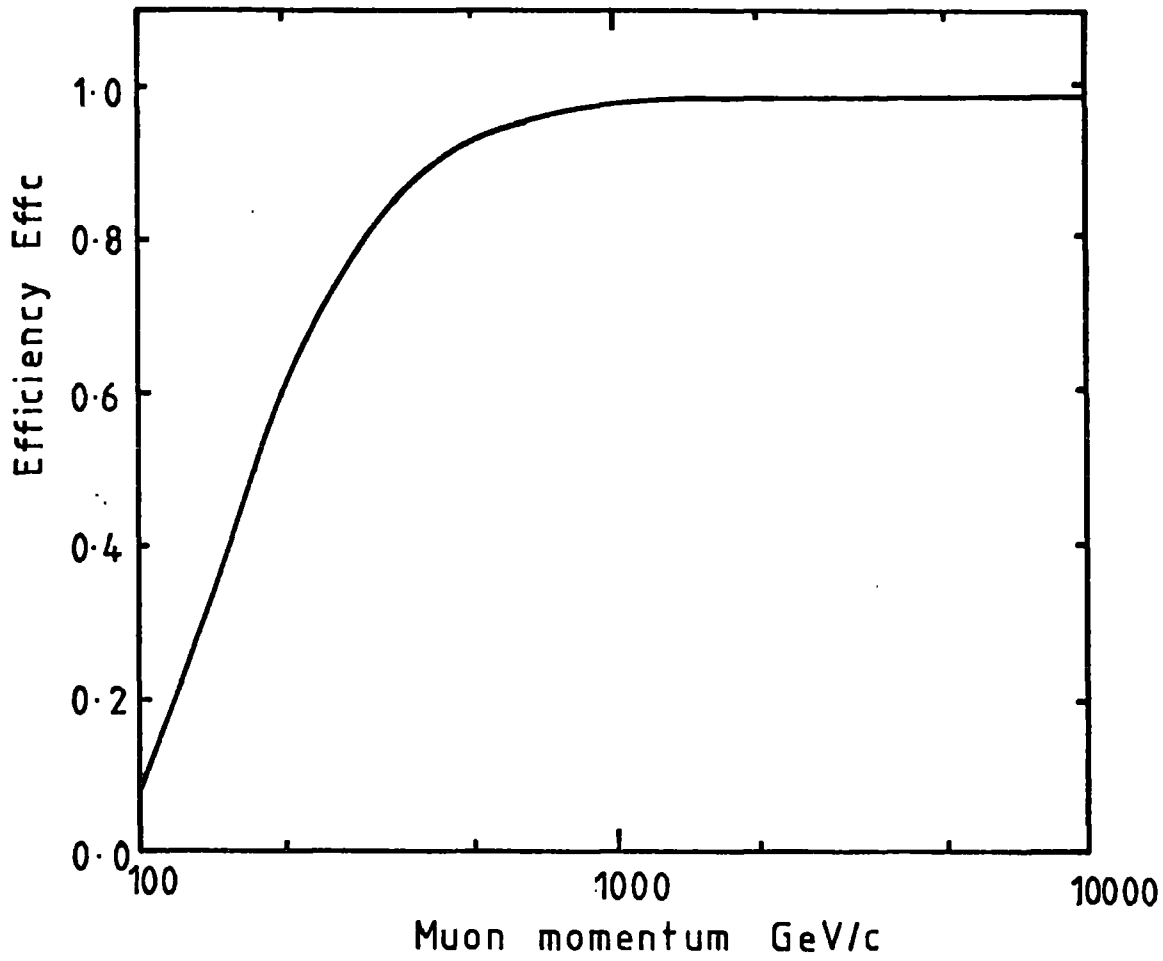

Figure 4.10 The momentum selector efficiency after correcting for bursts

insufficient flash-tubes may be discharged to allocate a cell. This effect is momentum independent and will lead to an overall decrease of the momentum selector efficiency.

The second reason for the non-allocation of a cell is that the cell allocation logic was not designed to be efficient for muons with large zenith angles. Figure 4.11, taken from Whalley (1974), shows the variation of the probability of a cell being allocated as a function of zenith angle, for flash-tubes of 100% efficiency. It can be seen that for zenith angles of interest in this work, i.e. ±7 degrees, the cell allocation probability is unity, and only the effect of flash-tube inefficiency needs considering when calculating the momentum selector tray efficiency.

4.5.2 MEASUREMENT OF THE FLASH-TUBE INEFFICIENCY

The probability of no cell being allocated by the three momentum selector trays was measured continuosly over the period of data collection for all events prior to momentum selection. This was done by using three scalers to count the number of times one or more cells were allocated in each of the momentum selector trays in a given time. Let these counts be N_c^1, N_c^3 and N_c^5. A fourth scaler counted the total number of events, N_t, in the same period. The probability of a cell being allocated in the momentum selector tray at each level is therefore given by $P_c^i = N_c^i/N_t$ with i = 1, 3 or 5. As this was done for all momenta P_c will include the effect of large zenith angles as well as flash-tube inefficiencies. Whalley (1974) has derived the relationship between flash-tube efficiency and the probability of no cell being allocated for the three momentum selector trays. His results are shown in figures 4.12a, b and c. The probability of zero celling is seen to be much less at level 3 compared with that at levels 1 and 5.

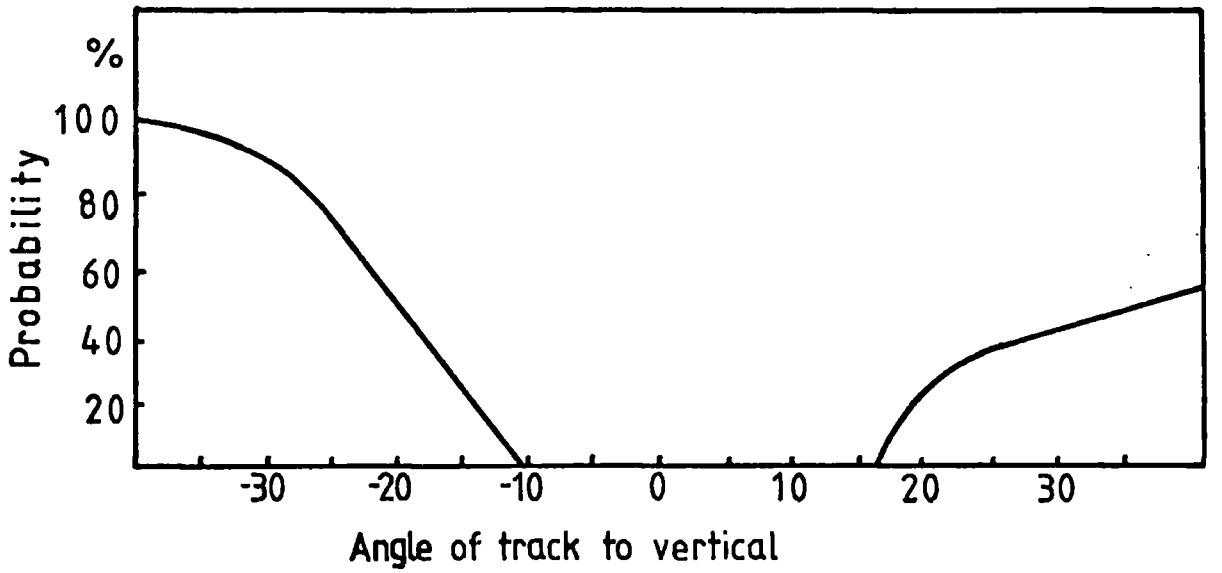

Figure 4.11 The percentage probability of no cells being set in the momentum selector tray as a function of angle of track (Whalley 1974)

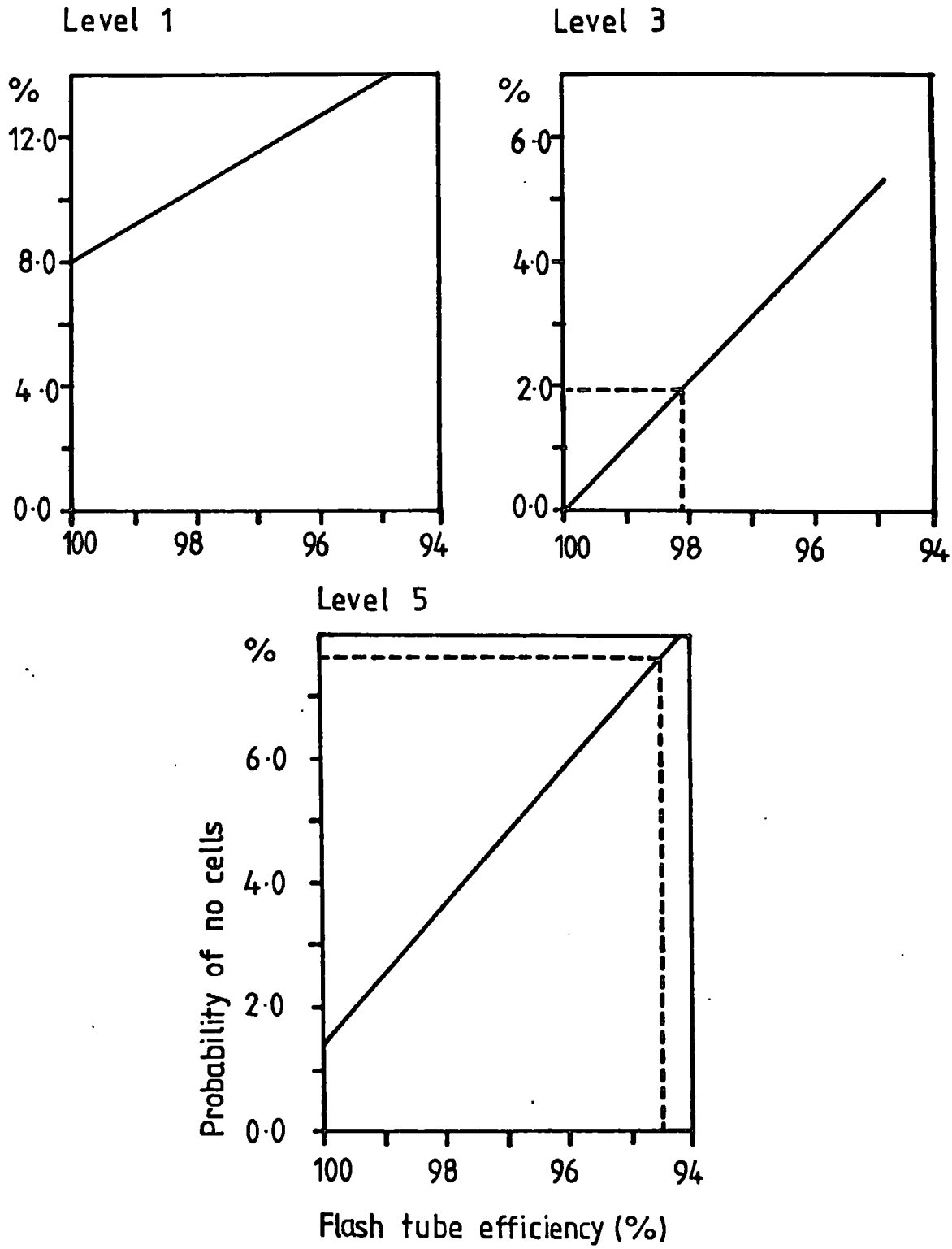

Figure 4.12 The probability that no cell is allocated, plotted as a function of flash-tube efficiency

After Whalley (1974)

This is because the range of zenith angles at level 3 is much smaller than at levels 1 and 5 due to the fact that the only way muons of low momenta can be accepted by the spectrograph is to have large incident and exit zenith angles and consequently small zenith angles at level 3.

The measured values of P_c^i and the corresponding flash-tube efficiencies Eft^i which have been obtained from figures 4.12a, b and c are given in table 4.8.

LEVEL	$(1 - P_c^i)\%$	$Eft^i\%$
1	7.31 ±0.01	100.0 ±0.5
3	1.92 ±0.01	98.1 ±0.5
5	7.61 ±0.01	94.5 ±0.5

TABLE 4.8 THE CELL ALLOCATION PROBABILITIES P_c^i AND THE CORRESPONDING FLASH-TUBE EFFICIENCIES Eft^i AT LEVELS i =1, 3 AND 5

4.5.3 THE CORRECTION TO THE MOMENTUM SELECTOR EFFICIENCY

It has been shown that the efficiency of the momentum selector trays at high momenta is only dependent upon the flash-tube efficiency. The measured flash-tube efficiencies shown in table 4.8 were incorporated into the Monte Carlo program used to calculate the momentum selector efficiency. If a muon passed through a flash-tube, a random number in the range 0 - 1 was generated and if it was greater than the flash-tube efficiency of that tray it was not allowed to discharge. The program, modified in this way, was used to recalculate the momentum selector efficiency for a range of momenta. The ratio of momentum selector efficiency with inefficient flash-tubes to that with 100% efficient

flash-tubes has the value 0.913 ±0.001. This is therefore the overall momentum selector tray efficiency which must be used to calculate the absolute height of the spectrum.

4.6 THE SCINTILLATION COUNTER EFFICIENCIES

When a muon passes through all three scintillation counters a pulse is generated at the output of the three-fold coincidence unit to which they are connected. This pulse is used to trigger the momentum selector and data storage system of MARS. Therefore to obtain an absolute measurement of the muon flux it is necessary to know how efficient the scintillation counters are in detecting muons. This is measured by means of an auxilliary, small area (29cm × 59cm) scintillation counter called a telescope. This is placed directly above the scintillation counter under test as shown in figure 4.13 for level 3. A four-fold coincidence unit coupled to a scaler counts how many times a muon is detected coincidentally in SC1, SC3, T and SC5 in a given time, while a three-fold coincidence unit coupled to a scaler counts how many times a muon is detected coincidentally in SC1, T and SC5 in the same time period. (SC1, SC3, SC5 and T refer to the scintillation counters at levels 1, 3 and 5 and to the telescope respectively). Assuming that any muon which passes through the telescope will also pass through SC3, then the inefficiency of SC3 is given by equation 4.3, where N_3 and N_4

$$I_3 = \frac{N_3 - N_4}{N_3} \pm \frac{I_3}{\sqrt{N_3 - N_4}} \qquad (4.3)$$

are the number of three-fold and four-fold coincidences in a given time.

The size of the telescope is small enough to permit four measurements over separate regions of the MARS scintillation counters SC1, SC3, and SC5. These measurements have been averaged with equal weight for SC1 and SC5, but for level 3 the measurements have been

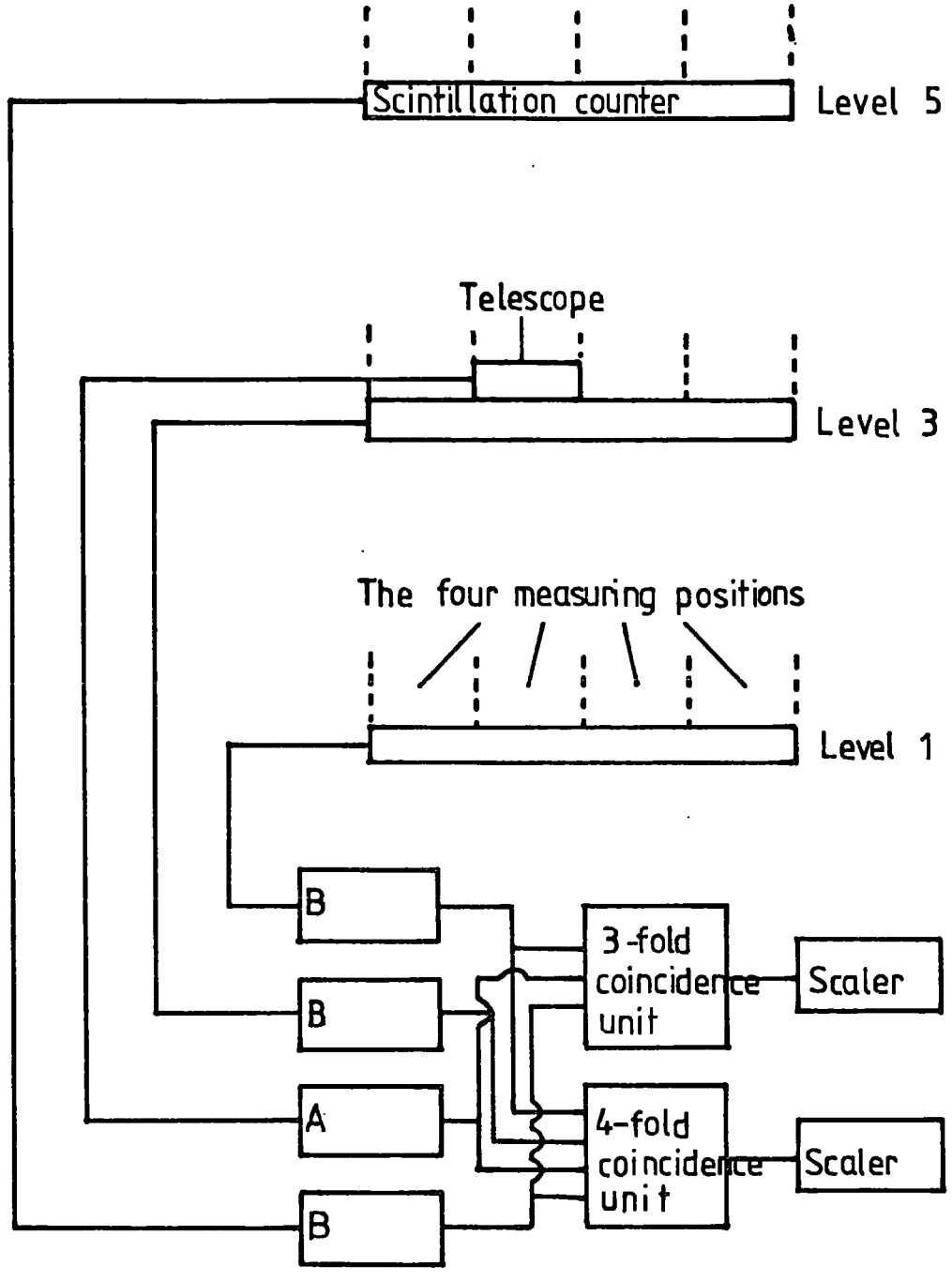

A - amplifier and discriminator

B - circuit of figure 2.6 (Up to main 3-fold coincidence unit)

Figure 4.13 Diagram showing apparatus for measuring the scintillation counter efficiencies

weighted towards the centre of the scintillation counter as a greater proportion of the muons pass through here. The discriminator settings on SC1, SC3 and SC5 were left as they were during data collection.

Experiments similar to the one described above were performed by Whalley (1974) and Piggott (1975) before data collection for the present experiment began. Their results are summerised in table 4.9 along with those for the present experiment which was performed at the end of data collection.

	EFFICIENCY %			
	LEVEL 1	LEVEL 3	LEVEL 5	OVERALL
M. R. W.	98.02 ±0.08	99.22 ±0.05	91.90 ±0.14	89.4 ±0.2
J. L. P.	99.10 ±0.4	96.80 ±0.3	92.70 ±0.3	88.9 ±0.6
PRESENT RESULTS	90.20 ±0.2	91.70 ±0.2	87.60 ±0.2	72.4 ±0.3

TABLE 4.9 THE MEASURED EFFICIENCY OF THE SCINTILLATION COUNTERS

It is apparent that the efficiency of the scintillation counters has deteriorated over the period of the experiment. However, this may be expected when it is realised that SC3 and SC5 are subjected to the heating effect of the magnetic field coils below.

It can be seen from table 4.9 that the efficiency of the scintillation counters at the end of data collection was approximately 81% of the efficiency before data collection. This compares well with the observed decrease in the rate of three-fold coincidences of SC1,

SC3 and SC5 of approximately 84% over the same period. This three-fold rate was observed to fall approximately linearly with time, as shown in figure 4.14. Thus the scintillation counter efficiency used in computation of the absolute intensity of muons is the mean of the efficiencies before and after data collection, i.e. 80.5 ±0.2%.

4.7 THE ENERGY LOSS AND MAGNET GAP CORRECTIONS

In the analysis technique described in Chapter 3, it is assumed that the spectrograph has one continuous magnet and that the energy loss of the muons is zero. The first assumption means that the magnetic path length, $\int B.dl$, and hence the muon momentum are overestimated. The ratio of the true momentum to the measured momentum is practically constant and equal to 0.7972 for momenta above 100 GeV/c when the incident zenith angle is zero and all five trays have been used in the analysis. For zenith angles up to 6 degrees the ratio changes by less than 1.3%.

All calculated momenta are multiplied by 0.7972 so that for events with less than five usable trays, an additional correction is needed. This is because the effect of the gaps between the magnets is different for other tray combinations. Also, a correction for energy loss is needed for all events. Wells (1972) calculated these corrections using a computer simulation of muons passing through the spectrograph. The energy loss equations of Sternheimer and Peierls (1971) together with corrections for pair production, bremsstrahlung and nuclear interations were used. Table 4.10 summarises the results of Wells. The corrections for zenith angles of +6 degrees and -6 degrees have been averaged and the corrections for some tray combinations are so similar that they too have been averaged. A fit of the form $Cr = a_0 + a_1 \ln p + a_2(\ln p)^2 + a_3(\ln p)^3 + a_4(\ln p)^4$, where p GeV/c is the muon momentum and Cr GeV/c is the correction, was used to interpolate

Figure 4.14 The variation of the blue side 3-fold coincidence rate with time over the period of the experiment

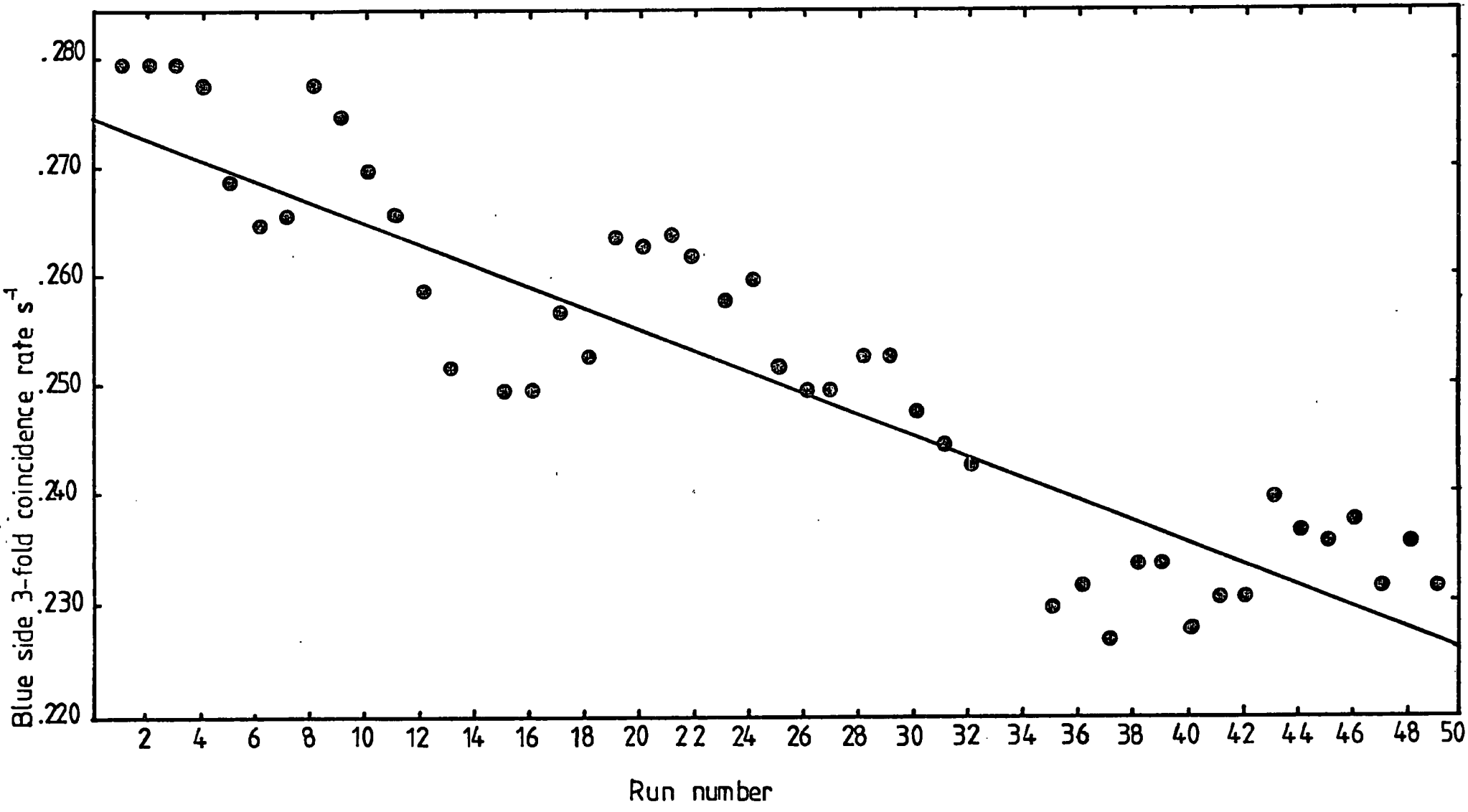

between momenta, and a linear interpolation was used to calculate the correction for angles between 0 and 6 degrees. The relative corrections to the calculated momenta are seen to be small, so any errors caused by these interpolations will have a small effect on the final result.

MOMENTUM GeV/c	ZENITH ANGLE°	TRAY COMBINATION								
		12345	2345 1234 135	1345 1235	1245 245 145 125 124	345	235	234	134	123
100	0	4.4	3.0	4.0	6.0	8.9	-1.1	-6.5	1.2	13.8
200	0	4.4	1.8	3.5	7.8	15.7	-6.0	-17.7	-2.8	21.7
500	0	4.5	-2.1	2.1	13.2	36.1	-20.5	-51.3	-14.9	45.5
1000	0	4.5	-8.7	-0.2	22.1	70.1	-44.9	-107.0	-35.2	85.1
5000	0	4.4	-61.9	-19.4	93.3	342.0	-240.0	-557.0	-198.0	401.0
100	±6	6.0	4.7	5.6	7.6	10.4	0.6	-4.7	2.9	15.3
200	±6	7.6	5.0	6.7	11.0	18.7	-2.6	-14.1	0.6	24.7
500	±6	12.6	6.1	10.2	21.0	43.7	-12.0	-42.2	-6.4	53.0
1000	±6	20.8	7.7	16.2	37.2	85.4	-27.8	-89.4	-18.2	100.2
5000	±6	86.1	20.7	62.6	173.5	418.0	-154.5	-466.5	-112.5	476.0

TABLE 4.10 THE CORRECTIONS TO BE ADDED TO THE COMPUTED MOMENTA

CHAPTER 5

THE SPECTRUM DEPENDENT CORRECTIONS

5.1 INTRODUCTION

To estimate the sea-level muon momentum spectrum, it is necessary to correct the measured spectrum for instrumental effects and experimental biases. Some of these have been dealt with in the previous chapter. Those to be described in this chapter are multiple Coulomb scattering of the muon in the magnet blocks and the error of trajectory location. The corrections arising from these two effects are characterised by their dependence upon the shape of the spectrum which is being measured. Therefore they cannot be calculated exactly.

In the front plane of the spectrograph, in which the muons are deflected, horizontal deflections caused by multiple scattering and trajectory location errors are symmetrically placed either side of the deflection caused by magnetic bending. Therefore, when calculating the corrections to the spectum, it is preferable to work in terms of inverse momentum, which is proportional to the deflection. If the momentum spectum is $N(p) = Ap^{-\gamma}$ and $d = 1/p$ (for convenience d will be called the deflection) then the deflection spectrum is given by

$$N(d) = N(p) \frac{dp}{dd}$$

$$= Ap^{-\gamma} \frac{1}{d^2}$$

$$= A' d^{\gamma-2}$$

Therefore, a deflection spectrum can be derived from a momentum spectrum simply by multiplying by the square of the momentum.

5.2 THE METHOD OF CALCULATING THE CORRECTIONS

If N(d) is the true deflection spectrum and R(d) is the resolution

function of the spectrograph, then the measured deflection spectrum is given by the convolution integral below

$$M(d) = \int N(d') R(d-d') dd'$$

and the corrections for multiple scattering and track location errors are

$$C(d) = M(d)/N(d)$$

The resolution function is defined as the response of the spectrograph to a beam of mono-energetic muons. R(d) is assumed to be a Gaussian distribution whose standard deviation is dependent upon the magnitude of the multiple scattering in the magnet blocks and on the trajectory location errors. The calculation of R(d) will be considered later in this chapter.

The corrections C(d) cannot be evaluated exactly because they depend upon the true spectrum N(d), which is being measured. Therefore, an initial value of N(d) is assumed. It is called a trial deflection spectrum, $N_o(d)$, and is a close approximation to the true spectrum. This is used to evaluate the convolution integral and hence calculate a first estimate of the corrections, $C_1(d)$, as shown below

$$M_1(d) = \int N_o(d') R(d-d') dd'$$

and $$C_1(d) = M_1(d)/N_o(d)$$

The corrections, $C_1(d)$, are then used to obtain a new estimate of the trial deflection spectrum, $N_1(d) = M(d)/C_1(d)$, which is then used to recalculate the corrections as shown below.

$$M_2(d) = \int N_1(d') R(d-d') dd'$$

and $$C_2(d) = M_2(d)/N_1(d)$$

and $$N_2(d) = M(d)/C_2(d)$$

This process can be repeated until the relative difference between successive estimates of the corrections becomes small. However, as the number of iterations increases, large errors may be

introduced into the result (Cooper 1977). These errors arise because of the fact that M(d) and R(d), to a lesser extent, contain noise. This noise leads to large variations in the high frequency terms of the Fourier transforms of M(d) and R(d), and as the number of iterations increases, the effect of these high frequency terms also increases. Thus, the best results are obtained if the number of iterations is kept small, and in this case only two have been made. Therefore the corrections $C_2(d)$ have been used to correct the measured spectrum.

5.3 THE TRIAL DEFLECTION SPECTRUM

The trial deflection spectrum depends upon the number of trays used in the analysis of the data, and on the momentum selector efficiency. This is because the five, four and three tray fit (or 5TF, 4TF and 3TF for short) spectra have different shapes because of the increasing production of bursts with momentum. This leads to a steepening of the 5TF spectrum, due to the loss of trays containing bursts, and a corresponding flattening of the 3TF and 4TF spectra. The momentum selector efficiency is important because it governs the spectrum of muons which pass through the spectrograph and causes the spectrum to be attenuated at low momentum compared to the true spectrum.

Three trial deflection spectra N_0^5, N_0^4 and N_0^3 are therefore required to calculate the corrections C^5, C^4 and C^3 to be applied to the 5, 4 and 3 tray fit spectra respectively. The first estimates of these spectra were calculated using the following formula:

$$N_0^i(d) = Nt(d) \times Effc \times Pi, \qquad \text{for } i = 3, 4 \text{ and } 5$$

where Effc is the momentum selector efficiency calculated in section 4.4, Pi is the probability of an event having i = 3, 4 or 5 usable trays and Nt(d) is calculated from equation 5.1 .

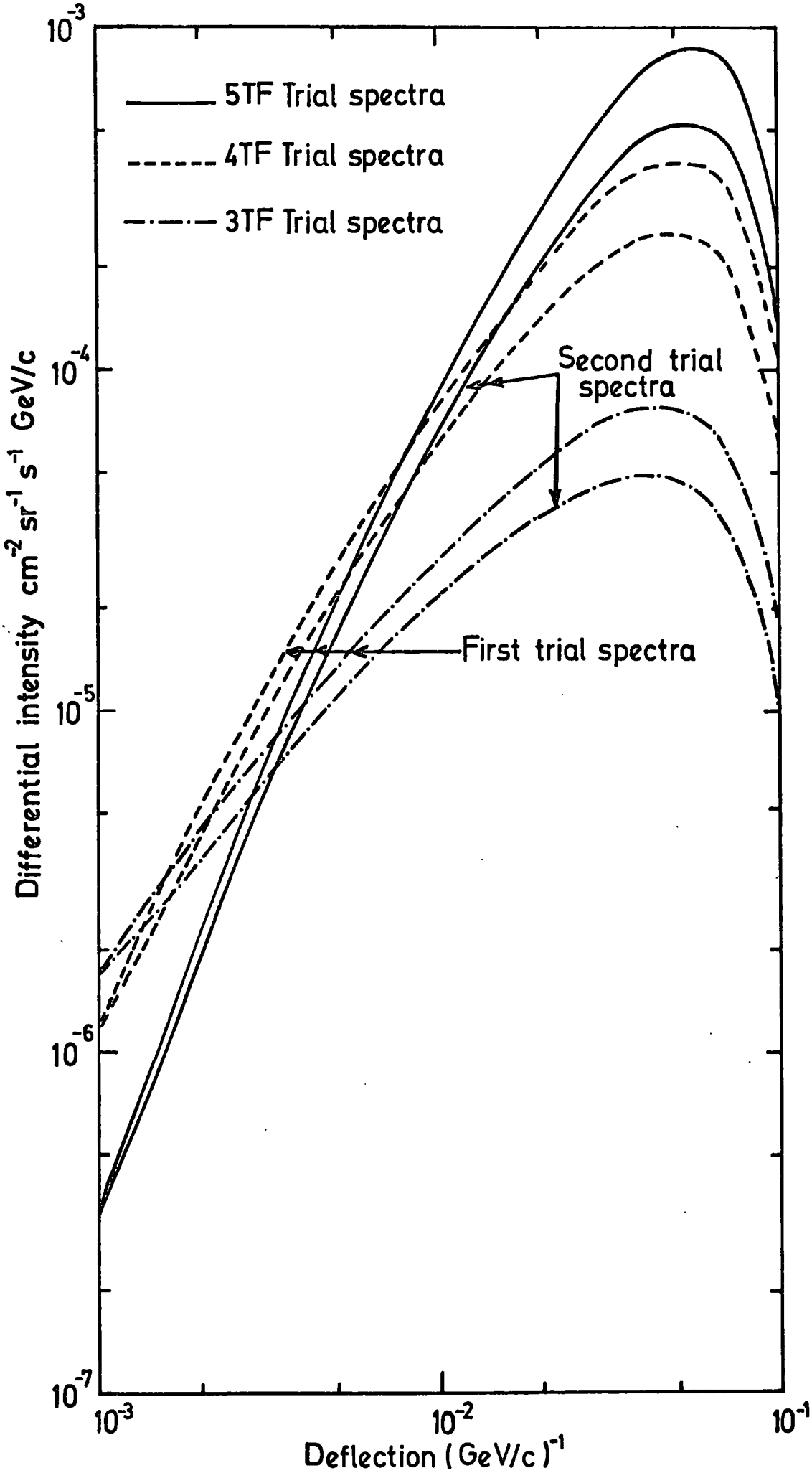

Figure 5.1 The trial deflection spectra

$$Nt(p) = \frac{Ap^{-\gamma}}{(1 + p/90)} \qquad (5.1)$$

This equation is derived from a simple model, developed by Barrett (1952) and Bull (1965), of the diffusion of cosmic rays through the atmosphere. It assumes a production spectrum of pions with a constant exponent γ. Thompson (1973) derived a value of $\gamma = 2.67 \pm 0.02$ from a fit to the magnetic spectrograph data of Appleton et al (1971), Nandi and Sinha (1972) and Allkofer (1971) whose measurements extend from approximately 1 to 1000 GeV/c. This value has been used to calculate the trial deflection spectra.

The probabilities, P_3, P_4 and P_5, of an event having 3, 4 or 5 usable trays are given in equations 5.2, 5.3 and 5.4.

$$P_5 = (1 - P)^4 \ (1 - P^t) \qquad (5.2)$$

$$P_4 = 4P(1 - P)^3 \ (1 - P^t) + (1 - P)^4 \ P^t \qquad (5.3)$$

$$P_3 = 6P^2(1 - P)^2 \ (1 - P^t) + 4PP^t(1 - P)^3 \qquad (5.4)$$

P and P^t are the probabilities that a tray at level 1, 2, 3 or 4 or a tray at level 5 are not used in the analysis. These probabilities are given by:

$$P = P_B + (1 - P_B) \ P_o$$

$$P^t = P_B^t + (1 - P_B^t) \ P_o$$

P_B and P_B^t are the probabilities that a tray at level 1, 2, 3, 4 or a tray at level 5 contains a burst and P_o is the probability that a tray is not used because of flash-tube inefficiencies and/or knock-on electrons.

The variation of the probability of a burst of electrons being produced when a muon passes through one of the magnet blocks as a function of momentum is shown in Figure 5.2. (Said 1966 and Hansen 1976). The two theoretical curves agree will in shape and show a strong increase in burst probability with momentum. The difference

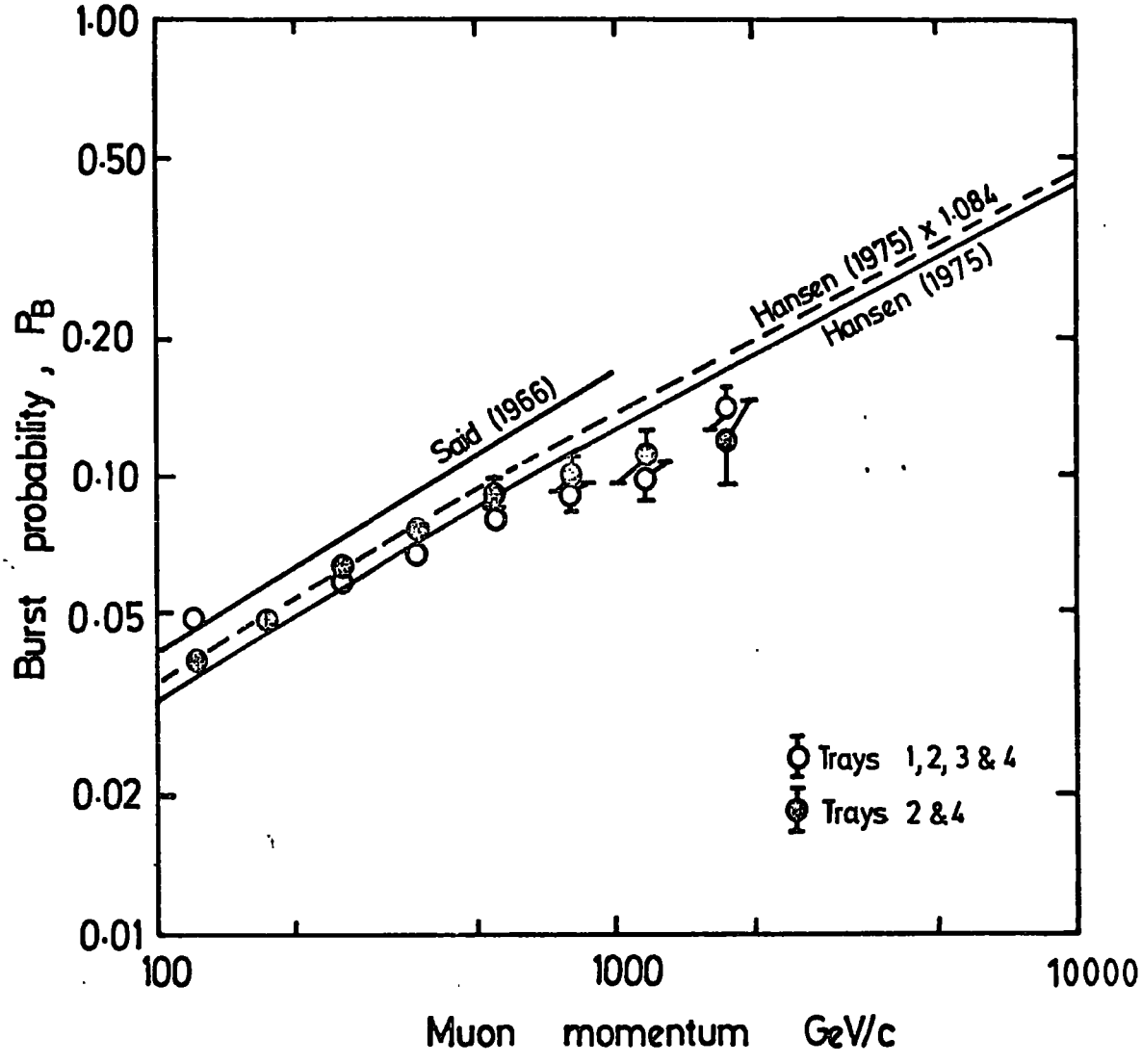

Figure 5.2 The probability of a burst accompanying a muon from a magnet block as a function of muon momentum

in their heights is due to the fact that Said assumed an electron detection threshold of 3 MeV whereas Hansen assumed one of 7 MeV. Also plotted on this figure are the burst probabilities derived from the experimental data. The points which include trays 1 and 3 show a systematic increase for momenta <150 GeV/c due to their pre-selection by the momentum selector. The data from trays 2 and 4 are independent of the momentum selector and they agree well in shape with the theoretical curves up to about 700 GeV/c. Above 1000 GeV/c the experimental points tend to flatten in comparison with the theoretical curves. This is thought to be a resolution effect caused by the low maximum detectable momentum of 4 and 3 tray fit events. The dotted line in figure 5.2 is a best fit through the data for trays 2 and 4 for momenta between 100 GeV/c and 1000 GeV/c and is 8.4% higher than the theoretical curve of Hansen. Therefore, the burst probability, P_B, has been made equal to the theoretical probability of Hansen (1976) multiplied by 1.084 to bring it into agreement with the measured burst probability between 100 and 700 GeV/c from the present data.

The burst probability for tray 5, P_B^t, has been measured from the collected data and is shown in figure 5.3 as a function of momentum. It has a weighted mean of 1.23 ±0.07% for the momentum range 100 -1000 GeV/c. The slight increase of this probability with momentum has been ignored.

The variation of the probability P_o, of losing a tray because of tube inefficiencies and/or knock-on electrons has also been derived from the experimental data and is given in figure 5.3. Theoretically, this should not be dependent upon momentum (Said 1966) and this is seen to be true up to about 1000 GeV/c. For momenta greater than this, however, P_o rises sharply. This is thought to be a resolution effect

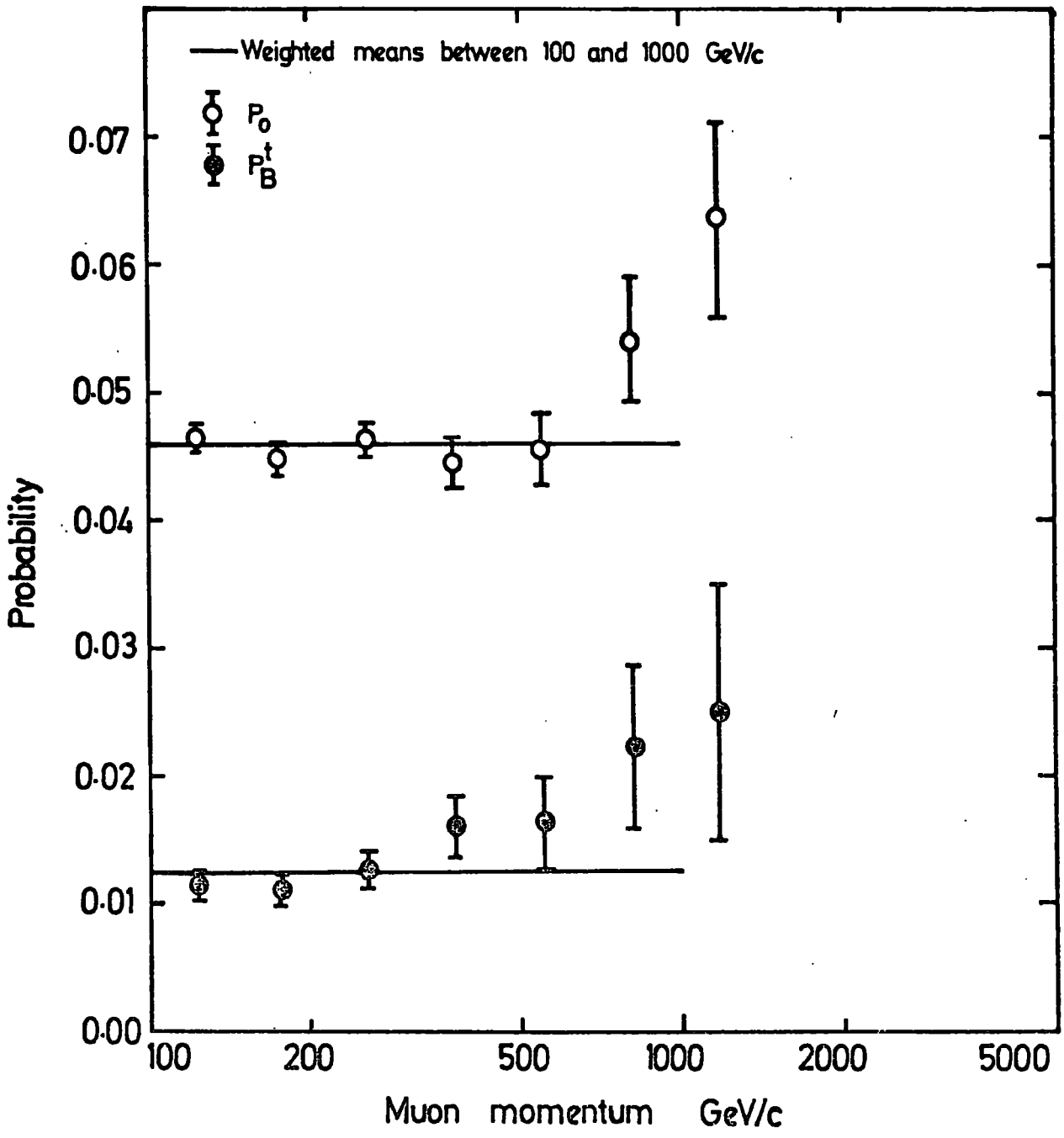

Figure 5.3 The experimentally observed variation of P_0 and P_B^t with momentum

caused by the low maximum detectable momentum of 3TF and 4TF events. The weighted mean value of P_o over the momentum range 100 - 1000 GeV/c is 4.60 ±0.06%. This has been used in the calculations of P_3, P_4 and P_5.

Figure 5.4 shows the variation of $P_n/(P_3 + P_4 + P_5)$, for n = 3, 4 and 5, with momentum. For comparison, the value of $N_n/(N_3 + N_4 + N_5)$, where N_n for n = 3, 4 or 5 is the number of 3TF, 4TF or 5TF events, has been calculated from the analysed data in the 'pass' category and plotted on the same figure. Good agreement is seen between the theoretical and experimental values, therefore giving confidence in the use of equations 5.2, 5.3 and 5.4 to calculate the trial deflection spectra.

The trial deflection spectra calculated in the way described above are shown in figure 5.1 and labelled 'first trial spectra'. The spectra are seen to increase in intensity as deflection increases until about 5.0×10^{-2} GeV/c^{-1} where they begin to fall because of the decreasing efficiency of the momentum selector. As expected, the 5TF spectrum is steeper than the 4TF spectrum which in turn, is steeper than the 3TF spectrum. Therefore, the track location errors and multiple scattering will have least effect on the 3TF spectrum. However, as the track location errors are greatest for the 3TF data (because fewer trays are used in their analysis) this will tend to have a counter-effect on the magnitude of the 3TF corrections.

Following the method of section 5.2, second estimates of the trial deflection spectra have been derived from the first trial spectra. These second trial spectra are also shown in figure 5.1 where it will be seen that at small deflections, where it is most important, the two sets of spectra are very similar, the second estimates being slightly flatter than the first. At large deflections, the spectra diverge most,

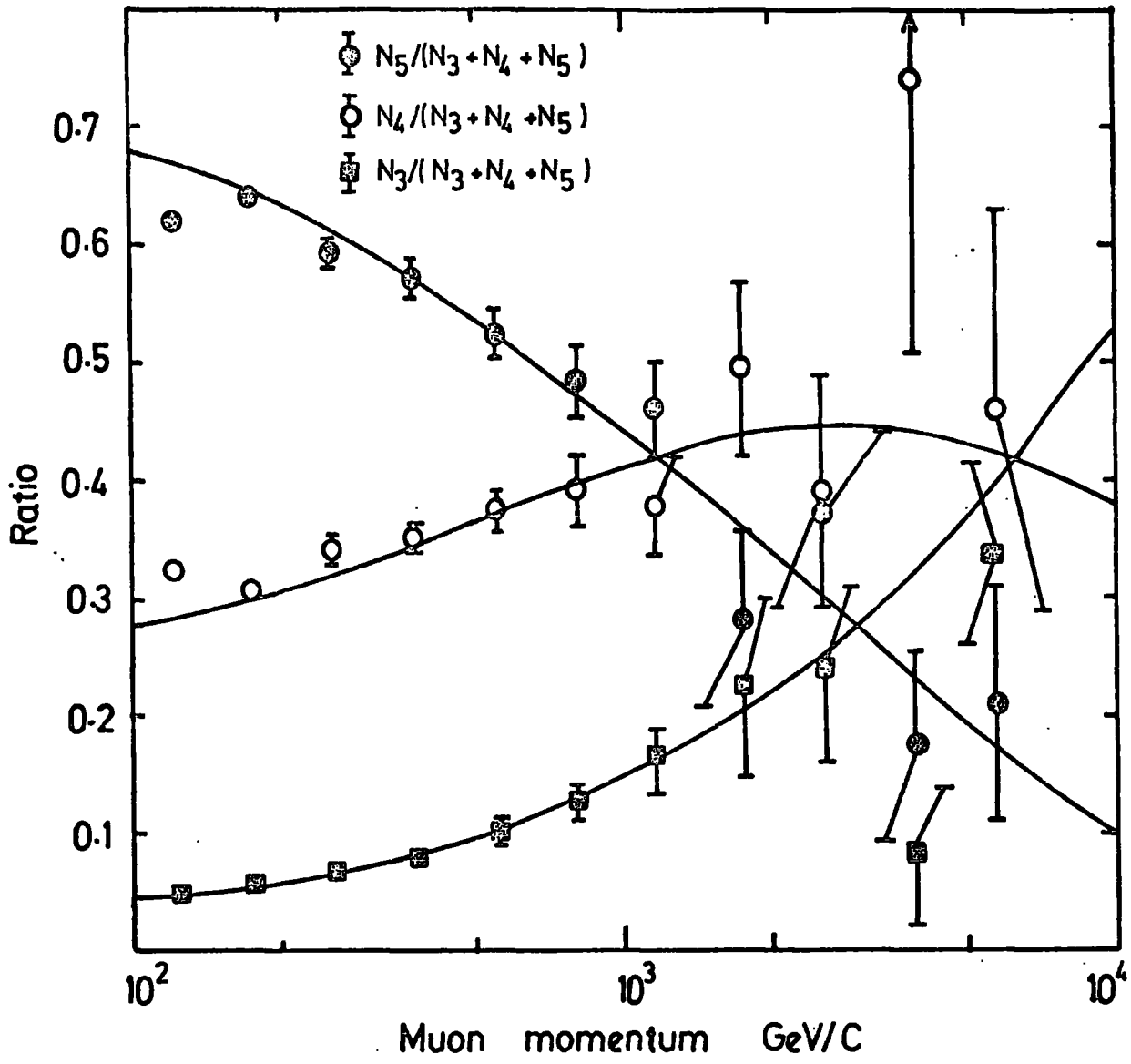

Figure 5.4 The ratio of the number of events with a given number of trays to the total number of events as a function of momentum. The points are observed values and the lines are based upon equations 5·2, 5·3 and 5;4.

but this is considered unimportant as here the corrections are small. The corrections which have been derived from these spectra are presented in section 5.6.

5.4 THE ERRORS IN TRAJECTORY LOCATION AND THE MAXIMUM DETECTABLE MOMENTUM OF MARS

5.4.1 INTRODUCTION

The maximum detectable momentum (or MDM for short) of the spectrograph is defined as the momentum at which the relative error on the momentum is unity. If Δp is the error on the momentum and p_{MDM} is the MDM then

$$\frac{\Delta p}{p} = \frac{p}{p_{MDM}} \tag{5.5}$$

or in terms of d,

$$\Delta d = 1/p_{MDM} \tag{5.6}$$

The error in momentum determination has two important effects on the momentum spectrum. Firstly, the spectum is flattened at high momenta, i.e. at momenta comparable to the MDM. Secondly, the charge ratio of muons approaches unity for momenta greater than the MDM, (for an explanation see chapter 7).

The flattening at high momenta is due to the fact that the spectrum falls steeply with momentum. Therefore more muons of low momentum are wrongly assigned to high momentum cells than are of high momentum to low momentum cells.

From the above considerations, it is apparent that to have any confidence in the data at high momenta, it is necessary to know the maximum detectable momentum as precisely as possible and to know how the errors in momentum measurement effect the shape of the spectum. Two approaches are then possible. One is to reject all the data which has an apparent momentum greater than the MDM. The other is to correct the spectrum up to momenta equal to and even greater than the MDM.

The second approach has been adopted here as it is considered wasteful to reject data without any consideration being given to them, and in any case, data with momenta less than the MDM should be corrected for the error in momentum determination.

5.4.2 THE CALCULATION OF THE MDM

There are two interrelated methods of calculating the MDM of the spectrograph. One of them is to directly consider the track location errors and use a method similar to that of Allkofer et al (1971(b)).

Assuming that the errors in track location of the five measuring trays are independent and all equal then it was shown by Wells (1972) that the MDM is given by

$$MDM = \frac{0.03\ B\ H}{2\ l\ F(x)\ \sigma n}$$

where B is magnetic field strength.

H is the total length of the magnets.

l is the height of the spectrograph.

F(x) is a function depending upon the geometry of the spectrograph and the number of trays used in the analysis.

σn is the standard deviation of the track location error.

The track location error is defined as $\Delta y = (y_R - y_C)$, where y_R is the true co-ordinate of the muon at a measuring level and y_C is the co-ordinate of the centre of the channel defined by the analysis program. The standard deviation of the track location error has been estimated using a Monte Carlo technique by Piggott (1975). Muon tracks in the zenith angular range $\pm 7°$ were simulated in a measuring tray and the patterns of discharged flash-tubes were obtained. Channels were defined through the flash-tube patterns using the same technique as the analysis program and the true muon co-ordinate was compared to the

co-ordinate defined by the channel. For 100% efficient flash-tubes σn had a value of 3.04×10^{-4} m giving an MDM of 5300 GeV/c. When flash-tube inefficiencies were considered, σn had a mean value of 5.80×10^{-4} m giving a reduced MDM of 2800 GeV/c.

However, there are two main limitations to this method. Firstly, the error in track location σn is not the same in each tray. This can be seen from table 3.2 which shows the mean tube density for each tray. Tray 3 is the least efficient tray having 4.31 ±0.01 tubes per track on average. Thus, tray 3 can be expected to have the worst track location error. Secondly, the track location errors are not totally independent. This is due to the fact that the analysis program employs a two stage process for finding the co-ordinates of the muon, see section 3.4. In the first stage the co-ordinates are defined in terms of the discharged flash-tubes in each tray and here the errors can be considered independent. However, in the second stage, the program uses the angle of the parabola in each tray as extra information in redefining the co-ordinates. As the parabola is based on a fit to the co-ordinates in all the trays, the errors in trajectory location at the second stage cannot be considered independent.

The alternative but related method of finding the MDM of the spectrograph is to simulate the paths of muons of infinite momentum through the spectrograph. The muon trajectories will be straight and they will not suffer from the effects of multiple scattering. When these events are analysed, the only contribution to the error in momentum is from the trajectory location errors, which arise in the measuring trays, and through the method of analysis. These errors will be symmetrically placed about the true paths of the muons and, as inverse momentum is proportional to deflection, they will also be

symetrical in inverse momentum. Therefore the distribution of inverse momentum from the analysed events will be the resolution fuction R(d) and from equation 5.6 the MDM is equal to the inverse of its standard deviation.

This is the method used in the present work to find the MDM of MARS. It has the advantage that no assumptions are made regarding the independence and size of the track location errors and it is possible to accurately include the contribution from the analysis program to the measuring errors.

5.4.3 THE SIMULATION PROGRAM

The paths of muons of infinite momentum were simulated by means of a Monte Carlo program. Muon trajectories were accepted if they were within the acceptance of the spectrograph as defined by the scintillation counters. The zenith angular distribution of muons was assumed to be flat over the $\pm 7^{\circ}$ angular acceptance of the spectrograph. The patterns of discharged flash-tubes at each level were calculated and the layer efficiencies given in table 3.2 were used to give the probability that a flash-tube would discharge on the passage of a muon through its sensitive volume. The production of knock-on electrons and spurious tubes was simulated in flash-tube layers in which the muon passed through a gap. The probability of this occuring is given by Wells (1972) as 0.0672 ± 0.094.

One of the most important features of the simulation program is that it generates an output file containing details of which flash-tubes discharged for each event, in the same format as the data file for the real events. Therefore the analysis program of chapter 3 can be used to analyse the simulated events, and any biases which it introduces will be automatically included.

A file of 10,000 infinite momentum events was generated and analysed, and the resulting inverse momentum distribution for all 5TF

events is shown in figure 5.5. It has a mean of $-5(\pm4) \times10^{-6}$ $(GeV/c)^{-1}$ a standard deviation, σ_{dn}, of $3.76(\pm0.03) \times10^{-4}$ $(GeV/c)^{-1}$, a skewness 0.019 ±0.027 and a kurtosis of 4.14 ±0.05. The distribution is therefore seen to be symmetrical about a mean of zero. However its kurtosis is significantly greater than 3, which is the kurtosis of a Gaussian distribution.

The corrections to the spectrum are to be calculated assuming that the inverse momentum distribution is Gaussian in shape. Therefore it is necessary to know the error in doing this. The corrections C(d) were calculated in two ways. Firstly by assuming that R(d), i.e. the inverse momentum distribution, was Gaussian with a standard deviation of 3.76×10^{-4} $(GeV/c)^{-1}$. Secondly by fitting a function to the inverse momentum distribution using a least squares minimising technique. This function was simply the sum of two Gaussian distrubutions of differing standard deviations and with unequal weights. This had a much better fit than the first case. The differences in the corrections were less than 1% for all momenta less than 5000 GeV/c and less than 0.1% for all momenta less than 1000 GeV/c. Therefore it is considered that the error introduced into the spectrum by assuming that the inverse momentum distribution is Gaussian is negligible compared with the statistical errors.

The MDM for 3TF and 4TF events is lower than that for 5TF events because fewer trays are used to define the trajectory. To calculate the MDM for the tray combination 2345, the file of infinite momentum events was analysed without the data for tray 1. Similarly, for the tray combination 145, the file was analysed without using the information in trays 2 and 3. Thus the data file was analysed 15 times, i.e. once for each tray combination, and the standard deviation, σ_{dn}, of the

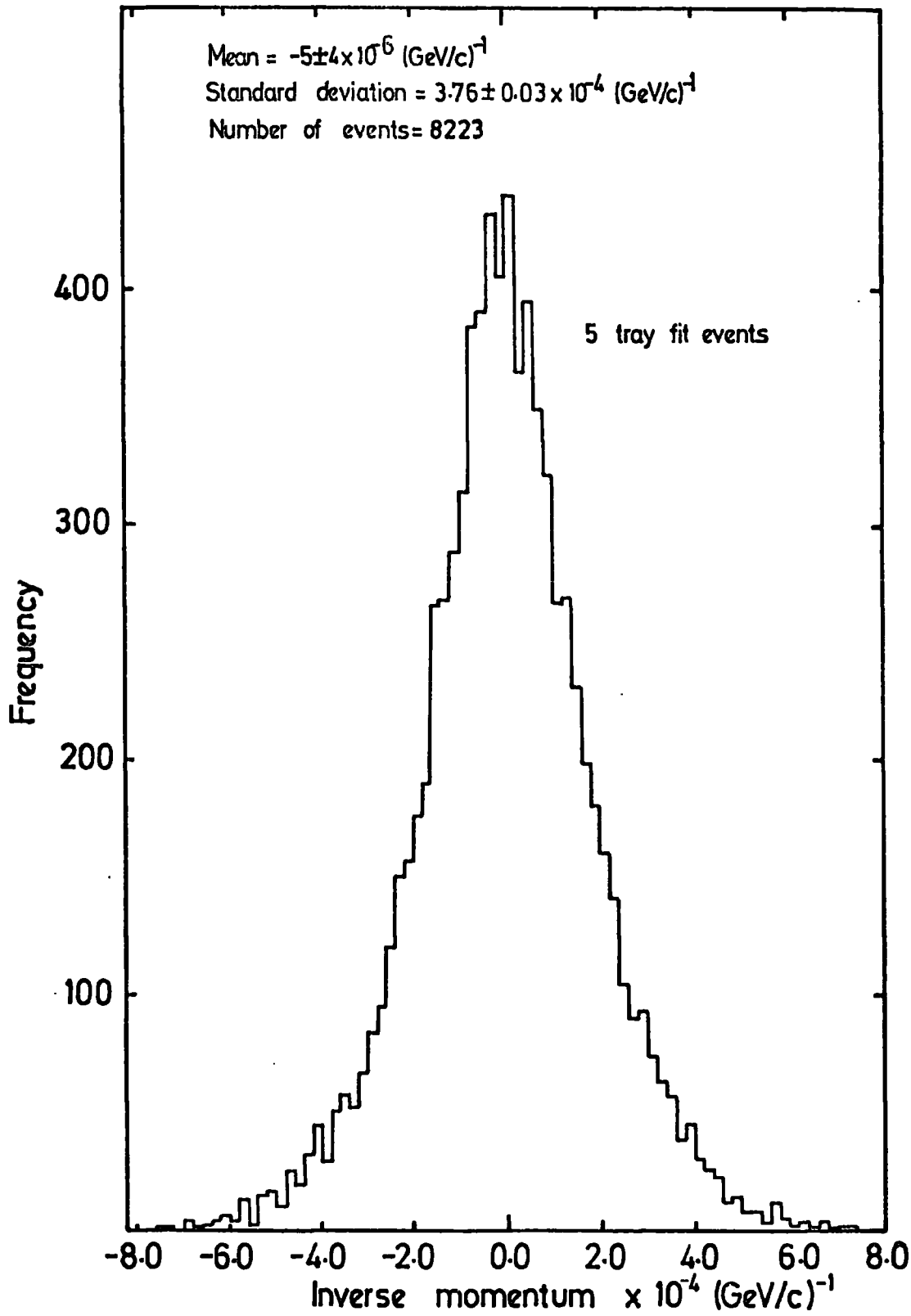

Figure 5.5 The frequency histogram of inverse momentum for simulated 5TF events

inverse momentum distribution, and hence the MDM, was measured in each case.

These results will be presented after the accuracy of the simulation program and the error on the MDM have been discussed.

5.4.4 THE ERROR ON THE MDM

It is important to know the error on the MDM of each tray combination so that the errors on the corrections to the spectrum are known.

The statistical error on the MDM is easy to estimate and it can be made small simply by increasing the sample of simulated events. However, there is a systematic error in the method which is hard to calculate. This is because it is dependent on how well the trajectory of the muon is simulated by the program.

The performance of the simulation program has been checked by comparing the analysis of simulated data with the analysis of real data. The point of comparison is the standard deviation of fit of the parabola around the co-ordinates of the muon trajectory which is defined in section 3.7. If s is the standard deviation, s_o a constant related to the trajectory location errors, and K is a constant related to the magnitude of the multiple scattering, then

$$\bar{s}^2 = \bar{s}_o^2 + K^2/\bar{p}^2 \qquad (5.7)$$

where the bar above the letter indicates the mean over a momentum range.

The simulation program was used to generate several files of 2000 muon events each at descreet momenta between 100 GeV/c and 316 GeV/c. This is the same program as the one used to simulate the paths of infinite momentum muons, except that the effects of energy loss, magnetic bending and multiple Coulomb scattering (according to the

theory of Rossi and Greisen 1942) were included in the calculation of the muon trajectories. Each file was analysed and the mean value of s was calculated for 5TF and 4TF events separately. The frequency distributions of s for 4TF and 5TF events of momentum 150 GeV/c are shown in figure 5.6.

The analysed real data with momentum between 100 GeV/c and 325 GeV/c were divided into a series of narrow momentum ranges and for each momentum range, the mean of s was calculated. Shown in figure 5.6 are the frequency distributions of s for 5TF and 4TF real events between 140 - 160 GeV/c for comparison with the simulated data.

The variation of $\bar{s}^2$ with $1/\bar{p}^2$ is shown in figures 5.7 and 5.8 for the 5TF and the 4TF events respectively. The lines through the data were fitted by a least squares technique and table 5.1 lists the coefficients of the lines.

		REAL DATA	SIMULATED DATA	RATIO OF SIMULATED TO REAL DATA
5TF DATA	K(m(GeV/c))	0.0334 ±0.0015	0.0340 ±0.0004	1.02 ±0.05
	S_o(m)	$3.32(\pm0.06)10^{-4}$	$2.95(\pm0.04)10^{-4}$	0.89 ±0.02
4TF DATA	K(m(GeV/c))	0.0242 ±0.0010	0.0244 ±0.0012	1.01 ±0.07
	S_o(m)	$2.23(\pm0.07)10^{-4}$	$1.91(\pm0.10)10^{-4}$	0.86 (±0.05)

TABLE 5.1 THE COEFFICIENTS OF THE STRAIGHT LINE FITS TO THE DATA IN FIGURES 5.7 AND 5.8

Good agreement is seen between the slopes of the lines and within the

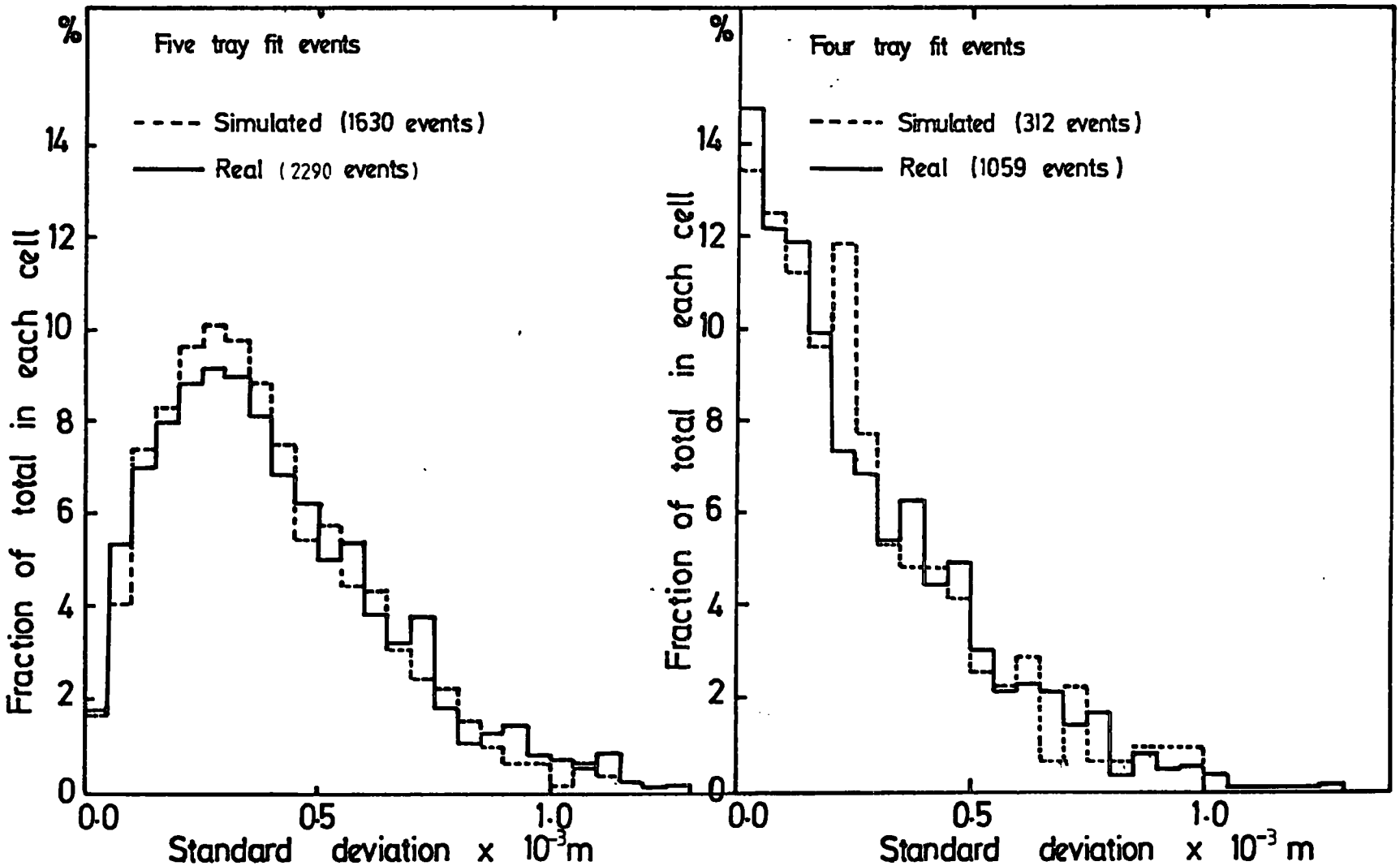

Figure 5·6 Diagrams showing the four and five tray fit standard deviation distributions of real events compared with those for simulated events of mean momentum 150 GeV/c

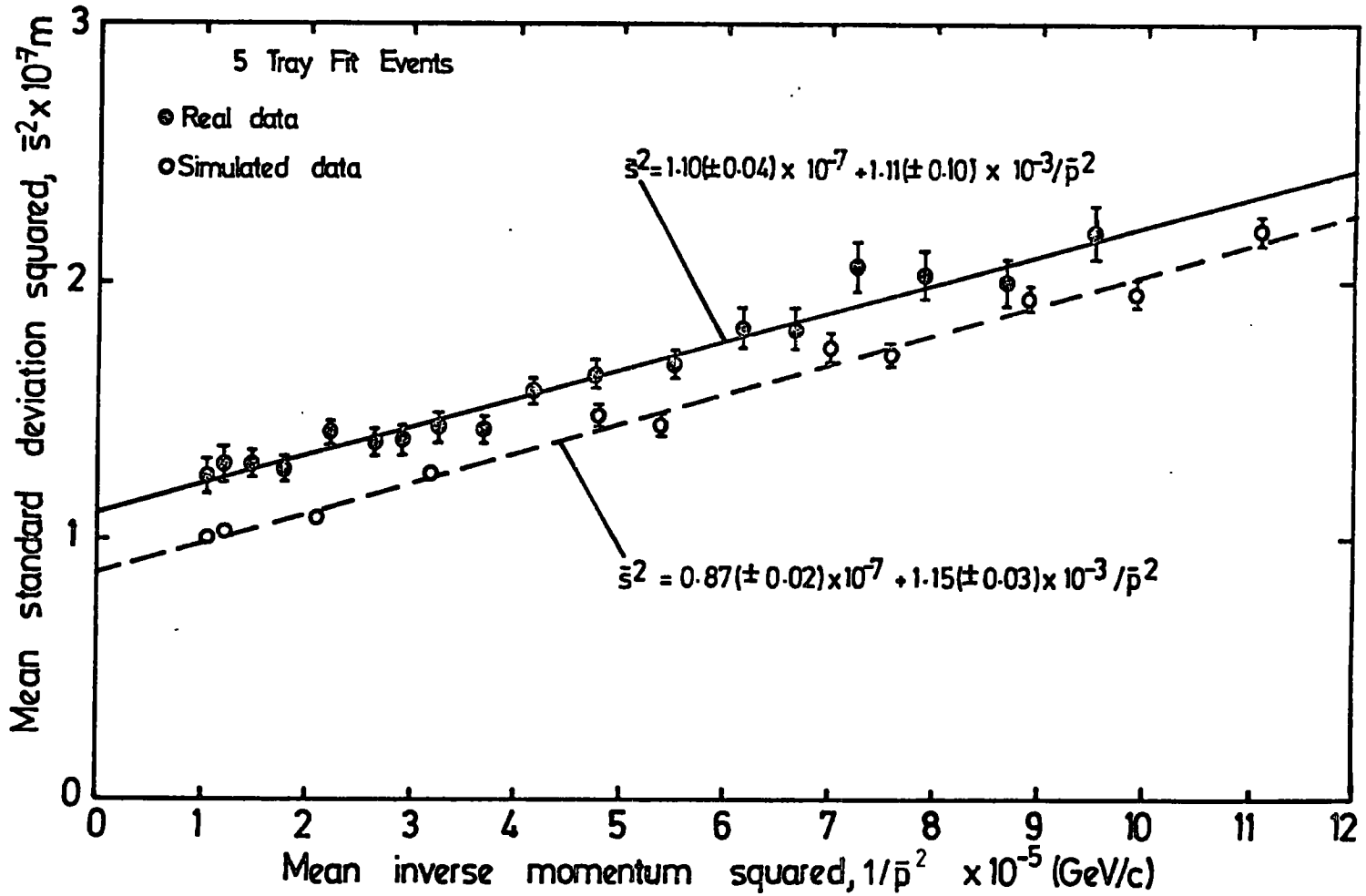

Figure 5.7 The variation of $\bar{s}^2$ with $1/\bar{p}^2$ for five tray fit events

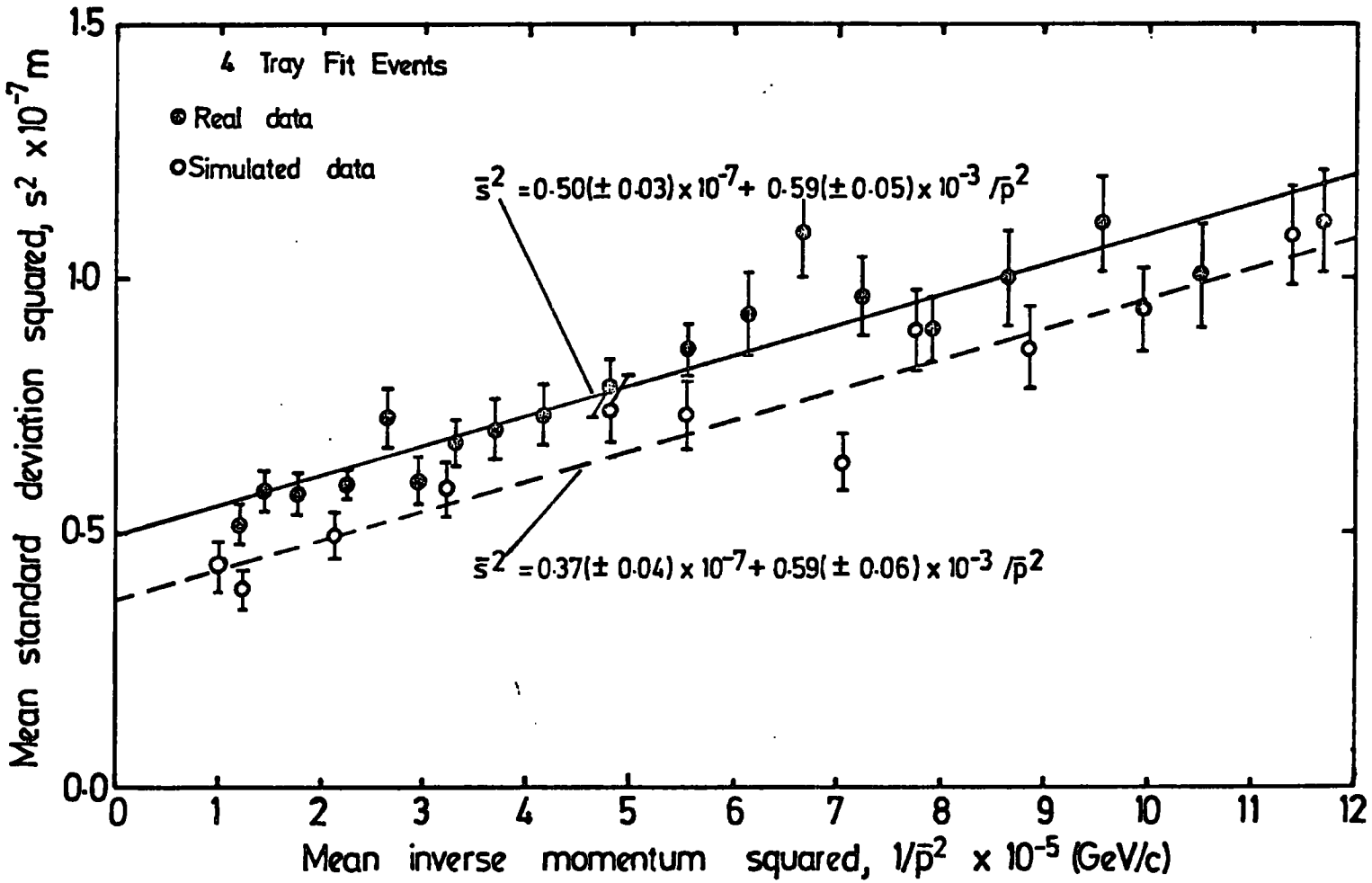

Figure 5.8 The variation of $\bar{s}^2$ with $1/\bar{p}^2$ for four tray fit events

the errors quoted it can be assumed that the theory of Rossi and Greisen adequately explains the multiple scattering in the spectrograph.

The comparison of s_o suggests that the simulation program underestimates the noise in the spectrograph. The reason for this is thought to be the fact that the program does not adequately simulate the production of bursts in the magnet blocks and the production of knock-on electrons in the measuring trays. Both processes are difficult to model and would lead to a large increase in the computing time.

To see how s_o is related to the MDM a second program was written to simulate trajectories of muons of infinite momentum in the spectrograph.

In this program, the horizontal co-ordinates of the muon at the five measuring levels were specified by picking numbers from a Gaussian distribution of standard deviation σ_n. This corresponds to the standard deviation of the track location error which was discussed in section 5.4.2. A parabola was fitted to these co-ordinates and the standard deviation of the fit, s, was measured. Also the momentum was calculated from the coefficiect of the squared term in the parabola and hence the inverse momentum, d, was derived. Therefore by generating a large sample of muons, the relationship between σ_n, $\bar{s}$ and σ_{dn} was found. The results of this program are shown in Table 5.2 where it can be seen that for the range of σ_n chosen, the ratio of σ_{dn} to $\bar{s}$ is practically constant.

In view of the proportionality between $\bar{s}$ and σ_{dn} it is considered reasonable to reduce the MDM for each tray combination calculated above by 12 ±1% to account for the inadequacy of the simulation program. The error on the MDM is still difficult to define but it is considered that the MDM is now known to within ±6%.

Table 5.3 shows the final MDM for each of the tray combinations.

$\sigma n \times 10^{-4}$ m	$\bar{s} \times 10^{-4}$ m	$\sigma dn \times 10^{-4}$ $(GeV/c)^{-1}$	$\sigma dn/\bar{s}$ $(GeV/c.\ m)^{-1}$
2.5	1.29 ±0.01	1.42 ±0.01	1.10 ±0.01
5.0	2.70 ±0.01	2.86 ±0.02	1.06 ±0.01
6.5	3.55 ±0.02	3.75 ±0.02	1.06 ±0.01
7.5	4.09 ±0.02	4.32 ±0.03	1.06 ±0.01
10.0	5.55 ±0.03	5.73 ±0.04	1.03 ±0.01

TABLE 5.2 THE RELATIONSHIP BETWEEN THE STANDARD DEVIATION OF THE TRACK LOCATION ERROR, σn, THE MEAN OF THE STANDARD DEVIATION OF THE TRAJECTORY, $\bar{s}$ AND THE STANDARD DEVIATION OF THE INVERSE MOMENTUM DISTRIBUTION, σdn.

TRAY COMBINATION	MDM GeV/c	TRAY COMBINATION	MDM GeV/c
12345	2400 ±150	125	1580 ±100
		135	1660 ±100
1234	1410 ± 80	345	520 ± 30
1235	2200 ±130	245	900 ± 50
1245	2000 ±120	235	850 ± 50
1345	2200 ±130	234	490 ± 30
2345	1230 ± 70	134	1030 ± 60
		124	1100 ± 70
145	1490 ± 90	123	460 ± 30

TABLE 5.3 THE MDM FOR EACH TRAY COMBINATION

5.4.5 THE RESOLUTION FUNCTION FOR TRACK LOCATION ERRORS

The resolution function of the spectrograph for the case of trajectory location errors is given by equation 5.8, where σ_{dn}

$$R(d) = \frac{1}{\sqrt{2\pi}\,\sigma_{dn}} \exp\left[-\frac{d^2}{2\sigma_{dn}^2}\right] \qquad (5.8)$$

equals $1/p_{MDM}$. The corrections for a given trial deflection spectrum N (d) are calculated using equation 5.9. This integral was evaluated numerically using Simpson's rule, the limits of integration being

$$C(d) = \frac{M(d)}{N(d)} = \int_{-\infty}^{\infty} N\,(d')\,R(d-d')\,dd' \Big/ N(d) \qquad (5.9)$$

reduced to $\pm 5\sigma_{dn}$.

If the deflection spectrum has the form $N\,(d) = Ad^{\gamma-2}$, then for $\gamma = 3$ or 4, equation 5.9 can be evaluated analytically with the results given below.

$$C(d) = \mathrm{ERF}\left[\frac{d}{\sqrt{2}\,\sigma_{dn}}\right] + \left[\frac{\sqrt{2}\,\sigma_{dn}}{\sqrt{\pi}\,d}\right]\exp\left[\frac{d^2}{2\sigma_{dn}^2}\right] \qquad \text{for } \gamma = 3$$

$$C(d) = 1 + \left[\frac{\sigma_{dn}}{d}\right]^2 \qquad \text{for } \gamma = 4$$

where $\mathrm{ERF}(x) = \frac{2}{\sqrt{\pi}}\int_0^x e^{-t^2}dt$ is the error function.

These analytical solutions were used to check the numerical calculations using Simpson's rule. In all cases, the agreement between the results was better than 1%. Figure 5.9 shows the variation of the corrections C(d) with γ for various momenta. The corrections calculated using the trial deflection spectra of section 5.3 are given in section 5.6.

5.5 MULTIPLE SCATTERING IN MARS

5.5.1 INTRODUCTION

A disadvantage of solid iron spectrographs such as MARS, is that

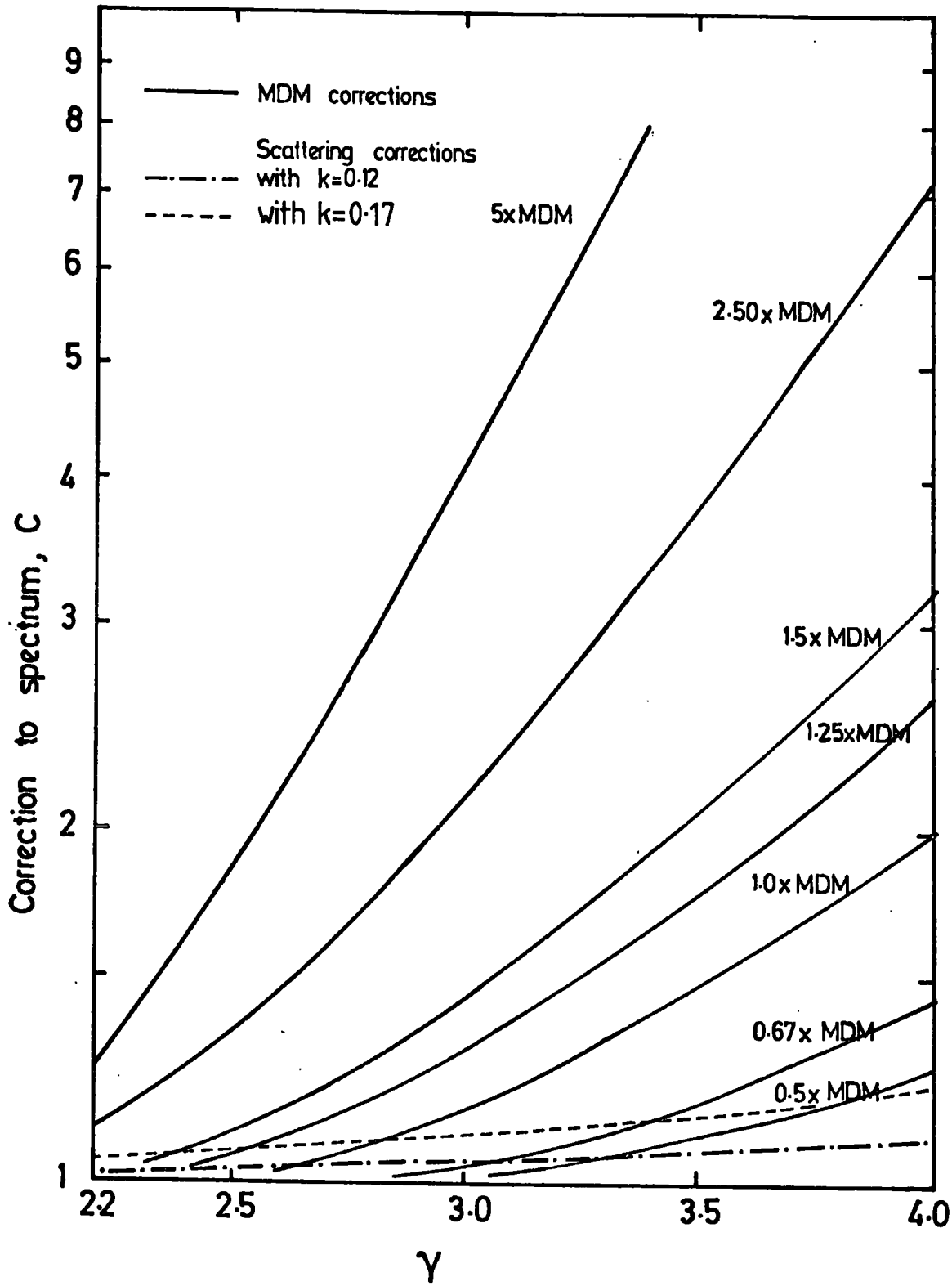

Figure 5.9 The correction C, to be applied to the measured spectrum as a function of momentum and slope of the differential spectrum

muons undergo scattering as they pass through the magnet blocks. This means that their apparent deflection is made up of two parts. One from magnetic bending and one from scattering. Thus scattering introduces an error into the measurement of muon momentum and leads to a distortion of the momentum spectrum.

The distortion of the momentum spectrum is due to the fact that it falls steeply with momentum. Hence the number of muons of low momentum which will, as a result of scattering, be wrongly given higher momenta is greater than the number of muons of higher momentum wrongly given low momenta. It will be shown later that the ratio of the r.m.s. deflection caused by scattering to the magnetic deflection is constant, and equal to 12% for muons which traverse four magnet blocks. Therefore for a power law spectrum with constant exponent, scattering simply causes an enhancement of the spectrum. In practice though, the differential exponent of the muon spectrum is seen to increase from $\sim$2.1 at 10 GeV/c to $\sim$3.5 at 1000 GeV/c. As a result of this, the enhancement of the spectum becomes more pronounced as momentum increases and leads to an overall flattening of the spectrum.

Most of the scattering is the result of elastic electromagnetic interactions between the charge on the muon and the Coulomb field of the iron nuclei. Other interactions such as electromagnetic interactions between the muon and the atomic electrons, and inelastic nuclear interactions also play a part in the scattering process but to a smaller degree. As the number of interactions is very large, the overall change in deflection of the muon is small. This type of scattering is called multiple scattering.

5.5.2 THE THEORY OF MULTIPLE SCATTERING

The multiple scattering theory of Rossi and Greisen (1942) has

been used to calculate the corrections to the spectrum. They assume that the individual deflections suffered by the muon are small and that the scattering is small angle multiple scattering. If $\lambda\!\!\!^{-}$ is the de Broglie wavelength of the muon, a represents the atomic radius, d represents the nuclear radius and θ is the angular deflection of the muon, then individual deflection of $\theta<\lambda\!\!\!^{-}/a$ and $\theta>\lambda\!\!\!^{-}/d$ are not allowed. These restrictions on θ allow for the effect of screening of the nucleus by the atomic electrons and for the effect of finite nuclear size respectively.

Rossi and Greisen deduce the probability, $F(t,y,\theta)$, that the particle, after traversing a plate of thickness t radiation lengths, will have a lateral displacement between y and y + dy and a projected angle between θ and $\theta + d\theta$. This is given in equation 5.10 below, where the scattering function $\omega = 2p\beta/Es$, p is the momentum of the particle,

$$F(t,y,\theta) = \frac{\sqrt{3}\ \omega^2}{2\pi\ t^2} \exp\left[-\omega^2\left[\frac{\theta^2}{t} - \frac{3y\theta}{t^2} + \frac{3y^2}{t^3}\right]\right] \qquad (5.10)$$

$\beta = v/c$ and Es is a constant having the value 21.2 MeV/c.

If $F(t,y,\theta)$ is integrated over θ, the distribution in y irrespective of angle, $H(t,y)$, is obtained. Similarly by integrating over y, the distribution in θ irrespective of lateral displacement, $G(t,\theta)$ is obtained. The distributions $H(t,y)$ and $G(t,\theta)$ given by equations 5.11 and 5.12, are seen to be Gaussian having standard deviations σ_y and σ_θ given by equations 5.13 and 5.14.

$$H(t,y) = \frac{\sqrt{3}\ \omega}{2\sqrt{\pi}\ t^{3/2}} \exp\left[-\tfrac{3}{4}(\omega^2 y^2/t^3)\right] \qquad (5.11)$$

$$G(t,\theta) = \frac{\omega}{2\sqrt{\pi}\ t^{\frac{1}{2}}} \exp\left[-\tfrac{1}{4}(\omega^2\theta^2/t)\right] \qquad (5.12)$$

$$\sigma_y^2 = \frac{1}{6}\frac{Es^2}{p^2\beta^2}\, t^3 \qquad (5.13)$$

$$\sigma_\theta^2 = \frac{1}{2}\frac{Es^2}{p^2\beta^2} t^3 \qquad (5.14)$$

Whalley (1974) showed that the distribution in projected angle, θ, at a particular lateral displacement, y, was also Gaussian with a mean value of

$$\theta = 3y/2t$$

and a standard deviation of

$$\sigma_{\theta y}^2 = \frac{Es^2\, t}{8p^2\beta^2}$$

In the simulation program previously described, the lateral deflection of the muon due to scattering, after passing through a thickness of iron of t radiation lengths, was selected from a Gaussian distribution of standard deviation σ_y. Then, using this value of y, the projected angular deflection, θ, was selected from a Gaussian distribution of mean 3y/2t and standard deviation $\sigma_{\theta y}$. The lateral and angular deflections due to scattering were added to the deflections due to magnetic bending.

In section 5.4.4 the constant K, defined in equation 5.7 and which is related to the magnitude of the multiple scattering, was derived from real and simulated data. There was found to be good agreement between the two values, thus indicating that the Rossi and Greisen theory adequately explains the multiple scattering in MARS.

5.5.3 THE SCATTERING CONSTANTS

In the introduction to this section, it was assumed that the ratio of the deflection caused by multiple scattering to the deflection caused by magnetic bending is independent of momentum. To show this, the angular deflection, θm due to magnetic bending must be derived.

If the muon moves a distance dl along the arc of a circle of radius r, then the angular deflection $d\theta m$ is given by $d\theta m = dl/r$. The

radius r is related to the muon momentum, p, and the magnetic field strength, B, through the relation p = Ber. Therefore $d\theta_m$ can be re-written as

$$d\theta_m = \frac{Be}{p}\, dl$$

and, by integration, the total angular deflection over the whole magnet is

$$\theta_m = \frac{e}{p}\int B\, dl$$

If the magnetic field strength is assumed uniform then B can be taken out of the integral to give

$$\theta_m = \frac{Bel}{p}$$

Therefore the ratio of the r.m.s. angular deflection caused by scattering, $\langle\theta\rangle$ (given by equation 5.13), to the angular deflection due to magnetic bending is given by equation 5.15 where $t = 1/X_o$

$$\frac{\langle\theta\rangle}{\theta_m} = k = \frac{Es}{\sqrt{2}Be\sqrt{X_o}\sqrt{l}} \qquad (5.15)$$

and X_o is the radiation length in iron in metres. The ratio has been set equal to the scattering constant k which, for a given material, is seen to depend only upon the length of the magnet l.

The angular deflection of a trajectory, θ, is proportional to its lateral deflection, Δ, and hence to the inverse momentum d. Therefore, the scattering constant k is also equal to σ_{ds}/d where σ_{ds} is the standard deviation of the inverse momentum distribution resulting from a beam of muons, of momentum p = 1/d, passing through the spectrograph. This inverse momentum distribution is therefore the resolution function R(d) for multiple scattering.

The scattering constant k has been calculated using the

simulation program previously described, by generating several files of 2000 muon events each, at discreet momenta between 100 GeV/c and 316 GeV/c. Each file of data was analysed and the standard deviation of the resulting inverse momentum distribution was calculated. These distributions are approximately Gaussian in shape and the standard deviation, σ_d, is made up of two parts, that due to track location errors, and that due to multiple scattering. Therefore, the standard deviation can be written:

$$\sigma_d^2 = \sigma_{dn}^2 + \sigma_{ds}^2$$

and given that $k = \sigma_{ds}/d$ this can be re-written:

$$\sigma_d^2 = \sigma_{dn}^2 + k^2 d^2$$

The constant k was evaluated by plotting the values of σ_d^2 from each file against $d^2 = 1/p^2$ and fitting a line by the method of least squares. The slope of this line was therefore equal to k^2. The variation of σ_d^2 with $1/p^2$ is shown plotted in figure 5.10 for 5TF events and the scattering constant derived from this line is $k = 0.121 \pm 0.001$. This is in good agreement with the value of 12% calculated by Whalley (1974) and the value of 11.5% calculated by Piggott (1975).

To calculate the scattering constant for 4TF and 3TF events, the files of simulated data were reanalysed a further 15 times. Each time a different tray or pair of trays was omitted from the analysis of the events, therefore allowing k to be calculated for all the tray combinations. The variation of σ_d^2 with $1/p^2$ for 4TF and 3TF events is shown plotted in figures 5.11 and 5.12 and the corresponding values of k are given in table 5.4. It can be seen that for events which traverse four magnet blocks, the scattering constant is $\sim$12%, for those which traverse three blocks it is $\sim$13.5% and for those which traverse

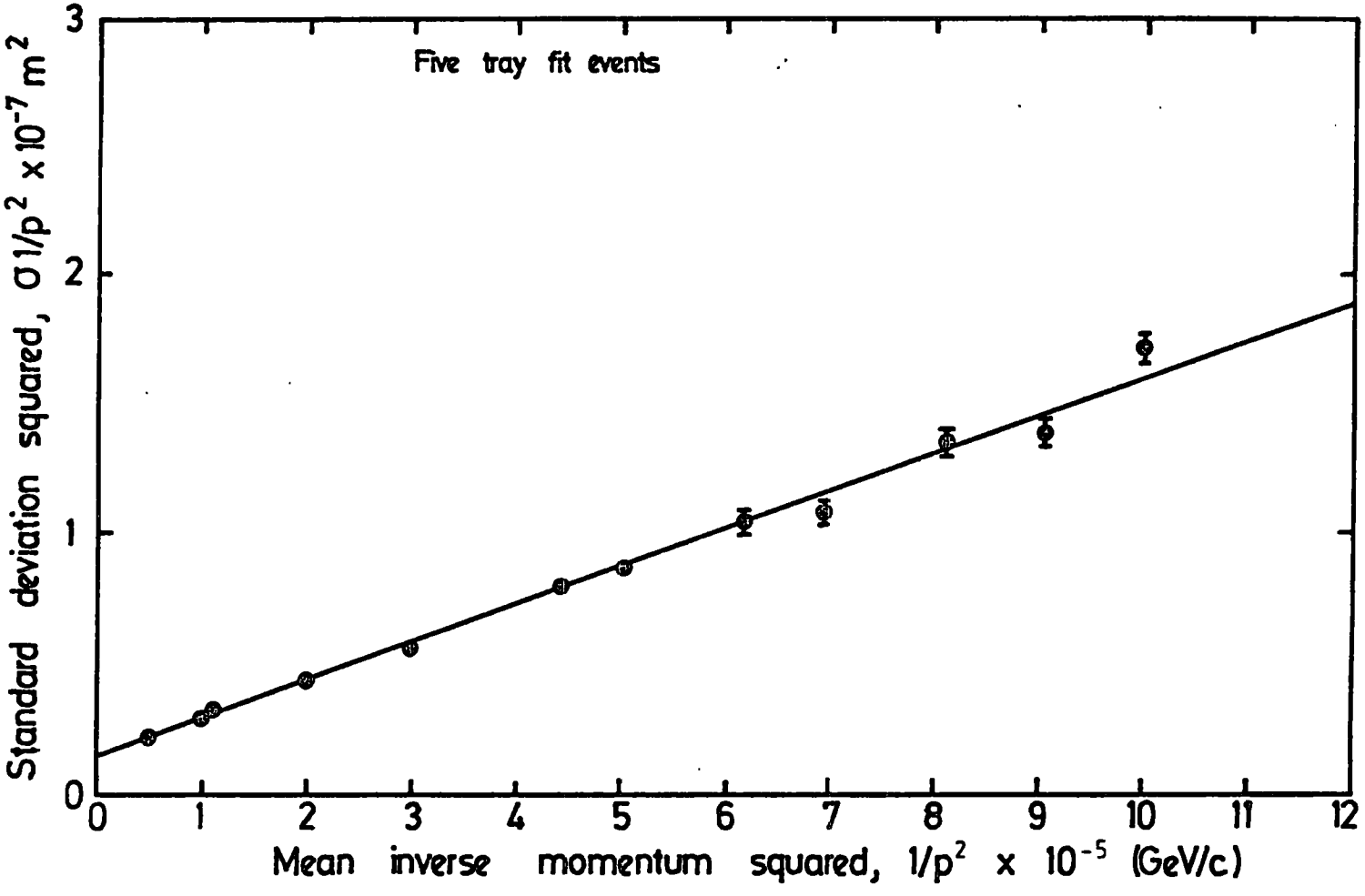

Figure 5.10 The variation of $\sigma\, 1/p^2$ with $1/p^2$ for simulated five tray fit events

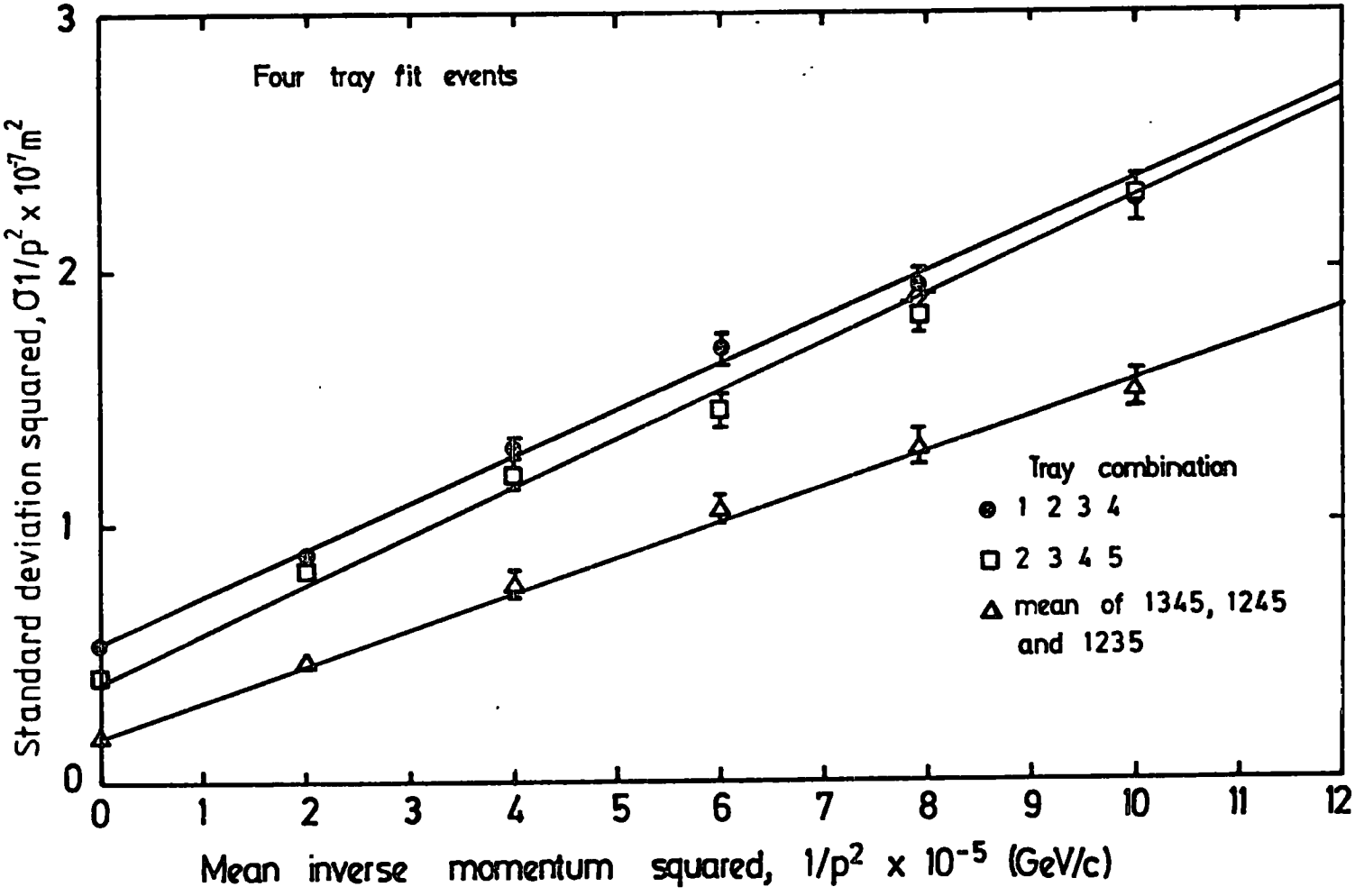

Figure 5.11 The variation of $\sigma 1/p^2$ with $1/p^2$ for simulated four tray fit events

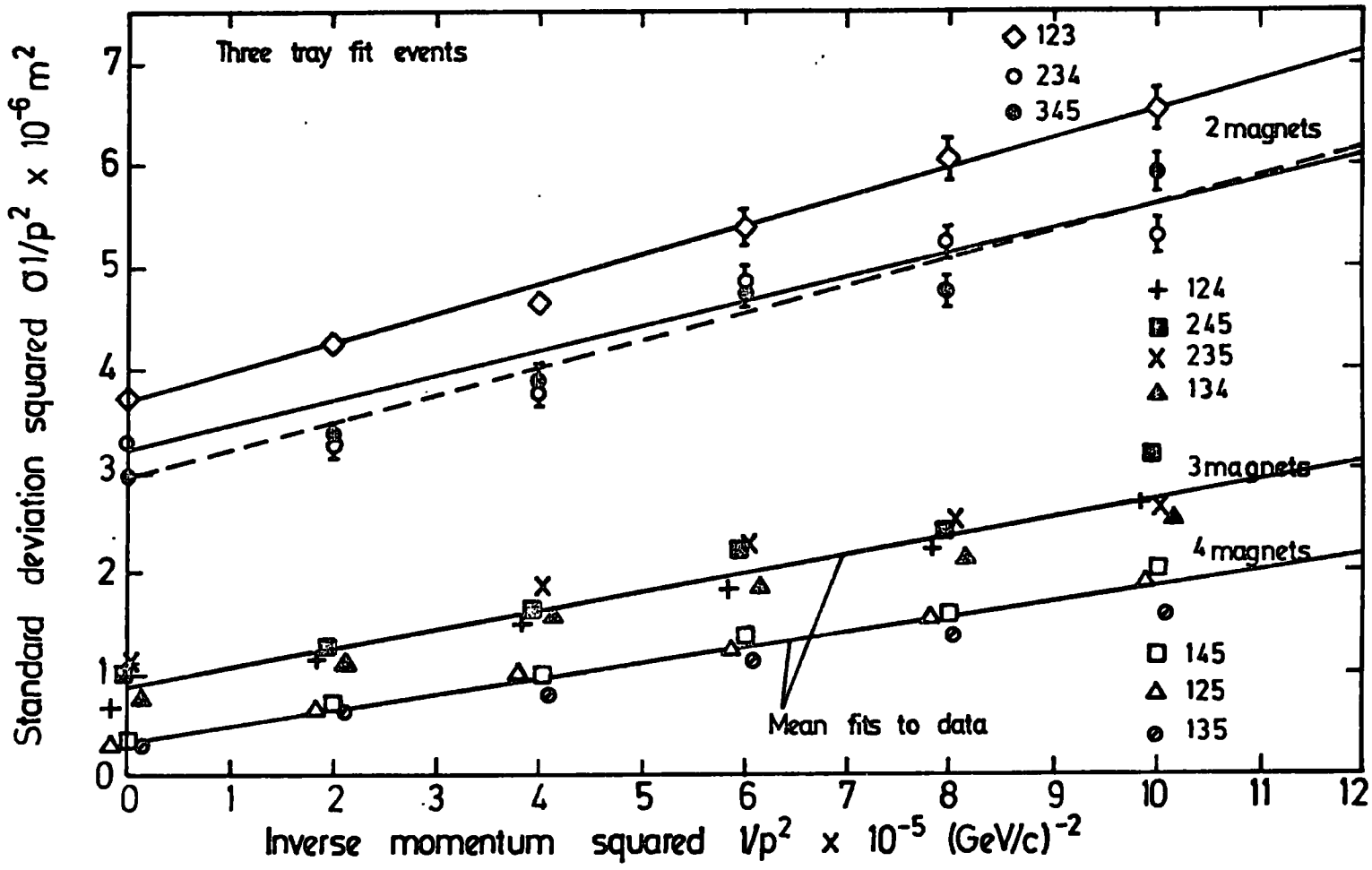

Figure 5·12 The variation of $\sigma 1/p^2$ with $1/p^2$ for simulated three tray fit events

TRAY COMBINATION	SCATTERING CONSTANT k %
12345	12.1 ±0.10
1234	13.7 ±0.20
1235	11.9 ±0.20
1245	11.7 ±0.20
1345	11.8 ±0.20
2345	13.4 ±0.20
345	16.4 ±0.70
245	13.7 ±0.20
235	13.1 ±0.20
234	14.7 ±0.30
145	12.6 ±0.20
135	11.6 ±0.20
134	13.4 ±0.20
125	12.5 ±0.20
124	14.1 ±0.30
123	16.9 ±0.30

TABLE 5.4 THE SCATTERING CONSTANTS FOR EACH TRAY COMBINATION

only two blocks it is ∿16%. This is broadly in agreement with equation 5.17 which shows that k is proportional to $1/\sqrt{l}$, where l is the length of the magnet. This equation does not, however, allow for the gaps in the magnets.

5.5.4 THE MULTIPLE SCATTERING CORRECTIONS

The inverse momentum distributions of the simulated data were approximately Gaussian in shape, as expected from the theory of Rossi and Greisen (1942). Therefore the resolution function R(d), for multiple scattering has been assumed to be Gaussian with a standard deviation $\sigma_{ds} = kd$.

The resolution function and the equation used to derive the multiple scattering corrections are shown below.

$$R(d) = \frac{1}{2\pi\ \sigma_{ds}} \exp\left\{-\frac{d^2}{2\sigma_{ds}^2}\right\} \qquad (5.16)$$

$$C(d) = \frac{M(d)}{N(d)} = \frac{1}{N(d)}\int_{-\infty}^{\infty} N(d')\ R(d-d')\ dd' \qquad (5.17)$$

The limits can be reduced from $\pm\infty$ because the Gaussian function is practically zero for d greater than five standard deviations from d'. If d_1 and d_2 are the lower and upper limits of integration and R is the range of integration in standard deviations then we require

$$d - d_1 = R\sigma_{ds} \qquad \text{and} \qquad d_2 - d = R\sigma_{ds}$$
$$= Rkd_1 \qquad\qquad = Rkd_2$$

therefore $d_1 = d/(1 + kR)$ therefore $d_2 = d/(1 - kR)$

Using d_1 and d_2 as the limits of integration, the convolution integral can be evaluated analytically for a deflection spectrum of constant exponent. If the trial deflection spectrum is given by $N(d) = Ad^{\gamma-2}$ then it can be shown that:

$$C(d) = ERF(R/\sqrt{2}) \qquad \text{for } \gamma = 1$$

$$C(d) = ERF(R/\sqrt{2})[1 + k^2 + 3k^4 + 3.5k^6 + 3.5.7k^8 + \ldots] \qquad \text{for } \gamma = 2$$

$$C(d) = ERF(R/\sqrt{2})[1 + 3k^2 + 3.5k^4 + 3.5.7k^6 + \ldots] \qquad \text{for } \gamma = 3$$

$$C(d) = ERF(R/\sqrt{2})[1 + 2.3k^2 + 3.3.5k^4 + 4.3.5.7k^6 + 5.3.5.7.9k^8 + \ldots] \qquad \text{for } \gamma = 4$$

Where $ERF(x) = \frac{2}{\sqrt{\pi}} \int_0^x e^{-t^2}\, dt$ is the error function.

As expected the corrections do not depend upon the deflection, d, for the case of a spectrum with a constant exponent.

In the present case, however, the trial deflection spectra of section 5.3 are to be used, and the convolution integral must be evaluated numerically. This has been done by using Simpson's rule and integrating from d_1 to d_2 using R equal to 5. The numerical calculations were checked for the case of deflection spectra with constant slope by comparing the numerical results with those calculated analytically from the equations above. The comparison is shown in table 5.5 where the agreement is seen to very good. The scattering corrections for k = 0.12 and k = 0.17 are shown plotted against γ in figure 5.9.

5.6 THE COMBINED CORRECTIONS FOR TRACK LOCATION ERRORS AND MULTIPLE COULOMB SCATTERING

The resolution function, R(d), which is needed to calculate the corrections for multiple scattering and trajectory location errors has been assumed to be Gaussian in both cases. Therefore the corrections for these two effects have been calculated together, using the joint resolution function given below, where $\sigma_d^2 = \sigma_{dn}^2 + \sigma_{ds}^2$, $\sigma_{ds} = kd$ and $\sigma_{dn} = 1/P_{MDM}$.

γ	C(d) ANALYTIC R = 5	NUMERICAL R = 5
1	1.000	1.000
2	1.015	1.015
3	1.047	1.046
4	1.096	1.097

TABLE 5.5 THE MULTIPLE SCATTERING CORRECTION CALCULATED USING THE ANALYTIC AND NUMERICAL METHODS FOR k = 0.12, AND γ THE EXPONENT OF THE DIFFERENTIAL MOMENTUM SPECTRUM

TRAY COMBINATION	MEAN MDM GeV/c	MEAN SCATTERING CONSTANT
1234, 1345	2200 ±120	0.118
123, 345, 234	490 ±30	0.160
124, 245, 235, 134	970 ±60	0.136
145, 125	1530 ±90	0.122

TABLE 5.6 THE GROUPING OF THE TRAY COMBINATIONS

$$R(d) = \frac{1}{\sqrt{2\pi}\ \sigma_d} \exp\left[-\frac{d^2}{2\sigma_d^2}\right] \qquad (5.18)$$

The convolution integral was evaluated using Simpson's rule, the lower limit of integration being $-R\sigma_{dn}$ or $d/(1 + kR)$ whichever was the smaller, and the upper limit of integration being $+R\sigma_{dn}$ or $d/(1 - kR)$ whichever was the greater, and R was set equal to 5.

Examination of tables 5.3 and 5.4 will show that certain tray combinations have a similar MDM and scattering constant. Where this is the case, those tray combinations have been grouped together for the purpose of calculating the corrections for multiple scattering and track location errors. The grouping of the tray combinations is shown in table 5.6.

As stated earlier, the combined corrections were evaluated using the first set of trial deflection spectra and the corrections were used to provide a second estimate of these spectra. The combined corrections derived from the second estimates of the trial deflection spectra were then used in the final calculation of the momentum spectrum. These corrections are shown in tables 5.7 and 5.8.

The corrections at low momentum are mainly due to the effect of multiple scattering, whereas at high momentum the track location errors dominate and are responsible for the large corrections needed for the spectrum. It is worth noting that the magnitude of the corrections needed for the 3TF spectra at high momentum are smaller than those needed for the 4TF or 5TF spectra although their maximum detectable momenta are greater. This is, of course, because the 3TF trial deflection spectum is much flatter than the 4TF and 5TF spectra.

The muon momentum spectrum, calculated using these corrections, is presented in the next chapter.

TRAY COMBINATION	12345	1234	1235 1345	1245	2345
MDM GeV/c	2400	1410	2200	2000	1230
SCATTERING CONSTANT	0.121	0.137	0.118	0.117	0.134
MOMENTUM GeV/c					
123	0.936	0.935	0.946	0.947	0.937
177	0.971	0.947	0.969	0.967	0.940
257	1.012	0.986	0.999	0.998	0.976
376	1.040	1.007	1.017	1.014	0.994
553	1.069	1.029	1.030	1.026	1.021
809	1.122	1.088	1.050	1.050	1.101
1183	1.249(±0.02)	1.259(±0.03)	1.110(±0.01)	1,126(±0.01)	1.329(±0.04)
1760	1.581(±0.06)	1.718(±0.06)	1.305(±0.03)	1.362(±0.04)	1.899(±0.10)
2584	2.398(±0.15)	2.738(±0.17)	1.797(±0.07)	1.940(±0.10)	3.132(±0.20)
3917	4.792(±0.40)	5.234(±0.40)	3.058(±0.20)	3.405(±0.20)	6.139(±0.40)
5729	10.83 (±1.10)	10.29 (±0.80)	5.661(±0.45)	6.415(±0.50)	12.23 (±0.90)
7868	22.94 (±2.50)	18.58 (±1.50)	9.906(±0.80)	11.32 (±0.90)	22.13 (±1.70)

TABLE 5.7 THE COMBINED CORRECTIONS FOR TRACK LOCATION ERRORS AND MULTIPLE COULOMB SCATTERING FOR THE 5 AND 4 TRAY FIT DATA

TRAY COMBINATION	123 345 234	124 245 235 134	145 125	135
MDM GeV/c	490	970	1530	1660
SCATTERING CONSTANT	0.160	0.136	0.122	0.122
MOMENTUM GeV/c				
123	0.969	0.955	0.995	0.954
177	0.846	0.936	0.960	0.962
257	0.829	0.956	0.986	0.989
376	0.850	0.952	0.991	0.996
553	0.954	0.945	0.984	0.990
809	1.306	1.004	0.983	0.987
1183	1.591(±0.04)	1.180(±0.03)	1.039(±0.01)	1.027(±0.01)
1760	2.321(±0.06)	1.593(±0.06)	1.231(±0.04)	1.193(±0.03)
2584	3.547(±0.10)	2.281(±0.10)	1.650(±0.07)	1.563(±0.06)
3917	5.813(±0.20)	3.649(±0.20)	2.509(±0.10)	2.349(±0.10)
5729	9.231(±0.30)	5.747(±0.30)	3.869(±0.20)	3.594(±0.20)
7868	13.41 (±0.40)	8.314(±0.40)	5.527(±0.30)	5.129(±0.30)

TABLE 5.8 THE COMBINED CORRECTIONS FOR TRACK LOCATION ERRORS AND MULTIPLE COULOMB SCATTERING FOR THE 3 TRAY FIT DATA

CHAPTER 6

THE MUON MOMENTUM SPECTRUM

6.1 INTRODUCTION

In this chapter, the results of the analysis of the MARS, class I, high momentum muon data will be presented and the muon momentum spectrum from 200 GeV/c to 3000 GeV/c will be calculated. The spectrum beyond 3000 GeV/c will also be calculated, but less emphasis will be placed on the result as it is beyond the MDM of the spectrograph.

An analysis of the errors on the spectrum will be given and the most likely slope of the pion production spectrum will be derived.

Finally, the present result will be compared with other direct and indirect measurements of the muon energy spectrum.

6.2 THE DATA

The data presented here were collected over a two year period and were analysed in one computer run using the MARS2 analysis program described in chapter 3. For convenience the data were split into files labelled A45, A6, A78MI, M2, M3 and M4 containing a total of 79,729 events. On analysis, 43,919 events passed the analysis, (some of which were multiple muons), 13,742 were put into the shower category and 22,068 events failed, being spread amongst the various error codes. Table 6.1 gives a breakdown of the data. In the analysis program, error codes SE1, SE3, SE19 and E91 are flagged before the error code E92 which flags a shower event, that is, an event with more than 30 columns of data in tray 5. Hence, on the first analysis, some of the events given the error codes SE1, SE3, SE19 and E91 are also shower events. Therefore the shower events had to be separately filtered out and the figures in

FILE		A45	A6	A78MI	M2	M3	M4
TOTAL		13900	7105	21115	10000	13804	13805
PASS		8142	4175	13960	5566	5945	6131
SHOWERS		1957	857	2585	1987	3203	3153
SE1	FAILED EVENTS	190 (190)	36 (33)	517 (506)	256 (255)	550 (547)	324 (322)
SE3		648 (301)	335 (195)	1217 (753)	1026 (527)	2353 (1383)	1686 (935)
SE19		613 (17)	347 (10)	1063 (50)	997 (25)	1347 (48)	1357 (45)
E91		560 (256)	252 (140)	796 (438)	512 (312)	1030 (678)	914 (553)
E92		710 (0)	265 (0)	739 (0)	315 (0)	579 (0)	727 (0)
E94		44	26	83	53	43	67
E95		446	240	652	312	339	335
E97		2355	1319	1753	783	1293	972
E99		192	110	329	180	325	1292
RUN TIME h:m:s		778:08:59	431:46:10	1649:01:54	697:17:51	736:00:07	826:09:30
PASS RATE h^{-1}		10.5	9.7	8.5	8.0	8.1	7.4
FIRST EVENT NUMBER		696371	1685669	2190891	4832888	6595085	7869957
LAST EVENT NUMBER		1685579	2161508	4822289	6594671	7869867	638289

TABLE 6.1 A BREAKDOWN OF THE DATA ACCORDING TO THE DATA FILES AND ERROR CODES

brackets in table 6.1 are the numbers of events with the given error code which do not contain showers. The analysis of the showers will be discussed in section 6.4.

Also shown in table 6.1 are the run times of each file and the rate of pass events per hour which is seen to decrease from 10.5 h^{-1} at the start of data collection to 7.4 h^{-1} at the end of data collection. This is broadly in agreement with the observed decrease in the rate of three fold coincidences from the blue side scintillation counters which was discussed in section 4.6.

The reclaimed events from the SE19, E99 and E95 files were added to the file of pass events and the momentum of each event was corrected for energy loss and for the effect of the magnet gaps in the manner described in section 4.7. The resulting momentum spectra for the various tray combinations are given in table 6.2. It can be seen that some tray combinations have been grouped together where the maximum detectable momenta and scattering constants for those combinations are similar.

The proportion of 5, 4 and 3 tray fit events are shown in table 6.3. The total number of events in this table is 31,134 and is less than the number of pass events in table 6.1 (43,919) because the muons of momentum less than 100 GeV/c have not been included. This, therefore, is the number of events which have been used to calculate the unassociated muon spectrum. There will be a further small contribution of events from the shower data.

6.3 THE UNACCOMPANIED MUON MOMENTUM SPECTRUM

The unaccompanied spectrum is the spectrum of muons excluding those accompanied by extensive air shower particles which discharge more than 30 columns in tray 5.

MOMENTUM RANGE GeV/c		100 147	147 215	215 316	316 464	464 681	681 1000	1000 1470	1470 2150	2150 3160	3160 4640	4640 6810	6810 10000	$>10^4$
TRAY COMBINATION														
12345	P	5867	6193	3552	1695	701	275	121	35	25	4	5	2	9
12345	S	32	15	7	3	1	2	1	1	0	0	0	0	0
12345	T	5899	6208	3559	1698	702	277	122	36	25	4	5	2	9
1234	P	343	338	218	132	47	22	13	8	2	3	2	2	0
1234	S	13	10	12	5	3	3	3	1	0	0	0	0	0
1234	T	356	348	230	137	50	25	16	9	2	3	2	2	0
1235	P	470	514	391	227	108	52	16	10	6	4	1	3	1
1235	S	20	9	8	8	1	1	0	0	0	0	0	0	0
1235	T	490	523	399	235	109	53	16	10	6	4	1	3	1
1345	P	370	472	384	187	98	42	23	9	5	2	1	2	4
1345	S	30	17	10	1	3	0	1	0	1	0	0	0	0
1345	T	400	489	394	188	101	42	24	9	6	2	1	2	4
1245	P	942	849	542	231	127	48	20	15	5	2	3	1	1
1245	S	36	32	27	18	3	5	1	0	0	1	0	0	0
1245	T	978	881	569	249	130	53	21	15	5	3	3	1	1
2345	P	927	785	506	264	121	57	27	20	8	6	4	5	3
2345	S	16	21	11	13	2	1	0	0	0	0	0	0	0
2345	T	943	806	517	277	123	58	27	20	8	6	4	5	3
123	P	17	20	12	11	3	1	3	1	1	0	1	0	1
345	P	57	59	34	26	18	11	4	6	2	0	1	3	2
234	P	49	39	29	8	10	5	7	0	1	2	0	2	1
123 / 345 / 234	S	14	12	5	3	7	2	2	0	1	2	0	0	0
123 / 345 / 234	T	137	130	80	48	38	19	16	7	5	4	2	5	4
145	P	65	59	57	32	16	4	1	2	1	0	0	0	1
125	P	65	75	40	30	19	7	2	2	4	0	0	0	1
145 / 125	S	6	3	6	11	1	1	1	1	0	0	0	0	0
145 / 125	T	136	137	103	73	36	12	4	5	5	0	0	0	2
235	P	70	80	61	42	13	13	8	10	4	0	3	0	3
124	P	48	61	28	12	8	4	3	2	0	0	1	0	1
245	P	134	96	80	35	22	11	6	3	3	0	1	1	0
134	P	22	29	20	6	8	7	2	1	0	0	1	0	0
124 / 245 / 235 / 134	S	17	12	8	7	3	0	0	1	0	0	1	0	0
124 / 245 / 235 / 134	T	291	278	197	102	54	35	19	17	7	0	7	1	4
135	P	40	39	30	25	14	7	6	1	0	0	0	1	1
135	S	3	2	0	0	1	0	0	0	0	0	0	0	0
135	T	43	41	30	25	15	7	6	1	0	0	0	1	1

P is the number of pass events plus the reanalysed E19 and E99 events.
S is the number of reanalysed E95 events.
T is the total number of events for that momentum range.

TABLE 6.2 THE MOMENTUM SPECTRA FOR THE VARIOUS TRAY COMBINATIONS AFTER CORRECTION FOR ENERGY LOSS AND THE EFFECT OF THE MAGNET GAPS

MOMENTUM RANGE GeV/c	5TF	%	4TF	%	3TF	%	TOTAL
100 - 147	5899	61.0	3167	32.7	607	6.3	9673
147 - 215	6208	63.1	3047	31.0	586	6.0	9841
215 - 316	3559	58.6	2109	34.7	410	6.7	6078
316 - 464	1698	56.0	1086	35.8	248	8.2	3032
464 - 681	702	51.7	513	37.8	143	10.5	1358
681 - 1000	277	47.7	231	39.8	73	12.6	581
1000 - 1470	122	45.0	104	38.4	45	16.6	271
1470 - 2150	36	27.9	63	48.8	30	23.3	129
2150 - 3160	25	36.2	27	39.1	17	24.6	69
3160 - 4640	4		18		4		26
4640 - 6810	5	19.6	11	50.0	9	30.4	25
6810 - 10^4	2		13		7		22
>10^4	9		9		11		29
>100	18546	59.6	10398	33.4	2190	7.0	31134

TABLE 6.3 THE NUMBER AND PROPORTIONS OF 5, 4 AND 3 TRAY FIT EVENTS

The spectrum has been calculated for the 5, 4 and 3 tray fit data separately to show the accuracy and consistancy of the method of calculation. The spectrum has also been calculated from the 5, 4 and 3 tray fit data combined.

Equations 6.1 to 6.4 show how the spectra have been calculated. The calculation of the spectrum from the 5TF data is straightforward. For the 4TF and 3TF data, the number of events in a given momentum cell are first corrected for multiple Coulomb scattering and the track location errors, then the events from different tray combinations, but with the same momentum, are added to find the total number of corrected events for that momentum cell.

$$N^5(\bar{p}) = \frac{N^5}{C^5} \propto \frac{1}{\Delta p \ Effc} \times \frac{C_1 \times C_{3,91}}{Acc \times Time \times E_{MST} \times E_{SCN}} \frac{1}{P_5}$$

$$= \frac{N^5}{C^5} \times \frac{1}{\Delta p \ Effc} \times A \times \frac{1}{P_5} \qquad (6.1)$$

$$\text{Where} \quad A = \frac{C_1 \times C_{3,91}}{Acc \times Time \times E_{MST} \times E_{SCN}}$$

$$= 1.88 \times 10^{-10} \ cm^{-2} \ sr^{-1} \ s^{-1}$$

$$N^4(\bar{p}) = \sum_{i=1}^{4} \frac{N_i^4}{C_i^4} \times \frac{1}{\Delta p \ Effc} \times A \times \frac{1}{P_4} \qquad (6.2)$$

$$N^3(\bar{p}) = \sum_{i=1}^{4} \frac{N_i^3}{C_i^3} \times \frac{1}{\Delta p \ Effc} \times A \times \frac{1}{P_3} \qquad (6.3)$$

$$N(\bar{p}) = \left(\frac{N^5}{C^5} + \sum_{i=1}^{4} \left[\frac{N_i^4}{C_i^4} + \frac{N_i^3}{C_i^3} \right] \right) \times \frac{1}{\Delta p. \ Effc} \times A \times \frac{1}{P_3 + P_4 + P_5} \qquad (6.4)$$

Where:-

N^5 is the number of 5TF events in a given momentum cell.

N_i^4 and N_i^3 for $i = 1,4$ are the number of events in a given momentum cell with tray combination i.

C^5 is the correction for track location error and multiple scattering for 5TF events.

C_i^3 and C_i^4	are the corrections for track location error and multiple scattering for 3TF and 4TF events of tray combination i.
Δp	is the momentum cell width.
Effc	is the momentum selector efficiency at momentum $\bar{p}$.
C_1	= 1.023 ±0.001 is the correction for events lost due to format errors.
$C_{3,91}$	= 1.014 ±0.001 is the correction for events lost due to an inefficient measuring tray.
Acc	= 408 ± 2cm^2 sr is the acceptance of the spectrograph.
Time	= 1.843 10^7 s is the live time of the spectrograph.
E_{MST}	= 0.9132 ±0.010 is the momentum selector tray efficiency.
E_{SCN}	= 0.805 ±0.002 is the scintillation counter efficiency.
$\bar{p}$	is the mean momentum of the cell.
$N^3(\bar{p})$, $N^4(\bar{p})$, and $N^5(\bar{p})$	are the 3, 4 and 5 tray fit spectra.
$N(\bar{p})$	is the combined muon spectrum.
P_3, P_4 and P_5	are the probabilities that an event will be a 3, 4 and 5 tray fit.

The calculation of the correction factors and efficiencies have been discussed in previous chapters. The mean momentum of each momentum cell, which was calculated from the experimental data, and the values of P_3, P_4 and P_5 used in calculations are shown in table 6.4. Table 6.5 shows the results of the calculation of the 3, 4 and 5 tray fit spectra and the spectra are shown graphically in figure 6.1. Only statistical errors are shown on the data points. Except for the intensity at 123 GeV/c the three spectra are seen to be consistent up

MOMENTUM RANGE GeV/c	MEAN MOMENTUM GeV/c	P_3	P_4	P_5
100 - 147	123	0.0477	0.282	0.666
147 - 215	177	0.0551	0.298	0.641
215 - 316	257	0.0662	0.319	0.608
316 - 464	376	0.0818	0.343	0.565
464 - 681	553	0.102	0.367	0.516
681 - 1000	809	0.128	0.389	0.462
1000 - 1470	1183	0.158	0.406	0.404
1470 - 2150	1760	0.195	0.416	0.341
2150 - 3160	2584	0.237	0.414	0.277
3160 - 4640	3917	0.287	0.394	0.207
4640 - 6810	5729	0.331	0.355	0.145
6810 - 10000	7868	0.358	0.306	0.100

TABLE 6.4 THE MEAN MOMENTUM OF EACH CELL AND THE PROBABILITIES OF AN EVENT HAVING 3, 4 OR 5 USABLE MEASURING TRAYS

$\bar{p}$ GeV/c	Δp GeV/c	Effc	$N_3(\bar{p})\bar{p}^3$ $cm^{-2}\,s^{-1}\,sr^{-1}$ GeV/c^2	$N_4(\bar{p})\bar{p}^3$ $cm^{-2}\,s^{-1}\,sr^{-1}$ GeV/c^2	$N_5(\bar{p})\bar{p}^3$ $cm^{-2}\,s^{-1}\,sr^{-1}$ GeV/c^2
123	46.8	0.220	0.451 ±0.018	0.404 ±0.007	0.321 ±0.004
177	68.7	0.524	0.334 ±0.014	0.309 ±0.006	0.288 ±0.004
257	101	0.744	0.281 ±0.014	0.283 ±0.006	0.246 ±0.004
376	148	0.868	0.250 ±0.016	0.244 ±0.007	0.225 ±0.005
553	217	0.929	0.228 ±0.019	0.215 ±0.010	0.201 ±0.008
809	319	0.962	0.174 ±0.020	0.181 ±0.012	0.173 ±0.010
1183	468	0.975	0.155 ±0.023	0.147 ±0.015	0.165 ±0.015
1760	687	0.981	0.144 ±0.026	0.151 ±0.019	0.101 ±0.017
2584	1010	0.983	0.103 ±0.025	0.099 ±0.019	0.122 ±0.025
3917	1480	0.984	0.019 ±0.009	0.086 ±0.020	0.031 ±0.016
5729	2170	0.985	0.072 ±0.024	0.063 ±0.019	0.053 ±0.024
7868	3190	0.986	0.056 ±0.021	0.089 ±0.025	0.025 ±0.018

TABLE 6.5 THE MUON MOMENTUM SPECTRUM CALCULATED FROM THE 5, 4 AND 3 TRAY FIT DATA SEPARATELY. THE ERRORS ARE STATISTICAL

Figure 6.1 The muon spectrum calculated from the 3,4 and 5 tray fit data separately.

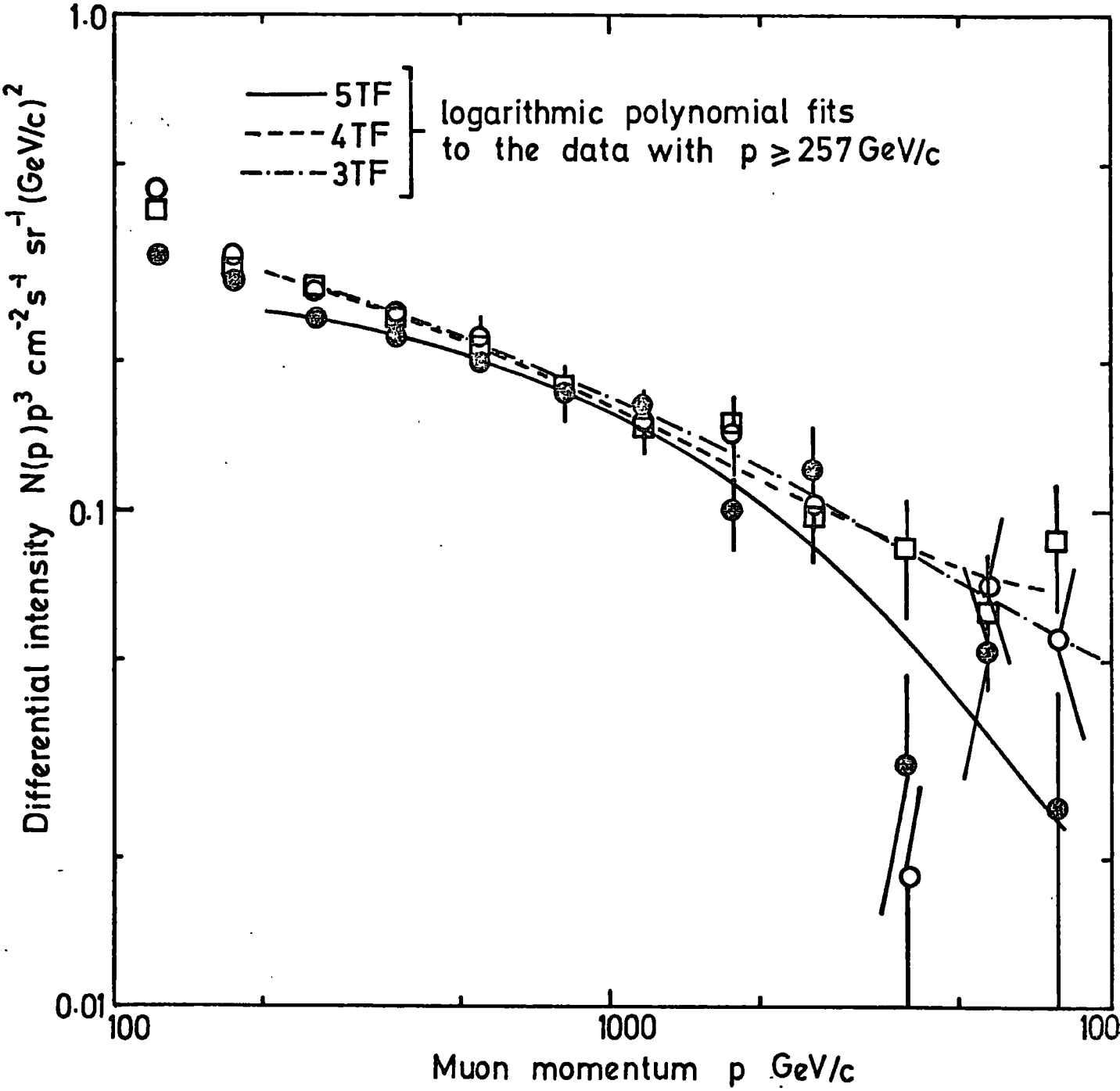

to about 3000 GeV/c. Above 3000 GeV/c the 5TF spectrum tends to steepen in comparison with the other two. This is either due to the fact that the 3 and 4 tray fit spectra are well above their respective maximum detectable momenta and the corrections for the track location errors have been underestimated or there is a systematic error in the probabilities P_3, P_4 , P_5 which are dependent upon the probability of burst production in the magnet blocks. In either case, the spectra cannot be relied upon here because they are higher than the maximum MDM of the spectrograph. The consistency of the three spectra up to 3000 GeV/c gives justification for combining them to give the best estimate of the muon spectrum.

The discrepancy in the three spectra at low momenta is thought to be due to the momentum selector pre-selecting 3 and 4 tray fit events due to the production of bursts in the magnet blocks above the momentum selector trays at levels 3 and 1.

The difference in absolute height between the three spectra is probably caused by a systematic error in P_3, P_4 and P_5. However, this should not be important when the three spectra are combined because the intensities are then only dependent upon the sum of P_3, P_4 and P_5, which is close to unity for most of the momentum range considered.

The momentum spectrum calculated from the combined data is given in table 6.6 and shown in figure 6.2. As expected it is in good agreement with the individual spectra presented earlier. The errors shown are statistical only.

6.4 THE MOMENTUM SPECTRUM OF MUONS ACCOMPANIED BY EXTENSIVE AIR SHOWERS

6.4.1 INTRODUCTION

A muon incident upon the spectrograph may be accompanied by an extensive air shower. If the density of electrons is low it is possible

$\bar{p}$ GeV/c	$\frac{N^5}{C^5}$	$\sum_{i=1}^{4} \frac{N_i^4}{C_i^4}$	$\sum_{i=1}^{4} \frac{N_i^3}{C_i^3}$	$P_3+P_4+P_5$	$N(\bar{p})$	$N(\bar{p})\ \bar{p}^3$
123	6.30×10^{3}	3.36×10^{3}	6.34×10^{2}	0.996	1.89×10^{-7}	0.351 ±0.004
177	6.39×10^{3}	3.18×10^{3}	6.36×10^{2}	0.995	5.36×10^{-8}	0.297 ±0.003
257	3.52×10^{3}	2.13×10^{3}	4.37×10^{2}	0.993	1.53×10^{-8}	0.260 ±0.003
376	1.63×10^{3}	1.08×10^{3}	2.62×10^{2}	0.990	4.39×10^{-9}	0.234 ±0.004
553	6.57×10^{2}	5.00×10^{2}	1.48×10^{2}	0.985	1.23×10^{-9}	0.209 ±0.006
809	2.47×10^{2}	2.17×10^{2}	6.87×10^{1}	0.978	3.33×10^{-10}	0.176 ±0.007
1183	9.77×10^{1}	8.77×10^{1}	3.58×10^{1}	0.968	9.42×10^{-11}	0.156 ±0.009
1760	2.28×10^{1}	4.13×10^{1}	1.86×10^{1}	0.952	2.42×10^{-11}	0.132 ±0.012
2584	1.04×10^{1}	1.25×10^{1}	7.51×10^{0}	0.928	6.22×10^{-12}	0.107 ±0.013
3917	8.35×10^{-1}	4.40×10^{0}	6.88×10^{-1}	0.888	8.61×10^{-13}	0.052 ±0.010
5729	4.62×10^{-1}	1.34×10^{0}	1.43×10^{0}	0.830	3.43×10^{-13}	0.064 ±0.013
7868	8.72×10^{-2}	9.27×10^{-1}	6.88×10^{-1}	0.764	1.33×10^{-13}	0.065 ±0.014

TABLE 6.6 THE MUON MOMENTUM SPECTRUM CALCULATED FROM THE 3, 4 AND 5 TRAY FIT DATA COMBINED. THE ERRORS ARE STATISTICAL ($N(\bar{p})$ is in units of $cm^{-2}\ s^{-1}\ sr^{-1}\ GeV/c^{-1}$ and $N(\bar{p})\bar{p}^3$ is in units of $cm^{-2}\ s^{-1}\ sr^{-1}\ GeV/c^{2}$)

Figure 6.2 The muon spectrum from the 3, 4 and 5 tray fit data combined.

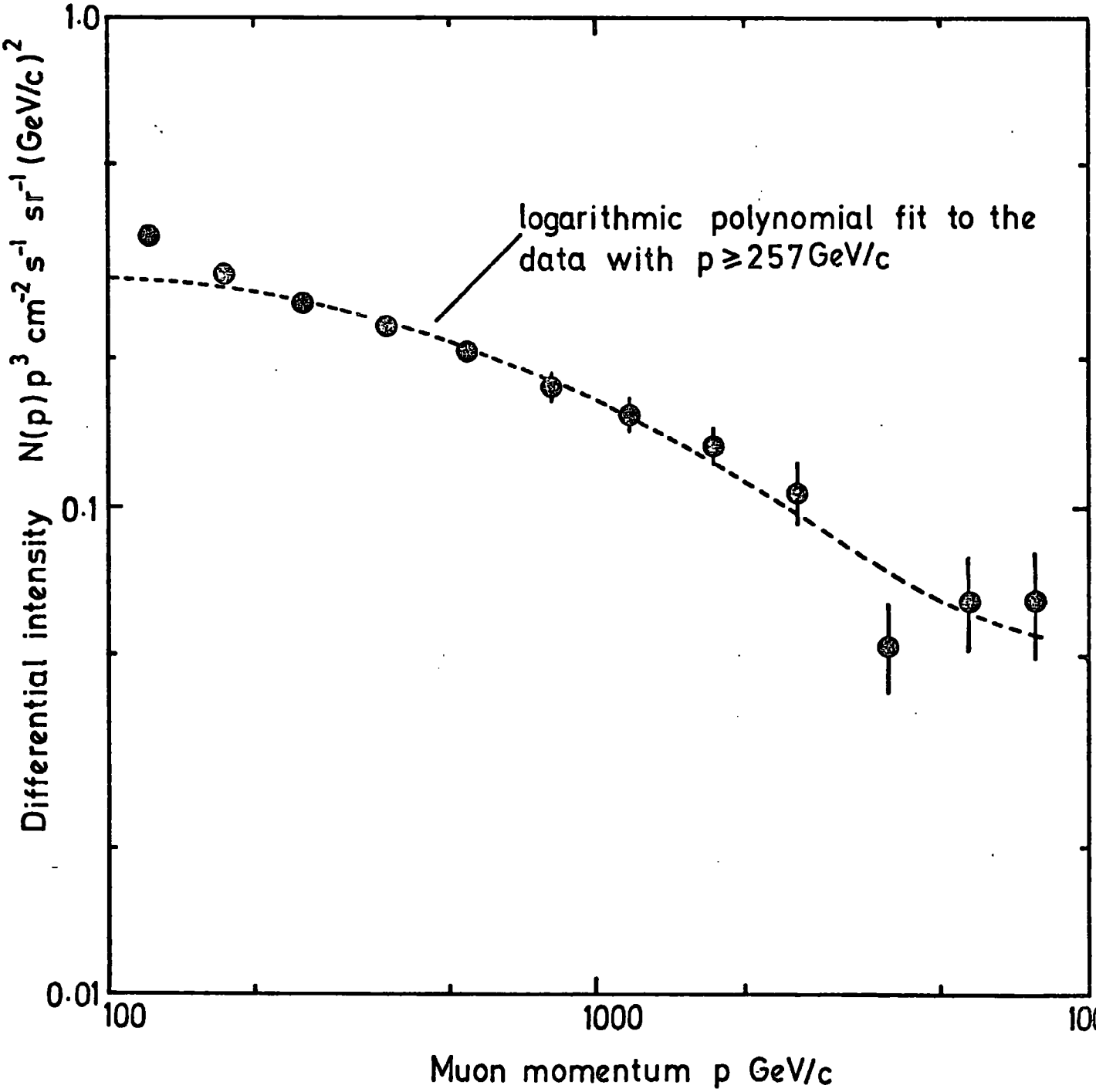

to differentiate the track of the muon in tray 5 from those of the electrons. The event can then be analysed in the usual way and be included in the spectrum of unaccompanied muons.

If the density of shower electrons is large, and there is consequently a large number of particle tracks in tray 5, it is difficult to differentiate the muon track from those of the electrons. In figure 6.3 is shown a frequency histogram of the number of columns containing at least one discharged flash-tube per event in trays 1 and 5. At 30 columns of data there is a wide divergence of the two histograms. This is the point at which it becomes difficult to abstract the muon track from the other tracks in tray 5, and this is the reason why the shower data has been treated separately.

This section will deal with the calculation of the spectrum of shower accompanied muons. First the efficiency of the spectrograph for these events will be discussed.

6.4.2 THE EFFICIENCY OF THE MOMENTUM SELECTOR TO SHOWER EVENTS

Muons accompanied by air shower electrons have a greater chance of triggering the momentum selector due to chance alignment of the muon tracks in trays 1 and 3 with an electron track in tray 5

The probability P_{ms} that a shower event will trigger the momentum selector is given by equation 6.5 (After Hawkes, 1978).

$$P_{ms} = P_{\mu ms}(p_\mu) + P_{ems}(\rho_e) - P_{\mu ms}(p_\mu) \times P_{ems}(\rho_e) \quad (6.5)$$

$P_{\mu ms}(p_\mu)$ is the probability that the muon will trigger the momentum selector (i.e. the normal momentum selector efficiency) and $P_{ems}(\rho_e)$ is the probability that there is a chance alignment of the muon tracks with an electron track which triggers the momentum selector. This is obviously dependent upon the electron density, ρ_e, in tray 5. Hawkes (1978) has calculated the relationship between $P_{ems}(\rho_e)$ and ρ_e and this

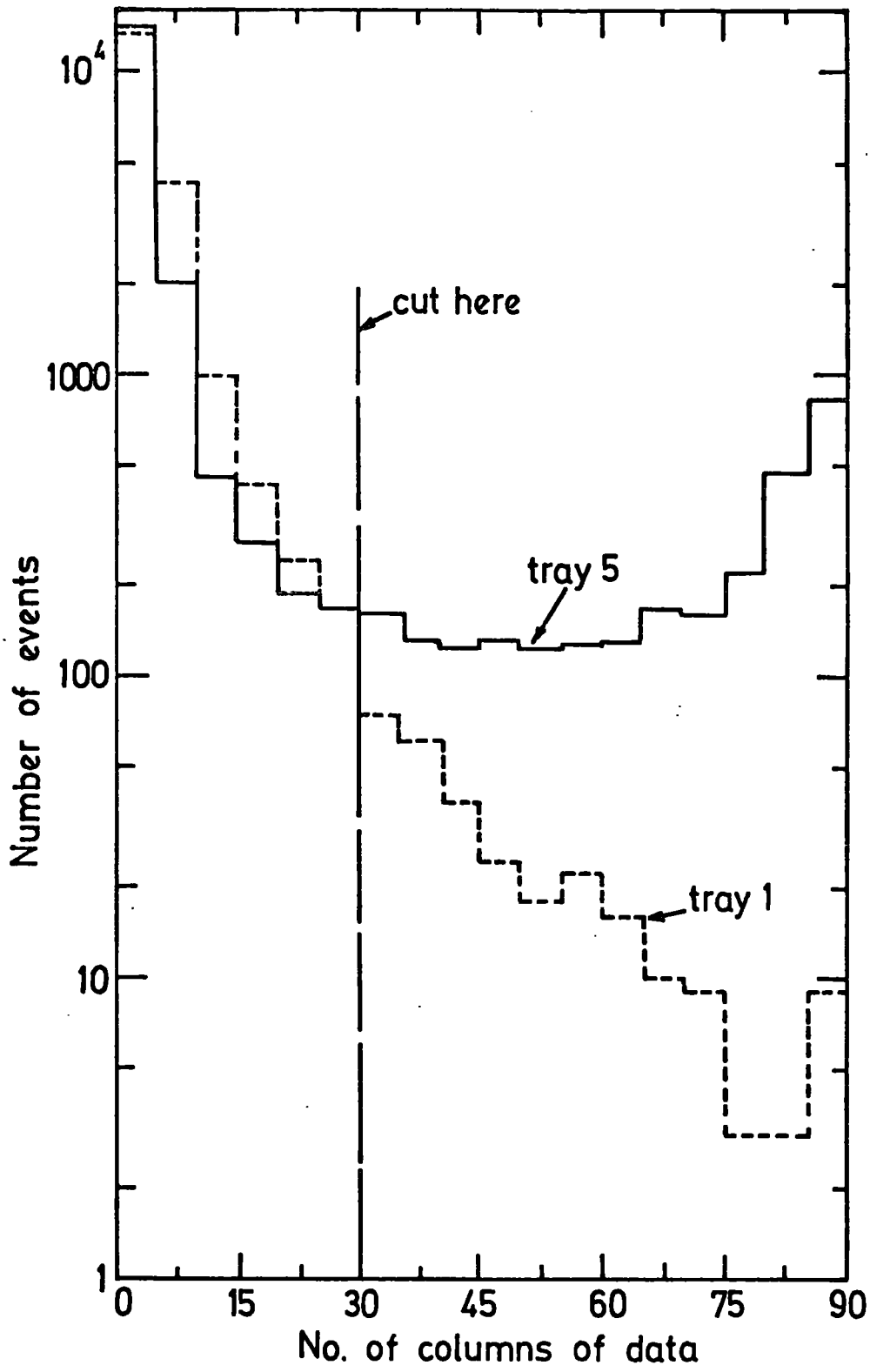

Figure 6.3 Distribution of number of columns of data per event in trays 1 and 5.

is shown in figure 6.4. Therefore, to evaluate equation 6.5, an estimate of ρ_e is needed.

The contributions to the rate of muon events from different radial distances from the shower core, and from different shower sizes have been calculated by Hawkes (1978) and are shown in figures 6.5 and 6.6. These curves have been integrated to give the mean radial distance $\bar{r}$ = 10.0 ±1.0 m and the mean shower size $\overline{Ne}$ = 3.25 (±0.1) $\times 10^5$, for muons of momentum ≥100 GeV/c.

The lateral distribution of electrons in air showers, as suggested by Greisen (1960), is given in equation 6.6, where r_1 is the Molière

$$\rho_e(Ne,r) = \frac{0.4}{r_1^2} Ne \left(\frac{r_1}{r}\right)^{0.75} \left(\frac{r_1}{r + r_1}\right)^{3.25} 1 + \left(\frac{r}{11.4\ r_1}\right) m^{-2} \qquad (6.6)$$

unit and equal to 79 m, Ne is the shower size and r is the radial distance from the core. Therefore, using the mean shower size and radial distance calculated above, it is found that the mean electron density in showers accompanying muons of momentum greater than 100 GeV/c is 67 ±10 m^{-2}.

The probability of triggering the momentum selector due to a chance alignment when the density of the electrons in 67 ±10 m^{-2} can be seen from figure 6.4 to be practically unity. Therefore, from equation 6.5, the momentum selector efficiency for shower events is also unity.

6.4.3 THE ACCEPTANCE OF THE SPECTROGRAPH TO SHOWER EVENTS

The acceptance of the spectrograph to muons accompanied by extensive air showers is greater than the acceptance to unaccompanied muons. This is because muons accompanied by shower particles can enter the front or back plane of the spectrograph between tray 5 and tray 4, the shower particles having triggered the spectrograph. Hawkes (1978) calculated the acceptance of the spectrograph under these

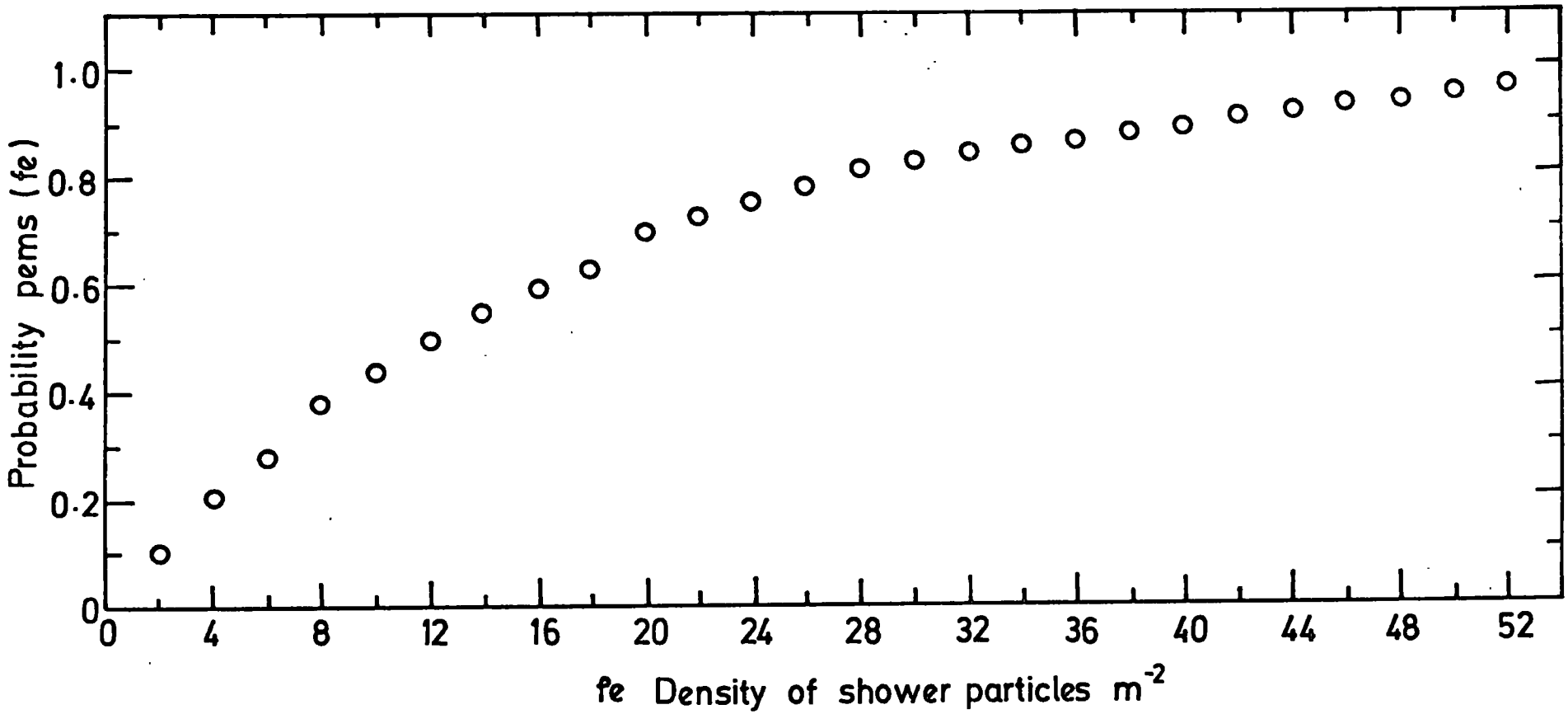

Figure 6.4 The probability of triggering the momentum selector vs density of shower particles.

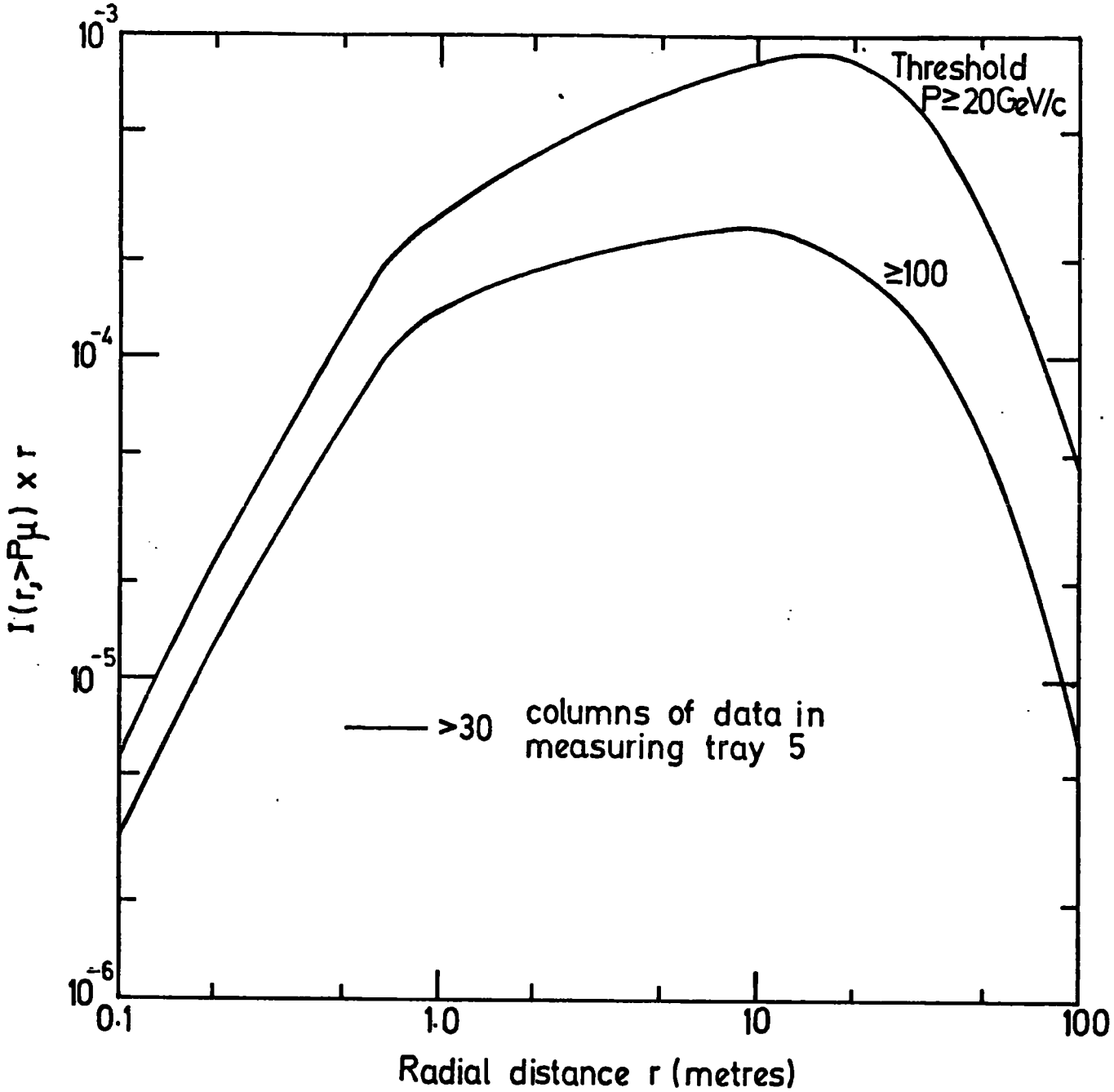

Figure 6.5 Contribution to the predicted rate of events from different radial distances.

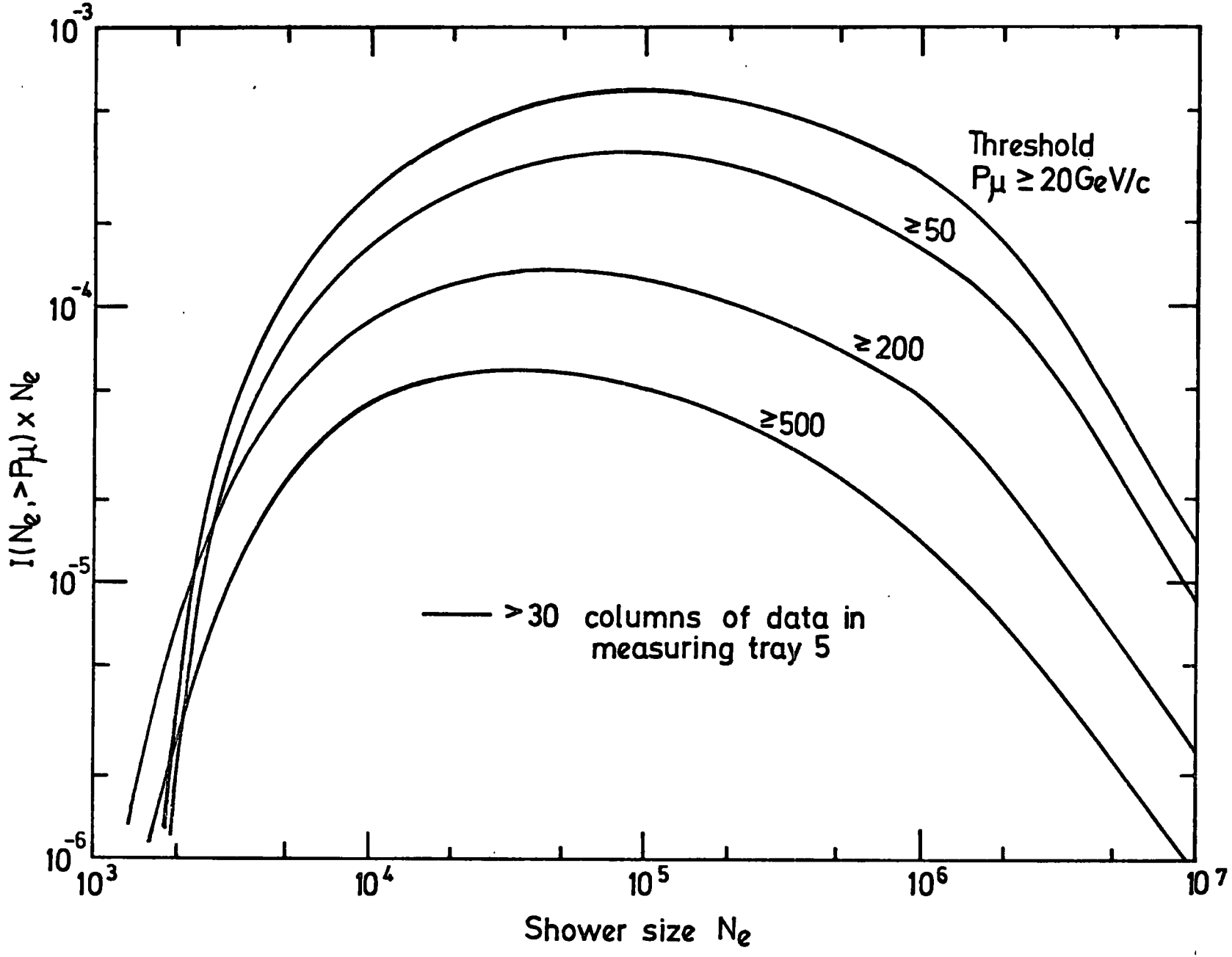

Figure 6.6 Contribution to the predicted rate of events from different shower sizes.

circumstances. and found that the acceptance for shower accompanied muons of momentum $\geq$100 GeV/c is 487 $\pm$3 cm^2 Sr.

6.4.4 THE EFFICIENCY OF THE SCINTILLATION COUNTERS AND MOMENTUM SELECTOR TRAYS

The efficiency of the scintillation counter at level 5 to muons accompanied by air showers can be assumed to be unity. Hence, the overall efficiency of the scintillation counter system is increased to 90.0 $\pm$0.2%.

In a similar way, the overall momentum selector tray efficiency will also increase, and its value for shower events is estimated to be 98 $\pm$1%.

6.4.5 THE ANALYSIS OF THE SHOWER EVENTS

The file of shower events was analysed by Hawkes (1978) as a part of a study of muons in extensive air showers. The MARS2 program described in Chapter 2 was used in the analysis and it was modified to disregard the flash-tube information in tray 5. Therefore, all the events which passed the analysis were either four tray fits (combination 1234) or three tray fits (combinations 123, 234, 134 and 124). There was a requirement, however, that for an event to pass the acceptance test, its trajectory when projected from the lower four trays must pass through tray 5.

All events which were shown to contain a muon and all events given an E94, E95, E96 or E97 error code had computer plots generated and were scanned manually to check the analysis. This was to check that the trajectory passed through the bottom four measuring trays and that there were no chance coincidences of tracks of independent air shower particles.

All four lower trays were used in the analysis whenever

possible. Extensive use was made of the editing facility of the analysis program so that any event which was returned with a three tray fit could be edited in an attempt to obtain a four tray fit. As a result of this, the ratio of the number of four tray fit events to three tray fit events is much higher than that for the unaccompanied data.

6.4.6 THE CALCULATION OF THE SPECTRUM OF ACCOMPANIED MUONS

The momentum spectrum of shower accompanied muons was calculated using equation 6.7.

$$N_{SH}(\bar{p}) = \left(\frac{N_4^{SH}}{C_4^{SH}} + \frac{N_3^{SH}}{C_3^{SH}}\right) \times \frac{1}{\Delta p} \times \frac{1}{Acc^{SH} \times Time \times E_{MST}^{SH} \times E_{SCN}^{SH}} \times \frac{1}{(P_3 + P_4)} \qquad (6.7)$$

Where:

N_4^{SH} and N_3^{SH} are the number of 4 and 3 tray fit shower events.

C_4^{SH} and C_3^{SH} are the 4TF and 3TF corrections for track location errors and multiple scattering.

Acc^{SH} = 483 ±3 cm^2 Sr is the acceptance of the spectrograph to shower events.

E_{MST}^{SH} = 0.98 ±0.01 is the momentum selector tray efficiency.

E_{SCN}^{SH} = 0.90 ±0.02 is the scintillation counter efficiency.

P_3 and P_4 are the probabilities of an event being a 3 or 4 tray fit event.

The corrections, C_4^{SH}, are equal to the corrections for a 4TF event with a tray combination 1234. The corrections C_3^{SH} are equal to the mean of the corrections for 3TF events with tray combinations 123, 234, 134 and 124. The error introduced by averaging the corrections in this way will be small, as the number of 3TF events is small.

To correct for the events which have less than three usable trays of data, the intensities are divided by $(P_3 + P_4)$ where P_3 and P_4

are the probabilities that 3 or 4 trays are usable in an event. For the case of shower events, $P_4 = (1 - P)^4$ and $P_3 = 4P(1 - P)^3$ where P is the probability of losing a tray.

Table 6.7 shows the results of the calculation of the spectrum of shower accompanied events. The errors shown are statistical only. Figure 6.7 shows the intensities plotted against momentum with the unaccompanied muon intensities for comparison, and table 6.8 gives the ratio of the spectrum of accompanied events to unaccompanied events.

It can be seen that the ratio gradually increases with momentum up to 3000 GeV/c, where it is $\sim$5%, and then suddenly jumps to $\sim$20% above 3000 GeV/c. This is probably caused by errors in the analysis due to the electron contamination of the data, leading to greater than expected track location errors. It is considered, therefore, that the data is not reliable above 3000 GeV/c.

6.5 THE SPECTRUM OF ACCOMPANIED AND UNACCOMPANIED MUONS

The accompanied and the unaccompanied muon spectra have been added to obtain the total spectrum of muons incident on the MARS spectrograph. This is given in table 6.9 and shown in figure 6.7. Data beyond a momentum of 3000 GeV/c have not been presented, as the shower data is considered unreliable here. Also this is beyond the maximum MDM of MARS and the individual 5, 4 and 3 tray fit spectra are seen to diverge in this region.

It could be argued that the five tray fit spectrum provides a good estimate of the spectrum up to twice the MDM if it is corrected for resolution errors. There are two main reasons why this has not been done. The first is that the statistics are poor, there being only 20 events greater than 3160 GeV/c and secondly the 5TF spectrum is highly dependent upon the value of P_5 which has a value less than 0.25 for

$\bar{p}$ GeV/c	No. 4TF SHOWERS N_4^{SH}	No. 3TF SHOWERS N_3^{SH}	C_4^{SH}	C_3^{SH}	$P_3 + P_4$	$N^{SH}(\bar{p})$ $GeV^{-1}\ cm^{-2}\ Sr^{-1}\ s^{-1}$
123	134	9	0.935	0.962	0.962	$4.28\ (\pm 0.36) \times 10^{-10}$
177	94	14	0.947	0.891	0.956	$2.21\ (\pm 0.21) \times 10^{-10}$
257	82	4	0.986	0.892	0.944	$1.16\ (\pm 0.12) \times 10^{-10}$
376	57	3	1.007	0.901	0.927	$5.52\ (\pm 0.71) \times 10^{-11}$
553	42	4	1.029	0.950	0.903	$2.90\ (\pm 0.43) \times 10^{-11}$
809	24	3	1.088	1.155	0.872	$1.12\ (\pm 0.21) \times 10^{-11}$
1183	11	1	1.259	1.386	0.834	$3.06\ (\pm 0.88) \times 10^{-12}$
1760	11	0	1.718	1.957	0.781	$1.51\ (\pm 0.46) \times 10^{-12}$
2584	4	0	2.738	2.914	0.715	$2.56\ (\pm 1.3\ ) \times 10^{-13}$
3917	6	0	5.234	4.731	0.623	$1.57\ (\pm 0.64) \times 10^{-13}$
5729	5	1	10.26	7.489	0.521	$6.90\ (\pm 2.8\ ) \times 10^{-14}$
7868	7	0	18.58	10.86	0.425	$3.50\ (\pm 1.3\ ) \times 10^{-14}$

TABLE 6.7 THE MOMENTUM SPECTRUM OF SHOWER ACCOMPANIED MUONS

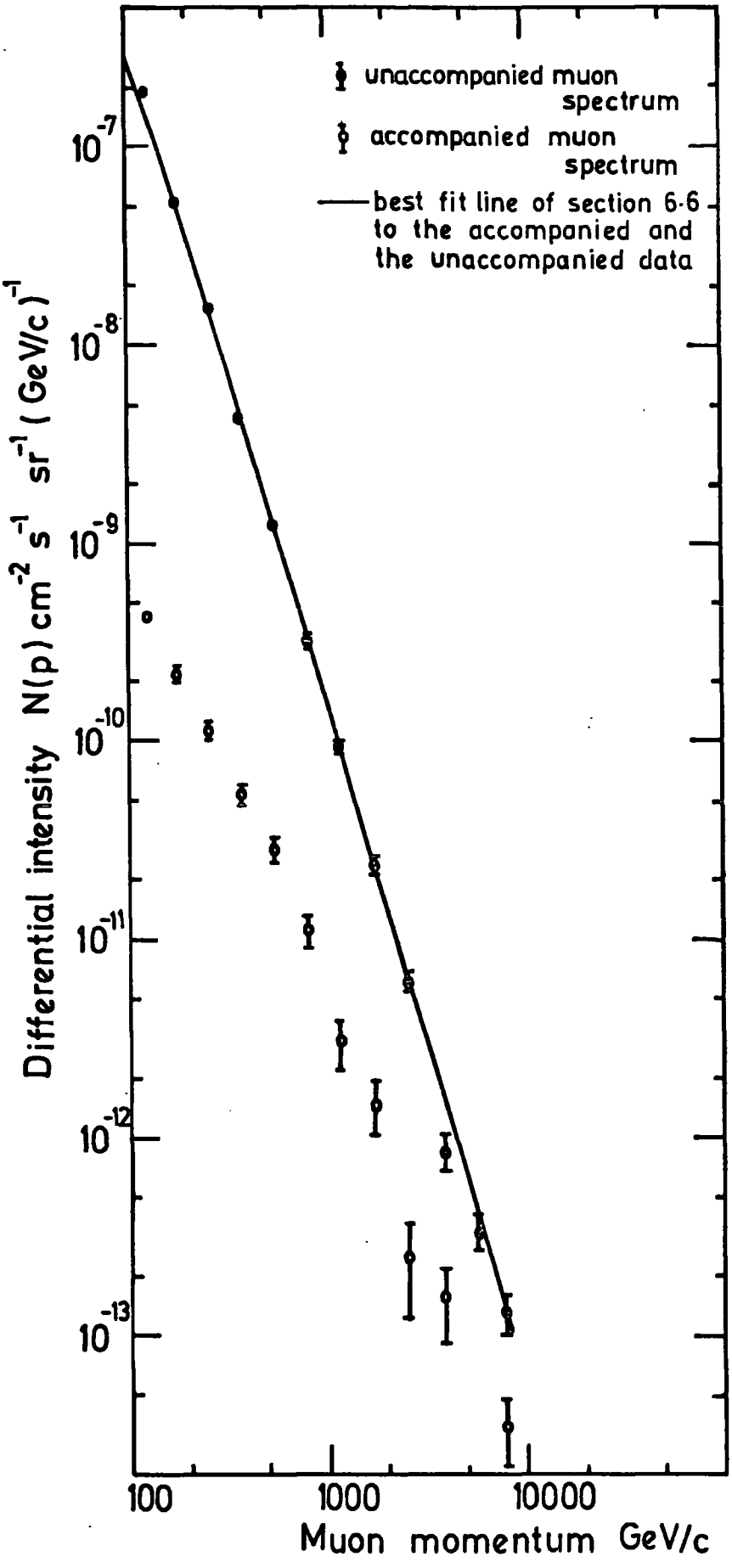

Figure 6.7 The unaccompanied and accompanied muon spectra.

MUON MOMENTUM GeV/c	RATIO %	MUON MOMENTUM GeV/c	RATIO %
123	0.2	1183	3.2
177	0.4	1760	6.2
257	0.8	2584	4.2
376	1.3	3917	18.0
553	2.4	5729	20.0
809	3.4	7868	26.0

TABLE 6.8 THE RATIO OF THE ACCOMPANIED MUON SPECTRUM TO THE UNACCOMPANIED MUON SPECTRUM

MUON MOMENTUM GeV/c	DIFFERENTIAL INTENSITY $cm^{-2}\ Sr^{-1}\ s^{-1}\ GeV/c^{-1}$	MOMENTUM DEPENDENT ERRORS %
123	1.89×10^{-7}	2.2
177	5.38×10^{-8}	1.4
257	1.54×10^{-8}	1.4
376	4.45×10^{-9}	1.9
553	1.26×10^{-9}	2.7
809	3.44×10^{-10}	4.2
1183	9.73×10^{-11}	6.2
1760	2.57×10^{-11}	13.0
2584	6.48×10^{-12}	21.0

TABLE 6.9 THE COMBINED SPECTRUM OF ACCOMPANIED AND UNACCOMPANIED MUONS. (THE ERROR ANALYSIS IS GIVEN IN THE NEXT SECTION)

momenta above 3000 GeV/c and is itself very dependent upon the value of the burst probability at high energies.

To calculate the intensities at standard momenta a logarithmic polynomial, of the form used by Whalley (1974) and given in equation 6.8, has been fitted into the data in table 6.9.

$$p^3N(p) = a_0 + a_1(\ln p)^1 + a_2(\ln p)^2 + a_3(\ln p)^3 \qquad (6.8)$$

The method of least squares was used to calculate $a_0 - a_3$, and the data points were weighted according to their errors. The resulting coefficients are as follows:

$a_0 = 3.2300$	$a_0 = -0.2208$
$a_1 = -1.2670$	$a_1 = 0.3295$
$a_2 = 0.1831$	$a_2 = -0.06110$
$a_3 = -0.009224$	$a_3 = 0.003130$
For a momentum range of	For a momentum range of
100 <P<3000 GeV/c	257 <P<3000 GeV/c

The two polynomials are shown plotted in figure 6.8 with the spectrum of Ayre et al (1975) for comparison. This was measured using the MARS spectrograph with the momentum selector trays as primary detectors. Further details of this experimement can be found in section 6.8.2. All that is required at this point is to know that this was a precise, absolute measurement of the muon spectrum over the momentum range 20 to 500 GeV/c and that it should join up smoothly with the present measurement. It is apparent, however, that the intensities at 123 GeV/c and 177 GeV/c do not fall on a smooth curve between the spectrum of Ayre et al and the present specrum above 257 GeV/c.

There are two reasons why these intensities may be higher than expected. Firstly, the effect of bursts on the momentum selector efficiency may have been underestimated and the momentum selector

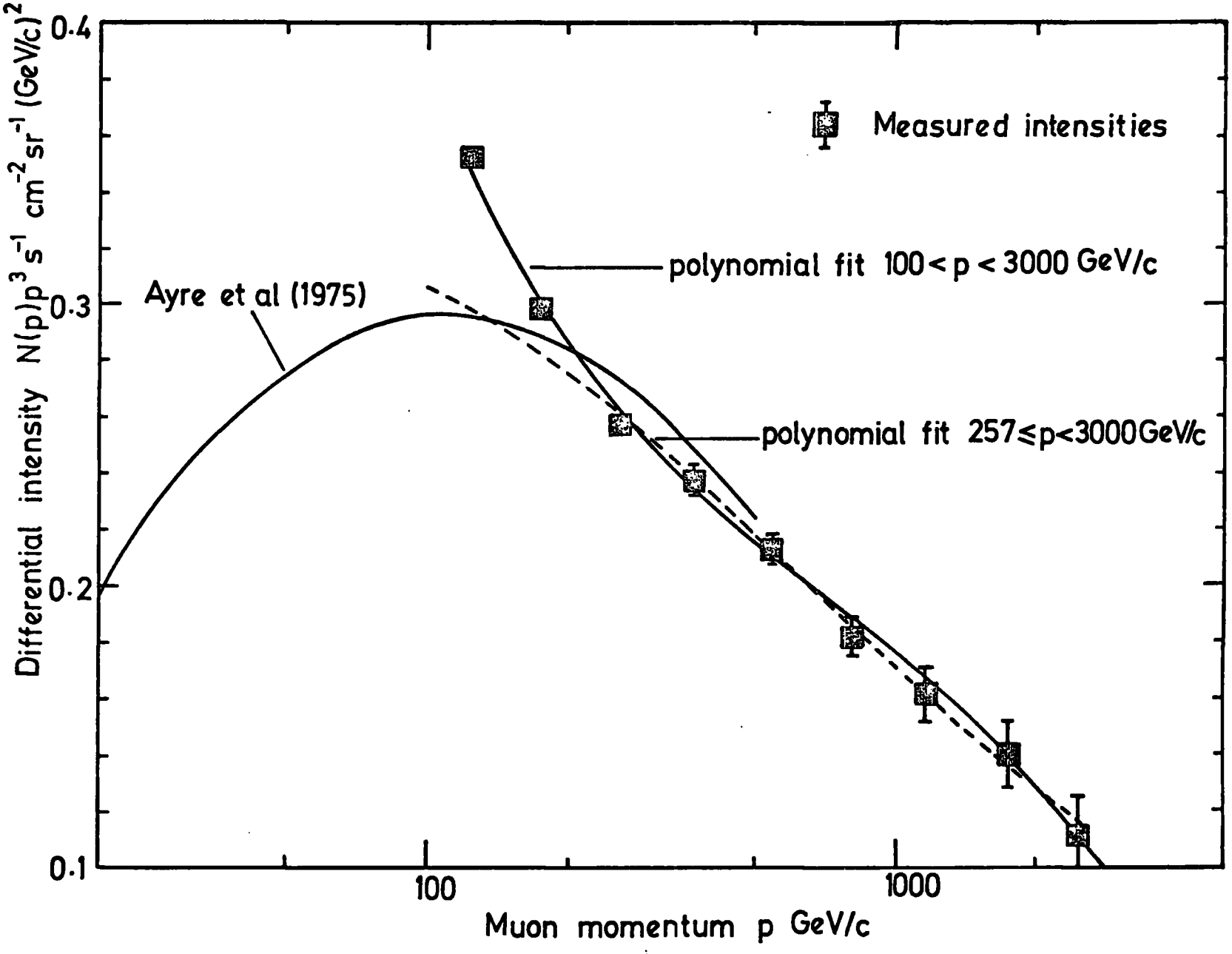

Figure 6.8 The best fit polynomials from the present work compared with the one from the spectrum of Ayre et al (1975).

efficiency between 100 and 200 GeV/c may be higher than has been calculated. Secondly, some of the data which were included in the Class I category were collected after the momentum selector had developed a fault. They were included in the Class I category if the rate of high momentum events was not significantly higher than normal. In this case it was assumed that the fault had occured near the end of the run. Therefore, this may have increased the proportion of events of low momentum. For these reasons, both associated with the momentum selector efficiency close to its cut-off momentum, the two lowest intensities have not been included in the calculation of the intensities at standard momenta. Further justification for this will be given in section 6.7.3.

The technique of fitting a logarithmic polynomial to the spectrum provides a model independent and practical way of calculating the differential and integral intensities at standard momenta. The integral momentum spectrum is given by equation 6.9, whose coefficients are uniquely related to the coefficients of equation 6.8 for the differential spectrum.

$$p^2N(>p) = b_0 + b_1(\ln p) + b_2(\ln p)^2 + b_3(\ln \bar{p})^3 \qquad (6.9)$$

where the coefficients are given by:

$$b_0 = -\left(\frac{a_0}{2} + \frac{a_1}{4} + \frac{a_2}{4} + \frac{3a_3}{8}\right) = 0.04213$$

$$b_1 = -\left(\frac{a_1}{2} + \frac{a_2}{2} + \frac{3a_3}{4}\right) = -0.1365$$

$$b_2 = -\left(\frac{a_2}{2} + \frac{3a_3}{4}\right) = 0.02820$$

$$b_3 = -\frac{a_3}{2} = -0.001565$$

The polynomials defined by equations 6.8 and 6.9 are only valid

within the momentum range $200 < p < 3000$ GeV/c. There are no constraints on their values outside this range.

The differential and integral intensities at standard momenta are given in table 6.10.

MOMENTUM GeV/c	DIFFERENTIAL INTENSITY $cm^{-2}\ s^{-1}\ sr^{-1}\ (GeV/c)^{-1}$	INTEGRAL INTENSITY $cm^{-2}\ s^{-1}\ sr^{-1}$
200	3.44×10^{-8}	3.06×10^{-6}
300	9.32×10^{-9}	1.22×10^{-6}
400	3.63×10^{-9}	6.25×10^{-7}
500	1.75×10^{-9}	3.71×10^{-7}
700	5.70×10^{-10}	1.67×10^{-7}
1000	1.71×10^{-10}	7.10×10^{-8}
1500	4.31×10^{-11}	2.67×10^{-8}
2000	1.60×10^{-11}	1.34×10^{-8}
3000	3.97×10^{-12}	5.14×10^{-9}

TABLE 6.10 THE DIFFERENTIAL AND INTEGRAL INTENSITIES AT STANDARD MOMENTA

6.6 THE ERRORS ON THE SPECTRUM

6.6.1 THE MOMENTUM DEPENDENT ERRORS

Equation 6.4 shows how the differential intensities have been calculated and therefore shows the sources of error in the results. All the terms except A have an error which is dependent upon momentum. Ignoring the error on A, the most probable error on $N(\bar{p})$ is given by

equation 6.10, where the summations are over all nine tray combinations

$$\left(\frac{\alpha_N}{N(\bar{p})}\right)^2 = \frac{\Sigma(\alpha_{Ni}/Ci)^2}{(\Sigma\ Ni/Ci)^2} + \frac{\Sigma(\alpha_{Ci}Ni/Ci^2)^2}{(\Sigma\ Ni/Ci)^2} + \left(\frac{\alpha_{Effc}}{Effc}\right)^2 + \left(\frac{\alpha P_3 + P_4 + P_5}{P_3 + P_4 + P_5}\right)^2 \qquad (6.10)$$

or groups of tray combinations.

The first term of equation 6.10 is due to the random errors on the number of events in each momentum cell and it contributes most to the momentum dependent errors, especially at high momentum where the number of events collected is small.

The second term is due to the errors in the values of the maximum detectable momenta and multiple scattering constants for each tray combination. The multiple scattering constants are known to better than 1% for the 5TF spectrum, 2% for the 4TF spectra and 4% for the 3TF spectra. Investigation of figure 5.9 will show that the multiple scattering correction is small and not very dependent upon the multiple scattering constants, therefore the contribution from the error on the multiple scattering constants to the C_i's has been neglected.

Of greater importance are the errors in the values of the maximum detectable momenta which are systematic in nature and are of the order of ±6% (see section 5.4.4).

The swing in values of the correction, C_i, corresponding to a ±6% swing in the maximum detectable momenta have been calculated, and the results are shown in tables 5.7 and 5.8.

The third term of equation 6.10 is due to errors in the calculation of the momentum selector efficiency. This is estimated to decrease from about 2% at 100 GeV/c, where the effect of burst production

in the magnet blocks is most important, to about 0.2% above 800 GeV/c. The errors arise from statistical errors in the Monte Carlo calculation of the momentum selector efficiency and errors on the quantities used to calculate the correction for burst production.

The fourth term of equation 6.10 is the contribution from the correction for the events lost when fewer than three trays are available for analysis. The probabilities P_3, P_4, P_5 depend upon P_B, P_B^t and P_0 (see section 5.3 for definitions). The latter two values have been determined from the experimental data and their errors are known. The error on P_B is a little uncertain as it is based on the theoretical calculations of Hansen (1976). It has therefore been ignored in the calculation of the fourth term of equation 6.10. The contribution from this term is found to insignificant.

6.6.2 THE MOMENTUM INDEPENDENT ERRORS

The momentum independent errors arise from the errors on the quantities used to calculate A in equation 6.4 and from the error in the magnetic field strength.

The values of the quantities used to calculate A are given in Section 6.3. The error on the run time is assumed to be negligible as it was measured with an electronic scaler counting mains frequency at 50 Hz. Combining the errors in quadrature results in the most probable error on A being equal to 1.2%.

A ±1% variation in the magnetic field strength was shown by Piggott (1975) to produce a ±3.5% variation in the absolute intensity of the spectrum (assuming it has a constant exponent of 3.5). Combining this with the error in A gives a total momentum independent error of ±3.7%.

A summary of the errors on the spectrum is given in table 6.11.

MOMENTUM GeV/c	MOMENTUM DEPENDENT ERRORS (EQUATION 6.10)					MOMENTUM INDEPENDENT ERRORS TOTAL
	TERM 1	TERM 2	TERM 3	TERM 4	TOTAL	
123	1.0	0.0	2.0	0.01	2.2	3.7
177	1.0	0.0	1.0	0.01	1.4	3.7
257	1.3	0.0	0.5	0.01	1.4	3.7
376	1.8	0.0	0.5	0.01	1.9	3.7
553	2.7	0.0	0.3	0.02	2.7	3.7
809	4.2	0.0	0.2	0.02	4.2	3.7
1183	6.1	0.8	0.2	0.03	6.2	3.7
1760	8.9	1.5	0.2	0.04	9.0	3.7
2584	12.3	2.5	0.2	0.04	13.0	3.7
3917	20.4	2.9	0.2	0.07	21.0	3.7
5729	20.9	3.0	0.2	0.08	21.0	3.7
7868	23.4	2.9	0.2	0.10	24.0	3.7

TABLE 6.11 A SUMMARY OF THE ERRORS ON THE MUON MOMENTUM SPECTRUM

6.7 THE DERIVATION OF THE PION AND KAON PRODUCTION SPECTRA

6.7.1 THE THEORETICAL MODEL OF THE MUON ENERGY SPECTRUM

Cosmic ray muons come almost entirely from the decay of charged pions and kaons in the upper atmosphere, the pions and kaons having been produced in interactions between primary cosmic rays (mainly protons and alpha particles) and air nuclei.

The standard theoretical model of the muon energy spectrum developed by Barrett (1952) and further by Bull (1965) has been used to relate the sea level muon spectrum with the production spectra of pions and kaons. This relationship is given in equation 6.11 which is a solution of the diffusion equations describing the interaction and decay of secondary cosmic rays in the atmosphere. The derivation of

$$N(E\mu)\, dE\mu = A\, P\mu\, (E\mu + \Delta E\mu) \left(\frac{r_\pi^{\gamma-1}\, B\pi}{E\mu + \Delta E\mu + B\pi} + \frac{K\, r_K^{\gamma-1} B_K}{E\mu + \Delta E\mu + B_K} \right) \qquad (6.11)$$

this equation and the assumptions made in doing so have been extensively covered in the publications given above and by Thompson (1973) and Whalley (1974) and they will not be repeated here. However, a description of the terms of the equation will be given.

A and γ are constants describing the production spectra of pions and kaons. It is assumed that the spectra have the form $AE^{-\gamma}$, and that the exponent, γ, is the same for pions and kaons. The constants A_1 and γ are to be derived by fitting equation 6.11 to the measured muon spectrum. γ is closely related to the exponent of the primary cosmic ray spectrum.

$P\mu$ is the survival probability of muons assuming they are all produced at a depth of 100 gm cm^{-2}. It is calculated using the formula of Rossi (1952):

$$P\mu(E_0) = \left(\frac{100}{1033} \cdot \frac{E_0}{E_0 + 933\varepsilon}\right)^{\frac{1.027}{E_0 + 1033\varepsilon}}$$

Where E_0 is the muon energy at sea level and ε is the rate of energy loss of muons in the atmosphere.

$E\mu$ and $\Delta E\mu$ are the sea level muon energy and the energy lost by the muon, mainly through the process of ionisation, when descending through the atmosphere. The rate of energy loss is calculated from the formula by Maeda (1964):

$$-\frac{dE}{dx} = 2.5 + 0.0025\ E \quad \text{MeV gm}^{-1}\ \text{cm}^2$$

where E is the muon energy in GeV .

r_π and r_K are the constant fractions of energy that a muon takes from a pion or kaon when it decays. This is an approximation because in any two-bodied decay, the energy of a daughter can have any value within a given range (e.g. $E\pi$ to $E\pi\ m\mu^2/m\pi^2$). The values of $r\pi$ and r_K are 0.76 and 0.52.

K is the ratio of the number of kaons to the number of pions produced in the interactions between primary cosmic rays and air nuclei. Its value has been measured in proton-proton collisions up to equivalent laboratory energies of 2000 GeV at the CERN intersecting storage rings facility. Its value ranges from 0.088 (Morrison and Elbert 1973) to 0.14 (Thompson and Whalley 1977) depending upon the data used and the way it is interpreted. The value of K at cosmic ray energies for primary cosmic ray-air nuclei collisions is even more uncertain. Thompson (1973) surveyed horizontal and vertical measurements of the muon spectrum and concluded that K = 0.3 ±0.15. Previous attempts to fit equation 6.11 to the sea level muon spectrum have not been successful because of poor statistics in the data above 100 GeV/c where most of

the contribution from kaons is expected. An attempt has been made here to derive K from the present measurement of the muon spectrum.

$B\pi$ and B_K are constants which depend upon the properties of the atmosphere and upon the mass and lifetime of pions and kaons respectively. Their values are $B\pi$ = 90 GeV and B_K = 450 GeV.

6.7.2 THE TECHNIQUE USED TO DERIVE THE PION AND KAON PRODUCTION SPECTRA

The variable parameters A, γ, and K of equation 6.11 have been derived by using the method of Whalley (1974). The theoretical spectrum is evaluated for given values of A, γ and K and compared to the measured spectrum by calculating the quantity χ^2 given in equation 6.12. I_0 and Ie are the observed and expected intensities and δI_0 is the

$$\chi^2 = \Sigma \left(\frac{I_0 - Ie}{\delta I_0}\right)^2 \qquad (6.12)$$

error on the observed intensity. It can be shown that when δI_0 is the statistical error on the intensity (i.e. $\propto\sqrt{N}$) then the χ^2 defined above is analogous to the usual χ^2 of a frequency histogram, and tables of percentile values of χ^2 can be used for hypothesis testing.

The parameters K and γ are fixed and the parameter A is allowed to vary until the minimum value of χ^2 is obtained. This is the best fit for those parameters. The value of γ is then changed a little and A is again allowed to vary until a new minimum of χ^2 is obtained. This is repeated for a range of values of γ until the value of γ which gives the best fit of equation 6.11 to the measured spectrum is obtained. The whole process is then repeated for a new value of K. Therefore the best fit value of γ for each value of K is found.

6.7.3 THE SELECTION OF THE DATA POINTS

In section 6.5, it was shown that the measured intensities at 123 and 177 GeV/c do not fall on a smooth curve between the low momentum

spectrum of Ayre et al (1975) and the present data above 250 GeV/c. It was suggested that there was a systematic bias in these intensities and they were subsequently left out of the calculation of the intensities at standard momenta. Further justification for this is provided below.

The theoretical energy spectrum was fitted to the measured intensities in three momentum ranges: $100 < p < 3000$ GeV/c, $177 \leq p < 3000$ GeV/c and $257 \leq p < 3000$ GeV/c. The data above 3000 GeV/c were excluded because they are above the five tray fit MDM of the spectrograph. The results of this are shown graphically in figures 6.9, 6.10 and 6.11.

Consider the first momentum range. The smallest value of χ^2 is 87.7, which is obtained for $K = 0.2$ and $\gamma = 2.71$. From tables of percentile values χ^2_p for the chi-square distribution, the value of $\chi^2_{0\cdot995}$ for 8 degrees of freedom (9 data points) is 22.0. This is much smaller than the measured value of χ^2 and it can be concluded that the fit is very poor.

For the momentum range $177 \leq p < 3000$ GeV/c, the smallest value of χ^2 is 16.76 which is obtained for $K = 0.1$ and $\gamma = 2.60$. The value of $\chi^2_{0\cdot98}$ for 7 degrees of freedom is 16.6. This is about equal to the measured value of χ^2 but the fit is still poor, having a 2% significance level.

Finally, consider the momentum range $257 \leq p < 3000$ GeV/c, i.e. with the first two intensities omitted. The best fit value of χ^2 is now 0.698 which is obtained for $K = 0.0$ and $\gamma = 2.491$. The value of $\chi^2_{0\cdot01}$ for 6 degrees of freedom is 0.872, therefore the fit is very good indeed and is significant at the 99% level. The agreement between the observed and expected intensities can be seen in figure 6.12 which

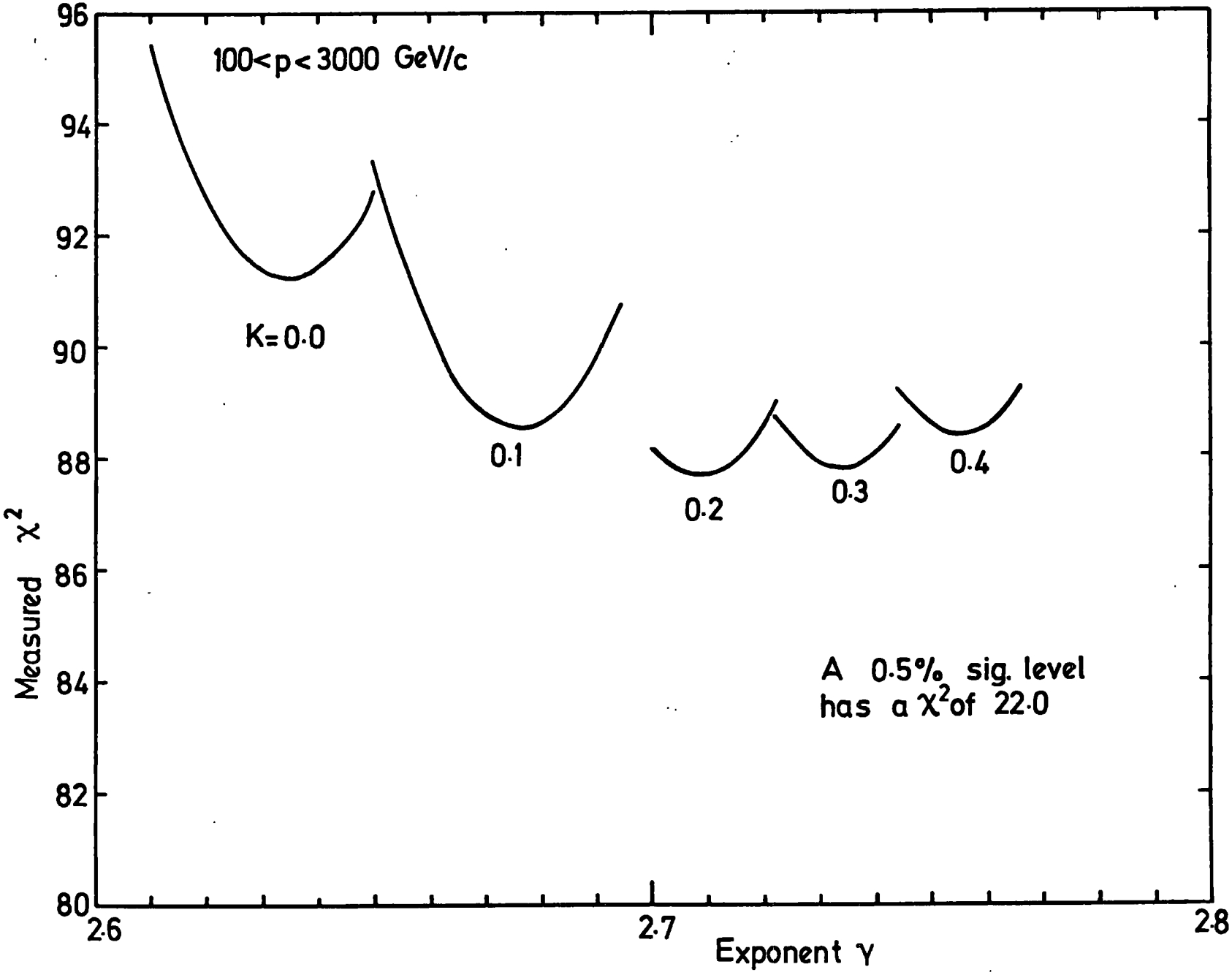

Figure 6.9 χ^2 versus γ for $100 < p < 3000$ GeV/c (9 data points)

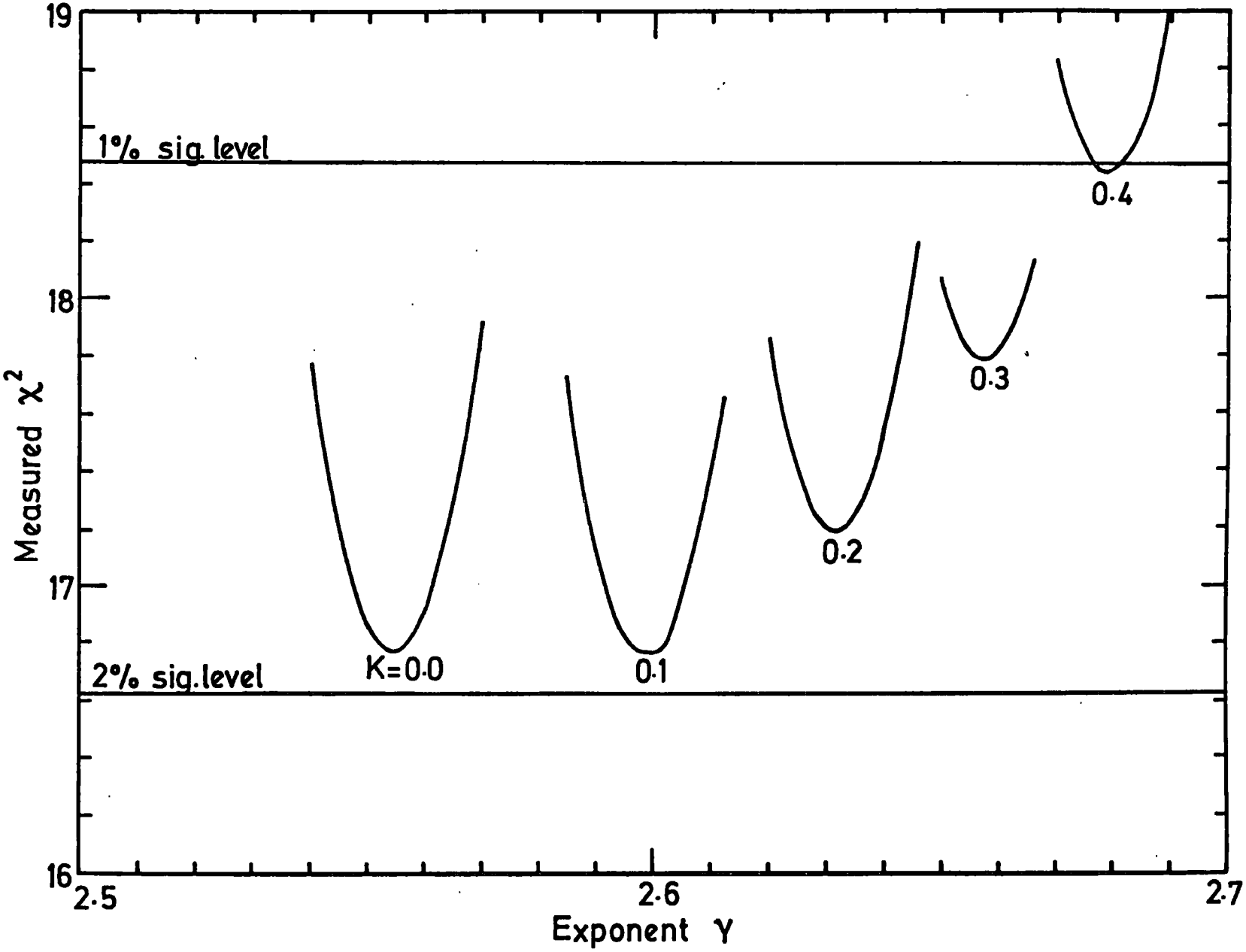

Figure 6.10 χ^2 versus γ for $177 \leq p < 3000$ GeV/c (8 data points).

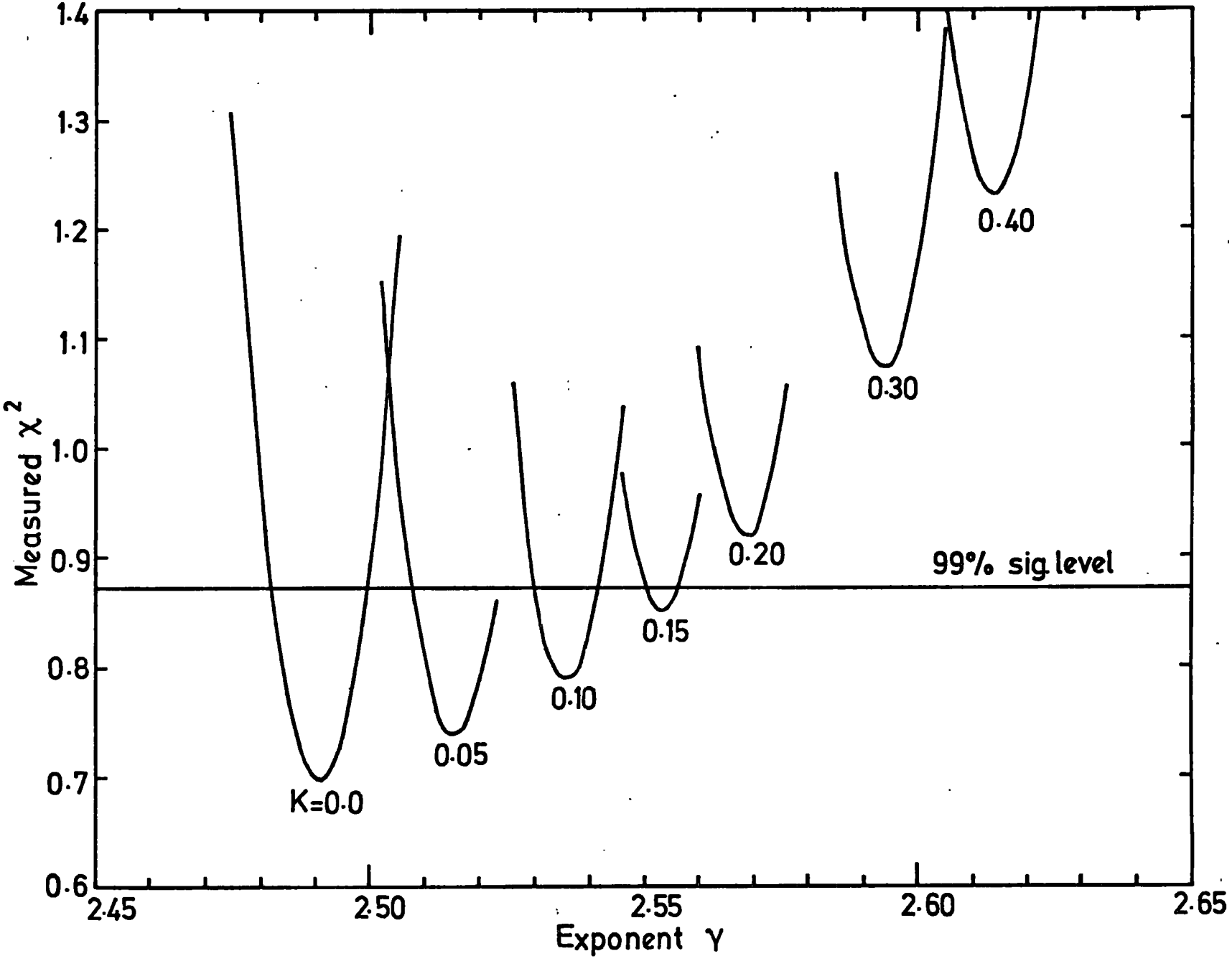

Figure 6.11 χ^2 versus γ for $257 \leq p < 3000$ GeV/c (7 data points).

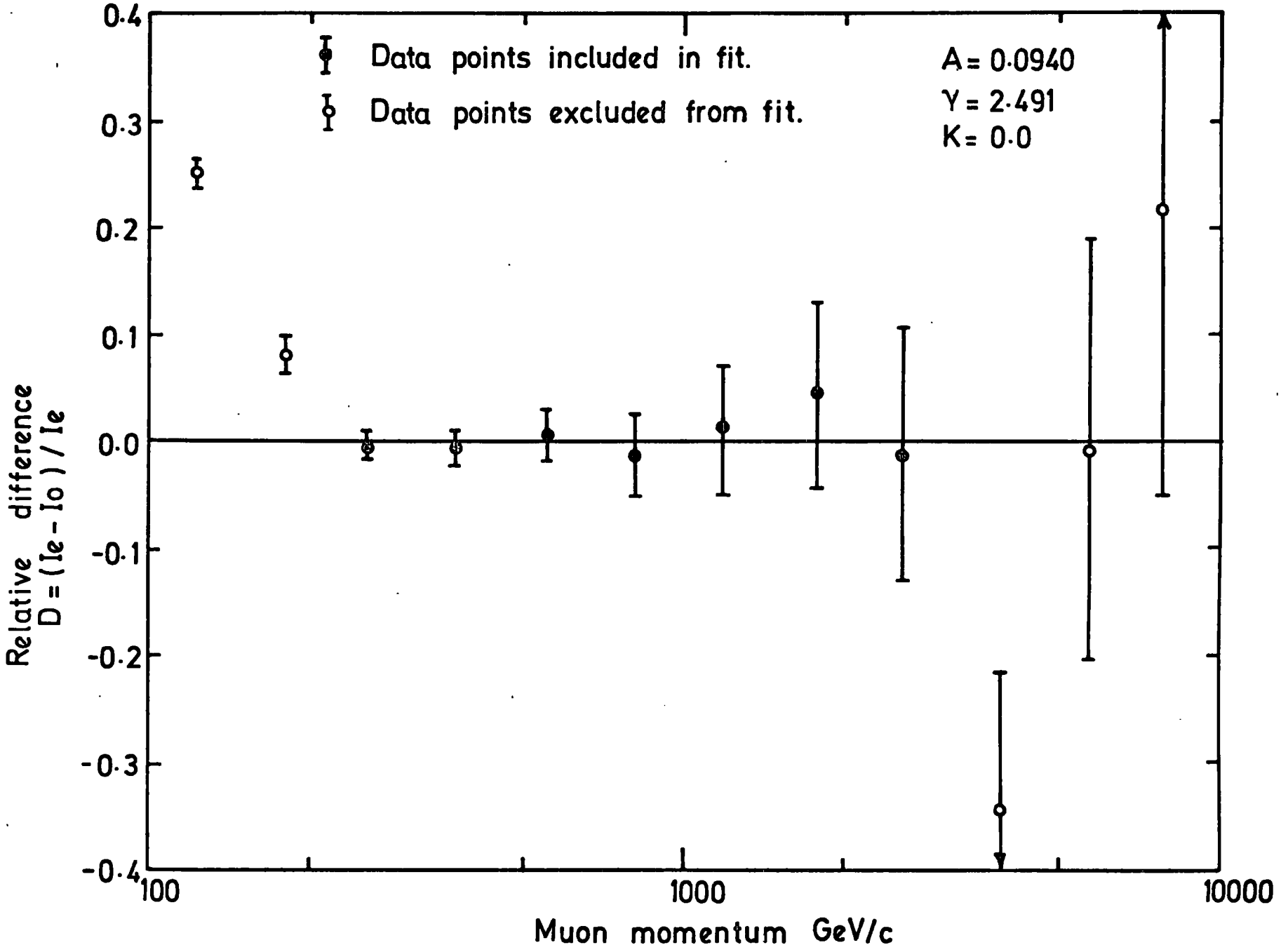

Figure 6.12 A comparison of the measured intensities with the best fit line.

shows D = $(I_0 - Ie)/Ie$ plotted against momentum. There is seen to be little systematic variation of the experimental points around the theoretical spectrum, except for the two points at 123 GeV/c and 177 GeV/c. It is believed therefore, that there is good justification for excluding these two data points.

6.7.4 THE BEST FIT PRODUCTION SPECTRA

It is concluded from figure 6.11 that the best fit of equation 6.11 to the measured intensities is obtained for values of K = 0.0, γ = 2.491 and A = 0.0940. There is no evidence for a minimum of χ^2 in the region $0.1 < K < 0.15$ as predicted from the ISR results. However a value of K in this range is not precluded from the present measurements as the significance level for such values of K is greater than 99%. Table 6.12 shows the best fit values of γ for values of K in the range 0.00 to 0.20.

K	γ
0.000	2.491
0.050	2.516
0.075	2.526
0.100	2.536
0.125	2.545
0.150	2.554
0.200	2.568

TABLE 6.12 THE BEST FIT VALUES OF γ FOR THE GIVEN VALUES OF K

The error on the exponent of the production spectrum can be estimated, somewhat arbitrarily, by finding the values of γ corresponding to the 20% significance level. Thus, in the present case, the best fit value of the exponent of the all pion production spectrum is 2.49 ± 0.06.

6.8 THE COMPARISON WITH DIRECT MEASUREMENTS OF THE MUON SPECTRUM

6.8.1 INTRODUCTION

In this section, the present measurement of the muon spectrum will be compared with some of the most recent direct measurements of the muon spectrum by othe experimentalists.

Up to 1-2 TeV/c the best estimates of the vertical muon spectrum have been obtained directly by using air gap or solid iron magnet spectrographs. However above 2 TeV/c the small acceptance and low MDM of existing spectrographs has limited the availability and precision of the data. In this region indirect measurements of the muon spectrum must be relied upon. These will be considered in the next section.

The results from magnetic spectrographs situated at Durham (UK), Nottingham (UK), Kiel (West Germany), Durgapur (India), San Diago (USA) and College Station, Texas (USA) have been used in comparisons with the present work. A brief summary of the characteristics of these spectrographs is shown in table 6.13. It can be seen that except for the UCSD spectrograph at San Diago, all other spectrographs have a smaller acceptance and MDM than MARS, therefore comparisons between results will not be very significant in most cases. Also, the results from the UCSD spectrograph are open to a little uncertainty because they were measured over a range of zenith angles and the results were combined to give the vertical spectrum.

The spectrum which has been compared with the results from these

LOCATION	AUTHORS	MDM GeV/c	ACCEPTANCE cm^2 Sr^1	ZENITH ANGLE	DETECTORS	MAGNET TYPE	RANGE OF MEASUREMENT GeV/c
DURHAM	HAYMAN & WOLFENDALE(1962)	657	8	0°	GM and FT	AIR GAP	1 - 1000
DURHAM (MARS)	AYRE ET AL (1975)	670	408	0°	S and FT	SOLID IRON	20 - 500
DURHAM (MARS)	PIGGOTT (1975)	2400	408	0°	S and FT	SOLID IRON	100 - 3000
DURHAM (MARS)	PRESENT	2400	408	0°	S and FT	SOLID IRON	200 - 3000
NOTTINGHAM	APPLETON ET AL (1971)	360	18.61	0°	GM and FT	SOLID IRON	3 - 1000
KIEL	ALLKOFER ET AL (1971)	1000	16	0°	S and OSC	SOLID IRON	0.2 - 1000
DURGAPUR	NANDI & SINHA (1972)	985	11.6	0°	GM and FT	SOLID IRON	5 - 1200
SAN DIAGO (UCSD)	BURNETT ET AL (1973)	2500	1550	0°-82°	WSC & S	SOLID IRON	25 - 2000
COLLEGE STATION (AMH)	ABDEL-MOMEM (1973)	700		0°	OSC & S	SOLID IRON	2 - 700

TABLE 6.13 THE SPECTROMETERS USED IN THE COMPARISON WITH THE PRESENT EXPERIMENT

(Key to the abbreviations: GM - Geiger-Muller Counters, S - Scintillation Counters, FT - Flash-tubes, OSC - Optical Spark Chambers, WSC - Wire spark Chambers.)

spectrographs is the best fit of equation 6.11 to the data in the range $257 \lesssim p < 3000$ GeV/c. The best fit parameters are A = 0.0940, γ = 2.491 and K = 0.0, i.e. an all pion production spectrum. The variation of the measured intensites around the best fit line is shown in figure 6.12.

6.8.2 THE DURHAM SPECTRA

Hayman and Wolfendale (1962)

The spectrograph used by Hayman and Wolfendale (1962) was the first to be built at Durham. It had an air gap magnet and an estimated MDM of 657 GeV/c. (Note that the MDM given by Hayman and Wolfendale is based upon the probable error of the trajectory location error and is 1.48 (i.e. 1/0.674) times higher than the MDM based upon the standard deviation of the trajectory location error which is used in the present work). The spectrum was corrected for the magnetic bias, the momentum selector characteristics and for track location errors. The best fit value of γ, the exponent of the pion production spectrum, was found to be 2.67 ± 0.10 for $70 \lesssim p \lesssim 700$ GeV/c. The Hayman and Wolfendale spectrum (or HW spectrum for short) is shown in figure 6.13 and the relative difference between it and the present spectrum is shown in figure 6.15. The large difference in absolute intensity is due to the fact that the HW spectrum was not an absolute measurement and was normalised to the standard intensity at 1 GeV/c givenby Rossi (1948). This intensity is 26% lower than the now accepted recent measurement at 1 GeV/c by Allkofer et al (1971) and 22% lower than the best fit line to a survey of recent measurements of the spectrum in the region $0.2 < p < 10$ GeV/c (see Thompson, 1973).

It can be seen that although the best fit to the HW spectrum is steeper than the present one, the data points are not in disagreement.

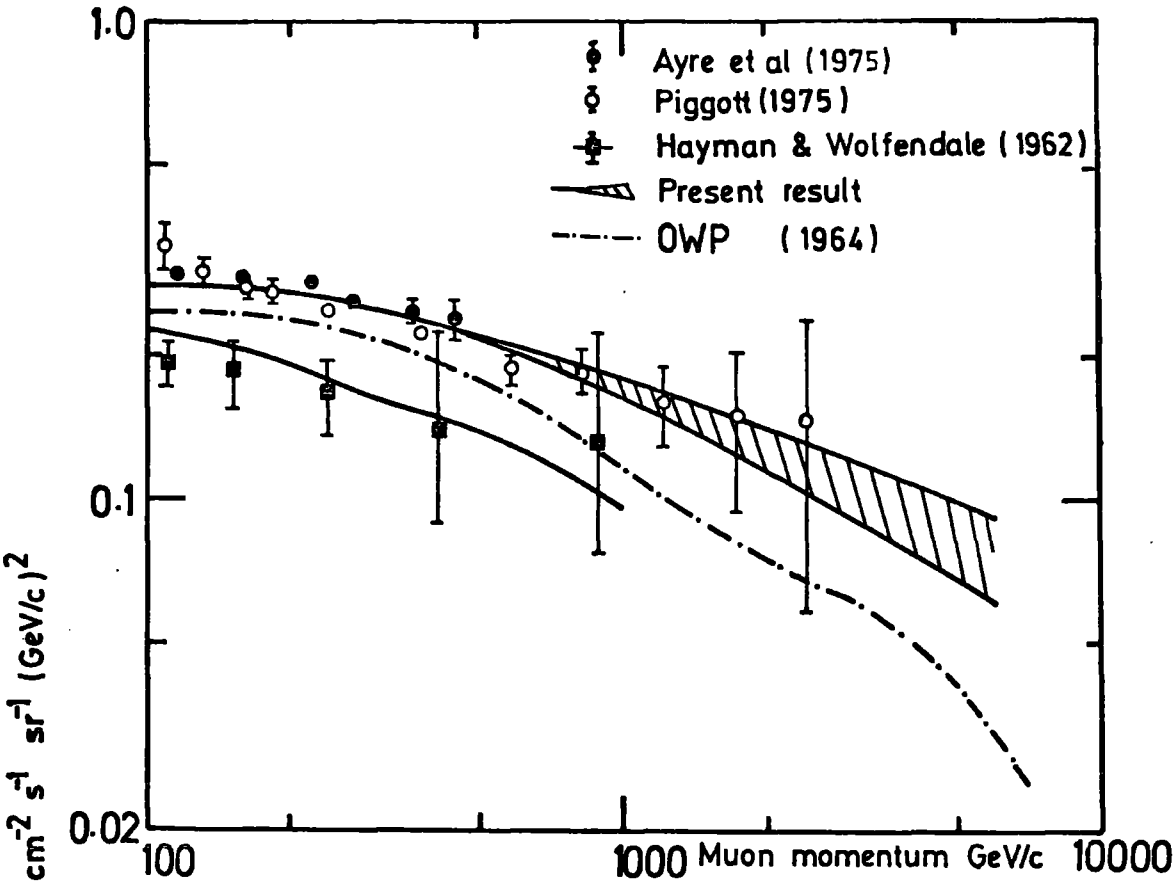

Figure 6.13 A comparison with previous measurements of the muon spectrum made at Durham.

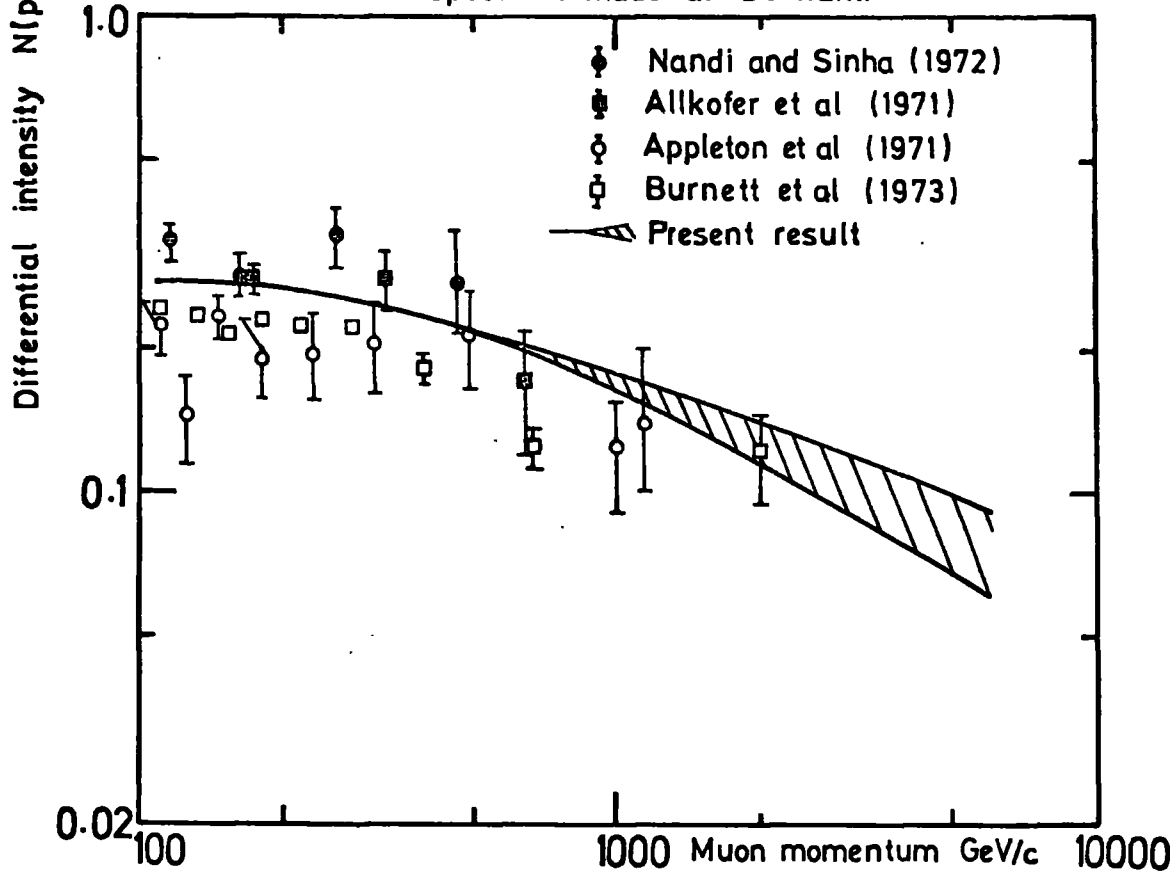

Figure 6.14 A comparison with other recent direct measurements of the main spectrum.

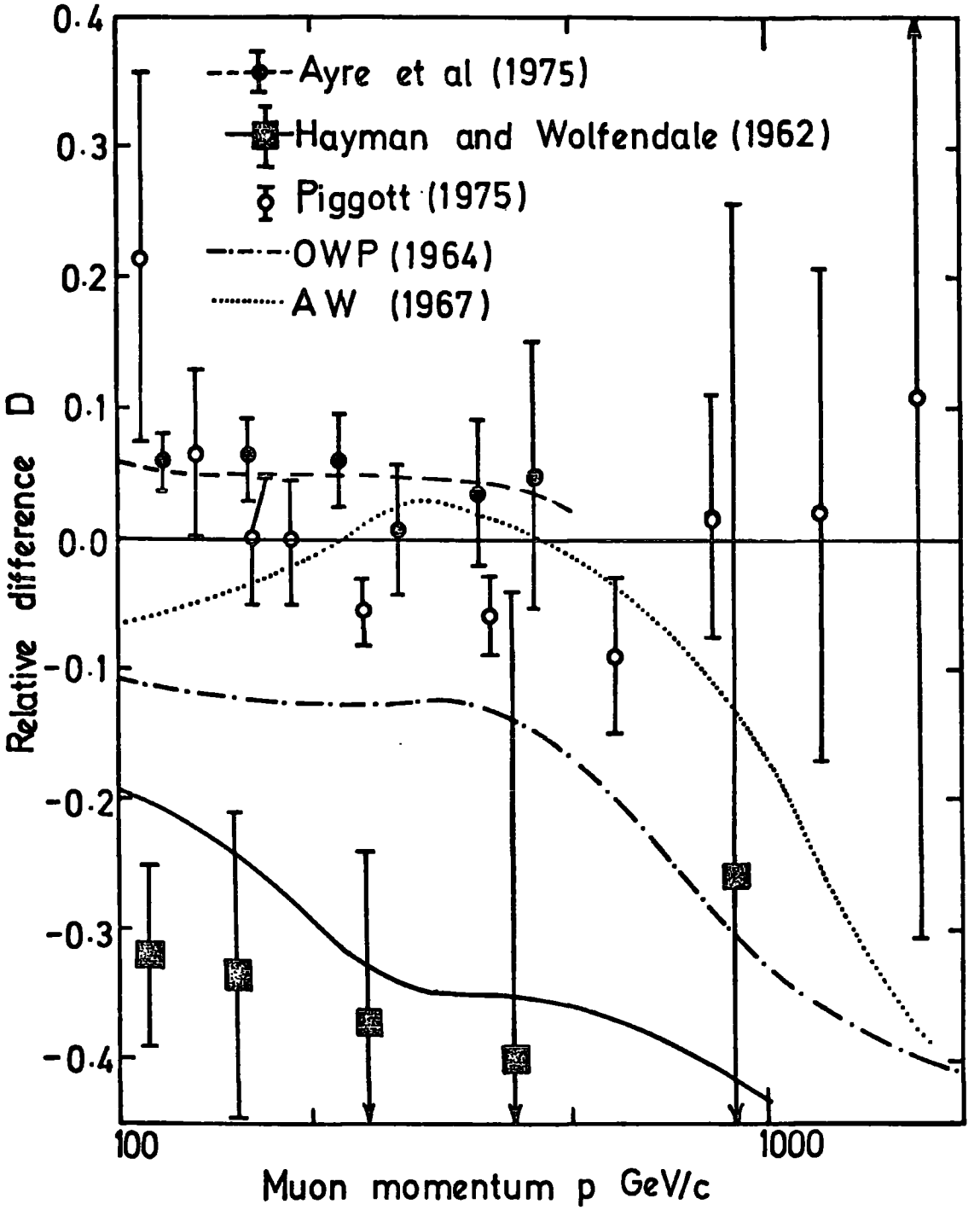

Figure 6.15 A comparison with other measurements of the muon spectrum made at Durham.

Ayre et al (1975)

An independent measurement of the muon spectrum between 20 and 500 GeV/c was carried out by Ayre et al (1975) on the MARS spectrograph, using the trays of large diameter flash-tubes as the trajectory location detectors. The MDM of MARS was estimated to be 670 GeV/c. The spectrograph was fully automated, the analysis of the discharged flash-tubes and the collection of the data being controlled electronically. The spectrum was corrected for multiple Coulomb scattering, the variation of the spectrograph acceptance with momentum, event rejection and for the category acceptance function. The spectrum, which is absolute, is shown in figures 6.13 and 6.15. The agreement in shape between the two spectra in their region of overlap is seen to be very good. However, the present measurement is about 5% lower in absolute intensity. A possible cause of this is thought to be a systematic error in the scintillation counter efficiencies. In section 4.6 it was shown how the overall efficiency of the scintillation counters had decreased over the period of the experiment and it was assumed that the fall had been linear with time. If this had not been the case, the true efficiency might well have been 5% lower than has been calculated.

Whalley (1974) used the model described in the previous section to find the best fit parameters of the pion and kaon production spectra from the spectrum of Ayre et al. It was found that a power law production spectrum with a constant γ over the entire energy range was inconsistent with the measurements. A better fit to the data was obtained by making a break in the spectrum at 70 GeV/c. The results obtained by Whalley are shown in table 6.14. It can be seen that γ is significantly lower for both values of K in the 70 - 500 GeV/c momentum range. The value of γ (2.51 $\pm$0.04) obtained in this momentum range, for

MOMENTUM RANGE GeV/c	K	γ	SIGNIFICANCE LEVEL %
20 - 70	0.00	2.63 ±0.02	35
20 - 70	0.15	2.64 ±0.02	35
70 - 500	0.00	2.51 ±0.04	90
70 - 500	0.15	2.56 ±0.04	90

TABLE 6.14 THE BEST FIT PARAMETERS OF THE PRODUCTION SPECTRA FOR THE SPECTRUM OF AYRE ET AL (1975)

a kaon to pion ratio of zero, is not significantly different from the value of γ (2.49 ±0.06) obtained in the present work for p > 200 GeV/c. Therefore the present result confirms the flattening of the pion production spectrum, for pion energies in excess of 100 GeV/c, which was reported by Whalley (1974).

Piggott (1975)

The spectrum of Piggott was based on approximately the first 25% of the data presented here. It is therefore not an independent measurement of the muon spectrum. However, because the corrections to the spectrum were calculated independently, it has been presented here.

The events were analysed using the MARS2 analysis program and the spectrum, which is absolute, was corrected for multiple Coulomb scattering and for the rejection of events. However, no correction was made for the trajectory location errors and this manifests itself in figures 6.13 and 6.15 in a definite rise in the measurements for p > 800 GeV/c. The increase in the measured intensities at low momentum is also seen in the spectrum of Piggott.

The best fit value of γ, the exponent of the all pion production spectrum, obtained by Piggott was 2.545. This is a little higher than in the present case, and is thought to be due to the inclusion of the measurements between 100 and 200 GeV/c which have been rejected in the present work.

6.8.3 THE UCSD SPECTRUM OF BURNETT ET AL (1973)

The results from the spectrograph at the University of California, San Diago, are statistically the most precise, and extend to the highest energy so far reported. The spectrograph has a solid iron magnet with scintillation counters and wire spark chambers for particle detection. It has an MDM of 2500 GeV/c, practically the same as that of MARS, and

an acceptance of 1550 cm^2 sr, about four times as great as that of MARS. The whole spectrograph is capable of rotation through 360°, allowing measurements to be made at any zenith angle. The measurements were made at eight angles from 0 to 82° and from 0 - 40 in terms of inverse energy $1/E\ (TeV)^{-1}$. The data at different zenith angles were combined in a fairly model independent way to give the vertical muon spectrum with small statistical errors. The model assumed an all pion source and a value of 2.715 ±0.015 was derived for the exponent of the pion production spectrum. Since publication at the Denver conference in 1973, the intensities have been raised by 15%. However, as figures 6.14 and 6.16 show, the absolute intensity of the spectrum is still 15 - 20% below the present result. The measured intensities are in good agreement with the shape of the present spectrum, although the slope of the pion production spectrum is significantly higher than in the present case.

6.8.4 THE RESULTS FROM OTHER SPECTROGRAPHS

The results from spectrographs at Nottingham (Appleton et al 1971), Durgapur (Nandi and Sinha 1972), Kiel (Allkofer et al 1971) and College Station, Texas (Abdel-Monem et al 1973) are summarised graphically in figures 6.14 and 6.16. All the measurements have been corrected for multiple Coulomb scattering and trajectory location errors. However, because of the small acceptance of these spectrographs there are large errors on the measurements for momenta above 100 GeV/c. Although this makes significant comparisons with the present spectrum difficult, it can be seen that the measured intensities from these spectrographs (with the exception of the AMH spectrograph at College Station) are not in serious disagreement with the shape of the best fit to the present measurements.

All the authors fitted an all pion production spectrum to their

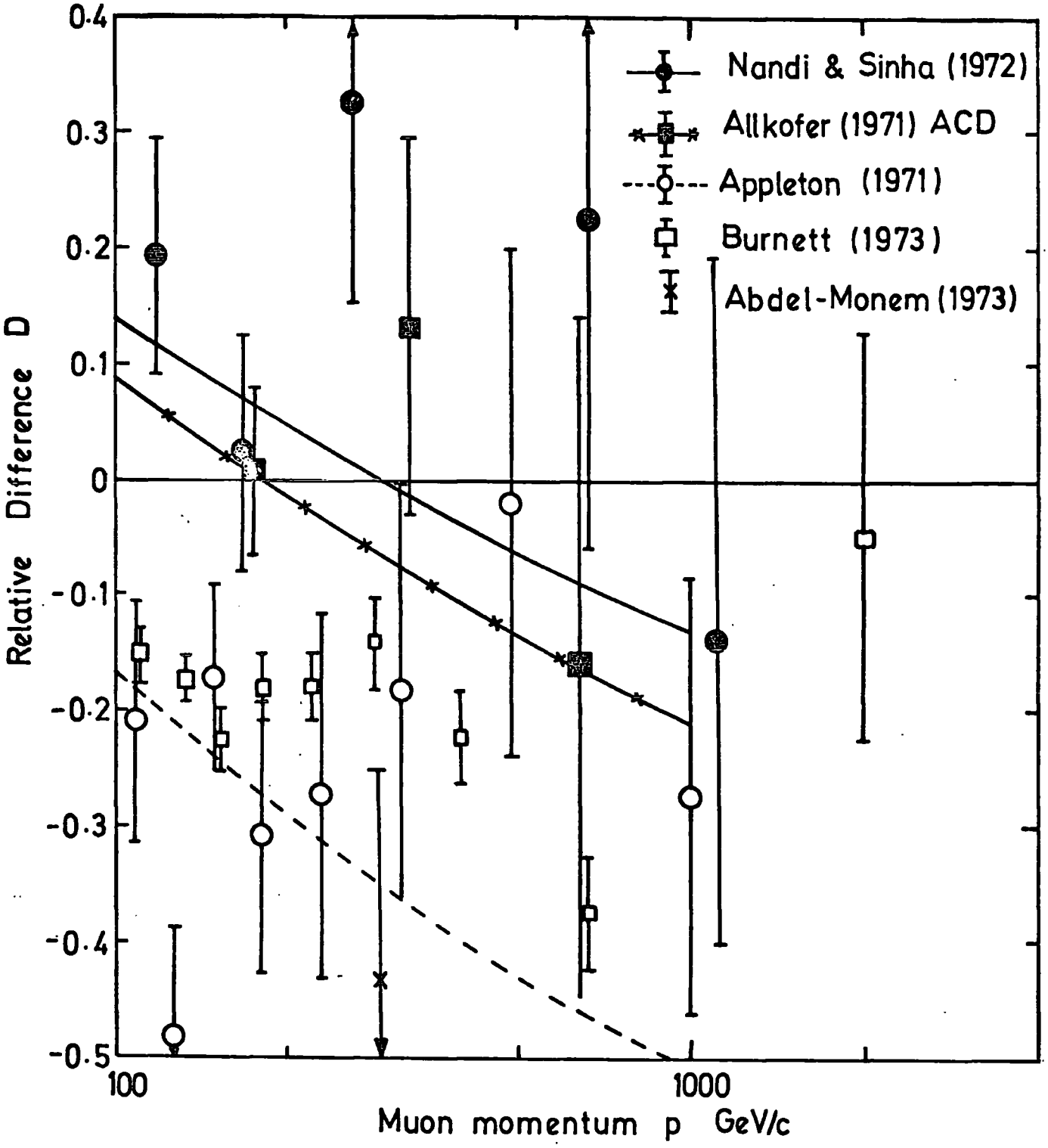

Figure 6.16 A comparison with other measurements of the muon spectrum.

measurements in a similar way to that used here. In all cases the exponent of the pion production spectrum was steeper than the present result. The best fit lines of Nandi and Sinha, Allkofer et al and Appleton et al are shown in figure 6.16. The values of the exponents are given in table 6.15.

The measurements of Appleton et al and Nandi and Sinha were not absolute. Appleton et al normalised their measurements to the 1 GeV/c integral intensity of Greison (1942). This is now known to be an underestimate and this explains why their results are significantly below the present measurements. Nandi and Sinha normalised their results to the now accepted standard intensity of Allkofer et al (1971) at 1 GeV/c. However, their results are significantly higher than the present measurements, and higher than the absolute measurements of Allkofer et al.

The masurements of Allkofer et al, which are absolute, are seen to be in good agreement with the present absolute measurements.

The spectrum of Abdel-Monem et al is also absolute, however, the single intensity at 293 GeV/c is significantly below the present best estimate.

6.8.5 CONCLUSIONS

The absolute intensity of the present measurement of the muon spectrum is in good agreement with previous measurements from the MARS spectrograph. It is $\sim$5% lower than the independent measurements of Whalley (1974) and $\sim$5% higher than the measurements of Piggott (1975). Of the other spectra considered, only the measurements of Allkofer et al (1971) are in agreement with the absolute intensity of the present result.

The disagreement in absolute intensity with the other results is thought to be due to either the method of normalisation (in the cases of Hayman and Wolfendale and Appleton et al) or to instrumental

difficulties (Burnett et al and Nandi and Sinha).

The shape of the present best fit spectrum is in agreement with the measured intensities from all the spectrographs considered although in most cases the errors are large. The situation regarding the value of the best fit exponent of the pion production spectrum is summarised in table 6.15.

For the measurements which extend from around 10 GeV/c, the value of the exponent is in the range 2.63 to 2,73. In these cases, the value of γ is heavily weighted by the results at low momentum. In contrast to this, the results from MARS, which extend from 70, 100 and 200 GeV/c respectively, give a value of γ in the range 2.49 to 2.545, which is significantly lower. It appears, therefore, that the conclusion of Whalley (1974) is correct and the pion production spectrum is flatter for pion energies in excess of 100 GeV/c. This is not inconsistent with the measurements extending from around 10 GeV/c because it can be seen in figure 6.16 that the measured intensities above 100 GeV/c are mainly above their respective best fit lines. The present measurements suggest that the flatter pion spectrum continues to a pion energy of about 4000 GeV/c and possibly further if the results above the MDM of MARS can be relied upon.

6.9 THE COMPARISON WITH INDIRECT MEASUREMENTS OF THE MUON SPECTRUM

6.9.1 INTRODUCTION

The present measurement of the vertical muon spectrum extends to higher energies than have hitherto been measured directly. Therefore, indirect measurements of the muon spectrum, which extend far beyond the range of magnetic spectrographs, will serve as a useful, but tentative comparison with the present result.

The two most common indirect methods of measuring the muon spectrum

AUTHORS	MOMENTUM RANGE GeV/c	BEST ESTIMATE OF γ
HAYMAN AND WOLFENDALE	70 - 700	2.67 ±0.1
AYRE ET AL	20 - 70	2.63 ±0.02
AYRE ET AL	70 - 500	2.51 ±0.04
PIGGOTT	100 - 3000	2.545
PRESENT RESULT	200 - 3000	2.49 ±0.06
APPLETON ET AL	3 - 1000	2.73 ±0.02
NANDI AND SINHA	5 - 1200	2.61 ±0.03
ALLKOFER ET AL	0.2 - 1000	2.63
ABDEL-MONEM ET AL	2 - 700	2.67
BURNETT ET AL	25 - 2000	2.715 ±0.015

TABLE 6.15 THE BEST ESTIMATE OF γ, THE EXPONENT OF THE ALL PION PRODUCTION SPECTRUM

are based upon depth-intensity measurements underground or underwater and measurements of showers induced in lead or iron plates at sea level. Both of these methods, however, rely upon a knowledge of interaction cross-sections at the highest energies, where they have not been verified experimentally. Further difficulties arise in depth-intensity measurements underground from estimating the atomic number, atomic mass and depth of the rock above the detector, and from straggling caused by bremsstrahlung and inelastic nuclear interactions.

Another indirect method is to measure the intensity of γ cascades with depth in the atmosphere. Then by assuming that all the γ's come from neutral pions and that neutral and charged pions are produced in equal proportions in nuclear interactions, the pion production spectrum and hence the sea level spectrum can be deduced. This is very dependent upon the model chosen to describe the production and propogation of cosmic rays in the atmosphere and it is therefore subject to many uncertainties.

Therefore, because of the difficulties associated with indirect measurements, the comparison with direct measurements can only be tentative.

6.9.2 INDIRECT MEASUREMENTS OF THE MUON SPECTRUM

The Spectrum Of Osborne et al (1964)

After the publication of the Hayman and Wolfendale spectrum, an instrumental bias was found in the result. In 1964, Osborne et al published a best estimate spectrum (known as the OWP spectrum) which followed the corrected HW spectrum up to 50 GeV, then followed the spectrum of Duthie et al (1962) up to 200 GeV (this was based on γ cascade measurements and was raised by 10% by Osborne et al and finally followed the spectrum based on the depth-intensity measurements of Miyake et al (1964) up to 7000 GeV. Therefore, for the purposes of this work, the OWP spectrum

is an indirect measurement.

The OWP spectrum is shown in figures 6.15 and 6.17 where it can be seen to be lower in absolute intensity but in good agreement with the shape of the present measurement up to about 500 GeV/c. Here the OWP spectrum steepens as it follows the depth-intensity spectrum.

The Spectrum Of Aurela And Wolfendale (1967)

The spectrum of Aurela and Wolfendale (known as the AW spectrum) was based on a new direct measurement of the muon spectrum using the spectrograph of Hayman and Wolfendale, modified by the inclusion of an iron plug in the magnet. It was also based on the OWP spectrum and on the underground measurememts of Achar et al (1965). The AW spectrum is shown for comparison with the present spectrum in figure 6.15 where it can be seen that the agreement is not good. This is thought to be due to difficulties in the normalisation of the various components making up the AW spectrum.

The Spectra Of Wright et al (1973) and Ng et al (1973)

Surveys of indirect measurments by Wright et al (1973) and Ng et al (1973) are shown in figure 6.17.

The line of Wright et al is calculated from depth-intensity measurements underground and underwater using a re-assesment of the range-energy relation for different materials.

The line of Ng et al is a fit of the form $AE^{-\gamma}/(1 + E/90)$ to magnetic spectrograph measurments, γ cascade measurements, burst measurements and depth-intensity measurements made underground. The best fit value of γ was found to be 2.69 ± 0.026.

The spectrum of Wright is seen to be in good agreement with the magnetic spectrograph data up to about 1000 GeV/c and then it steepens slightly in comparison with the present result. The best fit of Ng et al

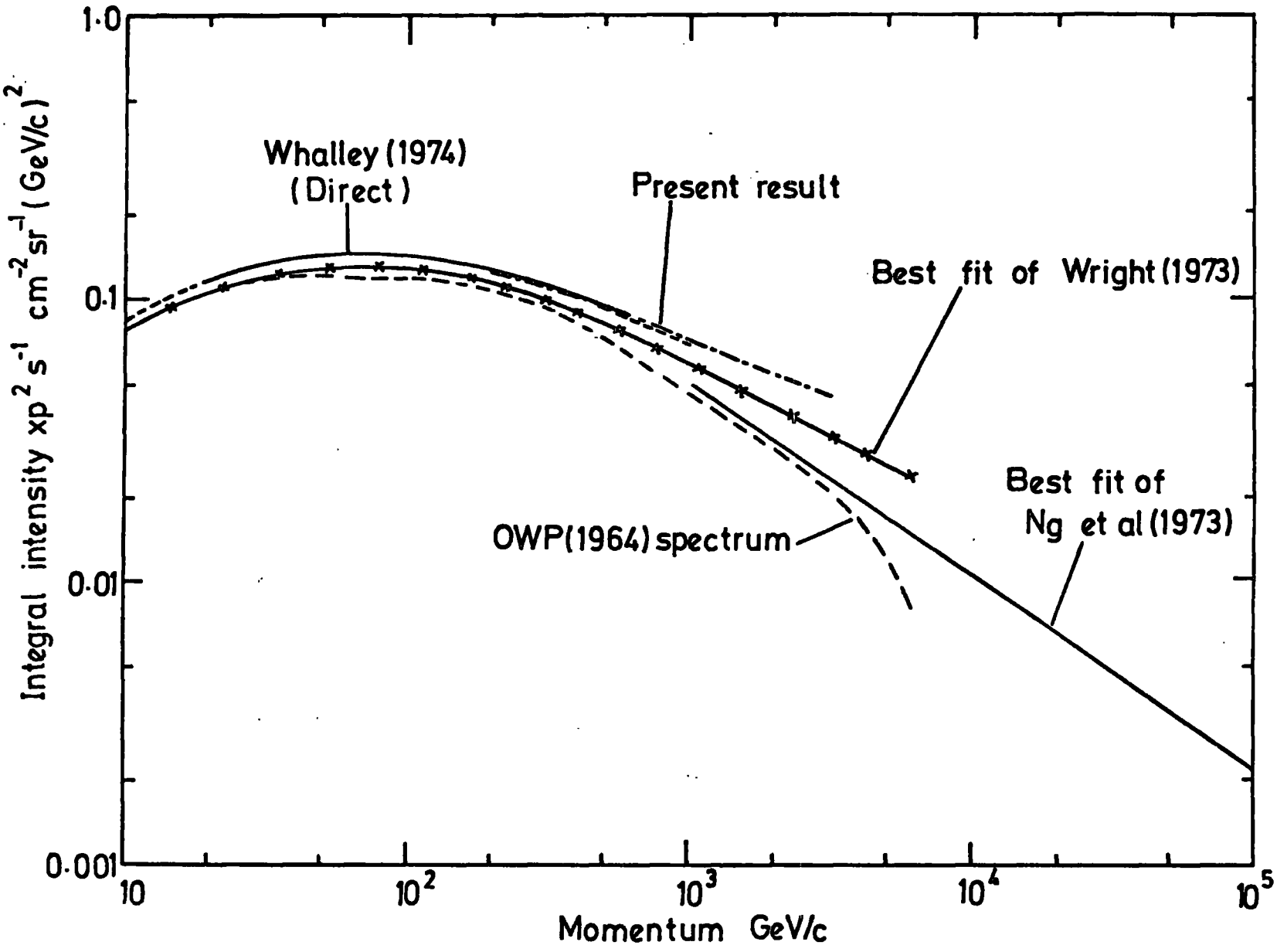

Figure 6.17 The present work shown in comparison with three surveys of indirect measurements of the muon spectrum.

is in disagreement with the present result and that of Wright et al, being steeper in both cases.

The Spectra Of Mizutani et al (1978) and Krisnaswamy et al (1977)

The integral intensities of the present measurements, based on equation 6.9, are compared in figure 6.18 with the recent burst measurements of Mitzutani et al (1978) and the underground measurements of Krisnaswamy et al (1977). It is seen that the indirect measurements are again steeper than the present best estimate of the muon spectrum.

6.9.3 CONCLUSIONS

Above 1000 GeV/c, the present measurement of the muon spectrum is seen to be flatter than the indirect measurements considered above. However, there is also disagreement between the indirect spectra, the line of Wright et al being significantly flatter than the OWP spectrum and the best fit of Ng et al. It is thought that the situation will remain unresolved until further direct measurements of the spectrum are made at energies above 1000 GeV/c.

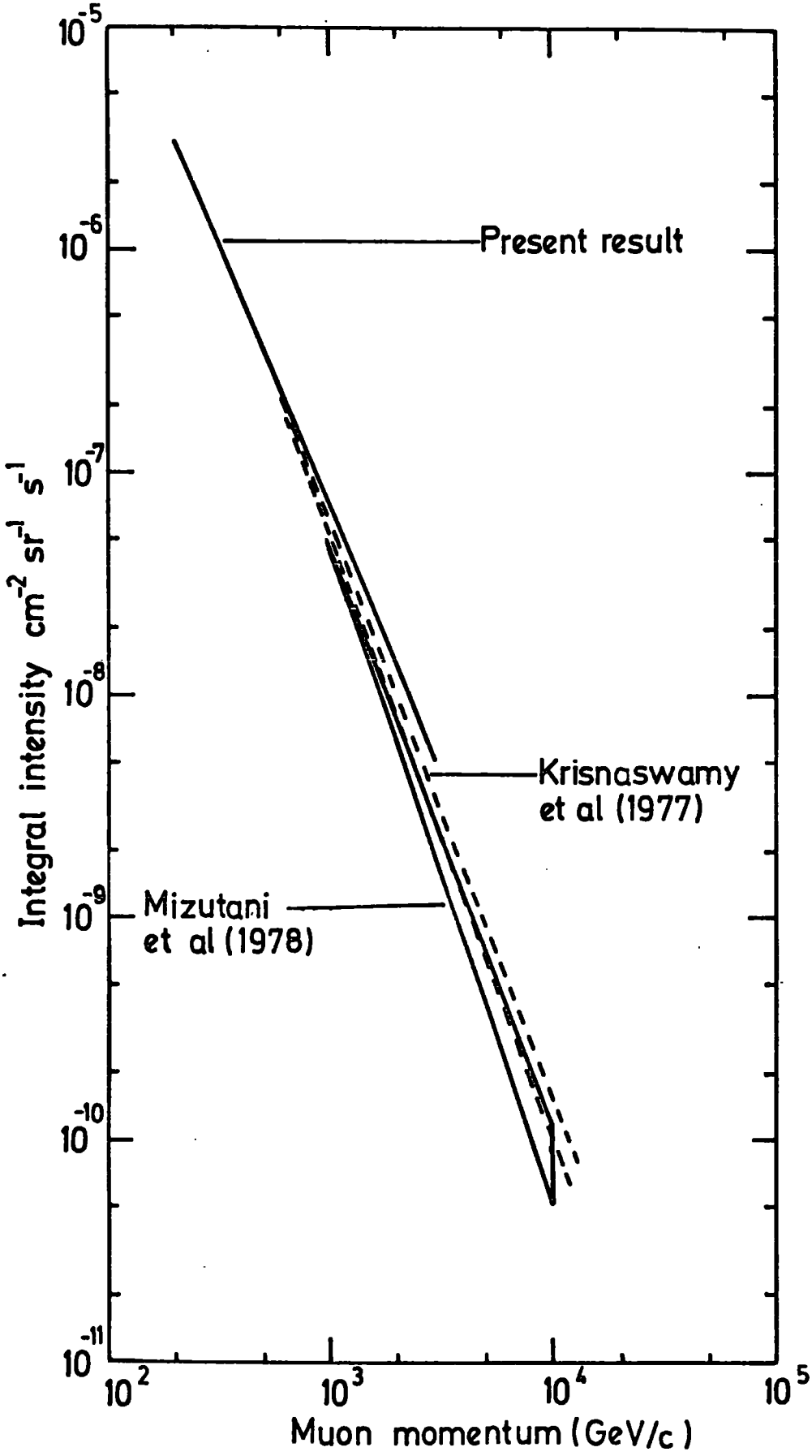

Figure 6.18 The present work shown in comparison with two recent indirect measurements of the muon spectrum.

CHAPTER 7

THE MUON CHARGE RATIO

7.1 INTRODUCTION

The data presented in the previous chapters have been used to measure the muon charge ratio above 100 GeV/c. The charge ratio is defined as the ratio of the number of positively charged muons to the number of negatively charged muons.

A previous independent measurement of the muon charge ratio by Baxendale et al (1975), using the MARS spectrograph, established its value to within a few per cent for momenta between 10 GeV/c and 100 GeV/c. The present measurement extends the MARS results up to 1000 GeV/c but with less precision. Above 1000 GeV/c the poor statistics limit the reliability of the data.

7.2 THE COLLECTION AND ANALYSIS OF THE DATA

Details of the collection and analysis of the data have been given in previous chapters. Of particular importance in charge ratio measurements is the bias caused by the different acceptance of the spectrograph to positively and negatively charge muons when operated in a particular field direction. The magnetic field was reversed once every 24 hours and table 7.1 shows the live times of the spectrograph in each field direction. The ratio of positive field run time to negative field run time is 0.9947. Therefore, it is considered that this bias has been kept to a minimum.

Another bias which can affect the measurement of the muon charge ratio is that caused by track location errors. As the muon momentum approaches the maximum detectable momentum of the spectrograph, the probability that the muon will be given the wrong sign increases. This is because the deflection of the muon becomes similar in magnitude to

MAGNETIC FIELD DIRECTION	LIVE TIME		
	HOURS :	MIN :	SEC
+	2551	03	55
-	2567	20	36
+ and -	5118	24	31

TABLE 7.1 THE LIVE TIMES IN THE TWO FIELD DIRECTIONS

the track location error of the measuring trays and the direction of curvature of the trajectory of the muon may be wrongly estimated. Therefore for momenta greatly in excess of the MDM of the spectrograph, the curvature of the trajectory of the muon will be assigned on a random basis and the charge ratio will approach unity. In fact this is not a great problem with the five tray fit data because, for momenta greater than the MDM, the poor statistics limit the accuracy of the measurements. However, the three tray fit and four tray fit data in excess of their respective maximum detectable momenta should not be used in the calculation of the charge ratio as they will dilute the charge ratio of the five tray fit events. Therefore, the approach has been to take each tray combination in turn and to reject those events which are greater than the MDM for that tray combination. Table 7.2 shows the data used to calculate the charge ratio. It is considered that this method minimises the bias caused by trajectory location errors.

The charge ratio, calculated using equation 7.1 for the 3, 4 and 5 tray fit data separately, is shown plotted against momentum in figure 7.1. It can be seen that within the errors, there is fairly good agreement between the three results and it is considered that there are no serious systematic differences between the three sets of data. Also, there is no indication that the charge ratio is approaching unity at high momenta.

The muon events which are accompanied by extensive air showers (i.e. the shower events described in section 6.4) have not been included in the calculation of charge ratio. This is because in the core of an air shower there are successive nuclear interactions which lead to the generation of charged pions and kaons. These successive interactions lead to a dilution of the original charge ratio of nucleons

TRAY COMBINATION	12345		1234		1235 1345		1245		2345		ALL 4TF EVENTS		123 345 234		145 125		124 245 235 134		135		ALL 3TF EVENTS	
MUON MOMENTUM GeV/c	−	+	−	+	−	+	−	+	−	+	−	+	−	+	−	+	−	+	−	+	−	+
100/147	2547	3325	147	209	391	499	444	534	404	539	1386	1781	65	72	68	68	129	162	18	25	280	327
147/215	2648	3560	152	196	430	582	383	498	345	461	1310	1737	59	71	66	71	129	149	15	26	269	317
215/316	1580	1979	97	133	350	443	263	306	234	283	944	1165	38	42	44	59	83	114	12	18	177	233
316/464	690	1008	70	67	191	232	99	150	121	156	481	605	18	30	34	39	42	60	8	17	102	146
464/681	302	400	20	30	99	111	52	78	48	75	219	294			16	20	21	33	7	8	44	61
681/1000	113	164	12	13	38	57	23	30	24	34	97	134			6	6	11	24	1	6	18	36
1000/1470	53	69	8	8	14	26	11	10			33	44			1	3			4	2	5	5
1470/2150	17	19			8	11	5	10			13	21										

TABLE 7.2 THE DATA USED TO CALCULATE THE MUON CHARGE RATIO

Figure 7.1 The muon charge ratio for the 5,4 and 3 tray fit data separately.

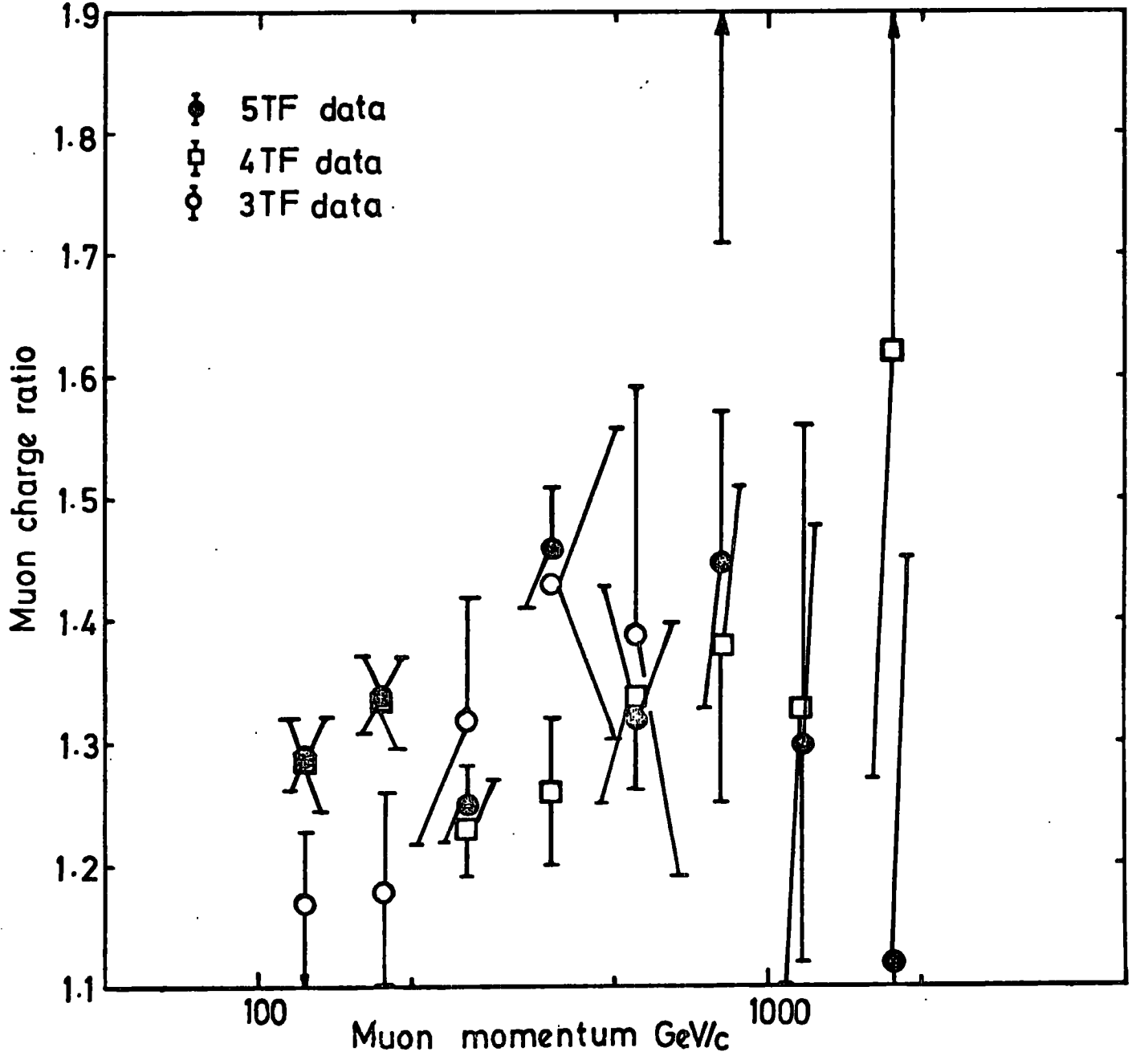

in the primary radiation to such an extent that the charge ratio of the pions and kaons approaches unity. Therefore, on theoretical grounds, the charge ratio of muons (which are the decay products of pions and kaons) will be unity in the core of extensive air showers. Hawkes (1978) has calculated the charge ratio of the shower accompanied muons in MARS with the result that it has the value 1.05 ±0.06, in agreement with the theoretical predictions.

7.3 THE CALCULATION OF THE CHARGE RATIO

Two methods of calculating the charge ratio were investigated. Let the numbers of positive and negative muons collected with a positive magnetic field be N_+^+ and N_-^+ and the number collected with a negative magnetic field be N_+^- and N_-^- respectively. Let the acceptance of the spectrograph to these muons be A_+^+, A_-^+, A_+^- and A_-^- respectively and let t^+ and t^- be the run time with a positive and a negative magnetic field respectively. Then the charge ratio may be calculated by dividing the total number of positively charged muons by the total number of negatively charged muons. This ratio will be called R_1 and is given by equation 7.1.

$$R_1 = \frac{N_+^+ + N_+^-}{N_-^+ + N_-^-} \qquad (7.1)$$

In the present case, the ratio of positive field run time to negative field run time is practically unity, hence it is unnecessary to normalise the number of events to equal run times. This method assumes that the four acceptances defined above are equal.

The second method which has been investigated is one in which the charge ratio measured with a positive magnetic field, R^+, and the charge ratio measured with a negative magnetic field, R^-, are combined geometrically. If I^+ and I^- are the intensities of positive and

negative muons, then using the notation defined above the following equations can be written:

$$N_+^+ = I^+ A_+^+ t^+ \qquad (7.2)$$

$$N_-^+ = I^- A_-^+ t^+ \qquad (7.3)$$

$$N_+^- = I^+ A_+^- t^- \qquad (7.4)$$

$$N_-^- = I^- A_-^- t^- \qquad (7.5)$$

The true charge ratio is $R_2 = I^+/I^-$ which can be re-written using equations 7.2 - 7.5 as follows:

$$R_2 = R^+ \frac{A_-^+}{A_+^+} \qquad (7.6)$$

and

$$R_2 = R^- \frac{A_-^-}{A_+^-} \qquad (7.7)$$

where $R^+ = N_+^+/N_-^+$

and $R^- = N_+^-/N_-^-$

The trajectory of a positively charged muon in a positive magnetic field has the same curvature as a negatively charged muon in a negative magnetic field. Similarly, the trajectory of a positively charged muon in a negative magnetic field has the same curvature as a negatively charged muon in a positive magnetic field. Therefore it is reasonable to assume $A_+^+ = A_-^-$ and $A_+^- = A_-^+$ and from equation 7.6 and 7.7 the charge ratio is given by:

$$R_2 = \sqrt{R^+ \times R^-}$$

The charge ratio R_2 is a better estimate of the true charge ratio than is R_1 because fewer assumptions have been used in its derivation.

The charge ratio was calculated using these two formulae with the result that the relative difference between the two calculations was less than 1% for all momenta. Therefore, it is considered that any bias caused by the acceptance of the spectrograph is small and the

charge ratio can be calculated using equation 7.1. The charge ratio is presented in table 7.3 and figure 7.2.

MEAN MUON MOMENTUM GeV/c	TOTAL NUMBER OF MUONS		CHARGE RATIO
	-ve	+ve	
123	4240	5433	1.28 ±0.03
177	4227	5614	1.33 ±0.03
257	2701	3377	1.25 ±0.03
376	1273	1759	1.38 ±0.05
553	565	755	1.34 ±0.07
809	228	334	1.46 ±0.13
1183	91	118	1.30 ±0.18
1760	30	40	1.33 ±0.32

TABLE 7.3 THE MUON CHARGE RATIO

7.4 THE ERROR ON THE CHARGE RATIO

If N muons are detected in an experiment, the relative probabilities of there being 0, 1, 2, ...N negatively charged muons are given by the binomial distribution. The standard deviation of this distribution is $\sqrt{Npq}$, where p and q are the probabilities that a detected muon is negatively or positively charged. p and q can be estimated from the numbers of negatively and positively charged muons collected, thus $p \doteq N^-/N$ and $q = N^+/N$. Therefore the standard deviation can be estimated from $\sqrt{N^+N^-}/N$.

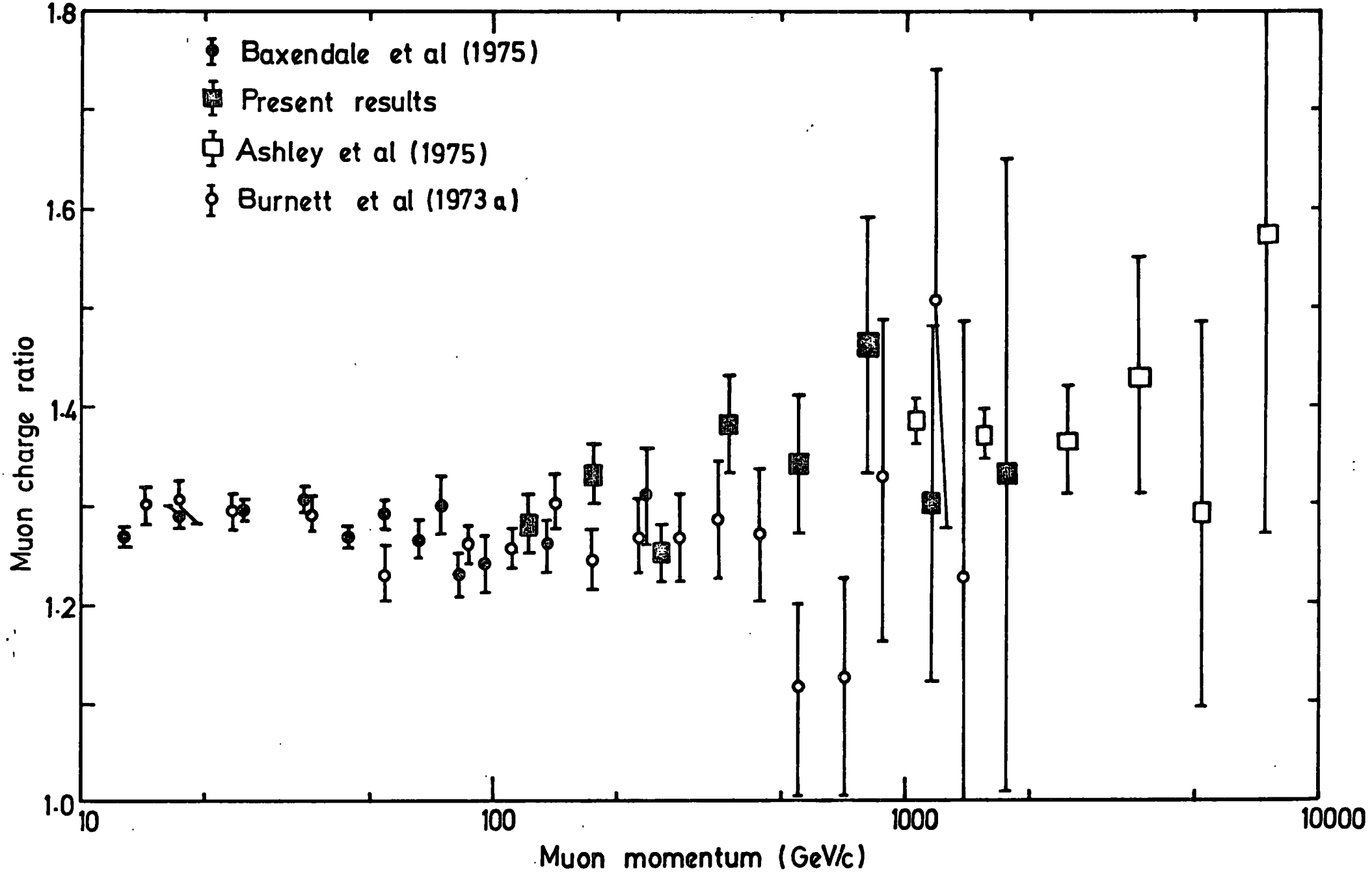

Figure 7.2 The muon charge ratio plotted as a function of momentum.

The charge ratio is given by $R = N^+/N^-$. Because N^+ and N^- are not independent quantities, the equation is re-written as $R = N/N^- - 1$, and the error on R can be calculated as follows:

$$\alpha_R^2 = \left(\alpha_{N^-} \cdot \frac{\delta R}{\delta N^-}\right)^2 = \frac{N^+ N^-}{N} \left(\frac{N}{N^- N^-}\right)^2$$

which by substitution and by re-arranging, becomes:

$$\alpha_R = R \sqrt{\frac{1}{N^+} + \frac{1}{N^-}}$$

This equation has been used to calculate the errors on the charge ratio.

7.5 THE COMPARISON WITH OTHER MEASUREMENTS

The results of the present measurement of the charge ratio are shown in figure 7.2 together with the previous MARS measurement of Baxendale et al (1975) and the measurements of Burnett et al (1973(a)), Ashley et al (1975).

The measurements of Baxendale et al were made on the MARS spectrograph using the momentum selector trays as primary detectors. The data collection and the analysis of the discharged flash-tubes was automatic, being controlled electronically. Approximately 1.3×10^6 near vertical muons of momentum greater than 10 GeV/c were collected and analysed. The data are consistent with a constant charge ratio of 1.285 ± 0.002, although there is a slight variation with momentum. Above 50 GeV/c the charge ratio is 1.261 ± 0.009 and above 100 GeV/c it is 1.274 ± 0.019. There is therefore a slight decrease in the charge ratio between 50 and 100 GeV/c with a small increase at higher momenta. The results of Baxendale et al are the most precise in this momentum range and are in good agreement with the results of Allkofer et al (1971(a)) who found a mean of $1,29 \pm 0.02$ for momenta >10 GeV/c and those of Nandi and Sinha (1972(a)) who found a mean of 1.28 ± 0.02 for momenta

> 5 GeV/c.

The measurements of Burnett et al were carried out on the sea-level cosmic ray spectrograph at the University of California, San Diago. For a description of this spectrograph see section 6.8.3. The charge ratio was measured at eight zenith angles between 0° and 90° with an angular acceptance of ±4°. Between 10 and 50 GeV/c the charge ratio is seen to decrease slightly with momentum and increase with zenith angle. Above 50 GeV/c however, the charge ratio is not dependent upon the zenith angle or the momentum and its overall value is 1.261 ±0.009. This is in good agreement with the result of Baxendale et al.

The work of Ashley et al was carried out on the underground Utah cosmic ray detector. The advantage of working underground is that the high energy muon spectrum is transformed to a low energy spectrum at the place of measurement due to energy loss in the rock above the detector. It is then possible to measure the spectrum using a solid iron magnetic spectrograph provided it has a large enough aperture to overcome the small flux of muons. The Utah spectrograph consists of two detector magnets seperated by a concrete absorber, four water Cherenkov detectors to trigger the apparatus and fifteen vertical planes of cylindrical spark chambers to locate the paths of the muons. The spectrograph is arranged horizontally and will accept muons within an angular range from 40° to 90°. In the energy range from 1 TeV to 7.5 TeV, the charge ratio showed no zenith angle dependence and was found to have the overall value of 1.378 ±0.015, which is significantly higher than the measurements of Baxendale et al and Burnett et al at lower momentum.

The overall charge ratio from the present work is 1.305 ±0.015 and there is an indication of a slight increase in the charge ratio with momentum. This result is consistent with an increase in the charge ratio from the accepted value of ∿1.29 below 50 GeV/c to a value of ∿1.38 above 1000 GeV/c which has been observed by Ashley et al. However, the present measurement is in general higher than that of Burnett et al although the large errors on the measurements around 1000 GeV/c do not allow significant comparisons to be made.

CHAPTER 8

CONCLUSIONS

The results of the final measurement of the vertical muon momentum spectrum and charge ratio using the MARS spectrograph have been presented in this work.

Approximately 80,000 events were analysed and about 31,000 events were found to be above 100 GeV/c and to be suitable for inclusion in the final spectrum. The data have been corrected for all known instrumental biases and for the rejection of events by the analysis program.

The maximum detectable momentum of the spectrograph has been calculated to be 2400 ±150 GeV/c. This is in reasonable agreement with the value of 2800 GeV/c calculated by Piggott (1975). The spectrum has been corrected for resolution effects up to $\sim 10^4$ GeV/c but only data below 3000 GeV/c have been used in the final spectrum.

The present measurement of the muon differential spectrum, which extends from 200 GeV/c to 3000 GeV/c, is found to be in good agreement with the previous measurement of the spectrum using the MARS spectrograph (Ayre et al, 1975) in the region of overlap between 200 GeV/c and 500 GeV/c. The present measurement is ∿5% lower in intensity.

The present measurement also agrees reasonably well with the measured intensities from other spectrographs (e.g. Hayman and Wolfendale, 1962, Allkofer et al, 1971 and Burnett et al, 1973) although there are large differences in absolute intensity in some cases.

A theoretical spectrum based upon an all pion production spectrum provided the best fit to the present data, yielding a value of 2.49 ±0.06 as the exponent of the production spectrum. The significance

level of this result is extremely high. A kaon production spectrum is not ruled out by this result, although it was not found possible to deduce a value for the kaon to pion ratio in nuclear interactions. If it is assumed to have a value of 0.1 (results from p-p interactions at the ISR facility at CERN indicate that it is in this region), then the exponent of the pion and kaon production spectra has a value of 2.54.

The present value of the exponent of the all pion production spectrum is lower than the value predicted by other workers (values range from 2.63 to 2.73) but it is in good agreement with the value of 2.51 ±0.04 obtained by Whalley (1974) from the spectrum of Ayre et al (1975) for momenta above 70 GeV/c. The disagreement with the results from other spectrographs is thought to be because those results are heavily weighted by the data at low momentum (10 -20 GeV/c). The present result therefore confirms the predictions of Whalley (1974) of a flatter production spectrum above 100 GeV/c and it indicates that this flatter spectrum extends a least up to 3000 GeV/c.

With regard to the indirect measurements of the muon spectrum at high energy, the present results are higher in intensity and have a flatter spectrum above 1 TeV/c. No reason is suggested to explain this, although it should be noted that there are significant differences between individual indirect spectra (for example the survey of indirect measurements of Wright (1973) has a flatter spectrum than the survey of direct and indirect measurements of Ng et al (1973)). It is believed that this conflict will only be resolved when further indirect measurements are carried out above 1 TeV/c.

If the present measurements are to be believed, then they would tend to indicate a flattening of the primary spectrum above 10^{13} eV/nucleon

which has been suggested by Wdowczyk and Wolfendale (1973) to bring agreement with the spectrum based on EAS data above 10^{15} eV. (See also Hillas, 1975). This could be caused by an increase in the proportion of heavy nuclei in the primary radiation as suggested by Thompson and Whalley (1977) and Erlykin et al (1974).

With regard to the measurements of the charge ratio, the present result gives an overall value of 1.305 ±0.015 for momenta above 100 GeV/c. This is in good agreement with the previous precise measurement of the charge ratio using the MARS spectrograph, reported by Baxendale et al (1975). There is also an indication of a rise in the charge ratio with momentum and the present results tend to confirm the measurements of Ashley et al (1975) who obtained a value of ∿1.38 above 1 TeV/c.

The results presented here conclude the measurements made using the MARS spectrograph. Together with the results of Ayre et al (1975) and Baxendale et al (1975), they provide a consistant picture of the muon spectrum and charge ratio over two orders of magnitude of momentum, and provide the basis for predictions concerning the nature of nuclear interactions and the shape and composition of the primary energy spectrum.

REFERENCES

Abdel-Monem, M.S., Benbrook, J.R., Osborne, A.R., Sheldon, W.R., Duller, N.M., Green, P.J., 1973, P.I.C.C.R., Denver, 3, 1811

Achar, C.V., Narasimham, V.S., Ramana Murthy, P.V., Creed, D.R., Pattison, J.M.B., and Wolfendale, A.W., 1965, Proc. Phys. Soc., 86, 1305

Allkofer, O.C., Carstensen, K., Dau, W.D., 1971, P.I.C.C.R., Hobart, 4, 1314

Allkofer, O.C., Carstensen, K., Dau., W.D., Fahnders, E., Heinrich, W., Jokisch, H., 1971(a). P.I.C.C.R., Hobart, 4, 1319

Allkofer, O.C., Carstensen, K., Dau. W.D., Jokisch, H., Frochlich, A., Seidman, A., and Yeiven, T., 1971 (b), P.I.C.C.R., Hobart, 4, 1596

Anderson, C.D., 1932, Science, 76, 238

Appleton, I.C., Hogue, M.T., Rastin. B.C., 1971, Nucl. Phys., B26, 365-389

Ashley, G.K., Keuffel, J.W., Larson, M.O., 1975, Phys. Rev. D, 12, 1, 20-35

Aubert, J.J., et al., 1974, Phys. Rev. Lett., 33, 1404

Augustin, J.E., et al., 1974, Phys. Rev. Lett., 33, 1406

Aurela, A.M., and Wolfendale, A.W., 1967, Ann. Acad. Sci. Fenn., A6, 226-40

Ayre, C.A., Thompson, M.G., 1969, Nucl. Inst. and Meth., 69, 106

Ayre, C.A., 1971, Ph.D Thesis, University of Durham

Ayre, C.A., Hamden, M.A., Hume, C.J., Stubbs, F.W., Thompson, M.G., Wells, S.C., and Whalley, M.R., 1972(a), Nucl. Inst. and Meth., 102, 19

Ayre, C.A., Hamden, M.A., Hume, C.J., Stubbs., F W., Thompson, M.G., Wells, S.C., and Whalley, M.R., 1972(b), Nucl. Inst. and Meth., 102, 29

Ayre, C.A., Baxendale, J.M., Daniel, B.J., Goned, A., Piggott, J.L., and Thompson, M.G., 1975(a), Nucl. Inst. and Meth., 124, 335-339

Ayre, C.A., Baxendale, J.M., Hume, C.J., Nandi. B.C., Thompson. M.G., Whalley, M.R., 1975, J. Phys. G: Nucl. Phys., 5, 584-600

Badhwar, G.D., Stephens, S.A., and Golden, R.L., 1977, Phys. Rev. D., 15, 3, 820

Barrett, P.H., Bollinger, L.M., Cocconi, G., Eisenburg, Y., and Greisen, K., 1952, Rev. Mod. Phys., 24, 3, 133-78

Bateman, B.J., Cantrell, W.G., Durda, D.R., Duller, N.M., Green, P.J., Jelinek, A.V., Nagy, T.A., and Sheldon, W.R., 1971, Phys. Lett., 36B, 144

Baxendale, J.M., Hume, C.J., and Thompson, M.G., 1975, J. Phys. G: Nucl. Phys., 7, 781-88

Benecke, J., Chou, T.T., Yang,N.N., and Yen, E., 1969, Phys. Rev., 188, 5, 2159

Blackett, P.M.S., Occhialini, G., 1933, Proc. of the Roy. Soc. (London), A139, 699

Bothe, W., and Kolhörster, W., 1928, Naturwissenschaften, 16, 1044, 1045

Bothe, W., and Kolhörster, W., 1939, Phys. Z., 30, 516

Bull, R.M., Nash, W.F., and Rastin, B.C., 1965, Nuovo Cim., 40A, 365

Burbidge, G.R., 1975, Phil. Trans. R. Soc., A277, 481

Burnett, T.H., Masek, G.E., Maung, T., Miller, E.S., Ruderman, H, and Vernon, W., 1973, P.I.C.C.R., Denver, 3, 1764-1770

Burnett, T.H., LaMay, L.J., Masek, G.E., Maung, T., Miller, E.S., Ruderman, H., and Vernon, W., 1973(a), Phys. Rev.Lett., 30, 19, 937-940

Clay, J., 1927, Proc. Amsterdam, 30, 1115

Close, F.E., 1979, Comtemp. Phys., 20, 3, 293-313.

Coates, R.B., 1967, Ph.D Thesis, University of Durham

Colgate, S.A., and White, R.H., 1966, Astrophys. J., 143, 626

Cooper, M., 1977, Physics Bulletin, 28, 10, 463

Cunningham, G., Pollack, A.T.M., Reid, R.J.O., and Watson, A.A., 1977, P.I.C.C.R. Plovdiv, OG-189

Daniels, B.J., 1975, Private Communication

Duthie, J., Fowler, P.H., Kaddoura, A., Perkins, D.H., and Pinkau, K., 1962, Nuovo Cim., 24, 122

Erlykin, A.D., Ng, L.K., and Wolfendale, A.W., 1974, J. Phys. A: Math., Nucl. Gen., 7, 16, 2059-2073 and 2074-2084

Feynman, R.P., 1969, Phys. Rev. Lett. 23, 24, 1415-1417

Fowler, P.H., Adams, R.A., Cowen. V.G., and Kidd, J.M., 1967, Proc. Roy. Soc. (London), 301A, 39-45

Fowler, P.H., et al, 1970, Proc. Roy. Soc. (London), 301A, 1-43

Ginzburg, V.L., 1975, Phil. Trans. Roy. Soc., A277, 463-479

Greisen, K., 1942, Phys, Rev. 61, 212-19

Greisen, K., 1960, Ann. Rev. Nucl. Sci., 10, 63

Greisen, K., 1966, Phys. Rev. Lett, 16, 748

Hansen, S., 1975, Ph.D Thesis, University of Durham.

Hansen, S., and Thompson, M.G., 1975(a), J. Phys. G: Nucl. Phys., 9, 995

Hansen, S., and Thompson, M.G., 1976, J. Phys. G: Nucl. Phys., 2, 523

Hawkes, R.C., 1977, Ph.D Thesis, University of Durham

Hayman, P.J., and Wolfendale, A.W., 1962, Proc. of the Phys. Soc., 80, 3, 515, 710-728

Hess, V.F., 1911, Phys. Z., 12, 998

Hess, V.F., 1912, Phys. Z., 13, 1084

Hillas, A.M., 1975, Phys. Rep., 20C, 2, 59-136

Hoffman, H.J., 1975, Phys. Rev. D, 12, 1, 82-91

Hume, C.J., Nandi, B.C., Thompson, M.G., Whalley, M.R., and Wolfendale, A.W., J. Phys. A: Math., Nucl. Gen., 6, 6, L73-6

Johnson, T.H., and Street, J.C., 1933, Phys. Rev., 43, 381

Karakula, S., Osborne, J.L., and Wdowczyk, J., 1974, J. Phys. A: Math., Nucl. Gen., 7, 437

Koshiba, M., 1977, J. Phys. Soc. Japan, 43, 2, 701-2

Krishnaswamy, M.R., Menon, M.G.K., Narasimham, V.S., Ito, N., Kawakami, S., and Miyake, S., 1977, P.I.C.C.R., Plovdiv, 6, 85

Lattes, C.M.G., Occhialini, G.P.S., and Powell, C.F., 1949, Nature, 160, 453, 486

Liland, A., 1978, Arkiv for Det. Fysiske Seminar i Trondheim, No. 8

Maeda, K., 1964, J. Geophys. Res., 69, 1725

Miller, D., 1978, Nature, 273, 705

Minorikawa, Y., and Saito, T., 1977, P.I.C.C.R., Plovdiv, 6, 12-17

Miyake, S., Narasimham, V.S., and Ramana Murthy, P.V., 1964, Nuovo Cim., 32, 1524

Mizutani, K., Misaki, A., Shirai, T., Watanabe, Z., Akashi, M., Takahashi, Y., 1978, Nuovo Cim., 48A, 4, 429-445

Morrison, J.L., and Elbert, J.W., 1973, P.I.C.C.R., Denver, 3, 1833

Nandi, B.C., and Sinha, M.S., 1972, J. Phys. A: Gen. Phys., 5, 1384-1394

Nandi, B.C., and Sinha, M.S., 1972(a), Nucl. Phys. B (Neth), B40, 1, 289-297

Ng, L.K., Wdowczyk, J., and Wolfendale, A.W., 1973, P.I.C.C.R., Denver, 3, 1781-1787

Osborne, J.L., Wolfendale, A.W., and Palmer, N.S., 1964, Proc. Phys. Soc., 84, 911-913

Perl, M.L., 1978, Nature, 275, 273-278

Piggott, J.L., 1975, Ph.D Thesis, University of Durham

Rada, W.S., 1977, Ph.D Thesis, University of Durham

Rochester, G.D., and Butler, C.C., 1947, Nature (London), 160, 855

Rossi, B., and Greisen, K, 1942, Rev. Mod. Phys., 13, 240

Rossi, B., 1948, Rev. Mod. Phys., 20, 537-83

Rossi, B., High Energy Particles, (New York: Constable), 1952

Said, S.S., 1966, Ph.D Thesis, University of Durham

Stecker, F.W., Comments Astrophys., 1978, 7, 4, 129-137

Sternheimer, R.M., and Peierls, R.F., 1971, Phys. Rev. B, 3, 11, 3681-3692

Street, J.C., and Stevenson, E.C., 1937, Phys. Rev., 52, 1003

Thompson, M.G., Cosmic Rays at Ground Level, Ed. Wolfendale, A.W., Institute of Physics, London and Bristol, 1973

Thompson, M.G., and Whalley, M.R., 1977, J. Phys. G (GB), 3, 1, 97-119

Thompson, M.G., Thornley, R., and Whalley, M.R., 1977, J. Phys. G (GB), 3, 2, L39-42

Wdowczyk, J., and Wolfendale, A.W., 1973, J. Phys. A: Gen Phys., 6, 1594

Wells, S.C., 1972, Ph.D Thesis, University of Durham.

Whalley, M.R., 1974, Ph.D Thesis, University of Durham

Wright, A.G., 1973, P.I.C.C.R., Denver, 3, 1709. (See also Whalley, 1974)

Wolfendale, A.W., 1973, Cosmic Rays at Ground Level, Institute of Physics, London and Bristol.

Yukawa, H., 1935, Proc. Phys. Math. Soc. Japan, 17, 48

Zatsepin, G.T., and Kuzmin, V.A., 1966, Soc. Phys. - J.E.T.P., 4, 114-117